

Alma Mater Studiorum – Università di Bologna

DOTTORATO DI RICERCA IN

Science della Terra, della Vita e dell'Ambiente

Ciclo 29°

Settore Concorsuale di afferenza: 04/A1

Settore Scientifico disciplinare: GEO/08

**DEVELOPMENT AND OPTIMIZATION
OF A THERMO-CHEMICAL PROCESS FOR RECYCLING
WASTE ELECTRICAL AND ELECTRONIC EQUIPMENT**

Presentata da: Peter Hense, M.Sc.

Coordinatore Dottorato

Relatore

Prof. Dr. Barbara Mantovani

Prof. Dr. Andrea Contin

Esame finale anno 2017

DEVELOPMENT AND OPTIMIZATION OF A THERMO-CHEMICAL PROCESS FOR RECYCLING WASTE ELECTRICAL AND ELECTRONIC EQUIPMENT

Entwicklung und Optimierung eines thermo-chemischen Verfahrens
zum Recycling von Elektro- und Elektronikschrott

Ph.D. Thesis

Dottorato di Ricerca in Scienze della Terra, della Vita e dell'Ambiente

Alma Mater Studiorum – Università di Bologna
Dipartimento di Scienze Biologiche, Geologiche e Ambientali

Ciclo 29°

Peter Hense, M.Sc.

Ph.D. Thesis Examination Board:

Coordinator: Prof. Dr. Barbara Mantovani

Tutor: Prof. Dr. Andrea Contin

Co-Tutor: Prof. Dr. Andreas Hornung

Bologna
2017

Acknowledgments

The present Ph.D. thesis was prepared in a collaboration of the University of Bologna and Fraunhofer UMSICHT, institute branch Sulzbach-Rosenberg.

Firstly of all, I am pleased to express my gratitude to my supervisor Prof. Andrea Contin and my co-supervisor Prof. Andreas Hornung for the chance they gave me to write this Ph.D. thesis at both institutes and especially for their material and immaterial support. Furthermore, I would like to thank both for the extensive advice they gave me and all the discussions we had. Additionally, I would kindly like to thank Prof. Barbara Mantovani and Prof. Alessandro Amorosi as very friendly coordinators of the Ph.D. committee at the University of Bologna.

Further thanks should be addressed to Prof. Maria Paola Luda from the University of Turin and Dr. Marianne Blazsó from the Hungarian Academy of Sciences, who reviewed this thesis and gave me much good advice.

Moreover, I thank both teams of the interdepartmental research centre for environmental sciences at the University of Bologna and of Fraunhofer UMSICHT. In particular, I would like to express my gratitude to Dr.-Ing. Matthias Franke and his team of the department of recycling management. Amongst many others, it was Matthias' input and information that was needed to write a conclusive thesis.

Special thanks also to Prof. Daniele Fabbri and Dr. Roberto Conti for the opportunity to conduct GC-MS analyses in their labs, Dr. Andreas Apfelbacher and Dipl.-Ing. Johannes Neumann for discussions about chemistry and energetic utilizations of fuels, and Dipl.-Ing. Ingrid Löh for the support during different analyses.

I am grateful having had the opportunity not only to work together with Prof. Mario Mocker for conducting EDRXF analyses at the Ostbayerische Technische Hochschule Amberg-Weiden (OTH) but also for the great discussions we had. Additional thanks goes to all the students that supported me on my topic, the mechanical and construction team of Fraunhofer UMSICHT, and Alyssa Albek, who checked this work as native speaker.

For financial support I would like to thank the German Federal Ministry of Education and Research, the Bavarian Ministry of Economic Affairs and Media, Energy and Technology as well as the German Association for Waste Management (DGAW e.V.).

Last but not least, I would like to acknowledge my friends and in special my family, who gave me energy, ideas, and time for discussions during the last three years.

Sincere thanks are given to them all!

Lock Flag

The present Ph.D. thesis “Development and Optimization of a thermo-chemical Process for Recycling Waste Electrical and Electronic Equipment” contains confidential information of Alma Mater Studiorum – Università di Bologna and Fraunhofer UMSICHT, Fraunhofer Institute for Environmental, Safety, and Energy Technology. Thus, this work contains a lock flag and should not be made available to the public in its full length.

Publication of the contents or any parts of it and the passing on third parties – also in digital format – is generally not allowed.

Exemptions require written permissions of:



ALMA MATER STUDIORUM
UNIVERSITÀ DI BOLOGNA

Alma Mater Studiorum
Università di Bologna
Dipartimento di Scienze Biologiche,
Geologiche e Ambientali

Via Selmi 3
40126 Bologna (Italy)

Phone: +39 051 20 9 4900

Fax: +39 051 20 9 4149

Email: bigea.segreteria@unibo.it
<http://www.bigea.unibo.it>



Fraunhofer UMSICHT, Fraunhofer Institute
for Environmental, Safety, and Energy
Technology
Institute Branch Sulzbach-Rosenberg

An der Maxhütte 1
92237 Sulzbach-Rosenberg (Germany)

Phone: +49 9661 908-400

Fax: +49 9661 908-469

E-Mail: info-suro@umsicht.fraunhofer.de
<http://www.umsicht-suro.fraunhofer.de>

Abstract

The steadily increasing amount of Waste Electrical and Electronic Equipment (WEEE) contains a number of economically relevant base, precious, and high-tech metals. However, recovery of these metals using state-of-the-art mechanical treatment is limited with the effect that, for instance, a significant amount of metals remains in residual waste fractions. Pyrolysis technology allows an extraction and accumulation of metals from such waste fractions in order to enable corresponding recycling. However, recycling of WEEE, especially using thermal and chemical processes could bring up a number of different challenges, for instance, due to feasible formations of harmful substances like highly-toxic polyhalogenated dibenzo-*p*-dioxins and -furans (PXDD/F).

In the present work, a process and a corresponding bench-scale plant for a thermo-chemical treatment of different fractions from WEEE were developed and optimized. As feedstocks, a shredder residue, which represents the main output with negative earnings from a treatment of WEEE, as well as tantalum capacitors and Liquid Crystal Displays (LCD), which contain the scarce/critical metals Ta, Ga and/or In, were selected. With the aim to accumulate and/or extract metals from feedstocks to enable downstream recycling as well as to dehalogenate pyrolysis products, the development of the pyrolysis process was accompanied with a number of different analyses: these were, amongst others, inductively coupled plasma mass and optical emission spectrometry (ICP-MS/-OES), energy dispersive x-ray fluorescence spectrometry (EDXRF), and x-ray diffraction (XRD) for quantitative and qualitative analyses of metal contents as well as statistical evaluations in order to analyze elemental and mainly metal allocations to different pyrolysis products. Regarding dehalogenation of pyrolysis products, the focus was on PXDD/F, which quantifications were conducted by high-resolution gas chromatography/mass spectrometry (HR GC-MS). For quantitative and qualitative analyzes of compounds, which are present in pyrolysis liquid products, amongst others, GC-MS analyses were conducted.

From pyrolysis tests with shredder residues, best results regarding metal accumulation and dehalogenation were achieved at a pyrolysis temperature of 650 °C and a residence time of 30 min. These results are based on comprehensive tests series from 43 pyrolysis tests under different conditions such as temperatures between 350 and 650 °C and residence times between 30 and 90 min. Analyses about allocations of metals from pyrolysis of shredder residues revealed, amongst others, that most metals were part of the pyrolysis solid products, but, for instance, Cd, In, and Mo were strongly mobilized to pyrolysis vapor. Due to these mobilizations, which accounted for up to 100 wt.-% in the case of In, a selective recovery of these metals could be enabled.

Due to optimizations of pyrolysis temperature and residence time, such an avoidance level of PXDD/F formations in the solid products was achieved, at which no threshold values of the German act on restriction of chemicals (GGVSEB) and German chemicals prohibition ordinance (ChemVerbotsV) were exceeded. In contrast, PXDD/F

concentrations in liquid products exceeded some of these values, even after an increase of pyrolysis temperature. Therefore, a polyolefin-reactor (PO-reactor) was designed, which enabled PXDD/F decomposition using blends of polypropylene (PP) and $\text{La}(\text{OH})_3/\text{LaOOH}$. HR GC-MS analyses revealed that due to the addition of such La compounds, a complete decomposition of polyhalogenated dioxins could be achieved. As decomposition products HX and X_2 were formed and became part of the pyrolysis liquid and gaseous products. In order to dehalogenate these pyrolysis products and thus, to enable (energetic) utilization of it, a halogen-filter with a novel filter-material was developed and tested. The filter-material consists out of a three-dimensional carrier structure, which is coated with a rare earth oxide (REO). Preliminary tests with Br_2 and HBr revealed that the developed halogen-filter is able to absorb more than 90 wt.-% of such compounds.

In order to investigate efficiencies of selective mobilizations of metals either to depollute feedstock or to recover valuable metals, different pyrolysis approaches with LCD as feedstock were conducted and allocations of metals analyzed. As approaches, pyrolysis of LCD, co-pyrolysis with polyvinyl chloride (PVC), and pyrolysis of PVC with LCD in vapor-phase mode were examined. The tests clearly revealed that co-pyrolysis with PVC could be used to completely mobilize As while a pyrolysis of PVC with LCD in vapor-phase mode enabled a selective extraction of In. In contrast, pyrolysis tests between 450 and 650 °C with Ta capacitors as feedstock were conducted to optimize pyrolysis process conditions for a great accumulation of Ta in pyrolysis solid products. These tests in combination with a sieving at 500 μm revealed that the highest rate of allocation to pyrolysis solid products <500 μm can be achieved at a pyrolysis temperature of 550 °C. The corresponding allocation of Ta accounted for nearly 90 wt.-%, representing an accumulation factor of 4.84 and a concentration of 55.7 wt.-% Ta in the corresponding fraction.

In an ecological and an economical assessment, the performance of a prospective, continuous pyrolysis process for shredder residues was compared to a treatment following the status quo. In the ecological assessment, in nine categories, impacts of the novel process were compared to the status quo, defined as thermal treatment of shredder residues in a waste incinerator. The assessment clearly revealed that in all of these categories exonerative effects concerning ecological aspects were stronger in the case of the pyrolysis process, mainly in categories regarding resources, acidification and photochemical ozone creation. For the economical assessment, an implementation of a continuous pyrolysis process was evaluated in three different scenarios, which can be mainly differentiated due to the way of energetic utilization of pyrolysis liquid and gaseous products. All different scenarios revealed positive rates of return with values up to 34.3 %. Such scenario, in which liquid and gaseous products are energetically utilized in a combustion unit showed the most economical benefits, for instance, represented by payback periods of minimal 2.73 (static) and 3.02 (dynamic) years.

Zusammenfassung

Die stetig wachsende Menge von Elektro- und Elektronikaltgeräten (EAG) enthält eine Reihe wirtschaftlich bedeutender Basis-, Edel- und High-Tech Metalle. Selbst mit Hilfe einer modernsten mechanischen Aufbereitung können jedoch nicht alle Metalle zurückgewonnen werden, so dass sich signifikante Mengen dieser in Rückständen der EAG-Aufbereitung finden lassen. Die Technologie der Pyrolyse ermöglicht es, Metalle aus diesen Fraktionen freizulegen und so anzureichern, dass ein adäquates Recycling möglich wird. Jedoch stellt das Recycling von EAG, insbesondere mittels thermischer und chemischer Prozesse, den Anwender unter anderem vor die Herausforderung der Bildung gefährlicher Substanzen wie beispielsweise hoch toxischer, polyhalogener Dibenzo-*p*-Dioxine und -Furane (PXDD/F).

In der vorliegenden Arbeit wurden ein Prozess sowie eine entsprechende Versuchsanlage für eine thermo-chemische Aufbereitung verschiedener Fraktionen aus der EAG-Aufbereitung entwickelt und optimiert. Als Einsatzstoffe dienten hierbei zum einen ein Shredderrückstand, der jene Fraktion mit den höchsten, absoluten Entsorgungskosten der EAG-Aufbereitung darstellt, sowie Tantal-Kondensatoren und Flüssigkristallanzeigen (LCD), welche die knappen und kritischen Metalle Ta, Ga und/oder In enthalten. Mit dem Ziel, enthaltene Metalle anzureichern und/oder extrahieren um ein nachgeschaltetes Recycling zu ermöglichen sowie die Pyrolyseprodukte zu dehalogenieren, wurden unter anderem folgende Analysen durchgeführt: Qualitative und quantitative Metallbestimmungen wurden mit Hilfe von Massen- und Atomemissionsspektrometrie mit induktiv gekoppeltem Plasma (ICP-MS/-OES), energiedispersiver Röntgenfluoreszenzanalyse (EDXRF) und Röntgendiffraktometrie (XRS) durchgeführt. Des Weiteren sind Element- und insbesondere Metallallokationen mittels statistischer Methoden untersucht worden. Mit Bezug auf die Dehalogenierung der Pyrolyseprodukte wurde der Fokus auf PXDD/F gelegt, deren Quantifizierung mittels hochauflösender Gaschromatographie mit Massenspektrometrie (HR GC-MS) durchgeführt worden ist. Die quantitative Bestimmung von Komponenten der flüssigen Pyrolyseprodukte ist neben anderen mittels GC-MS durchgeführt worden.

Pyrolyseversuche mit Shredderrückständen zeigten, dass bei einer Pyrolysetemperatur von 650 °C und einer Verweilzeit von 30 min die besten Ergebnisse bezüglich einer Metallanreicherung und Dehalogenierung erzielt werden konnten. Diese und weitere Ergebnisse basieren auf umfangreichen Testreihen mit 43 Pyrolyseversuchen bei Temperaturen zwischen 350 und 650 °C sowie Verweilzeiten zwischen 30 und 90 min. Allokationsanalysen zu Metallen aus Shredderrückständen zeigten unter anderem, dass sich der Großteil der Metalle in den festen Pyrolyseprodukten wiederfinden ließ, aber auch, dass beispielsweise Cd, In und Mo in die Dampfphase gingen. Durch diese Mobilisierung, die, wie im Fall von In, bis zu 100 Ma.-% betrug, ließe sich eine selektive Rückgewinnung dieser Metalle ermöglichen.

Durch Optimierungen von Pyrolysetemperatur und Verweilzeit wurden in den festen Pyrolyseprodukten so geringe PXDD/F-Belastungen gemessen, dass keine Grenzwerte der Gefahrgutverordnung GGVSEB sowie der Chemikalien-Verbotsverordnung ChemVerbotsV überschritten wurden. Demgegenüber sind selbst nach einer Erhöhung der Pyrolysetemperatur einige der Grenzwerte in den flüssigen Produkten überschritten worden. Aus diesem Grund wurde ein Polyolefin-Reaktor entworfen, der es basierend auf Mischungen von Polypropylen (PP) und $\text{La}(\text{OH})_3/\text{LaOOH}$ ermöglicht, PXDD/F zu zerstören. HR GC-MS Analysen zeigten, dass durch den Zusatz der Lanthanverbindungen eine vollständige Zerstörung polyhalogener Dioxine erzielt werden konnte. Abbauprodukte zugrundeliegender Reaktionen sind X_2 und HX , welche Teil der flüssigen und gasförmigen Pyrolyseprodukte wurden. Um diese Pyrolyseprodukte zu dehalogenieren und so eine (energetische) Nutzung zu ermöglichen, wurde ein Halogenfilter mit einem neuartigen Filtermaterial entwickelt und getestet. Das Filtermaterial basiert auf einer dreidimensionalen Struktur, welche mit einem Seltenerdoxid beschichtet ist. Vorversuche mit Br_2 und HBr zeigten, dass das entwickelte Filtermaterial mehr als 90 Ma.-% dieser Komponenten absorbieren kann.

Um die Effizienz einer selektiven Mobilisierung von Metallen zur Schadstoffentfrachtung oder zur Rückgewinnung werthaltiger Metalle zu untersuchen, sind drei unterschiedliche Ansätze zur Durchführung einer Pyrolyse mit dem Einsatzstoff LCD durchgeführt und die Metallallokation untersucht worden. Die Ansätze waren im Einzelnen eine Pyrolyse von LCD, eine Co-Pyrolyse mit Polyvinylchlorid (PVC) sowie eine Pyrolyse von PVC, bei der LCD in der Dampfphase zur Reaktion gebracht wurde. Die Versuche zeigten sehr deutlich, dass mit Hilfe einer Co-Pyrolyse eine vollständige Mobilisierung von As möglich ist, während eine Dampfphasenreaktion von LCD in einer Pyrolyse von PVC eine selektive Extraktion von In ermöglichte. Im Gegensatz hierzu wurden Pyrolyseversuche mit Ta-Kondensatoren als Einsatzstoff zwischen 450 und 650 °C durchgeführt, um die Prozessbedingungen einer Pyrolyse für eine möglichst hohe Anreicherung von Ta im festen Pyrolyseprodukt zu erzielen. Die Versuche in Kombination mit einer Siebtrennung bei 500 µm zeigten, dass die stärkste Allokation von Ta zum Produkt <500 µm bei einer Pyrolysetemperatur von 550 °C erzielt werden konnte. Die entsprechende Allokationsrate belief sich auf knapp 90 Ma.-% was einen Anreicherungsfaktor von 4,84, respektive eine Ta-Konzentration von 55.7 Ma.-% im festen Pyrolyseprodukt darstellt.

In einer Nachhaltigkeitsbewertung zu einem anvisierten, kontinuierlichen Pyrolyseprozess für Shredderrückstände wurde die ökologische und ökonomische Performance in Relation zur jetzigen Aufbereitung nach dem Status Quo gesetzt. In der ökologischen Bewertung sind hierzu in neun Kategorien mögliche Auswirkungen auf die Umwelt mit einer thermischen Verwertung in einer Abfallverbrennung (Status Quo) verglichen worden. Die Bilanzierung zeigte deutlich, dass durch den Pyrolyseprozess in allen Kategorien, vor allem solchen, die Ressourcen-, Versauerungs- und photochemische Ozonbildungsaspekte betreffen, deutliche Vorteile offenbart werden. Im Rahmen der ökonomischen Bewertung wurden Kalkulationen für eine Implementierung in drei verschiedenen Szenarien durchgeführt, die sich dahingehend unterschieden, wie flüssige

und gasförmige Produkte energetisch genutzt werden. Alle Szenarien zeigten positive Renditen mit Werten von bis zu 34,3 % auf. Die Szenarien, in denen flüssige und gasförmige Pyrolyseprodukte in einem Brenner energetisch genutzt werden, zeigten hierbei die größten ökonomischen Vorteile, beispielsweise ausgedrückt durch Amortisationszeiträume von 2.73 (statisch), respektive 3.02 (dynamisch) Jahre.

Content

Acknowledgments	4
Lock Flag	5
Abstract	6
Zusammenfassung	8
Content	11
Abbreviations	13
List of figures	17
List of tables	23
1. Introduction	26
2. Motivation and objectives of the thesis	30
3. Current state of WEEE-handling in Europe.....	31
3.1 Legal framework of WEEE-handling	31
3.2 Quality and quantity of WEEE in Europe	31
3.3 Mechanical and metallurgical treatment of WEEE	38
3.3.1 Mechanical treatment.....	38
3.3.2 Pyrometallurgical treatment of WEEE	42
3.4 Potential fractions from WEEE treatment as feedstock for a thermo-chemical process	45
3.4.1 Residual fractions from WEEE treatment.....	45
3.4.2 Selected fractions containing scarce and critical metals	46
4. Chemical reactions during thermo-chemical treatment of WEEE.....	51
4.1 Decomposition of additive-free thermoplastics and thermosetting plastics	51
4.2 Decomposition of halogenated polymers and plastics	54
4.2.1 Brominated polymers in plastics	55
4.2.2 Chlorinated polymers and plastics	60
4.2.3 Formation and avoidance of (poly-)halogenated aromatic compounds.....	63
4.3 Pathways for dehalogenation	67
4.3.1 Two-stage pyrolysis	68
4.3.2 Use of metal-free additives.....	70
4.3.3 Halogen fixation by metals and metal oxides	72
4.4 Conclusion: Chemical reactions concerning a thermo-chemical treatment of WEEE ...	85
5. Material and methods.....	89
5.1 Raw materials.....	89
5.1.1 Shredder residues from WEEE treatment	89

5.1.2	Selected fractions containing scarce and critical metals	90
5.2	Analysis: Instrumentation	92
5.3	Analysis: Statistical methods.....	97
5.4	Bench-scale plant	99
5.4.1	Structure and components.....	100
5.4.2	Development, optimization, and preliminary tests.....	104
5.5	Sustainability assessment of a continuous pilot plant.....	111
5.5.1	Ecological assessment.....	111
5.5.2	Economical assessment.....	117
6.	Results.....	124
6.1	Raw material characterization	124
6.1.1	Shredder residues from WEEE treatment	124
6.1.2	Selected fractions containing scarce and critical metals	127
6.2	Pilot tests in bench-scale plant	131
6.2.1	Pyrolysis tests with shredder residues from WEEE treatment.....	131
6.2.2	Pyrolysis tests with selected fractions containing scarce and critical metals.....	165
6.3	Sustainability assessment of a continuous process.....	169
6.3.1	Ecological assessment.....	169
6.3.2	Economical assessment.....	173
7.	Discussions.....	177
7.1	Pyrolysis tests with shredder residues from WEEE treatment	177
7.2	Pyrolysis tests with selected fractions containing scarce and critical metals.....	192
7.3	Sustainability assessment	194
7.3.1	Interpretation of results from ecological assessment.....	194
7.3.2	Economical assessment.....	195
8.	Conclusions.....	196
9.	Outlook	198
	References	200
	Appendix	231

Abbreviations

Abbreviation	Full term	Unit
AADP	Anthropogenic stock extended Abiotic resource Depletion Potential	kg Sb-Eq.
ABS	Acrylonitrile Butadiene Styrene	
ADP	Abiotic resource Depletion Potential	kg Sb-Eq.
AP	Acidification Potential	kg SO ₂ -Eq.
BFR	Brominated Flame Retardants	
B_p	Boiling Point	°C
CHCs	Chlorinated Hydrocarbons	
ChemVerbotsV	German chemicals prohibition ordinance	
CHP	Combined Heat and Power plant	
CTA	Cellulose Triacetate	
CVAS	Cold-Vapor Atomic Spectrometry	
deca-BB	Decabromobiphenyl	
deca-BDE	Decabromodiphenyl Ether	
deca-BDO	Decabromodiphenyl Oxide	
deca-BDPE	Decabromodiphenyl Ethane	
d	Density, relative	kg·m ⁻³
ρ	Density, specific	
DSC	Differential Scanning Calorimetry	
DTA	Differential Thermal Analysis	
DTG	Differential Thermogravimetric analysis	
EDXRF	Energy Dispersive X-Ray Fluorescence spectrometry	
EEE	Electrical and Electronic Equipment	
EoL-RR	End of Life Recycling Rates	wt.-%

EP	Eutrophication Potential	kg PO ₄ ³⁻ -Eq.
EPDM	Ethylene-Propylene-Diene Monomer	
FAME	Fatty Acid Methyl Ester	
FTIR	Fourier Transform Infrared Spectroscopy	
GC-MS	Gas Chromatography/Mass Spectrometry	
GGVSEB	German act on restriction of chemicals	
GWP	Global Warming Potential	kg CO ₂ -Eq.
<i>HHV</i>	Higher Heating Value	MJ·kg ⁻¹
HIPS	High-Impact Polystyrene	
HR GC-MS	High-Resolution GC-MS	
IC	Integrated Circuits	
ICP-MS	Inductively Coupled Plasma Mass Spectrometry	
ICP-OES	Inductively Coupled Plasma Optical Emission Spectrometry	
<i>IRR</i>	Internal Rate of Return	%
LCD	Liquid Crystal Displays	
LHA	Large Household Appliances	
<i>LHV</i>	Lower Heating Value	MJ·kg ⁻¹
<i>M_p</i>	Melting Point	°C
MWI	Municipal Waste Incinerator	
ODP	Ozone Layer Depletion Potential	kg R11-Eq.
PAH	Polycyclic Aromatic Hydrocarbons	
PAN	Polyacrylonitrile	
PBB	Polybrominated Biphenyls	
PBDE	Polybrominated Diphenyl Ethers	
PBDD/F	Polybrominated Dibenzo- <i>p</i> -Dioxins and Furans	
PBP	Polybrominated Phenols	

PBT	Polybutylene Terephthalate	
PCABS	Polycarbonate Acrylonitrile Butadiene Styrene	
PCB	Polychlorinated Biphenyls	
PCDD/F	Polychlorinated Dibenzo- <i>p</i> -Dioxins and Furans	
PE	Polyethylene	
Penta-BDE	Pentabromodiphenyl ether	
PET	Polyethylene Terephthalate	
PGM	Platinum Group Metals	
POCP	Photochemical Ozone Creation Potential	kg C ₂ H ₄ -Eq.
POM	Polyoxymethylene	
PP	Polypropylene	
PS	Polystyrene	
PVA	Polyvinyl Acetate	
PVC	Polyvinyl Chloride	
PVOH	Polyvinyl Alcohol	
PWB	Printed Wiring Boards	
PXAH	Polyhalogenated Aromatic Hydrocarbons	
PXB	Polyhalogenated Biphenyls	
PXDD/F	Polyhalogenated Dibenzo- <i>p</i> -Dioxins and Furans	
REE	Rare Earth Elements	
REO	Rare Earth Oxides	
SAN	Styrene Acrylonitrile	
SBR	Styrene-Butadiene Rubber	
SBS	Styrene-Butadiene-Styrene block copolymer	
SEM	Scanning Electron Microscope	
SMD	Surface Mounted Device	

SHA	Small Household Appliances
TBBPA	Tetrabromobisphenol A
TEQ	Toxic Equivalency Factor
TGA	Thermo Gravimetric Analyzis
THT	Through Hole Technology
TTDE	TTBPA-TBBPA-Diglycidyl Ether Copolymer
WDXRF	Wavelength Dispersive X-Ray Fluorescence
WEEE	Waste Electrical and Electronic Equipment
XRD	X-Ray diffraction

List of figures

Figure 1:	Ranking of raw materials with regard to supply risk and economic importance [EC 2014].	27
Figure 2:	Amounts of products put on the market, waste collected, waste pre-treated, and metals recovered concerning selected metals from IT and telecommunication equipment 2010 in Germany (own diagram based on [Buchert et al. 2012; Sander et al. 2012]).	28
Figure 3:	Calculated average composition* of WEEE in EU-28 (2013) for categories 1, 2, 3, 4, 6, and 7 (in wt.-%) (own diagram based on [Eurostat 2016; Haig et al. 2012; Jofre, Morioka 2005; Reuter et al. 2013]).	32
Figure 4:	Content of Critical Metals in selected EEE (from PWB) and corresponding PWB separately (own diagram based on [Blaser et al. 2011]).	33
Figure 5:	Collection groups in Italy and Germany in combination with the corresponding WEEE categories and those amounts (own diagram based on [CDC RAEE 2014; Eurostat 2016; Magalini et al. 2012]).	35
Figure 6:	Annual growth for 2009 till 2013 and total growth between 2008 and 2013 of WEEE collected in EU-27* (own diagram based on [CDC RAEE 2008; 2009; 2010; 2011; 2013; 2014; Eurostat 2016]).	36
Figure 7:	Share of WEEE collected in the different WEEE categories in EU-28*, Italy, and Germany for 2013 (own diagram based on [CDC RAEE 2008; 2009; 2010; 2011; 2013; 2014; Eurostat 2016]).	36
Figure 8:	Estimated flows of WEEE in the EU-28 in 1 000 Mg (modified according to [Huisman et al. 2015]).	37
Figure 9:	Mechanical treatment of WEEE categories 1 and 10 (modified according to [VDI 2012]).	39
Figure 10:	Mechanical treatment of WEEE categories 2, 3, 4, 6, 7, 8, 9 excluding visual display units (modified according to [VDI 2012]).	40
Figure 11:	Metal content in wt.-% of a dust fraction <0.3 mm from WEEE-treatment (modified according to [Gaggl et al. 2014]).	41
Figure 12:	Structure of a LCD (modified according to [Wang, Xu 2016]).	48
Figure 13:	Components of a molded Ta capacitor [Vishay 2015].	49
Figure 14:	Average composition of Ta capacitors (in wt.-%) (own diagram based on [Cal-Chip 2016]).	50
Figure 15:	Mass yields of pyrolysis liquid and gaseous products (in groups) from a pyrolysis of phenol-formaldehyde resins at different temperatures (own diagram based on [Wong et al. 2015]).	53
Figure 16:	Mass yields of pyrolysis liquid and gaseous products (single compounds) from a pyrolysis of phenol-formaldehyde resins at different temperatures (own diagram based on [Wong et al. 2015]).	54
Figure 17:	Structures of TBBPA (left) and deca-BDE (right).	55
Figure 18:	Schematic diagram of continuous pyrolysis plant for a pyrolysis of ABS-Br and HIPS-Br [Miskolczi et al. 2008].	59

Figure 19:	Concentration of Br (left) and Sb (right) in char as well as light, middle, and heavy oil distillates from pyrolysis of HIPS-Br at temperatures between 360 and 440 °C [Miskolczi et al. 2008].....	59
Figure 20:	Chemical structures of PXDD, PXDF, and PXB.....	63
Figure 21:	Formation of 2,7-dibenzo- <i>p</i> -dioxin on the pyrolysis of 2,4-dibromophenol [Balabanovich et al. 2005b].....	65
Figure 22:	Formation of tribromodibenzofuran on the pyrolysis of 2,4-dibromophenol [Balabanovich et al. 2005b].....	65
Figure 23:	Yields of PBDF from pyrolysis of PBT + 7 wt.-% deca-BDE and 7 wt.-% Sb ₂ O ₃ (primary ordinate) and from pyrolysis of deca-BDE (secondary ordinate) (in wt.-%). Second named yields are shown in reverse order (own diagram based on [Dumler et al. 1989]).....	66
Figure 24:	Reductive debromination of Br containing radicals by using PE or PP (RH) [Hornung et al. 2003].	71
Figure 25:	Amount of HCl fixed by different metal oxides in stoichiometric mixture at 300 °C (in wt.-%) (own diagram based on [Horikawa et al. 1999]).	76
Figure 26:	Ratio of trapped Cl at water trap for pyrolysis tests of PVC and different PVC-metal oxide mixtures at 400 and 800 °C (own diagram based on [Masuda et al. 2006]).....	78
Figure 27:	Friedel-Crafts chlorination of benzene with Cl ₂ with a Lewis acid (FeCl ₃) as catalyst [Holleman et al. 2007; Fels et al. 2016].	78
Figure 28:	Reaction scheme for the destruction of CCl ₂ XY (with X = H and Y = Cl for CHCl ₃ and X = Y = H for CHCl ₂) over La ₂ O ₃ in the presence of steam [van de Avert et al. 2004].	81
Figure 29:	Pyrolysis product yields from fast-pyrolysis of HIPS-Br at 460 °C in a fluidized bed reactor with and without adding CaO/Ca(OH) ₂ (in wt.-%) [Jung et al. 2012].....	81
Figure 30:	Bromination of different metals and metal oxides with TBBPA and TTDE over temperature (own diagram based on [Grabda et al. 2009; Grabda et al. 2010; Rzyman et al. 2010; Oleszczek et al. 2013a; Oleszczek et al. 2013b; Oleszczek et al. 2013c; Terakado et al. 2011]).....	83
Figure 31:	Experimental setup of the bench-scale pyrolysis plant.	100
Figure 32:	Sectional drawing of the polyolefin-reactor.	102
Figure 33:	TGA, DTG, and DSC of PP (HP 570 U natural); 5 K·min ⁻¹ ; argon.	106
Figure 34:	DSC of glass spheres; 20 K·min ⁻¹ ; air.	108
Figure 35:	Figures from SEM of coated glass spheres (magnification of 300 for figures 35a and 35b).	108
Figure 36:	System boundary, direct emissions, and credits in the case of treatment by pyrolysis.....	112
Figure 37:	System boundary, direct emissions, and credits in the case thermal treatment in MWI.	112
Figure 38:	Product systems “allocating” (at the top) and “subtracted-extending” (at the bottom).	113

Figure 39:	Earnings for sold power in accordance with [KWKG 2016].	122
Figure 40:	Particle size distribution of SR1.....	124
Figure 41:	TGA (solid line), DTG (dotted line), and DSC (dashed line) of SR1; 5 K·min ⁻¹ ; argon.....	127
Figure 42:	DTG and DSC of Ta Capacitors “SMD Yellow” and “SMD Black”; 5 K·min ⁻¹ ; argon.....	129
Figure 43:	TGA, DTG, and DSC of “LCD-Dark”; 5 K·min ⁻¹ ; argon.	130
Figure 44:	TGA, DTG, and DSC of PVC; 5 K·min ⁻¹ ; argon.	131
Figure 45:	Product allocation from tests with SR1 as feedstock (in wt.-%).	133
Figure 46:	Results of significance tests regarding product allocation.....	138
Figure 47:	Results of significance tests regarding pyrolysis solid products.	139
Figure 48:	Results of significance tests regarding pyrolysis liquid products (filtered).	140
Figure 49:	Results of significance tests regarding pyrolysis gases.	141
Figure 50:	Yields of waxes, unfiltered, and filtered liquid product over temperature.	143
Figure 51:	Ignition loss and content of H of pyrolysis solid products over temperature.	143
Figure 52:	TAN value, Ratio of C/H, as well as contents of N and H ₂ O of filtered liquid pyrolysis products over temperature.....	144
Figure 53:	Contents of H ₂ corr, CO, CO ₂ , and C _x H _y in pyrolysis gases over temperature.	145
Figure 54:	LHV (wt), HHV (wt), and (relative) density of pyrolysis gases over temperature.	145
Figure 55:	Pyrolysis temperature and pressure during test “low heating rate”.	148
Figure 56:	Product allocation from pyrolysis test “low heating rate” and the average values for tests at 550 °C and 60 min.....	148
Figure 57:	Sums of PXDD/F according to GGVSEB / ChemVerbotsV of feedstock SR1, solid products from conventional tests, as well as from a test with a low heating rate.	149
Figure 58:	Sums of PXDD/F in different pyrolysis liquid products, according to GGVSEB / ChemVerbotsV.	150
Figure 59:	Allocation of C, H, N, and S from pyrolysis at 650 °C for 30 min with PO-reactor based on analyses using Vario MACRO Cube elemental analyzer.	152
Figure 60:	Degrees of enrichment for metals in pyrolysis solid products, filtration residue, and filtered liquid product; calculations based on ICP-MS/OES analyses.....	154
Figure 61:	Degrees of enrichment for non-metals, P, and halogens in pyrolysis solid products, filtration residue, and filtered liquid product; calculation of C, H, N, and S based on analyses using Vario MACRO Cube elemental analyzer, of P by ICP-MS/OES, of Br and Cl by ion chromatography.....	155

Figure 62:	Allocation of metals, halogens, and P with <99 wt.-% allocation to solid product from pyrolysis at 650 °C for 30 min with PO-reactor. Analyses were conducted using EDXRF with C, H, N given and O as missing component.....	156
Figure 63:	Enrichments of halogens and selected metals in pyrolysis solid products relative to those at 450 °C (residence time 30 min); black line = enrichment due to decreased solid products yields (in %). Analyses were conducted using EDXRF with C, H, N, and S given.....	157
Figure 64:	Allocations of Critical Metals from pyrolysis solid product to sieve fractions. Analyses were conducted using EDXRF with C, H, N given and O as missing component.....	158
Figure 65:	Allocations of metals, which are applicable for a recycling in an integrated copper smelter, from pyrolysis solid product to sieve fractions. Analyses were conducted using EDXRF with C, H, N given and O as missing component.....	159
Figure 66:	Degree of enrichment vs. MP of metal chlorides (left) and BP of metal bromides (right).	160
Figure 67:	Content of halogens in pyrolysis liquid products from pyrolysis tests (650 °C, 30 min) with and without PP+La, and halogen-filter (H.F.) (in wt.-%). Analyses were conducted using EDXRF with C, H, N given and O as missing component.	163
Figure 68:	Distillation ranges of pyrolysis liquid products from tests with SR1 and with SR1 with polyolefin-reactor and halogen-filter (SR1 + PP+1.5 + H.F.) in comparison to those of conventional fuels (modified according to [Luo et al. 2016]).	164
Figure 69:	Allocation of Ta, Ag, Mn, and Si to sieve fraction >500 and <500 µm from different pyrolysis tests with Ta capacitors "SMD Yellow" as feedstock. Analyses were conducted using EDXRF with C, H, N, S given and O as missing component.....	166
Figure 70:	Main components of Ta capacitors "SMD yellow", solid products <500, and >500 µm from pyrolysis test at 550 °C, 30 min (in wt.-%). Analyses were conducted using EDXRF with C, H, N, S given and O as missing component.....	167
Figure 71:	Product allocation from pyrolysis tests with LCD (in wt.-%). Analyses were conducted using EDXRF with C, H, O as missing components.....	168
Figure 72:	Allocation of Ga, As, In, and Sn to pyrolysis solid and liquid products as well as NaOH (precipitated and in solution) from different pyrolysis tests with LCD and PVC as feedstocks (in wt.-%). Analyses were conducted using EDXRF with C, H, O as missing components.....	169
Figure 73:	LCA-Results in impact categories ADP, AADP, AP, Areatime, Energy, EP, GWP, ODP, and POCP for a treatment of 1 Mg shredder residues.....	171
Figure 74:	Results of sensitivity analysis from ecological assessment expressed as dimensionless factor between balances of pyrolysis and MWI.	173

Figure 75:	Performance figures for scenario I (in 1 000 €·y ⁻¹).....	173
Figure 76:	Performance figures for scenario II (in 1 000 €·y ⁻¹).	174
Figure 77:	Performance figures for scenario III (in 1 000 €·y ⁻¹).	174
Figure 78:	Cumulative cash-flows of all scenarios (in 1 000 €·y ⁻¹).	175
Figure 79:	Net present value (NPV) of all scenarios (in 1 000 €·y ⁻¹).....	175
Figure 80:	Results of sensitivity analysis from economical assessment as relative change of IRR (in %).	176
Figure 81:	DTG curves of SR1 (solid line) and selected polymers (dotted, dashed lines); 5 K·min ⁻¹ ; argon.....	179
Figure 82:	Energy-flow diagram for a pyrolysis-test with SR1 + PP+La4.5 + H.F. (650 °C; 30 min).....	180
Figure 83:	PBDF concentrations in feedstock plus solid and liquid products from pyrolysis at 650 °C, 60 min (in µg·kg ⁻¹).....	182
Figure 84:	Formation pathways of PBDF during thermal degradation of deca-BDE (modified according to [Weber, Kuch 2003]).	183
Figure 85:	Expected reaction schemes for halogenation and dehalogenation of aromatic compounds using LaOOH in the presence of steam.....	185
Figure 86:	CAD drawing of a pyrolysis pilot plant for 70 kg shredder residues per hour [Kautz 2016].....	198
Figure 87:	Different capacitor types: THT blue, yellow disks; THT green drops; THT orange, yellow drops; SMD brown; SMD black; SMD yellow; SMD orange.	231
Figure 88:	Pyrolysis bench-scale reactor.	232
Figure 89:	Bottom of pyrolysis bench-scale reactor.....	233
Figure 90:	Polyolefin-reactor (based on [Hornung 1997]).	233
Figure 91:	Spectra for EDXRF analysis from La coated glass spheres, spectrum from Figure 35a.	234
Figure 92:	Spectra for EDXRF analysis from La coated glass spheres, spectrum from Figure 35b.	234
Figure 93:	XRD pattern of spheres from absorption tests with Br ₂ at 450 °C (%-values after normalization).	235
Figure 94:	GC-MS Chromatogram of pyrolysis liquid product (450 °C, 30 min). ...	246
Figure 95:	GC-MS Chromatogram of pyrolysis liquid product (550 °C, 30 min). ...	246
Figure 96:	GC-MS Chromatogram of pyrolysis liquid product (650 °C, 30 min). ...	247
Figure 97:	GC-MS Chromatogram of pyrolysis liquid product (650 °C, 30 min, PP, H.F.).	249
Figure 98:	GC-MS Chromatogram of pyrolysis liquid product (650 °C, 30 min, PP+La1.5, H.F.).	249
Figure 99:	GC-MS Chromatogram of pyrolysis liquid product (650 °C, 30 min, PP+La4.5, H.F.).	250
Figure 100:	XRD pattern of pyrolysis sieve fraction <63 µm from pyrolysis tests with SR1 (650 °C, 30 min) regarding S compounds (%-values after normalization).....	251

Figure 101: XRD pattern of fine fraction (<500 μm) from pyrolysis tests with Ta capacitors (550 $^{\circ}\text{C}$, 30 min) regarding Mn oxides (%-values after normalization).....	252
--	-----

List of tables

Table 1:	Minima, maxima, and total amount of WEEE treated in another member state or outside the EU than in IT, D, and the EU-28 [Eurostat 2016].....	37
Table 2:	Material and thermal recovery paths as well as disposal for fractions from WEEE treatment [VDI 2014].	38
Table 3:	Maximum concentration of different metals in Al cast alloys [VDI 2012].	43
Table 4:	Content of metals in LCD panels of different electronic devices (in mg·kg ⁻¹) [Savvilotidou et al. 2014].....	47
Table 5:	Values of activation energy E and frequency factor A for first and second stage of PVC decomposition as well as full decomposition [Gupta, Viswanath 1998; Sivalingam et al. 2003].....	75
Table 6:	Nature of metal chlorides formed during co-pyrolysis of PVC and metal oxides [Gupta, Viswanath 1998].....	76
Table 7:	Activation energy E_a and its temperature ranges of different REO.....	79
Table 8:	Effects and feasible opportunities of varied parameters during pyrolysis.	86
Table 9:	Concentrations of As, Ga, In, and Sn in both tested LCD layers (in mg·kg ⁻¹).....	91
Table 10:	Concentrations of selected metals in different capacitors (shortly Cap.) (in wt.-%).....	92
Table 11:	Sample weight and weighting accuracy for quantification of TAN	94
Table 12:	EDXRF results from La coated glass spheres, spectrum from Figure 35a.	109
Table 13:	EDXRF results from La coated glass spheres, spectrum from Figure 35b.	109
Table 14:	Yields of precipitated and dried AgBr and corresponding efficiencies from test runs with Br ₂ and HBr at 300, 450, and 600 °C.....	111
Table 15:	Impact categories used for environmental impact assessment.	114
Table 16:	Determined transport distances for the ecological assessment (in km)..	115
Table 17:	Investment costs for a pyrolysis pilot plant (in €).	120
Table 18:	Calculation of labor costs for different admin labor, technical supervisor, and operational labor (in €·h ⁻¹).	121
Table 19:	Variable costs of operating materials, disposal, transports, and energy.	122
Table 20:	Basic characteristics of SR1.....	124
Table 21:	Content of nonmetals and metalloids in SR1.	125
Table 22:	Content of metals in SR1 (determination by EDXRF and ICP-MS/-OES).	126
Table 23:	Basic characteristics of Ta capacitors.....	127
Table 24:	Content of C, H, and S in “SMD Yellow” and “SMD Black” determined with Vario MACRO Cube elemental analyzer.....	127
Table 25:	Elemental Composition of “SMD Yellow” and “SMD Black” Ta Capacitors based on EDRXF (in wt.-%).	128
Table 26:	Basic characteristics and contents of C, H, and S of LCD-Dark.	129

Table 27:	Metals, metalloids, and non-metals found in LCD-Dark based on EDXRF* (in mg·kg ⁻¹).	130
Table 28:	Metals, metalloids, and halogens found in PVC based on EDXRF* (in mg·kg ⁻¹).	130
Table 29:	Number of conducted test runs with SR1.	132
Table 30:	Quality of pyrolysis solid products from tests with SR1 as feedstock.	134
Table 31:	Quality of pyrolysis liquids products (filtered) from tests with SR1 as feedstock.	135
Table 32:	Quality of pyrolysis gases from tests with SR1 as feedstock.	136
Table 33:	Pairs of values for significance tests.	137
Table 34:	PXDD/F concentration in SR1 as well as six different pyrolysis solid products (in µg·kg ⁻¹).	147
Table 35:	PXDD/F concentrations in four different pyrolysis liquid products (in µg·kg ⁻¹).	151
Table 36:	Content of metals, P (determination by ICP-MS/OES ^{1,2}), Br, and Cl (determination by ion chromatography ³) in products from pyrolysis at 650 °C for 30 min with SR1 as feedstock.	153
Table 37:	Terms of logarithmic regression lines for filtration residues, and filtered liquid product with halides, metals, and oxides (determination of metal concentrations were conducted by ICP-MS/OES).	160
Table 38:	Relative abundances and origins of compounds detected in pyrolysis liquid products from tests at 450, 550, and 650 °C (residence time 30 min) by GC-MS.	161
Table 39:	Semi-quantitative changes of compounds in pyrolysis liquid products due to addition of PP and La.	162
Table 40:	Parameters of pyrolysis liquid products regarding energetic utilization.	164
Table 41:	Yields and Properties of pyrolysis products for the ecological assessment.	169
Table 42:	Amount of metals recycled from pyrolysis solid products and filtration residue in copper smelter processes.	170
Table 43:	Content of Al, Cu, and Fe in bottom ash >2 mm and those amounts as well as recovered amounts in bottom ash >2 mm.	170
Table 44:	Internal rates of return (IRR , in %) and paypack periods (in years) of the economical assessment in the different scenarios (Sc).	176
Table 45:	PXDF concentrations in pyrolysis solid and liquid products (in µg·kg ⁻¹). ..	182
Table 46:	Comparison between pyrolysis liquid products, fuel E5 and diesel fuel.	189
Table 47:	Internal rates of return (IRR , in %) with and without earnings for the sale of heat in the different scenarios (Sc).	195
Table 48:	List of all sums of PXDD/F and corresponding congeners according to the German act on restriction of chemicals (GGVSEB) and German chemicals prohibition ordinance (ChemVerbotsV).	234
Table 49:	Product allocation from tests with SR1 as feedstock.	236

Table 50:	Results of significance tests regarding product allocation with values <0.05.	237
Table 51:	Results of significance tests regarding quality of solid products with values <0.05.	237
Table 52:	Results of significance tests regarding quality of liquid products with values <0.05.	238
Table 53:	Results of significance tests regarding quality of gaseous products with values <0.05.	238
Table 54:	Results of chi-squared test HHV (in MJ·kg ⁻¹) versus H _{2corr} (in vol.-%).....	239
Table 55:	Results of chi-squared test HHV (in MJ·kg ⁻¹) versus CO (in vol.-%).....	239
Table 56:	Results of chi-squared test HHV (in MJ·kg ⁻¹) versus CO ₂ (in vol.-%).	239
Table 57:	Results of chi-squared test HHV (in MJ·kg ⁻¹) versus C _x H _y (in vol.-%).	239
Table 58:	Dataset about concentrations of PCDD/F in feedstock and pyrolysis solid products.	240
Table 59:	Dataset about concentrations of PBDD/F in feedstock and pyrolysis solid products.	241
Table 60:	Dataset about concentrations of PXDD/F in feedstock and pyrolysis liquid products.	242
Table 61:	Allocation of metals, halogens, and P from pyrolysis at 650 °C for 30 min with polyolefin-reactor (normalized, in wt.-%); analyses based on ICP-MS-/OES analyses.	243
Table 62:	Allocations of metals, Br, Cl, P, and S from pyrolysis solid product to sieve fractions (Pyrolysis at 650 °C for 30 min with polyolefin-reactor, normalized, in wt.-%); analyses based on EDXRF with C, H, N given and O as missing component.	244
Table 63:	Retention times and absolute abundances of compounds in pyrolysis liquid products from different pyrolysis temperatures, detected by GC-MS....	245
Table 64:	Retention times and absolute abundances of compounds in pyrolysis liquid products from pyrolysis tests with polyolefin-reactor, detected by GC-MS.	248
Table 65:	Degree of enrichment of metals found in filtration residue and filtered liquids from pyrolysis tests (650 °C, 30 min, polyolefin-reactor with PP+La1.5) with corresponding melting and boiling points of metals, its oxides and halides (in °C) determined using ICP-MS-/OES [DGUV 2016; Holleman et al. 2007; Perry, Phillips 1995].	253

1. Introduction

The raw material supply of many industrial nations (e.g. in the European Union (EU)) is vulnerable due to fading geogenic resources, export restrictions, and political conflicts in countries of exploration. In order to enable a continuous and sustainable supply, the recovery of raw materials from secondary resources offers promising potential. Waste Electrical and Electronic Equipment (WEEE) is a source of various metals and polymers, but also includes hazardous substances. It has become one of the fastest growing waste streams in the world, especially in industrial nations. As an example, the amount of officially collected small household appliances (SHA) in EU-27 countries¹ has been more than doubled from roughly 123 800 to 294 300 Mg between 2007 and 2014 [Eurostat 2017].

Following state-of-the-art processing technologies, collected WEEE gets dismantled and processed in a number of different treatment steps in order to depollute the devices and to recover valuable fractions such as metals or plastics. However, in spite of best techniques available, every WEEE treatment discharges an amount of waste as residual fractions, mainly shredder residues, which are either incinerated or landfilled. Thus, remaining metals are marginally or not at all extracted and in the case of incineration, only small amounts of energy are recovered. In contrast, a thermo-chemical treatment of shredder residues could enable a concentration of metals, which is high enough to recycle these metals in existing pyro- and hydrometallurgical processes.

In addition to base metals and plastics, WEEE contains a number of so called “Critical Metals”. These metals are part of a list of 14 Critical Raw Materials, which were defined by the EU in 2010. This list was actualized in 2014 and contains 20 elements and materials (eleven metals, three metal groups as well as six minerals/others) (Figure 1). For this ranking, the economic importance and the supply risk was analyzed for each material [EC 2014]. Many of the critical metals (e.g. Ga, Ge, or In) can be further characterized due to their low end of life recycling rates (EoL-RR), which are often below one percent [Bakas et al. 2014; Buchert et al. 2012; Graedel et al. 2011]. However, for the production of new electrical and electronic equipment (EEE) many critical metals, such as Ga, In, or Pd are indispensable.

¹ For calculations just officially collected amounts of WEEE from category 2 in EU-27 countries were taken into account without Italy, Spain, and Cyprus due to unreported amounts [Eurostat 2017].

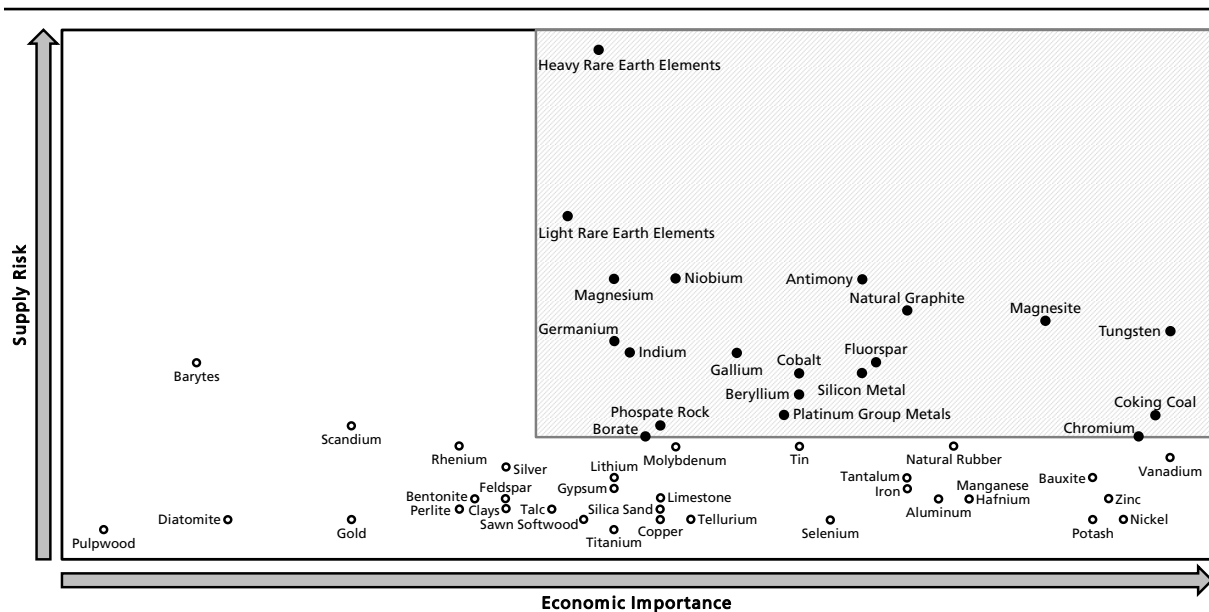


Figure 1: Ranking of raw materials with regard to supply risk and economic importance [EC 2014].

Two key reasons for the low EoL-RR are very small amounts of these metals in WEEE, which dissipate through the WEEE treatment processes, as well as the property of many critical metals to be chemically ignoble. As mentioned above, this characteristic is the main reason why a recycling in established pyrometallurgical processes is typically not possible due to thermodynamic restrictions.

In order to estimate the mass of elements, which get lost during different steps of WEEE recycling, Figure 2 shows the potential of some metals from IT and telecommunication equipment as well as their losses after collection, pre-treatment, and recycling [Buchert et al. 2012; Sander et al. 2012]. Shown metals can be clustered in three different groups, depending on (1) existing recycling, (2) full losses during recycling processes, or (3) during pre-treatment processes. However, even if recycling of metals such as Ag, Au, Co, or Pd exists, the recycling rates are only between 14.3 and 38.0 wt.-% for IT and telecommunication equipment. Besides losses during collection of WEEE, two of the main reasons for these low recycling rates are insufficient liberation and separation of metals [Reuter et al. 2013].

Considering this background information, processes such as pyrolysis with an oxygen free atmosphere and wide range of possible temperatures offer opportunities to separate valuable metals from organic matrixes, mainly plastics, to lower the amount of waste, depollute it, and to produce liquid and gaseous fuels at the same time. In a corresponding process chain, pyrolysis could be used in order to produce marketable concentrates of one or more scarce and critical metals, which could be delivered to specialized processes of pyro- and/or hydrometallurgical recycling.

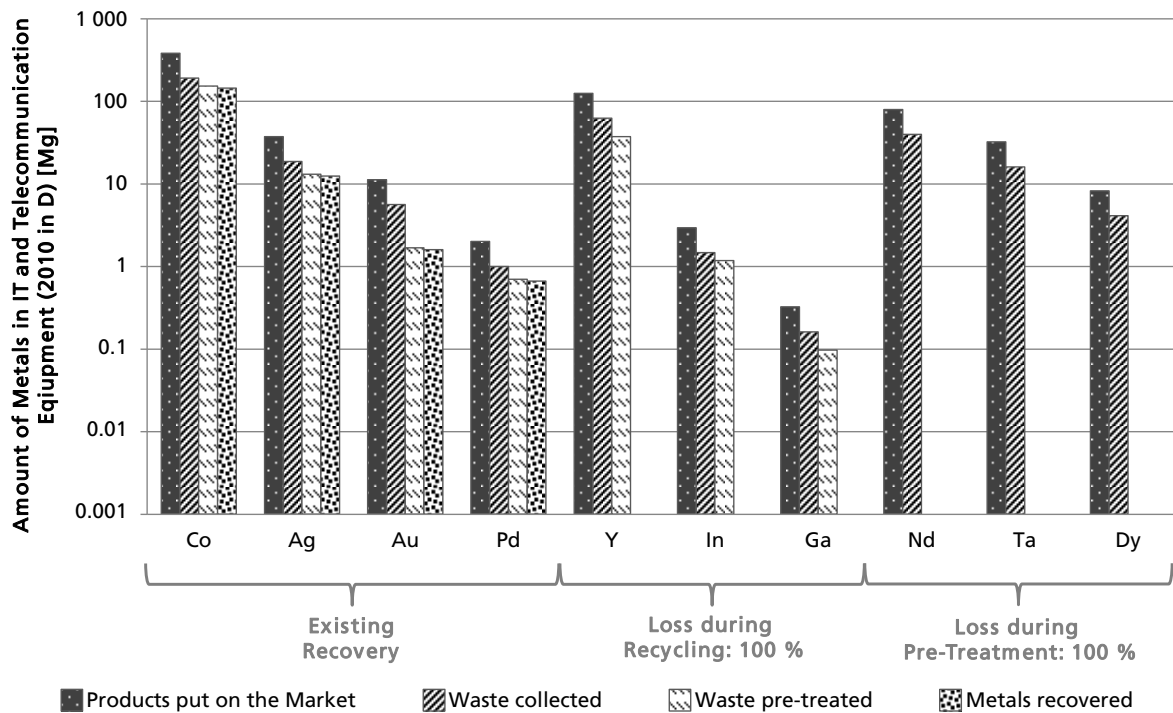


Figure 2: Amounts of products put on the market, waste collected, waste pre-treated, and metals recovered concerning selected metals from IT and telecommunication equipment 2010 in Germany (own diagram based on [Buchert et al. 2012; Sander et al. 2012]).

Pyrolysis is an endothermic, thermo-chemical process under absence of oxygen (air) at temperatures above those decomposition points of present (organic) material, which leads to the breaking of bonds and a formation of smaller molecules. In general, pyrolysis processes can be classified by temperature in low (<400 °C), medium (400 - 600 °C) and high temperature (>600 °C) processes. Besides temperature, further process conditions such as pressure, heating rate, or addition of catalysts can be varied. Additionally, depending on the aim of pyrolysis processes, different reactor types can be used. Most common types are extruders, screw conveyers, tubular reactors, stirred tank reactors, vertical or shaft reactors, fixed bed reactors, fluidized bed reactors, rotary kilns, and autoclaves [Buekens 2006]. With regard to formation of different products, usually pyrolysis processes can be divided in three different phases [Scholz et al. 2001]:

- 1) *Drying phase* at temperatures up to 200 °C, in which water vapor is the main product
- 2) *Carbonization* at temperatures between 200 and 500 °C. During this phase, mainly side groups become split off from higher-molecular substances, which lead to a formation of aromatic and aliphatic substances as well as tar and waxes. A solid pyrolysis product (char) is remaining.
- 3) *Gas formation phase* at temperatures above 500 °C in which products from the previous step get split further under formation of H₂, CO, CO₂, and CH₄.

Due to a huge number of different components and materials used for the production of EEE, pyrolysis of WEEE as well as the purposed extraction of metals, depollution, and (energetic) utilization of pyrolysis products is more complex compared to these basic phases of single polymers or plastics. Additionally, during pyrolysis of WEEE many chemical reactions between present educts and intermediate products take place. Commonly, plastics used in EEE contain brominated flame retardants (BFR), which can cause formations of caustic and toxic emissions such as HBr, brominated dioxins, or furans during thermal treatment. In this context, key procedural challenges for such a pyrolysis process are avoidance of toxic emissions and generation of products with low contents of halogens (dehalogenation), as well as preparation and accumulation of metals for downstream recycling processes. For environmental and economic reasons, an efficient energetic utilization of formed liquid and gaseous fractions should be considered besides an effective depollution.

With regard to already existing research on pyrolysis of different fractions from WEEE, many publications outline thermo-chemical treatment of brominated plastics (c.f. [Hall, Williams 2007a]), selected components such as printed wiring boards (PWB) (c.f. [Hall, Williams 2007b]), or small devices such as mobile phones (c.f. [Moltó et al. 2009]). Additionally, different studies outline the influence of metals and metal containing compounds on these reactions (c.f. [Bhaskar et al. 2003a]). With regard to different household and industrial wastes, information is given even for industrial scale plants [Quicker et al. 2014]. As an example, designed as pretreatment step for the utilization of a waste mixture out of a number of different household and industrial wastes, the so called "ConTherm" process was installed as part of a conventional, hard coal fired power plant in Hamm, Germany. This plant consisted out of two rotary pyrolysis kilns, each with an annual throughput of 50 000 Mg·a⁻¹ in which about 13.3 Mg waste per hour were pyrolyzed at 500 °C [Reinhardt, Richers 2004]. However, information on pyrolysis of residual fractions from WEEE treatment is limited. Along with this lack of information, information pertaining to critical metals from WEEE is limited, as well.

2. Motivation and objectives of the thesis

The purpose of this work is to develop and to optimize a thermo-chemical process for different fractions from Waste Electrical and Electronic Equipment (WEEE) in order to enable downstream metal recycling. Therefore, a bench-scaled plant will be designed and tested. Due to a very heterogeneous composition of WEEE and a number of partly toxic and carcinogenic compounds in the materials, the development of such a process brings up different challenges.

Therefore, a thermo-chemical process for two different fraction groups from WEEE, namely shredder residues and fractions containing scarce and critical metals, should be developed, tested, and optimized in a new designed bench-scale plant. In the bench-scale plant, optimal adjustments of the main parameters of temperature and residence time for designing a continuous plant should be identified by varying these parameters and evaluating the impacts on pyrolysis products using statistical methods. To achieve these objectives, a series of tests will be conducted with a shredder residue from a common WEEE treatment plant. Additionally, options for an optimization of mentioned parameters should be discussed, which increase either the possibility for a recycling of metals in (pyro-)metallurgical processes or the revenues for such a recycling. Amongst others, allocations of metals to different pyrolysis products will be investigated and analyzes about quality and quantity of different metals and compounds conducted in order to select recycling options accordingly. In order to find optimal utilization options for pyrolysis liquid and gaseous by-products, analyzes of properties with regard to an energetic utilization will be conducted, as well. Due to feasible formations of highly-toxic polyhalogenated aromatic compounds, a number of analyzes using high-resolution gas chromatography/mass spectrometry (HR GC-MS) will be conducted as well as solutions for dehalogenation and corresponding depollution developed.

With regard to scarce and critical metals, the efficiency of liberation and concentration of such metals from two different fractions containing Ga, In, and/or Ta will be tested. On the one hand, the thesis should present first results of corresponding pyrolysis tests in order to check if pyrolysis treatment offers clear advantageous for a recycling chain of these metals from WEEE; on the other hand, mainly with regard to Ga and In, different types of extraction via pyrolysis should be tested and assessed.

In order to evaluate environmental benefits and the loads of a technological approach regarding treatment of shredder residues, an ecological assessment following DIN EN ISO 14040/14044 will be conducted. Within this assessment, treatment via pyrolysis will be compared with an energetic utilization in an incineration plant (status quo) following a holistic approach. In addition, an economical assessment will be calculated for a continuous pilot plant in order to detect strengths and weaknesses for designing a continuous plant in an industrial plant scale.

3. Current state of WEEE-handling in Europe

3.1 Legal framework of WEEE-handling

In 2002, two directives were set into force by the European Union (EU) concerning Waste Electrical and Electronic Equipment (WEEE). In order to protect the environment and human health, restrictions for the use of harmful substances in Electrical and Electronic Equipment (EEE) as well as for the management and treatment of WEEE were defined. Both, directive 2002/96/EC on WEEE [EU 2003a] and directive 2002/95/EC on “the restriction of the use of certain hazardous substances in electrical and electronic equipment” (RoHS) [EU 2003b] have been updated to the present time.

By directive 2012/19/EU, the EU defined purposes concerning the product design of EEE and the collection, re-use, treatment, disposal, shipment, and recovery of WEEE as well as the financing of it. Actually, there are ten categories of EEE defined during a transitional period in effect until August 14th 2018 and six after that date. The different categories in connection with minimum targets for WEEE, which shall be recovered or be prepared for re-use and recycling for the time till August 14th 2018 and afterwards, can be found in [EU 2012]. Actually, the different rates vary between 75 and 85 wt.-% for recovery and 55 and 80 wt.-% for re-use and recycling.

Directive 2011/65/EU [EU 2011] concerns restrictions for use of hazardous substances in EEE. In this directive, a maximum concentration is defined for Pb, Hg, hexavalent Cr, polybrominated biphenyls (PBB), and polybrominated diphenyl ethers (PBDE) of about 0.1 wt.-% as well as for Cd of 0.01 wt.-%. The polybrominated compounds PBBs and PBDEs have been used as flame retardants, which are compounds of polymers for EEE. From July 2019, further restrictions of maximum 0.1 wt.-% will be in force for the four phthalates di-(2-ethylhexyl)-phthalate (DEHP), butylbenzylphthalate (BBP), dibutylphthalate (DBP), and diisobutylphthalate (DIBP) [EU 2015]. However, exceptions for these limit values are defined e.g. on Hg in lamps or Pb in medical devices and monitoring instruments.

3.2 Quality and quantity of WEEE in Europe

Driven by the huge number of different applications of EEE, heterogeneity of WEEE composition is very high. From literature, compositions of different selected EEE are known, however, often limited to main materials glass, plastics, Fe, Cu, and Al (e.g. [Goosey 2012; Reuter et al. 2013]). Based on data by [Eurostat 2016; Haig et al. 2012; Hense et al. 2015a; Jofre, Morioka 2005; Reuter et al. 2013], an average composition of WEEE was calculated (Figure 3). Besides base metals like Fe, Al, and Cu, WEEE mainly consists of different plastics like acrylonitrile-butadiene-styrene (ABS), polystyrene (PS), polypropylene (PP), polycarbonate-ABS (PCABS), polyethylene (PE), polyvinyl chloride (PVC), styrene acrylonitrile (SAN), polycarbonate (PC), or ethylene-propylene-diene

monomer (EPDM). Selected parts of WEEE, such as TV or monitor housings, are commonly made out of a much smaller number of plastics. However, as shown by [Schlummer et al. 2007], such plastics are often compounds of mixed plastics like PPO-PS, PVC-ABS, or PC-ABS and/or they contain flame retardants, which makes a straight separation and recycling complex or impractical.

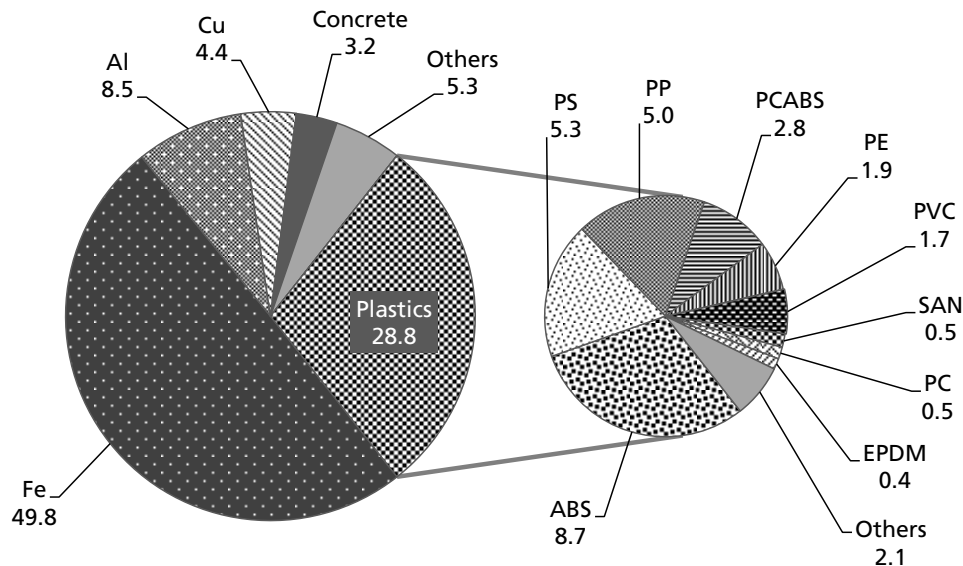


Figure 3: Calculated average composition* of WEEE in EU-28 (2013) for categories 1, 2, 3, 4, 6, and 7 (in wt.-%) (own diagram based on [Eurostat 2016; Haig et al. 2012; Jofre, Morioka 2005; Reuter et al. 2013]).

*Composition without categories 5, 8, 9, 10; composition stands for 97.1 wt.-% of all WEEE collected.

In addition to these main components, WEEE contains a number of precious and critical metals; however, compared to entire EEE, more detailed compositions are available almost for selected components, mainly printed wiring boards (PWB) (e.g. in [Blaser et al. 2011; Chancerel et al. 2009; Maurell-Lopez 2012; Moltó et al. 2009; Morf, Taverna 2004; Reuter et al. 2013; Sander et al. 2012; Williams 2010]). In Figure 4, the content of critical metals in PWB of selected EEE is shown as well as the calculated mass of such metals for the whole corresponding device (content of metals just from PWB) [Blaser et al. 2011]. Mainly due to high concentrations of platinum group metals (PGM) in addition to Cu, Ag, and Au, devices such as laptops and personal computers get dismantled in order to separate PWB for a pyrometallurgical recycling. In the case of mobile phones, which are usually separately collected, devices are commonly treated directly in such recycling processes. In contrast, small EEE such as video or digital cameras do not get dismantled manually, but crushed directly (c.f. chapter 3.3.1). Thus, a separation of PWB is difficult and often incomplete, which leads to allocation of many metals to non-adequate fractions such as plastics or residual fractions.

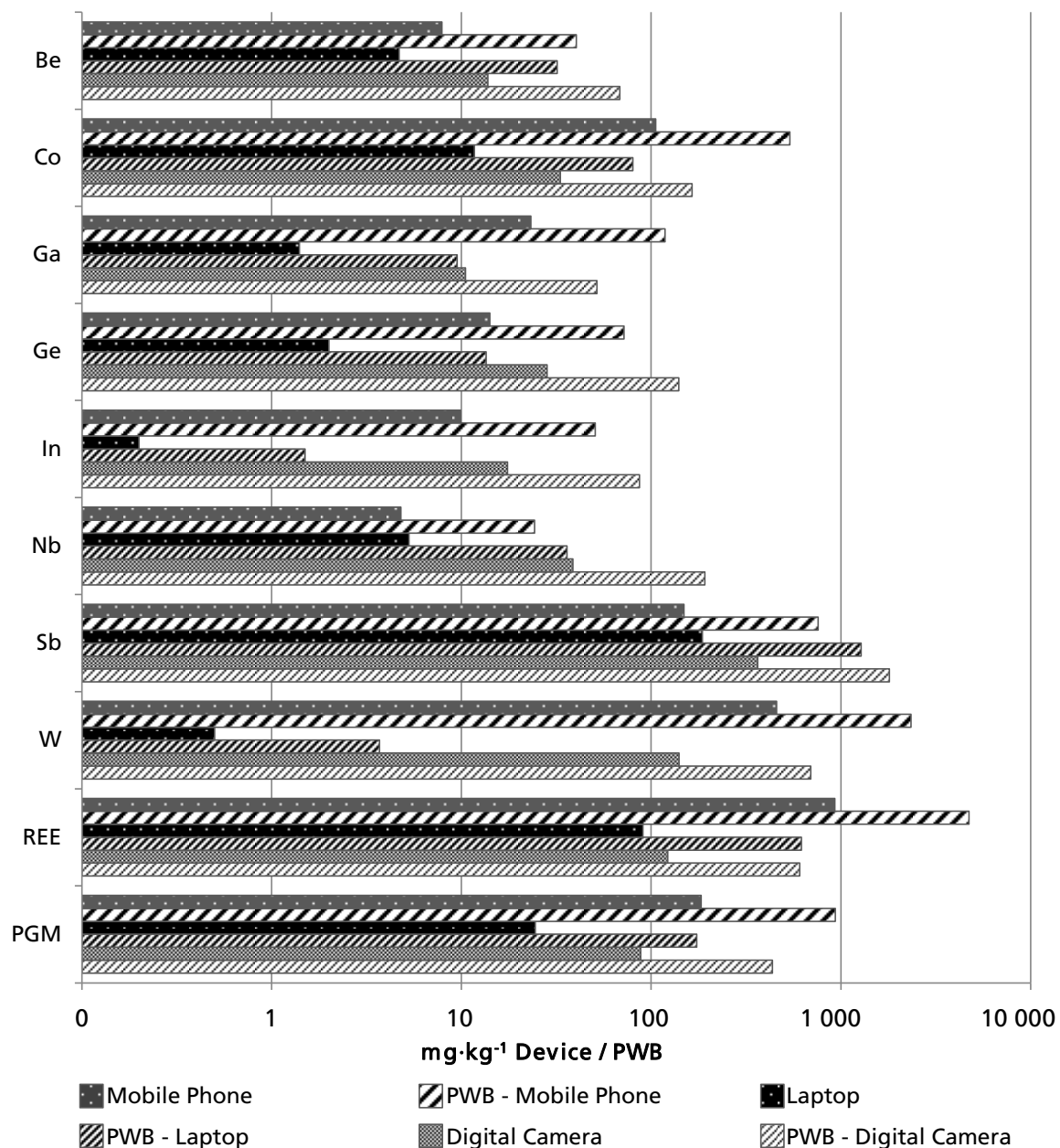


Figure 4: Content of Critical Metals in selected EEE (from PWB) and corresponding PWB separately (own diagram based on [Blaser et al. 2011]).

Besides clean plastics and metals, there are also components that cause problems in recycling processes. In this regard, mainly plastics containing heavy metals such as Cd, Cr, Pb, Sb, and Zn, as well as those containing flame retardants should be noted. Flame retardants for the production of EEE can be clustered in four groups [LAGA 2009]:

- halogenated organic compounds,
- inorganic compounds,
- halogen-free organic compounds based on phosphor, and
- halogenated organic compounds based on phosphor.

Generally, about one quarter of plastics from WEEE contain flame retardants [Eionet 2013], of which one third are based on halogens [EFRA 2007]. However, the amount of halogens in plastic fractions from WEEE could reach up to 10.9 wt.-% Br [Hall, Williams 2008] and 57.8 wt.-% Cl [Ma et al. 2002]. Since the use of selected brominated substances as flame retardants, namely PBB and PBDE, is restricted in EU countries by RoHS directive [EU 2011], alternative materials, mainly phosphorous- or nitrogen-based, have been developed. However, the production of halogenated flame retardants is still increasing due to an increasing total amount of plastics. Most are combined with phosphoric esters, inorganic compounds like aluminum or magnesium hydroxide ($\text{Al}(\text{OH})_3$, $\text{Mg}(\text{OH})_2$) and antimony compounds like antimony trioxide (Sb_2O_3), pentoxide (Sb_2O_5) or sodium antimonite (NaSbO_3) [Dettmer 2011]. For example, the amount of Sb in brominated acrylonitrile butadiene styrene (ABS) and high-impact polystyrene (HIPS) could reach between 3.2 wt.-% and 4.6 wt.-%, respectively [Hall et al. 2008].

In Italy and Germany, WEEE get collected in five (Italy) and six (Germany) collection groups. The compositions of these groups are different in both countries (c.f. Figure 5). WEEE categories 1, 2, 3, and 4 represent those categories with the highest amounts of collected WEEE, and stood for about 98.5 wt.-%, 92.2 wt.-% and 93.9 wt.-% of total WEEE in 2013 in Italy, Germany, and the EU-28, respectively (c.f. Figure 7) [CDC RAEE 2014; Eurostat 2016; Magalini et al. 2012].

In the year 2013, the total amount of WEEE collected in the EU-27 reached nearly 3.5 Mio. Mg. The amount of collected WEEE increased between 2008 and 2013 with up to 9.1 wt.-% per year (2008 - 2009); however, in 2012 the amount decreased by 2.2 wt.-% (Figure 6). The highest annual rate of growth (31.8 wt.-% in 2009) as well as the highest rate over the full period between 2008 and 2013 (51.7 wt.-%) was found for electrical and electronic tools (category 6). Additionally, high rates of growth in that time period were found for categories 4 (46.7 wt.-%), 10 (35.1 wt.-%), 2 (29.5 wt.-%), and 3 (17.9 wt.-%) [Eurostat, 2016].

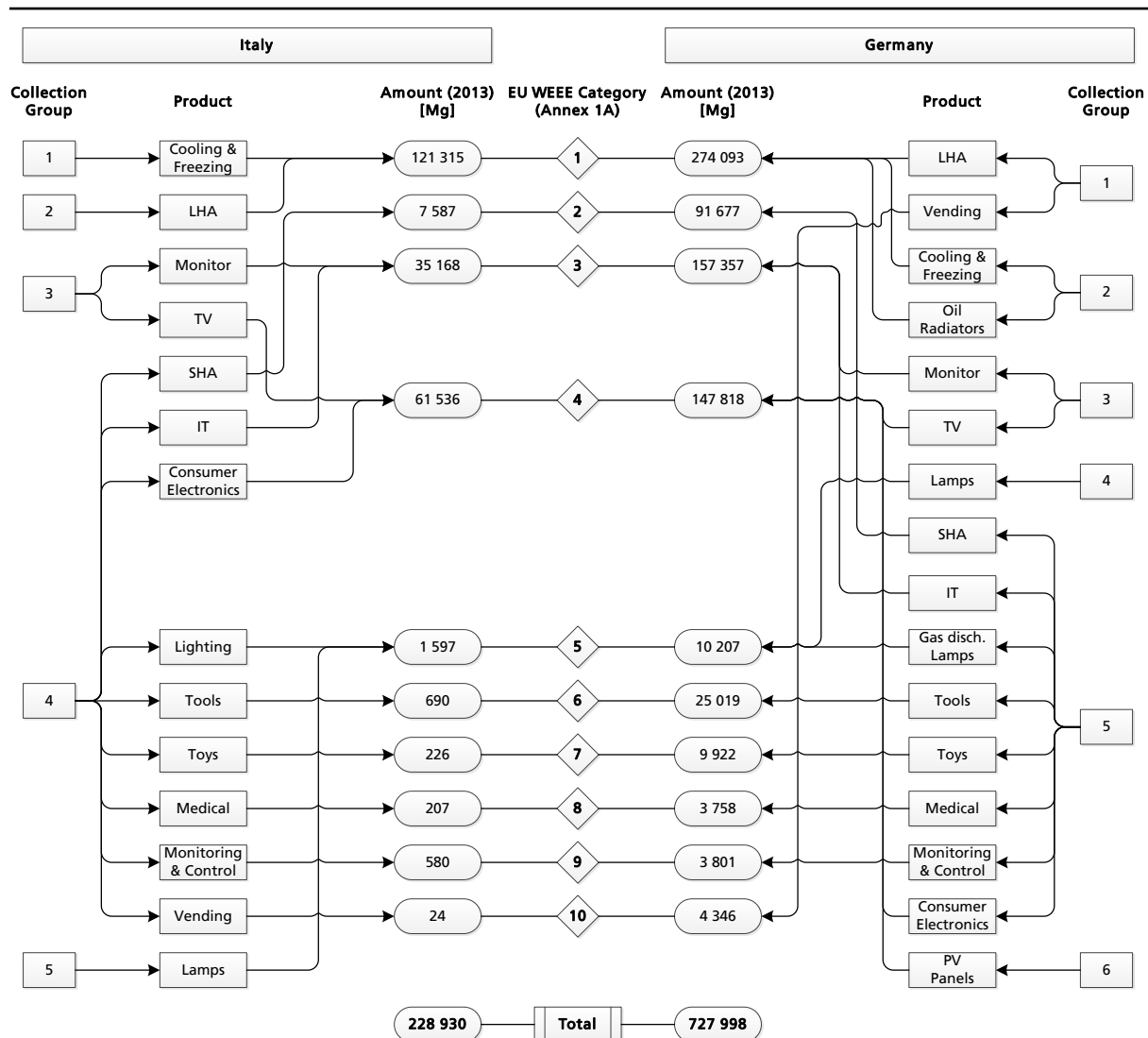


Figure 5: Collection groups in Italy and Germany in combination with the corresponding WEEE categories and those amounts (own diagram based on [CDC RAEE 2014; Eurostat 2016; Magalini et al. 2012]).

SHA: small household appliances, LHA: large household appliances, Gas disch. Lamps: gas discharge lamps; IT: information technology and telecommunications equipment; Medicals: medical devices; Monitoring & Control: monitoring and control instruments; Tools: electrical and electronic tools; Toys: toys, leisure and sports equipment; Vending: automatic dispensers; PV panels: photovoltaic panels.

The main amount of collected WEEE gets treated in that country, where it was collected; however, significant amounts are also exported and treated in other member states of the EU. Between 2007 and 2012, annual amounts of up to 175 135 Mg were officially treated in another member state of the EU related to the country of collection. Additionally, in total, 568 783 Mg were treated outside the EU-28 during this period of time (Table 1). However, the informal sector concerning collection, transport, export, and treatment of WEEE is very strong as reported by [Huisman et al. 2015]. As shown in Figure 8, just about 3.3 Mio. Mg (34.9 wt.-%) of all WEEE (9.45 Mio. Mg) generated in the EU-28 in 2012 was officially collected. Additional 0.75 Mio. Mg (7.9 wt.-%) end up in residual waste fractions plus 2.2 Mio. Mg (23.2 wt.-%) which are collected and recycled non-compliant. Concerning the remaining 3.2 Mio. Mg ("Gap"), there is a lack of information. Mainly based on estimations, the authors calculated that there are

mainly additional non-compliant collection and recycling activities (0.95 Mio. Mg, 10.1 wt.-%) as well as different undocumented exports (1.3 Mio. Mg in sum, 13.8 wt.-%) of WEEE and used Electrical and Electronic Equipment (UEEE).

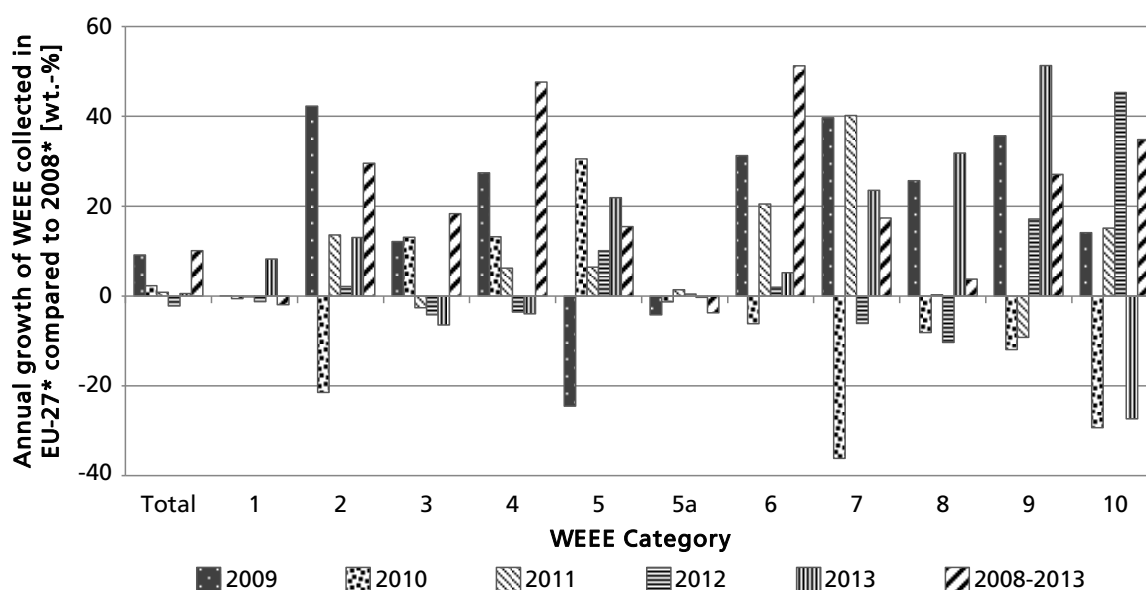


Figure 6: Annual growth for 2009 till 2013 and total growth between 2008 and 2013 of WEEE collected in EU-27* (own diagram based on [CDC RAEE 2008; 2009; 2010; 2011; 2013; 2014; Eurostat 2016]).

*All data without Rumania; category 5a without Italy and Portugal due to missing data.

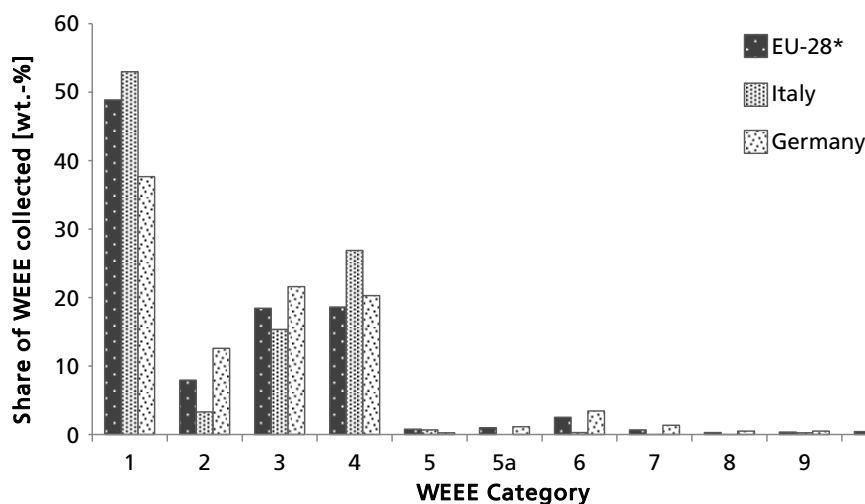


Figure 7: Share of WEEE collected in the different WEEE categories in EU-28*, Italy, and Germany for 2013 (own diagram based on [CDC RAEE 2008; 2009; 2010; 2011; 2013; 2014; Eurostat 2016]).

* All data without Rumania; category 5a without Italy due to missing data.

Table 1: Minima, maxima, and total amount of WEEE treated in another member state or outside the EU than in IT, D, and the EU-28 [Eurostat 2016].

[Mg]	Treated in another member State of the EU-28 2007-2013			Treated outside the EU-28 2007-2013		
	Min.	Max.	Total	Min.	Max.	Total
IT	7 021	27 786	127 102	55 904	98 013	573 302
D	3 827	17 593	69 139	1 436	2 486	9 544
EU-28	96 561	175 135	972 935	62 253	101 930	568 783

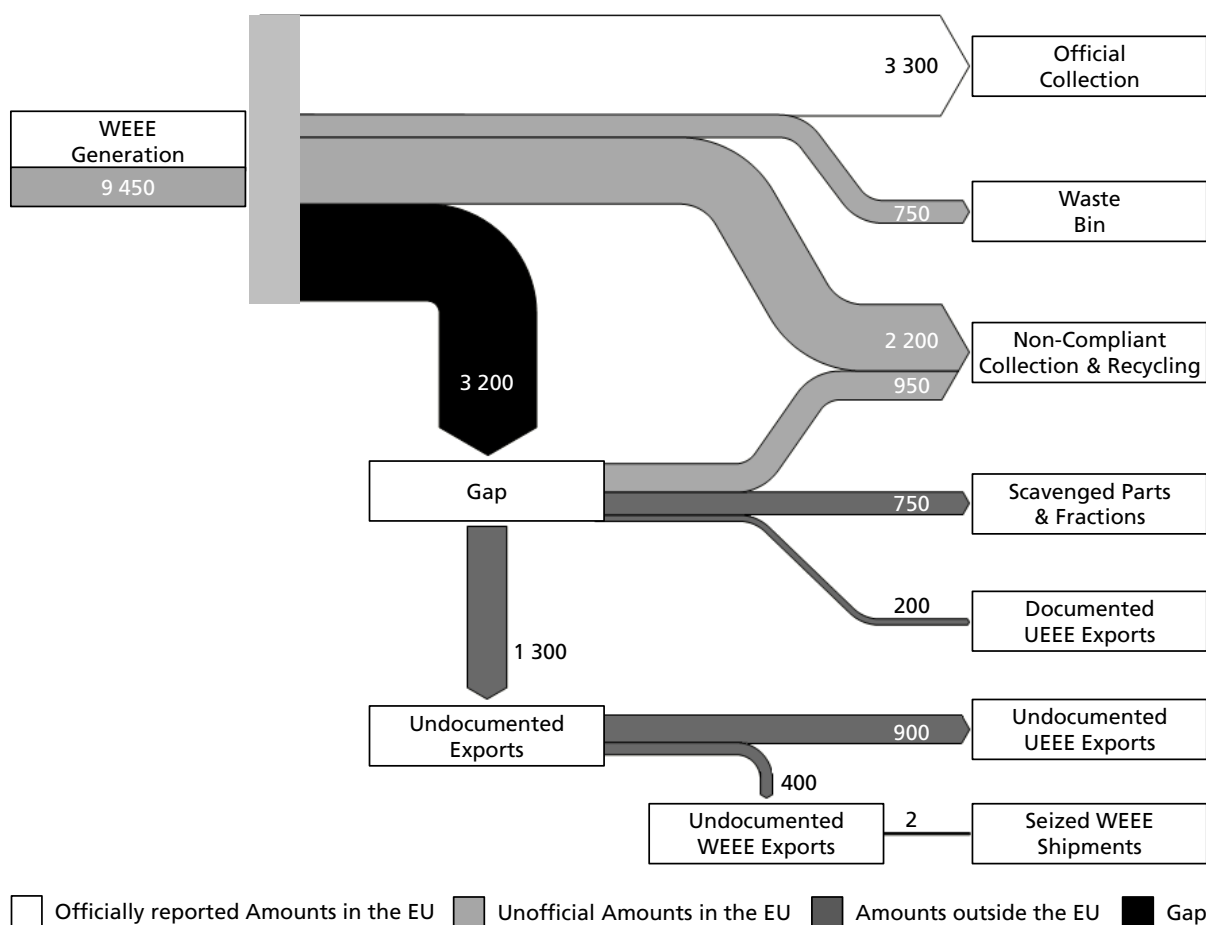


Figure 8: Estimated flows of WEEE in the EU-28 in 1 000 Mg (modified according to [Huisman et al. 2015]).

3.3 Mechanical and metallurgical treatment of WEEE

As mentioned above, WEEE is a source not only for reusable resources such as metals and plastics, but also for hazardous materials. Therefore, besides recovery of valuable materials, one of the main aims of WEEE treatment is depollution. Typical sources for pollutants are batteries, capacitors, toners, halogen containing plastics, and lead-containing materials like glasses of cathode ray tubes (CRT). For this reason, appropriate classification and separation of materials to the different recovery and disposal paths is required during WEEE treatment. Table 2 shows different paths for material and thermal treatment as well as disposal including examples of treatment and corresponding material flows [VDI 2014].

Table 2: Material and thermal recovery paths as well as disposal for fractions from WEEE treatment [VDI 2014].

Recovery and disposal paths	Material recovery	Thermal treatment	Disposal
Examples of treatment	<ul style="list-style-type: none"> - Pyrometallurgy - Hydrometallurgy - Regranulation and Compounding - Gasification - Blast furnace 	<ul style="list-style-type: none"> - Waste Incineration Plants - Industrial combustion Plants - Cement Industry - Power Plants 	<ul style="list-style-type: none"> - Landfilling - Underground disposal
Examples of material flows	<ul style="list-style-type: none"> - Ferrous Metals - Non-Ferrous Metals - Precious Metals containing fractions - Synthetics fractions 	<ul style="list-style-type: none"> - Timber - Filter dust - Capacitors 	<ul style="list-style-type: none"> - LCDs - Mineral fibers/rock wool - Mercury-containing switches

In order to gain appropriate fractions for the different recovery routes, WEEE usually gets treated in manual and mechanical steps (chapter 3.3.1). Following recycling via pyro- and hydrometallurgical processes will be detailed in chapter 3.3.2.

3.3.1 Mechanical treatment

In most industrialized countries, state-of-the-art initial treatment of WEEE is a combination of different mechanical processes and physical and/or optoelectronic separation systems. The mechanical treatment of WEEE will be explained on the basis of two examples, which could be relevant for a thermo-chemical treatment: these are, on the one hand LHA, and automatic dispensers (Figure 9) and on the other hand, SHA, consumer electronics, IT and telecommunications equipment, medical devices, toys, leisure and sports equipment, electrical and electronic tools, as well as monitoring and control instruments excluding visual display units (Figure 10) [VDI 2012].

In the case of LHA and automatic dispensers, whole devices get crushed using a shredder. From shredded material, metals get separated by density, for example using an air classifier with a cyclone. The remaining shredded light material consists mainly of plastics and can be used in upstream recycling steps or can be incinerated, depending on the purity, market prices, and further circumstances. By using magnetic separators, followed by eddy-current separators, ferrous and non-ferrous metals get separated. In contrast to ferrous metals, non-ferrous metals should be further reconditioned in an aluminum-rich fraction and a copper-rich fraction with precious metals, Bi, In, Ni, Pb, Sb, Se, Sn, and Te [Hagelüken and Corti 2010].

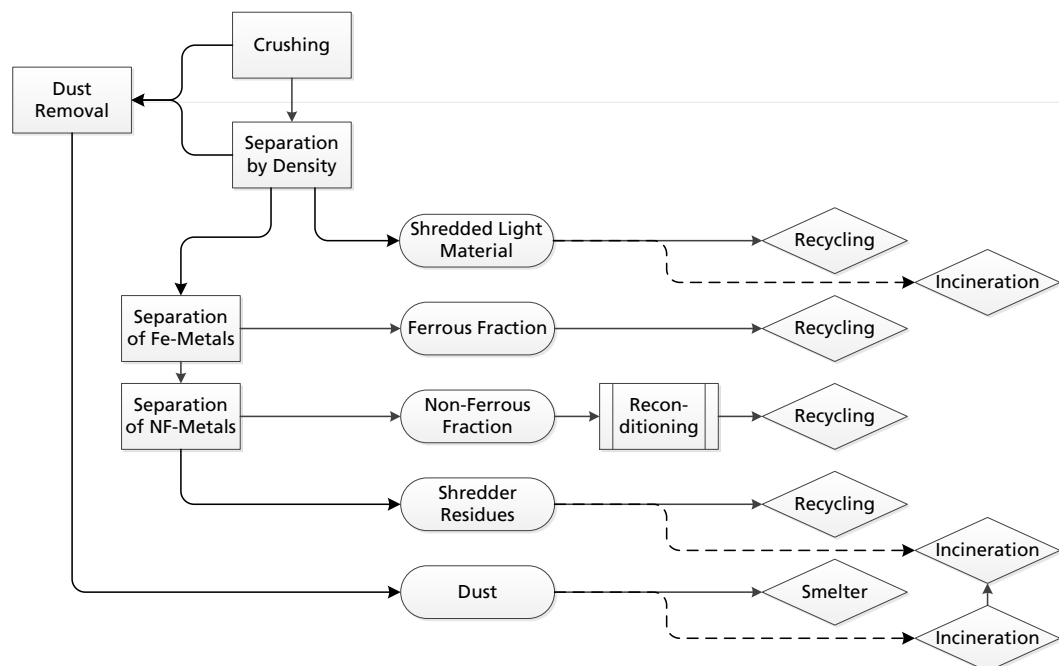


Figure 9: Mechanical treatment of WEEE categories 1 and 10 (modified according to [VDI 2012]).

The treatment as shown in Figure 10 starts with a manual dismantling, followed by shredding and separation, for example with magnetic, eddy-current, or infrared systems. Main processes are similar to the above mentioned recycling of LHA and automatic dispensers. However, due to the large number of different electronic devices, a significantly greater number of plastics could be found which entail a profound sorting of plastics. Due to the complexity of different sorting processes, just a few first steps of this sorting are conducted on-site a WEEE treatment facility and most of them are in specialized facilities. The sorting usually starts using sieving or air separation in order to remove foils, paper, dust, pieces of textiles, foams, and other light materials, followed by sink-float processes using water and salt solutions. In a first cell, which is filled with a salt solution with a density in between 1.08 and 1.20 g·cm⁻³, high-density plastics such as polyoxymethylene (POM) or polyethylene terephthalate (PET), halogenated plastics like PVC as well as plastics with fillers, and remaining metals represents a sinking residuum. Plastics with lower densities such as PE, PP, ABS, and PS float and get transferred to a second cell, which is filled with water in order to separate the polyolefins PE and PP on the one side (floating fraction) as well as PS and ABS on the

other side (sinking fraction). A further separation of economically and quantitative important polymers, PS and ABS, is usually conducted using electrostatic separation systems [Köhnlechner 2014]. Other modern options for splitting heterogeneous fractions, like mixed plastics, into halogenated and non-halogenated plastics are based on optoelectronic systems [Husemann et al. 2010]. For an effective sorting with good results concerning the separation of different plastics, the particle size should be >2 mm for eddy-current separation or sensor-supported sorting [VDI 2012] and <50 mm for sink-float processes. However, concerning sink-float processes, air bubbles could adhere to very small particles, the effect being that the separation of heavy materials is not effective [Köhnlechner 2014]. This means that in addition to those separated fractions like halogenated plastics, a further fraction with a very small particle size (<2 mm) arise from the treatment of WEEE, which will not be recycled yet. Recovered fractions like non-halogenated plastics or metals are handed over to recycling processes to recover secondary raw materials, while all other materials like halogenated plastics or small particle size fractions get landfilled or incinerated typically [VDI 2012].

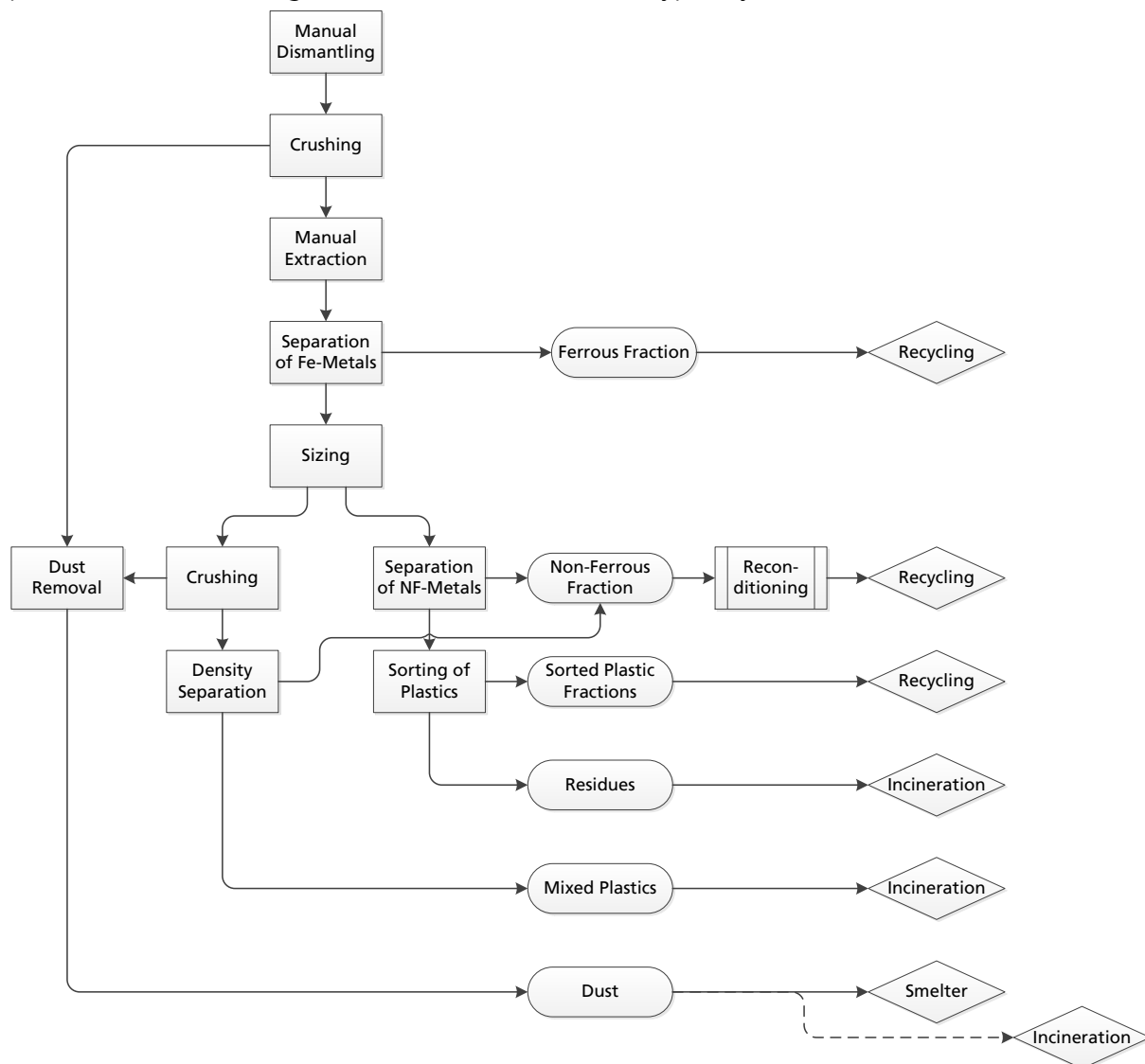


Figure 10: Mechanical treatment of WEEE categories 2, 3, 4, 6, 7, 8, 9 excluding visual display units (modified according to [VDI 2012]).

Dust fractions very often show significant concentrations of precious metals. If those concentrations are high enough that recovery is economically advantageous, dust fractions can be pelletized in order to connect small particles and to reduce volume for transports. In this compacted form, they can be treated in pyrometallurgical processes (chapter 3.3.2). As an example, composition of a dust fraction <0.3 mm was reported by [Gaggl et al. 2014], which showed significant yields of base and precious metals (Figure 11).

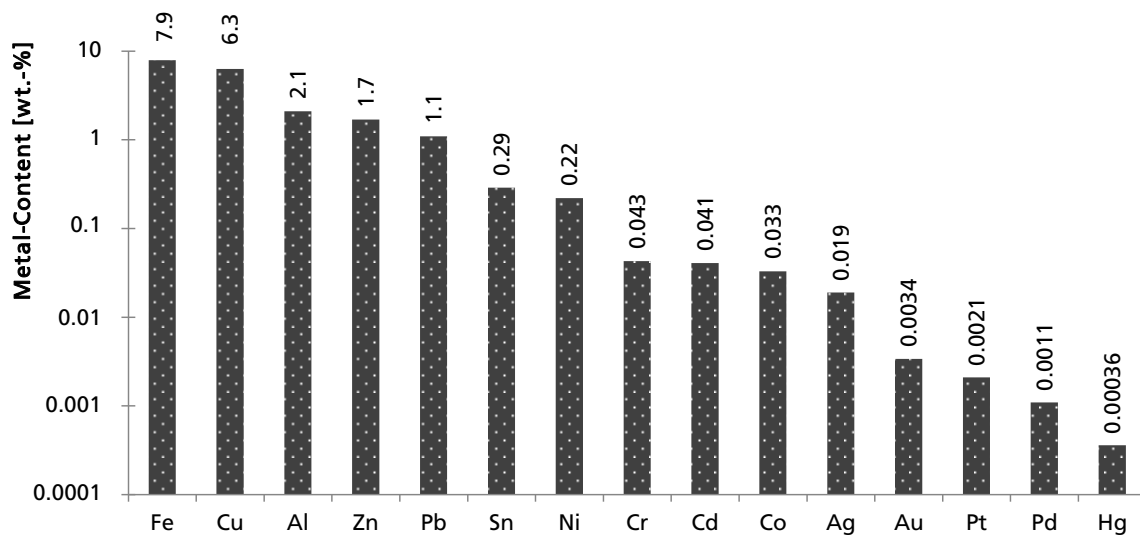


Figure 11: Metal content in wt.-% of a dust fraction <0.3 mm from WEEE-treatment (modified according to [Gaggl et al. 2014]).

Mixed plastics and mainly shredder residues are very heterogeneous and show a mixture of many different materials, which make further treatment difficult or impossible. One of the key reasons for the imperfect sorting during treatment processes is an incomplete material liberation, which means liberation by kinetic energy. Kinetic forces in commonly used shredding processes are not able to adequately liberate (all) glued, coated/painted, and foamed connections [Reuter et al. 2013]. As a result, especially small particle size fractions, often still contain relatively high amounts of non-ferrous and precious metals [VDI 2012]. For instance, as shown by [Chancerel et al. 2009], after pre-sorting, manual sorting and depollution, pre-shredding and manual sorting, as well as (second) shredding and automated sorting, approximately 49.9 wt.-% of Pd, 72.9 wt.-% of Au and 86.9 wt.-% of Ag ends up in non-adequate fractions like ferrous metals and plastics. With regard to scarce metals such as critical metals, mass flow analyses of these metals during WEEE treatment are incomplete. However, actual data from mass flow analyses of scarce metals during passenger vehicle treatment were conducted by [Widmer et al. 2015]. Both treatment processes regarding passenger vehicles and WEEE are similar, which allows a restricted comparison. From passenger vehicle treatment, mainly five fractions (Fe, Al, shredder light fraction, screen fraction, and mix) are gained,

from which shredder light fraction is comparable to those shredder residues from WEEE treatment. In the cases of passenger vehicle treatment, 15² of 31 analyzed scarce metals showed the highest allocation mainly to shredder light fraction. Therefore, such shredder residues could offer a source of many scarce and critical metals.

Concerning base metals, such as Cu, the Swedish Company Stena estimated that residual fractions from their WEEE recycling facilities contain up to 50 Mg Cu per year [Andersson et al. 2012]. In order to assess how many metals get lost during WEEE treatment in Italy, Germany, or the European Union, the concentrations of metals should be set in relation to the amount of residual fractions. For one of Germany's biggest WEEE treatment facilities, "Electrocycling GmbH", [Kramer 2013] presented yields of different output fractions from WEEE treatment and showed that the yield of residuals and mixed plastics ("shredder residues") for an energetic utilization accounts for about 20.1 wt.-%. Additional 2.3 wt.-% of waste goes to special treatment and hazardous waste incineration plants. Taking into account that the amount of WEEE collected in Italy, Germany, and EU-28 in 2013 was 437 090, 727 998, and 3.49 Mio. Mg, respectively, the corresponding amount of shredder residues could account for nearly 88 855, 146 328, and 701 655 Mg·y⁻¹ [Eurostat, 2016].

Possibilities for a further processing of different residual fractions from WEEE treatment by a thermo-chemical treatment will be discussed in chapter 3.4.1. In contrast, established recycling systems for recovered metals and metal-rich fractions such as PWB from WEEE will be shown in the next chapter 3.3.2.

3.3.2 Pyrometallurgical treatment of WEEE

Selected metal fractions, and metal-rich WEEE like mobile phones or components like PWB are given to pyrometallurgical plants to recover metals and to use remaining plastics as energy source and reduction agent.

Recycling of ferrous metals happens in converters or electric arc furnaces in combination with other secondary ferrous metal wastes in order to produce different kinds of steel qualities [Lüngen et al. 2006]. Usually, amounts of different metals besides Fe are limited: From VDI 4085 for European steel qualities, maximum concentrations are set of 0.25 wt.-% for Cu and Ni as well as 0.20 wt.-% for Cr. If the concentrations are higher than these values, revenues for sold iron-rich fractions decrease accordingly [VDI 2012].

Compared to the recycling of ferrous metals, recycling of non-ferrous metals is often more complex. Additionally, values for minimum concentrations of target metals are higher in some cases. As an example, Al-rich fractions with Al contents of more than

² Ce, Dy, Gd, La, Mo, Nd, Pr, Rb, Ru, Sb, Sm, Sr, Tb, W, and Y.

90 wt.-% could be recycled in specialized re-melting plants. However, very often, the minimum values are set to 98 wt.-%, which requires further treatment. In order to meet the requirements, Al-rich fractions could be sorted in sink-flow processes. From scrap Al, two different kinds of alloys could be produced, namely cast and wrought alloys. The concentrations of elements besides Al have to be lower than 2 wt.-% in the case of wrought alloys and 12 wt.-% in the case of cast alloys. Typical maximum values for such elements are listed in Table 3 [VDI 2012].

Table 3: Maximum concentration of different metals in Al cast alloys [VDI 2012].

Element	Maximum Values [wt.-%]	Element	Maximum Values [wt.-%]
Fe	1.3	Sn	0.1
Ni	3.0	Ti	0.25
Pb	0.35	Zn	0.15

For recycling of Cu in combination with precious metals such as Ag, Au, and PGM, the copper industry developed and optimized modern processes for such materials containing precious metals. The corresponding plants are so called integrated precious metals smelters such as ISASMELT™ from Umicore or the Kayser Recycling System (KRS) from Aurubis. These processes combine smelter and converter processes and are able to recycle up to 18 metals³, however they are limited to base and precious metals [Hagelüken 2010; Lossin 2006]. Depending on the content of copper and precious metals, the recycling starts either under reductive atmosphere (SO₂) in processes such as a Pierce-Smith-Converter or a Noranda reactor, or oxidative in the above mentioned combined processes such as the ISASMELT™ or a Top Blown Rotary Converter (TBRC) as part of the KRS. According to this, the products are blister Cu (reductive processes) with 96.0 - 99.5 wt.-% Cu or black Cu (combined processes) with about 90 - 95 wt.-% Cu. Further valuable products are iron silicate, Sn containing dross, and ZnO. In order to produce Cu with a high purity grade, further pyrometallurgical, electrolytic, and remelting/refining processes follow, subsequently. Impurities, mainly Sulphur, become oxidized in a first step of the pyrometallurgical refining, which is called poling. After this step a reductive process starts, in which dissolved hydrogen reacts with oxygen (from Cu₂O) to lower the content of oxygen to about 0.03 - 0.2 wt.-%. In a last step, anodes get casted for the electrolytic refining. During the electrolytic refining, Cu anodes are dissolved in an adequate electrolyte, which is mainly based on H₂SO₄, at temperatures between 55 and 65 °C. In the process, Cu is forming a cathode with purities of about 99.99 wt.-% Cu while impurities of the anode forming an anode sludge, which contains for instance 98.6 wt.-% Au, 97.7 wt.-% Ag, 97.6 wt.-% Se, and Te, 98.0 wt.-% Pb,

³ Example: Umicore's Precious Metals Refining Processes: Ag, As, Au, Bi, Cu, Ga, In, Ir, Ni, Pb, Pd, Pt, Rh, Ru, Sb, Se, Sn, Te, and H₂SO₄ [Hagelüken 2010].

3.7 wt.-% Ni, 24.7 wt.-% As, and 58 wt.-% of Sb compared to the content of these metals in the anodes [Lossin 2006]. Besides these metals, further precious metals, mainly PGM, get recycled from the anode sludge in specialized metallurgical facilities using precipitation, solvent extraction, reduction, oxidation, distillation, ion exchange techniques, hydrolysis, and calcination [Brumby et al. 2005; Hagelüken 2010].

In contrast to the above mentioned dust fractions, treatment of shredder residues in pyrometallurgical processes is limited: in 2004, a trial run with shredder residues containing approximately 76 wt.-% plastics⁴ and 10 wt.-% metals was conducted in Umicores Precious Metals Refining Plant at Hoboken near Antwerp, Belgium. Center-piece of this plant is a copper smelter with a capacity of roughly 250 000 Mg·y⁻¹ (2004), which already recycles PWB (approximately 10 wt.-% of the smelters capacity). From the trial run, in which 6.4 wt.-% of the smelters capacity was additional shredder residues, it was shown that no operational problems were obvious up to this input amount. The authors revealed that a further increase is limited by steam production and by a maximum temperature at the top of the furnace. Both parameters increased heavily due to added shredder residues. However, due to the addition of 1.0 Mg of shredder residues, 0.6 Mg of fossil coke, and 0.1 Mg of fossil fuel oil were substituted [Brusselaers et al. 2006]. Presently, the capacity of Umicores copper smelter increased and should reach 500 000 Mg·y⁻¹ [Katz 2013]. Taking this into account, Umicore would be able to treat about 32 000 Mg·y⁻¹. Similar to Umicore, two further companies in Europe recycle copper: the Swedish Company “Boliden AB” and the German company “Aurubis AG”. Actually, smelters of Boliden and Aurubis have a capacity of each 350 000 Mg·y⁻¹ [Kawohl 2011; Boliden 2016]. Taking this capacity into account, presumably all of these smelters would be able to treat about 6.4 wt.-% shredder residues, the treatment capacity for shredder residues in Europe would be at about 76 800 Mg·y⁻¹. Compared to the above mentioned amount of 701 655 Mg shredder residues per year in the EU-28, just 10.9 wt.-% of all shredder residues formed each year could be treated in copper smelters.

As pyrometallurgical recycling usually starts with or contains a smelter process, critical metals like Be, Ge, Nb, W, and a number of Rare Earth Elements (REE) contained in WEEE oxidize and become slagged due to their ignoble character [Bakas et al. 2014; Kumar et al. 2014]. Due to this, the end-of-life recycling rates (EoL-RR) of most critical metals from WEEE are less than one percent [Bakas et al. 2014; Buchert et al. 2012; Graedel et al. 2011]. An extraction of those critical metals prior to a pyrometallurgical recycling offers the opportunity to recycle both critical as well as base metals, like Cu, and precious metals like PGM. Additionally, remaining base metals such as Al could be recovered, too. For this, a thermo-chemical process could solve different metals from

⁴ In tested material 0.20 - 0.24 wt.-% Br and 2.2 - 3.2 wt.-% Cl were detected [Brusselaers et al. 2006].

their compounds, followed either by an extraction or separation of corresponding metals, alloys, or components. Chapter 3.4.2 will list some different fractions from WEEE containing critical metals, which could be extracted and separated by using a thermo-chemical process.

3.4 Potential fractions from WEEE treatment as feedstock for a thermo-chemical process

A thermo-chemical process for WEEE offers an opportunity for the recovery of metals, a reduction of waste, and a production of fuels for an energetic utilization. Compared to an incineration process, there is no oxidation of metals and, additionally, the gas flow through the process itself is very small, which lowers emission of dust particles greatly. Due to these circumstances, most metals stay stable in the solid fraction of a pyrolysis process [Andersson et al. 2012]. The pyrolysis char itself is very brittle and shows no effects of vitrification, which makes it easy to recover metals from it [Hense et al. 2015b].

In developed countries, many fractions yielded from WEEE treatment are already successfully handled by mechanical or pyrometallurgical treatment. As an example, as mentioned above PWB could efficiently be recycled in copper smelting processes, as far as the recycling of base and precious metals is concerned [Hagelüken and Corti 2010]. Therefore, PWB are not further pursued in the following chapters. However, it should be noted that a thermo-chemical treatment of PWB (c.f. [Williams 2010]) or many other fractions from WEEE could be a matter in countries where those pyrometallurgical treatment processes are missing and transports to corresponding plants are not economically feasible.

3.4.1 Residual fractions from WEEE treatment

As mentioned in chapter 3.3.1, the mechanical treatment of WEEE yields a number of different fractions, which are not getting recycled yet. These fractions, such as different plastic fractions with or without flame retardants, dust fractions, and shredder residues, are commonly treated by a thermal treatment. Thereby, the energy content from organic compounds could be utilized to produce power and heat. As an example, modern German municipal waste incinerators (MWI) are able to recover energy with an average gross plant efficiency of $\eta_{el} = 13 \%$ and $\eta_{th} = 30 \%$ for power and heat, respectively [UBA 2008]. However, state-of-the-art technology is not able to recover remained metals from the incineration slags: one reason being their relatively small particle size [Mark et al. 2006] and oxidation of a number of metals. While some metals such as Sn could be recovered from the filter dust as a product from the flue gas cleaning, the recovery is very complex. Besides thermal treatment, in many countries above mentioned fractions often end up in landfills after or instead of an appropriate

WEEE treatment. This means not only a loss of metals and energy, but also a potential risk to the environment, e.g. due to leaching of heavy metals [Andersson et al. 2012; Lee et al. 2007; Oguchi et al. 2013].

With respect to the above mentioned facts (e.g. concerning the high amount of residual fractions), the limited recycling capacity in copper smelters, the risk of landfilling, and high material values in it, treatment by pyrolysis seems to show many advantages. Due to thermo-chemical treatment, dehalogenation of pyrolysis products, extraction of metals, and a formation of fuels are theoretically feasible.

However, just a very small number of publications are about treatment of such residual fractions by pyrolysis e.g. [Andersson et al. 2012; Gaggli et al. 2014; Hee 2016; Quicker 2016]. As an example, [Gaggli et al. 2014] developed a bench-scaled, continuous pyrolysis process based on a heated screw conveyor in order to prepare dust materials for pyrometallurgical recycling. The reactor was designed for a throughput of 20 kg dust and a residence time of 120 min at 450 °C. Formed vapor from pyrolysis was condensed in a bubble tray tower to gain pyrolysis oil and gas. Unfortunately, no complete mass and/or energy balance was reported, just a reduction of mass of about 30.13 wt.-%. As a further challenge, mainly compaction of produced pyrolysis solid products was defined in order to enable a further recycling in pyrometallurgical processes.

As mentioned in chapter 3.3.1, the amount of shredder residues was estimated to be about 146 328 Mg·y⁻¹ in Germany for 2013. In relation to the number of WEEE treatment facilities (approximately 270 in Germany [EAR 2016]), an average amount of 542 Mg·y⁻¹ was formed per treatment facility, which could be potentially treated in thermo-chemical processes.

3.4.2 Selected fractions containing scarce and critical metals

Besides the above mentioned residual fractions as well as typical output fractions of WEEE recyclers like Cu- or Fe-rich fractions, further selected components can be separated in order to extract and recycle contained metals. Mainly, metals such as critical metals, which cannot be recycled due to thermodynamic reasons in smelter processes, should be extracted previously [Reuter et al. 2013]. A (manual) separation of those components before mechanical treatment of WEEE offers the opportunity to recycle contained metals in specialized recycling processes. Pyrolysis technology could be used to extract and concentrate those metals from separated fractions [Hense et al. 2016]. Therefore, in this subchapter the focus should be to set two selected components from WEEE containing mainly scarce and critical metals.

Indium-tin-oxide from liquid crystal displays

Approximately 70 wt.-% of the world's used In is applied for the production of indium-tin-oxide (ITO) films, which typically consists of 90 wt.-% In_2O_3 and 10 wt.-% SnO_2 . One of the most important applications for ITO films is the production of Liquid Crystal Displays (LCD), e.g. for flat screens [Zhang et al. 2015]. Thicknesses of ITO films could be between 30 and 2 990 nm [Buchert et al. 2012] and have densities of approximately $7.14 \text{ g}\cdot\text{cm}^{-3}$, while the density of the whole LCD is at about $3.2 \text{ g}\cdot\text{cm}^{-3}$ [Yang et al. 2013a]. Due to wide ranges of the ITO film thicknesses, ITO contents are between 72 and 7 176 $\text{mg}\cdot\text{m}^{-2}$ (56 - 5 597 $\text{mg In}\cdot\text{m}^{-2}$) [Buchert et al. 2012]. For In contents, [Jalalpoor et al. 2013] reported ranges of 40 - 650 $\text{mg}\cdot\text{kg}^{-1}$ for mobile phones (mean: 330), 50 - 250 $\text{mg}\cdot\text{kg}^{-1}$ for TV devices (mean: 170), and 140 - 220 $\text{mg}\cdot\text{kg}^{-1}$ for PC monitors (mean: 170). Besides these valuable metals, LCD could contain toxic metals such as As or Cr. Analyses concerning content of these and some further metals were conducted by [Savilotidou et al. 2014] (Table 4). With regard to complete EoL-devices, [Bakas et al. 2016] reported In concentrations of between 0.4 and 36.7 (average 13.2) $\text{mg}\cdot\text{kg}^{-1}$ for flat screens and TV monitors and 15 $\text{mg}\cdot\text{kg}^{-1}$ for laptops and notebooks.

Table 4: Content of metals in LCD panels of different electronic devices (in $\text{mg}\cdot\text{kg}^{-1}$) [Savilotidou et al. 2014].

	TV	PC	Tablet	Detection Limit (DL)
Al	4.87	5.08	7.78	$3.56\cdot 10^{-6}$
As	626.85	606.23	3.46	$6.94\cdot 10^{-5}$
Cd	<DL	<DL	<DL	$1.29\cdot 10^{-4}$
Cr	154.75	160.50	220.24	$1.37\cdot 10^{-3}$
Cu	23.24	13.69	15.98	$3.48\cdot 10^{-4}$
Fe	<DL	<DL	<DL	$1.5\cdot 10^{-6}$
Hg	<DL	<DL	<DL	$7\cdot 10^{-6}$
Ni	130.34	134.04	169.42	$1.25\cdot 10^{-4}$
Sn	144.84	255.20	762.69	$1.21\cdot 10^{-4}$
Zn	1 141.57	1 304.81	1 134.00	$1.67\cdot 10^{-3}$

Besides this treatment option, most of these flat TVs end up in incineration processes or get landfilled [Wang, Xu 2016; Zhang et al. 2015]. Modern treatment processes for flat EoL-TVs starts with a manual or automatic dismantling under a special air treatment system in order to collect Hg from carbon ray tubes, which are used for the background lighting. Concerning a recovery of critical metals, the most interesting part is the ITO-film as part of the LCD. Usually, a LCD consists of a sandwich-structure with a number of different layers such as two polarizing films, glass substrates, and liquid crystals (Figure 12), where the ITO films are nearly in the middle of this structure, next to the liquid crystals. Based on results by [Kim et al. 2009], different parts of LCD account for 87.2 wt.-% glass, 12.7 wt.-% plastics, and 0.1 wt.-% liquid crystals. Elemental analyses of the LCD by [Chien et al. 2005] showed approximately 77.1 wt.-% C, 8.4 wt.-% H, 14.5 wt.-% N and O. The polarizing film consists of 52.57 wt.-% C, 5.56 wt.-% H,

39.62 wt.-% O, and 0.06 wt.-% N [Wang, Xu 2016] as cellulose triacetate (CTA) (83.38 wt.-%), polyvinyl alcohol (PVOH) (4.44 wt.-%), and triphenyl phosphate (TPP) (12.18 wt.-%) [Wang et al. 2015a].

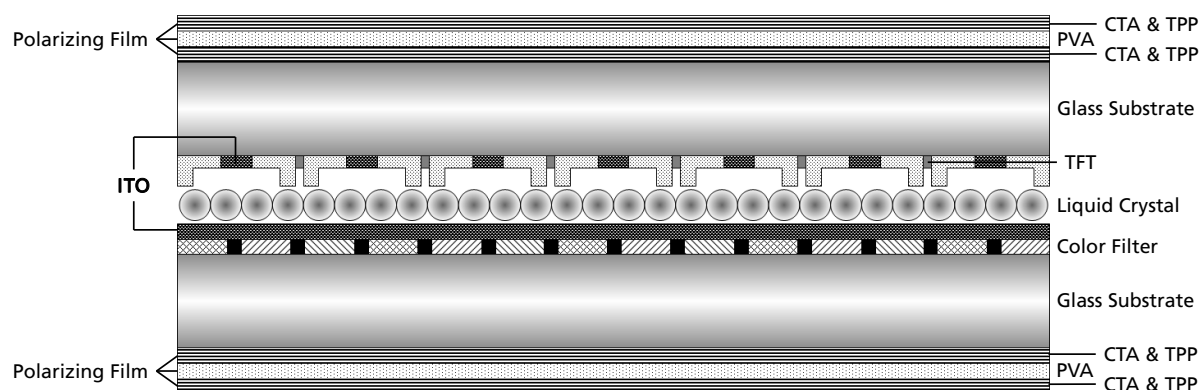


Figure 12: Structure of a LCD (modified according to [Wang, Xu 2016]).

In order to recover organic material and/or In from LCD, pyrolysis tests were conducted by a number of researchers (e.g. [Lu et al. 2012; Ma et al. 2013; Park et al. 2009; Wang, Xu 2014; Wang, Xu 2016]). With regard to a volatilization of organic material, from pyrolysis at 570 - 580 °C between 67 and 71 wt.-% of liquid plus between 12 and 14 wt.-% of gaseous products could be formed [Lu et al. 2012; Wang et al. 2016]. At lower temperature (300 °C) and under vacuum (50 Pa) the yield of liquid products could be increased to about 79 wt.-% in favor of gaseous products (2.9 wt.-%) [Ma, Xu 2013]. Generally, the gaseous products mainly consist of hydrocarbon compounds such as 1-butene, trans-2-butene, and 2,2,3-trimethyl-butane, while the main compounds of the oil were acetic acid and TPP. The liquid fraction could be further separated in a light fraction (71.8 wt.-%), which mainly consists of acetic acids, and a heavy fraction (28.2 wt.-%) [Wang, Xu 2016].

In order to recover In from pyrolysis solid products or directly from LCD, processes based on chlorination of In are analyzed in some studies. This process could enable an extraction as well as dissolution from LCD in one step. Therefore, NH_4Cl or PVC could be used as Cl donating additive. A feasible process developed by [Ma, Xu 2013] reached a nearly complete recovery of In (99.97 wt.-%) using 50 wt.-% NH_4Cl + 50 wt.-% pyrolyzed LCD (grinded to <0.16 mm) at 450 °C for 10 min. Pyrolysis tests with PVC and a LCD powder (12.0 wt.-% In_2O_3) in a Cl:In molar ratio of 11 at 350 °C for one hour could not reach that high efficiency. These tests, conducted by [Park et al. 2009], just reached a recovery rate of 66.7 wt.-%; however, in this procedure PVC could be used, which is a comparable cheap chlorination agent.

Tantalum pentoxide from capacitors

For the production of electrolytic capacitors, tantalum pentoxide (Ta_2O_5) is a widely used solid dielectric medium. Besides some Nb, Al, or ceramic based capacitors, Ta based capacitors are used at low voltage (1 - 60 V) and a medium capacitance (100 nF - 200 μF) for power supply in integrated circuits (IC) [Angerer et al. 2009]. Figure 13 shows the main components of a molded Ta-Capacitor. The core piece is a sintered Ta pellet, which is coated with nitrate solution containing Ag, MnO_2 , Graphite, NH_4OH , and different types of resins. The exterior mold usually consists of an epoxy and/or phenol resin encapsulation, which contains SiO_2 . Average amounts of materials⁵ used for the production of a Ta-Capacitor are shown in Figure 13 [Cal-Chip 2016; Vishay 2015].

Actually, Ta is not defined as a critical metal; however, mainly due to low recycling rates and its primary production from so called conflict minerals such as columbium [USGS 2016], new pathways are required for a recycling mainly from EoL goods.

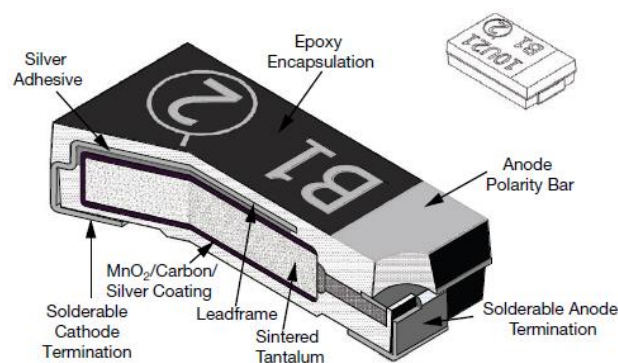


Figure 13: Components of a molded Ta capacitor [Vishay 2015].

Two different examples for a recovery of Ta from Ta capacitors should be highlighted. [Fujita et al. 2014] as well as [Mineta, Okabe 2005] developed process chains for a recovery of Ta. Both processes started with an oxidation step, which was followed by magnetic and eddy-current separation and sieving. After these steps, a product as a mixture of Ta_2O_5 , MnO_2 , and SiO_2 was formed, which was either treated thermally in an air atmosphere a second time at temperatures up to 600 °C (see [Fujita et al. 2014]) or treated with a wet sieving as well as leaching and reduction steps (see [Mineta, Okabe 2005]). After the last step of the second mentioned method (magnesiothermic reduction at about 1 000 °C), Ta with a purity of 99 wt.-% was recovered. In contrast, using steam gasification with NaOH at 530 °C, [Katano et al. 2014] investigated a recovery

⁵ The so called "42alloy" chemically consists out of 57.45 wt.-% Fe, 41 wt.-% Ni, 0.8 wt.-% Mn, 0.3 wt.-% Si, 0.25 wt.-% Cr, 0.10 wt.-% Al, 0.05 wt.-% C, 0.025 wt.-% P, and 0.025 wt.-% S [NEA 2016].

process for Ta pellets. From their findings they revealed that an extraction of Ta from exterior mold was impossible without any addition of NaOH, while the resin decomposed under addition of 33 - 100 wt.-% of NaOH.

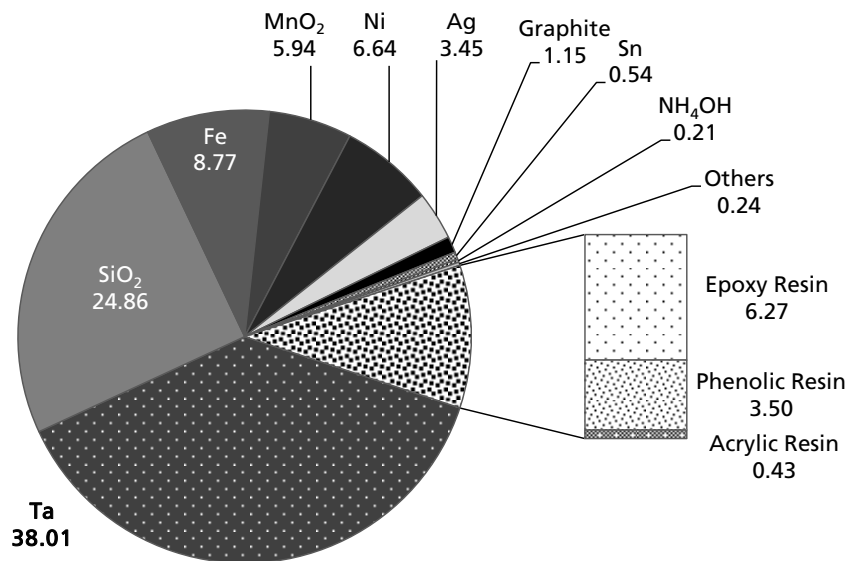


Figure 14: Average composition of Ta capacitors (in wt.-%) (own diagram based on [Cal-Chip 2016]).

In contrast to LCD, no pyrolysis processes with regard to an extraction of Ta₂O₅ from Ta capacitors, are actually known. As shown for LCD, pyrolysis offers the opportunity to remove hydrocarbons from fractions containing critical metals without oxidizing such (chemically) ignoble metals. However, there is still a huge lack of information, if pyrolysis – as thermo-chemical separation of materials – can become part of a process chain for recovering such metals.

4. Chemical reactions during thermo-chemical treatment of WEEE

Waste Electrical and Electronic Equipment (WEEE) consists of different plastics, a number of metals, as well as minerals. A comprehensive knowledge is needed on chemical reactions and interactions during thermo-chemical treatment, in order to develop a pyrolysis process treating many different fractions from WEEE, like residual fractions (chapter 3.4.1) or selected fractions containing critical metals (chapter 3.4.2).

This chapter gives a detailed view on how pyrolysis processes are influenced for treating plastics from WEEE by the main parameters⁶ of temperature, heating rate, residence time, operation mode (one- vs. two-stage), and additives as well as the influence of these parameters on quality and quantity of pyrolysis products and emissions. Using this information, adequate strategies and opportunities should be developed for focused feedstocks from WEEE. As an example, besides just mobilization of all volatile hydrocarbons, pyrolysis at different temperature stages could be used to volatilize compounds, such as hazardous components, selectively.

4.1 Decomposition of additive-free thermoplastics and thermosetting plastics

Most additive-free thermoplastics like polyethylene (PE), polyethylene terephthalate (PET), polypropylene (PP), or polystyrene (PS) decompose in one single step with, for instance, maximum rates of decomposition at approximately 430 °C, 440 °C, and 450 °C for PET, PS, and PP, respectively [Blazsó et al. 1995; Czégény et al. 2012; Jakab et al. 2003; Ma et al. 2015; Suzuki, Wilkie 1995]: For example, PS, which is one of the most widely used polymers in WEEE (c.f. chapter 3.2), decomposes between 360 and 450 °C with the formation of mainly styrene monomers and oligomers at moderate temperatures due to end-chain and random scission as well as depropagation and intra-/intermolecular transfer reactions [Suzuki, Wilkie 1995]. With an increase of temperature or pressure, a greater fragmentation was shown with the formation of mainly ethylene as well as styrene, toluene, and benzene [Madorsky, Straus 1959]. In both cases, no residues were obtained. (Low density) PE (LDPE), as an example for an aliphatic compound, decomposes between 390 and 505 °C. With regard to pyrolysis products, the yields of alkadienes increase from less than 1 wt.-% at 400 °C to approximately 6 wt.-% at 800 °C. The formation of alkenes and alkanes increases as well; however, it peaks at a temperature of 600 °C resulting in values of 7 and 15 wt.-% for alkanes and alkenes, respectively. With a further increase of temperature, aromatic hydrocarbons are formed: at 1 000 °C a total yield of 2.6 wt.-% naphthalene, acenaphthalene, and

⁶ The parameter particle size is not discussed in detail, because it does not influence pyrolysis very strongly [Andersson et al. 2012; Chiang et al. 2007]. As shown by [Quan et al. 2009], an influence on the pyrolysis due to different particle sizes is not significantly below 5 mm and just very small above this size.

phenanthrene are formed (at 800 °C: 0.0 wt.-%) [Blazsó et al. 1995]. These product formations are typical for degradation behavior of polymers, which takes place by the three reaction types of depolymerization, elimination, and cyclization [Shie et al. 2002].

Another plastic, which is widely used in the production of Electrical and Electronic Equipment (EEE), is the copolymer acrylonitrile butadiene styrene (ABS). Additive free ABS decomposes in one step with a maximum at about 419 °C [Czégény et al. 2012] and leaves a solid residual yield of 4 wt.-% at 600 °C [Suzuki, Wilkie 1995]. The decomposition of ABS itself starts at about 340 °C by forming butadiene monomers, shortly followed (350 °C and above) by aromatic compounds, mainly styrene. Additionally, between 400 and 450 °C acrylonitrile gets formed. The decomposition of polyacrylonitrile takes place in a temperature range between 290 and 480 °C with the main products being NH₃ and acrylonitrile (oligomers). Additionally, small amounts of CH₄ (>550 °C) and highly-toxic HCN (290 - 800 °C) were formed [Suzuki, Wilkie 1995]. On this account, sorting of ABS before pyrolysis makes sense in order to prevent a formation of HCN. Additionally, to focus sorting on this technical polymer is economically more reasonable compared to other thermoplastics: ABS could show a higher value of +21.6 %, +30.3 %, and +93.5 % compared to PS, PP, and polyvinyl chloride (PVC), respectively (values from 10/2016 [EUWID 43.2016a; 43.2016b]).

For the production of some modern electronic equipment, such as liquid crystal displays (LCD) (see chapter 3.4.2) or photovoltaic modules, polyvinyl alcohol (PVOH) is used in combination with some other compounds in layers. In contrast to the above mentioned polymers, PVOH contains a pendant OH-group, from which H₂O can be formed during thermal treatment by elimination of H₂O (dehydration). Thermal decomposition of PVOH takes place in two stages approximately up to 364 °C and above. In the first stage, depolymerization and dehydration can occur simultaneously, and in the second phase, gasification is dominant. Major gaseous products of a pyrolysis of PVOH are hydrocarbons (40.4 wt.-%), H₂O (20.9 wt.-%), CO₂ (19.2 wt.-%), and CO (18.9 wt.-%). Hydrocarbons in turn mainly consist of C₆ compounds (80.3 wt.-% benzene and 19.2 wt.-% toluene) and CH₄. Additional H₂O can be collected in the liquid phase, which consists out of 41.8 wt.-% oil (mainly heavy naphtha and heavy gas oil) and 58.2 wt.-% H₂O [Shie et al. 2002].

In the case of phenolic resin, it is known that there are three stages of decomposition under pyrolytic conditions: (1) formation of additional crosslinks, followed by (2) breaking and disappearing of the crosslinks and (3) off-stripping of hydrogen from ring structure [Ouchi, Honda 1959]. [Trick et al. 1995] investigated these mechanisms by using Fourier Transform Infrared spectroscopy (FTIR) and gas evolution analysis of carbon-phenolic prepreg: the first region occurred at temperatures between 300 and 550 °C, where mainly H₂O as well as phenol and cresol were formed, both with two peaks at about 150 - 200 °C and 400 °C. The maximum rate of evolution was at 406 °C. In the second stage, which ranged between 400 and 800 °C with maximum

evolution rates at 566 and 594 °C, CO (37.7 wt.-%), CH₄ (25.3 wt.-%), H₂O (24.3 wt.-%), and H₂ (12.7 wt.-%) evolved. In the last stage at temperatures between 560 and 900 °C, increased amounts of CO (50.8 wt.-%) and H₂ (33.0 wt.-%) as well as a smaller amount of H₂O (16.7 wt.-%) could be found in the evolved gases; evolution peaked at 688 and 745 °C (CH₄ was not found).

Additionally, [Wong et al. 2015] conducted batch pyrolysis and thermo gravimetric analyses (TGA) of a phenol-formaldehyde resin and investigated the formation of products by gas chromatography/mass spectrometry (GC-MS). From TGA, it was shown that the maximum weight loss was at about 490 °C. The yield of solid products after pyrolysis tests at temperatures of approximately 1 020 °C was 39.2 wt.-%. Concerning the different pyrolysis products of the vapor, (Figure 15 and Figure 16) it was measured that water was the main product at temperatures up to 535 °C. With an increase above 535 °C up to the final temperature of the pyrolysis tests (930 °C), mainly H₂, CH₄, CO, and CO₂ were the main products. At temperatures between 280 and 580 °C phenol and cresol as well as subdominant di- and trimethylphenol were formed, with a peak of formation at about 490 °C. Benzene, toluene, and xylene were detected mainly between 430 and 580 °C with a peak for benzene and toluene at 535 °C and for cresol at 490 °C. At temperatures >535 °C no di- and trimethylphenol, >585 °C no xylene and cresol and >715 °C no more phenol were formed.

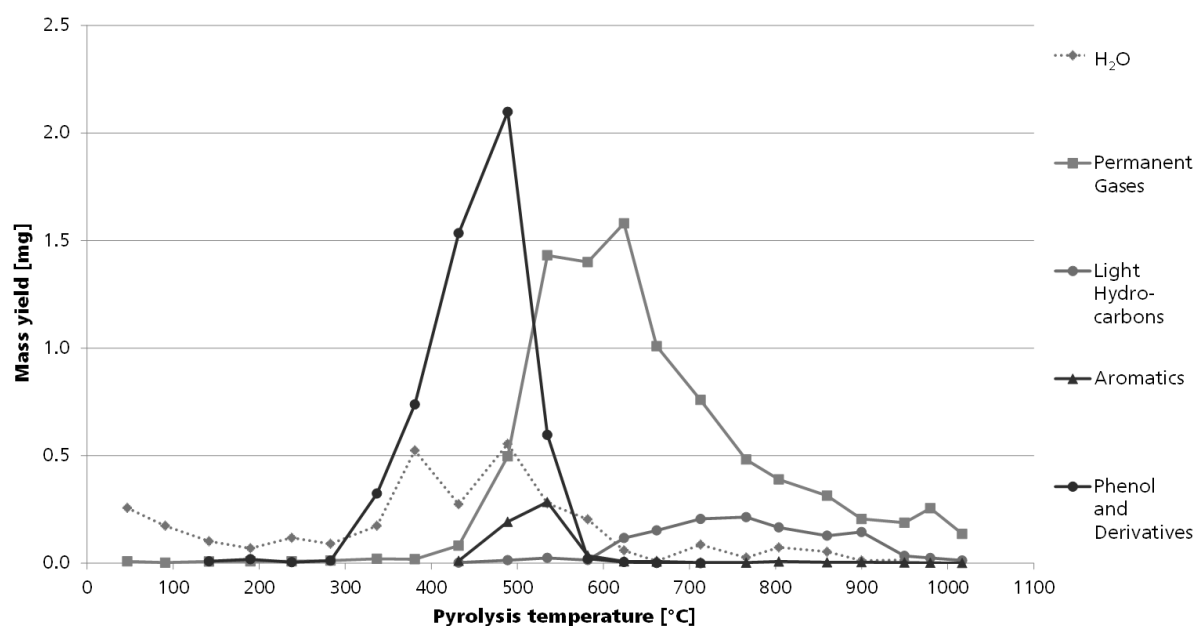


Figure 15: Mass yields of pyrolysis liquid and gaseous products (in groups) from a pyrolysis of phenol-formaldehyde resins at different temperatures (own diagram based on [Wong et al. 2015]).

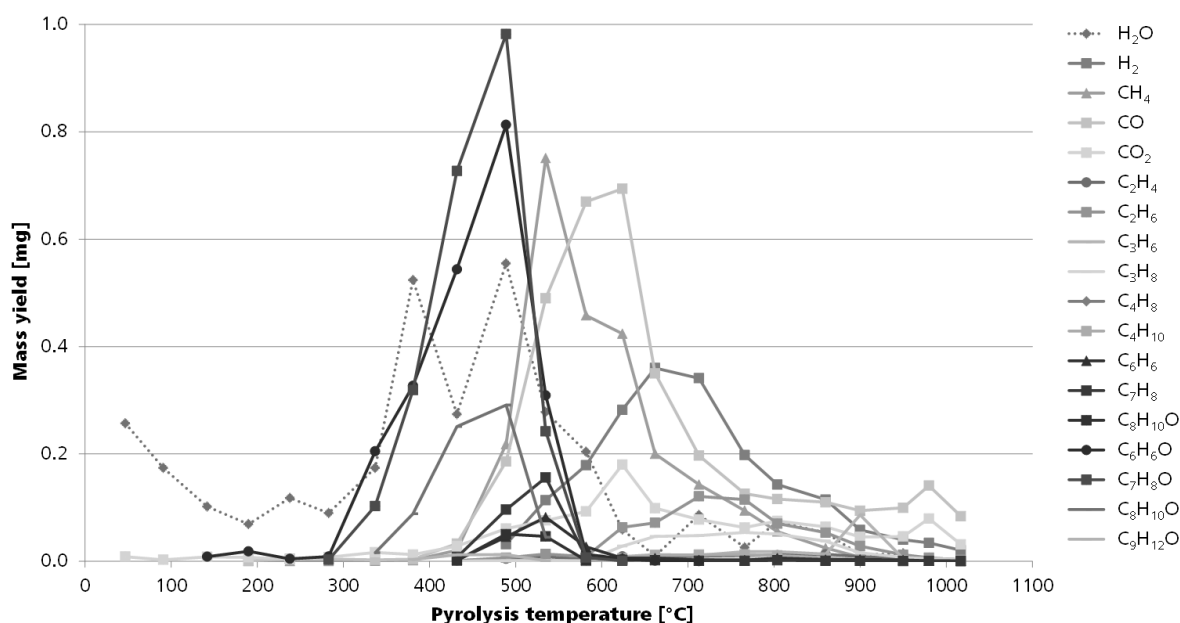
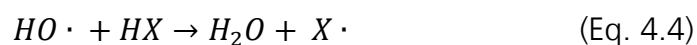
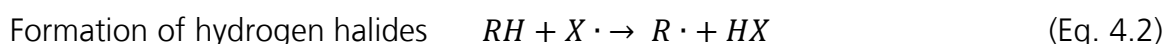
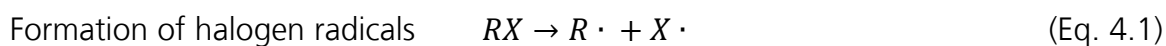


Figure 16: Mass yields of pyrolysis liquid and gaseous products (single compounds) from a pyrolysis of phenol-formaldehyde resins at different temperatures (own diagram based on [Wong et al. 2015]).

As mentioned above, $>535^{\circ}\text{C}$ the formation switched to permanent gases, but also light hydrocarbons were formed. The light hydrocarbons peaked at about 765°C with the dominant gases ethane and ethene. Concerning water and the permanent gases, water peaked at 380 and 490°C , CH_4 at 535°C followed by CO and CO_2 at 625°C and H_2 at 660°C . The formation of the permanent gases corresponded to an increase of pressure, which peaked at about 625°C . From the findings regarding phenol resins, it can be concluded that, with regard to an energetic utilization of pyrolysis liquid and gaseous products, pyrolysis temperatures should be higher than 580°C in order to reduce the amount of aromatics in favor of permanent gases mainly H_2 , C_2H_6 , and C_3H_8 .

4.2 Decomposition of halogenated polymers and plastics

Flame retardants like halogen containing compounds are commonly used additives in the production of plastics for EEE. During combustion of plastics, endothermic processes of warming, decomposition, and ignition take place. Due to the presence of oxygen, free radicals like energy-rich $\text{H}\cdot$ or $\text{HO}\cdot$ are formed, which initiate a degradation of the polymer. Products of these complex reactions are saturated and unsaturated hydrocarbons, which combust due to the presence of a foreign flame or by self-ignition after passing the self-ignition temperature [Dettmer 2001]. Flame retardants weaken these ignition processes by forming other free radicals. According to the “radical trap” theory by [Green 1996], halogenated flame retardants discharge free radicals ($\text{X}\cdot$), which abstract H atoms from olefins by forming hydrogen halides (HX), e.g. HBr in the case of brominated flame retardants (BFR). These molecules are able to weaken the ignition of polymers, because they react with free radicals via radical substitution (Equation 4.1 - 4.5) [Green 1996].



Although under pyrolytic conditions, due to the absence of oxygen, formation of $H \cdot$ and $HO \cdot$ is substantially suppressed, halogen radicals and thereby hydrogen halides are still formed. Formation of these halogen radicals could promote substitution as well as addition reactions. Corresponding reactions will be presented in the next two chapters for brominated (chapter 4.2.1) and chlorinated substances (chapter 4.2.2).

4.2.1 Brominated polymers in plastics

The following sections will give a brief overview at which temperatures thermal degradation of BFR containing plastics takes place and how thermal decomposition is affected by additives like Ca compounds or BFR synergists, like Sb_2O_3 . Two of the most widely used BFR are Tetrabromobisphenol A (TBBPA), e.g. in epoxy resins, and decabromodiphenyl ether (deca-BDE), mainly in a wide range of plastics (Figure 17) [UBA 2007].

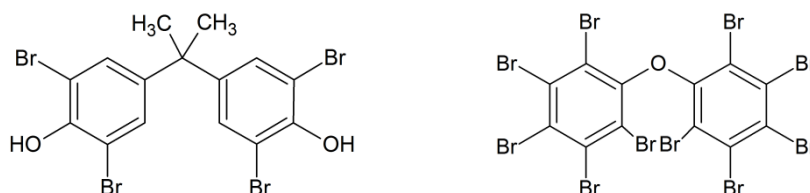


Figure 17: Structures of TBBPA (left) and deca-BDE (right).

In order to understand different decomposition ways of BFR, [Marongiu et al. 2007] developed a detailed kinetic model for the decomposition of TBBPA in a pyrolysis process. They showed four representative reaction classes: initiation, propagation, molecular, and termination reactions. An increase of process temperature or residence time starts debromination with a release of bisphenol A as well as HBr , and later phenol. By a further increase of temperature or time, larger organic compounds, and later, char are produced, while CH_4 and CO are emitted.

[Luda et al. 2002a] investigated the decomposition of a brominated epoxy resin (20 wt.-% Br), based on a mixture of bisphenol A and TBBPA-diglycidyl ether with 4,4-diaminodiphenylsulphone. TGA revealed that the epoxy resin decomposed rapidly in a first step between 295 and 360 °C as well as slowly above 360 °C. During the first step, there are two peaks at 297 °C and 336 °C with weight losses of 32 wt.-% and 30 wt.-%, respectively. Up to a temperature of 600 °C, there is a further decrease of weight of about 13 wt.-% due to char formation. During the first step at about 297 °C,

the brominated additive decomposed because O-CH₂ bonds become broken, brominated aromatic ring structures changed, and some secondary alcohols dehydrated. Formed HBr lowers the stability of the resin and caused that formation of brominated aromatics: The products of these reactions were mono- and di-brominated phenols as well as brominated aromatic and aliphatic ethers [Balabanovich et al. 2005a]. In the second step (at 336 °C), unbrominated compounds of the resin disintegrated while leaving substituted phenols as well as aromatic and aliphatic ethers [Luda et al. 2002a]. Concerning the allocation of Br, it was presented that just a small amount of HBr, but methyl, ethyl, propyl, and propilenyl bromides were formed. As mentioned in chapter 4.1, [Luda et al. 2010] examined the thermal behavior of brominated and non-brominated anhydride-cured epoxy resins based on bisphenol A and phthalic anhydride. They presented that up to a temperature of 340 °C there is no difference between the weight losses of these different resins. However, with an increase of temperature, the presence of Br reduces the thermal stability with the effect that the thermal decomposition of brominated resin starts at lower temperature compared to non-brominated resins. It was concluded that from pyrolysis of anhydride-cured epoxy resins with BFR at a low temperature (approximately 390 °C) the main educts of a (brominated) resin could be recovered, such as bisphenol A diglycidyl ether, TBBPA, and phthalic anhydride. At moderate temperatures (between 420 and 500 °C), mainly brominated aliphatic compounds are produced, char gets formed and the amount of oil decreases. At even higher temperatures (>590 °C) brominated phenols and HBr are produced. However, in previous test series the authors tested another brominated epoxy resin at temperatures between 275 and 350 °C under pyrolytic conditions and found up to 11.9 wt.-% HBr at 275 °C (for 45 min) in a typical closed system and up to 4.5 wt.-% HBr at 325 °C (for 40 min) in a fluidized system [Luda et al. 2005]. The comparison of both studies ([Luda et al. 2005] and [Luda et al. 2010]) shows that there are no strict temperature ranges at which a formation of selected products such as HBr could be depressed or stimulated. This could be underlined by a further study about the decomposition of paper-phenol resin: [Grause et al. 2008] investigated the pyrolysis behavior of TBBPA containing paper-phenol resin laminated PWB. TGA in a temperature range between 40 and 1000 °C and degradation experiments in a temperature range between 50 and 800 °C were performed. Brominated products generated during different temperature levels were characterized. Three levels were found in which the samples degraded. In a first step, with a maximum at 272 - 280 °C, H₂O and CO₂ evaporated from decomposition of cellulose. During the second step (270 - 370 °C), the contained fire retardants degraded by forming Br-products. The production of HBr, as the main product from decomposition of BFRs, proceeded in a temperature range between 270 and 500 °C and was characterized by two single peaks, located at 305 °C and 398 °C. During the third step, beginning with a temperature of 370 °C, phenol resins decomposed and char was formed. The generation of brominated aromatic compounds took place only in a temperature range between 270 and 400 °C. Above 400 °C, Br-products were formed primarily as HBr, so that phenol products generated at 450 °C showed a low concentration of Br. In summary, from [Grause et al. 2008; Luda

et al. 2005; 2010] it can be concluded, that a pyrolysis at 450 °C or higher produces mainly HBr, which is easily separable in a water trap, and just a small yield of brominated aromatic compounds, which could act as precursors for the generation of PBDD/F [Marongiu et al. 2007]. Such allocation of Br to HBr is advantageous regarding an effective debromination of pyrolysis solid products. However, due to the presence of metal oxides, both levels of degradation and Br containing products as well as the yield of solid, liquid, and gaseous products can vary.

As mentioned above, BFR are often used in combination with metal oxides like Sb_2O_3 . Sb_2O_3 acts as synergist in the condensed and gaseous phase of a flame [Efra 2007]. In addition, decomposition products of Sb_2O_3 are catalysts for recombination of hydrogen, hydroxyl, and oxygen radicals [Dettmer 2001; Lewin 2001]. To figure out the reaction behavior of Sb_2O_3 on the thermal decomposition of HIPS with BFR (HIPS-Br), whereat selected samples contained Sb_2O_3 , many authors conducted correspondent tests (e.g. [Bhaskar et al. 2003a; Brebu et al. 2007; Hall et al. 2007; Jakab et al. 2003; Jung et al. 2012; Wu et al. 2014]). The thermal decomposition of HIPS is not affected by presence of BFR: HIPS-Br decomposes between 380 and 520 °C, mainly in one single peak at about 440 °C [Jakab et al. 2003]. In contrast, the thermal decomposition of HIPS-Br with addition of Sb_2O_3 took place in two single stages. The first stage of decomposition is at about 310 to 350 °C, while the second one is from 360 to 450 °C [Wu et al. 2014]. However, depending on the BFR itself, the stages could diversify a bit [Bhaskar et al. 2003a; Jakab et al. 2003] as well as the pyrolysis products [Hall et al. 2007].

As suggested by [Luijk et al. 1991], pyrolysis tests confirmed that Br vaporized during the first stage of decomposition in the form of SbBr_3 and different brominated organic compounds. This reduction on the thermal stability of the plastic also explains that a formation of pyrolysis oil starts at lower temperatures [Brebu et al. 2007]. Without Sb_2O_3 most of the initial Br leaves the system as HBr (in gaseous phase), in contrast, with the BFR synergist this amount decreases in favor of SbBr_3 (in oil) [Bhaskar et al. 2003a; Brebu et al. 2007]. The temperature range, at which the maximum yield of SbBr_3 (above 60 wt.-%) vaporized is between 440 and 650 °C [Rzyman et al. 2010].

Due to an addition of Sb_2O_3 to HIPS-Br, cumulative liquid volumes are not significantly affected and the main oil compounds are ethylbenzene and styrene in both cases. However, the composition of the oils changes: in the cases of tests with Sb_2O_3 , the amounts of styrene, isopropenylbenzene, as well as phenyl- and phenylmethyl-naphthalenes decrease while those of isopropylbenzene, toluene, and ethylbenzene increase [Brebu et al. 2007].

Similar to resins, thermal decomposition of thermoplastics is also influenced due to the addition of Br. For instance, the presence of a BFR decreases the temperature at which the degradation of ABS starts by about 50 °C. Most of the Br could be found in the pyrolysis gas in the form of HBr and just small amounts in the other products. [Bhaskar et al. 2003b] investigated the allocation of Br and N in these non-gaseous products.

They found that during a pyrolysis at 450 °C between 56.0 and 78.8 wt.-% of Br was allocated to a wax fraction, which is part of the solid products and condensate on the reactor walls. Concerning N, between 37.7 and 50.2 wt.-% of N was allocated to the oil phase. The content of Br and N in the oil was 0.615 - 0.712 and 6.000 - 6.150 wt.-% for Br and N, respectively. With regard to the different liquid products, there is no significant change on the main products due to the presence of Br (c.f. chapter 4.1): The main products from a pyrolysis at 450 °C were aromatics such as styrene, toluene, cumene, and ethylbenzene [Bhaskar et al. 2003b].

In order to investigate the influence of Br and Sb_2O_3 in a commercially available ABS copolymer (ABS-Br), which contains a tribromophenol terminated brominated epoxy oligomer and Sb_2O_3 (in sum: 9.3 wt.-% Br and 3.8 wt.-% Sb), [Czégény et al. 2012] conducted TGA on this polymer and additive-free ABS. They found that the temperature of maximum degradation was almost unchanged (419 °C for ABS and 415 °C for ABS-Br); however, in contrast to pure ABS, decomposition of ABS-Br showed one additional peak at a lower temperature (approximately 340 °C), at which Sb_2O_3 increased the decomposition of the Br-containing copolymers by forming SbBr_3 . However, additionally they found out that the amount of this peak is a product not only from the decomposition of Br- and Sb-containing reagents, but also from ABS itself. The authors reasoned that due to an H-abstraction, the decomposition of ABS starts slowly at lower temperatures. In further tests with TGA and GC-MS they investigated the thermal decomposition of mixtures of ABS-Br, PET, and PVC. They showed that all different polymers influence the decomposition of each other. For example, the dehydrochlorination of PVC is increased by adding other polymers. With regard to a pyrolysis of plastics from WEEE, which presents a manifold mixture of polymers, this effect is presumably observable.

More or less, all above reported studies concerning thermal decomposition of polymers and plastics were conducted in small, lab-scaled tests, mainly using quartz-tube glass ampules. In these tests, systematic errors could happen due to small samples sizes, continuous tests cannot be conducted, and residence times of volatile products in the hot zone are extremely short. In order to conduct pyrolysis tests with bigger sample sizes ($0.5 \text{ kg}\cdot\text{h}^{-1}$) and long residence times of volatile products, [Miskolczi et al. 2008] designed a pyrolysis reactor with an extruder as feeding system as well as distillation columns to separate light (B_p : <170 °C), middle (B_p : 170 - 300 °C) and heavy distillates (B_p : >300 °C) besides char and gases. The corresponding schematic diagram of their test plant is shown in Figure 18.

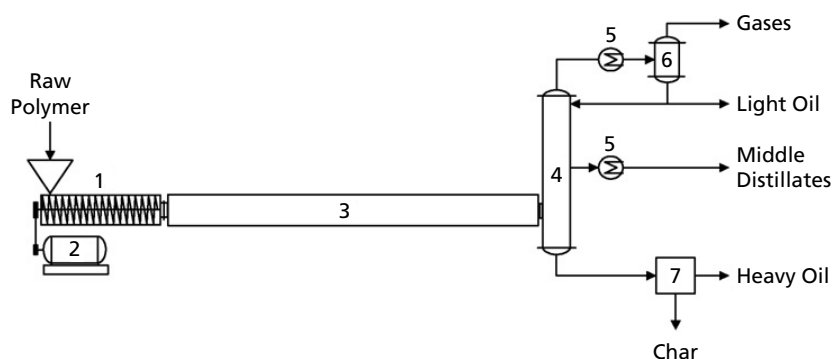


Figure 18: Schematic diagram of continuous pyrolysis plant for a pyrolysis of ABS-Br and HIPS-Br [Miskolczi et al. 2008].

1: Extruder; 2: Electric Motor; 3: Tube Reactor; 4: Distillation Column; 5: Cooler; 6: Separator; 7: Filter.

In pyrolysis tests of ABS-Br and HIPS-Br, which contained 3.2 and 4.6 wt.-% Sb, respectively, at 360 to 440 °C, no gases were formed in the case of HIPS-Br and <5 wt.-% in the case of ABS-Br. Figure 19 shows the concentrations of Br and Sb, respectively, in formed char as well as in the three different distillates from pyrolysis of HIPS-Br. First of all, it can be seen that light oil was more or less free of Br and Sb (maxima were 0.14 and 0.09 wt.-% Br and Sb, respectively) and that the fate of Br and Sb was not affected by temperature concerning concentration in char, middle, and heavy fractions. In the light oil fraction, there is a significant increase of both with an increased temperature. Concerning the content of Br, it was reported that light oil did not contain any organobromine compounds and just small amounts of SbBr_3 . Middle oil contained very low concentrations of Br and in the case of ABS-Br small concentrations of SbBr_3 , too. In contrast, middle oil from HIPS-Br contained high concentrations of SbBr_3 . The authors explained Br-allocation by the reactor design in which volatile products have a long residence time, which promotes thermal degradation of organobromine forming small Br containing molecules, mainly HBr.

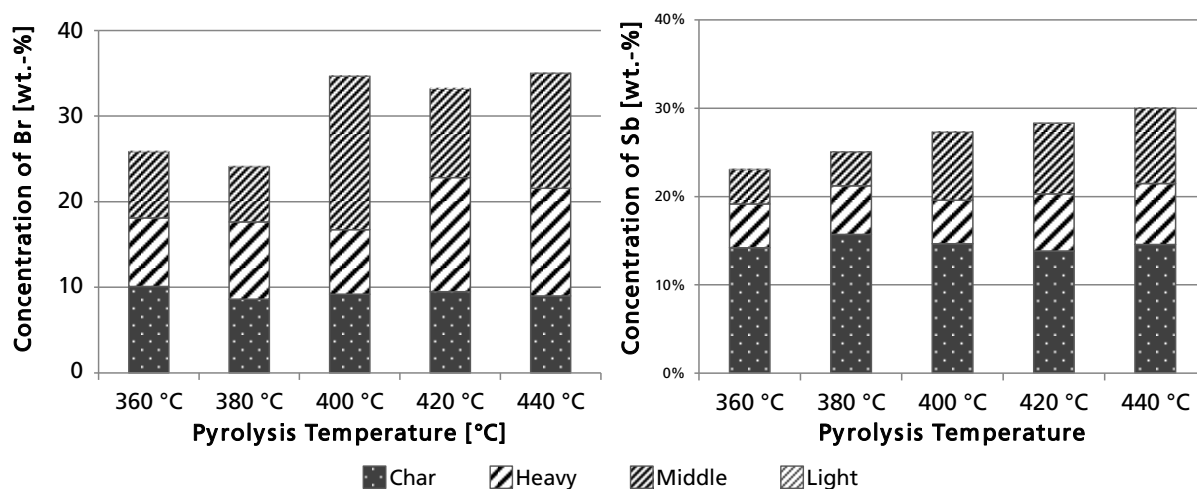


Figure 19: Concentration of Br (left) and Sb (right) in char as well as light, middle, and heavy oil distillates from pyrolysis of HIPS-Br at temperatures between 360 and 440 °C [Miskolczi et al. 2008].

Besides Sb_2O_3 as a synergist for flame retardation, other compounds such as CaCO_3 , NH_3 , or NaOH were tested in pyrolysis experiments with thermoplastics. During pyrolysis and combustion, CaCO_3 , NH_3 , or NaOH could react with halogens and halogen containing compounds in order to fix these in the solid phase [Luda et al. 2005].

4.2.2 Chlorinated polymers and plastics

The decomposition of the most common used chlorinated polymer PVC under pyrolytic conditions is widely analyzed (e.g. [Marongiu et al. 2003; Zhu et al. 2008]), due to the fact that an effective dehydrochlorination of this polymer (first step) is feasible prior to its decomposition (second step), which presents an interesting pre-treatment step for thermal treatment of PVC. The release of Cl and elimination of HCl starts at 252 °C (± 2 °C) [Castro et al. 2012] and could be occurred up to a temperature of 360 °C depending on the heating rate [Castro et al. 2012; Knümann, Bockhorn 1994; Ma et al. 2002]. During this first stage, the mass of solids decreases by about 55 wt.-%, corresponding to the initial Cl content of PVC (56.8 wt.-%) [Ma et al. 2002]. In summary, during first stage of PVC decomposition, the efficiency of dehydrochlorination of pyrolysis solid products is between 96.8 and 99.93 wt.-% [Castro et al. 2012; Ma et al. 2002]. In addition to dehydrochlorination reactions, some first, negligible formations of benzene and naphthalene take place.

A further decrease of pyrolysis solid products mass could occur with an increasing temperature, mainly in a range between 400 and 560 °C [Zhu et al. 2008], where the remaining polyene becomes decomposed by condensation and fragmentation [Marongiu et al. 2003; Miranda et al. 1999]. The products during this second stage of decomposition are substituted and unsubstituted aromatics as well as polyaromatics benzene, naphthalene, and anthracene. Additionally to this cyclisation as well as to the above mentioned condensation and fragmentation, char could be formed due to bridging of the (resulting) polyene structure [Masuda et al. 2006]. The first temperature range starts with a break of C-Cl bonds followed by C-C and C-H bonds, which are more stable due to the higher binding energy [Castro et al. 2012]. In summary, it is known that from a (fast) pyrolysis at 520 °C about 56.0 wt.-% HCl, 28.6 wt.-% gases, 6.3 wt.-% condensates, and 9.1 wt.-% solid char can be gained [Scott et al. 1990]. From breakages of C-Cl bonds, not only HCl but also Cl_2 are formed. Typical mass ratios of $\text{HCl}:\text{Cl}_2$ are $1:1.31 \cdot 10^{-6}$ (by weight) at 250 °C and $1:2.66 \cdot 10^{-6}$ (by weight) at 375 °C [Karama et al. 2013]. However, as shown in tests at 300 °C, a small amount of Cl remains in solid products due to formation of isolated C-Cl bonds in polyene structures ($-\text{C}=\text{C}-\text{CCl}-\text{C}=\text{C}-$). In the corresponding tests, just 92.6 wt.-% of Cl ions evolved as HCl [Horikawa et al. 1999].

In order to increase the effectivity of dehydrochlorination, the flow of a purging gas could be increased. This effects the removing of HCl from the pyrolysis reactor and therefore lowers the possibility of degradation of other polymers or the remaining polyene chain [Yanik et al. 2001].

Similar to dehydrobromination, dehydrochlorination of PVC is (catalytically) influenced due to the presence of other polymers as well as formed HCl (c.f. chapter 4.2.1). However, PVC and formed HCl could affect the decomposition of other polymers, too. As an example, on one hand, in a co-pyrolysis of 95 wt.-% LDPE and 5 wt.-% PVC the intensity of the second decomposition step of PVC is lowered due to the presence of PE. On the other hand, the formation of alkenes from PE (c.f. chapter 4.1) takes place at higher temperatures. Additionally, yields of aromatics, mainly naphthalene, acenaphthalene, and phenanthrene, could be observed already at a temperature of 800 °C instead of 1 000 °C [Blazsó et al. 1995].

For the production of plastics, PVC is often combined with Ca based fillers such as dolomite (CaMgCO_3)₂, CaO, Ca(OH)_2 , or CaCO_3 . These compounds react during the pyrolysis process with simultaneously formed HCl by forming solid chlorinated products [Zhu et al. 2008]. In contrast to other metal oxides (see below), the bridging of polyene chains seems to be diminished [Masuda et al. 2006]. Compared to Ca compounds, the decomposition of PVC is much more influenced with an addition of ZnO. From TGA it can be seen that in a PVC-ZnO mixture (1:1 molar ratio) the mass loss begins at about 200 °C, which reveals that activation energy for the first step of PVC dehydrochlorination (approximately 140 kJ·mol⁻¹) is lowered due to present ZnO [Kosuda et al. 2012]. From this temperature to approximately 280 °C, ZnO reacts with PVC by forming water and ZnCl_2 in a solid-solid reaction [Kosuda et al. 2012; Zhang et al. 2000]. During this reaction, two kinds of dehydrochlorination mechanisms take place: one of which includes C-C single bonds forming due to cross-linking and the other mechanism includes side isomerization of these previously formed compounds forms olefins and aromatics [Kosuda et al. 2012].

Besides these reactions, those with several alternate metals, metal oxides and metal chlorides have been studied. Co-pyrolysis tests with PVC and different metal oxides (Al_2O_3 , CeO_2 , Co_3O_4 , Cr_2O_3 , CuO , Fe_2O_3 , MoO_3 , PbO_2 , TiO_2 , ZrO_2 ; 5 wt.-% by weight) were conducted by [Sivanlingam et al. 2003] in order to analyze the influence of these metal oxides on the thermal degradation of the polymer. It was shown that just some of the metal oxides ($\text{Fe}_2\text{O}_3 > \text{Co}_3\text{O}_4 > \text{MoO}_3 > \text{CuO} > \text{Cr}_2\text{O}_3 > \text{pure PVC}$) decrease the temperature of first stage decomposition, while other increased that temperature (pure PVC). However, no metal oxide influenced the second stage degradation temperature by more than 10 °C. In further tests with corresponding metal chlorides, a strong influence on the decomposition of PVC was shown, which revealed that metal chlorides are formed from oxides during dehydrochlorination and influence the degradation afterwards. Additionally, a good correlation between Lewis acidity of the metal chloride and the onset temperature of the thermal degradation during co-pyrolysis was obtained.

Similarly, tests by [Müller, Dongmann 1998] revealed a strong correlation between the Lewis acidity of different metal chlorides and the maximum yield of formed char: with a decrease of Lewis acidity ($\text{AlCl}_3 > \text{GaCl}_3 > \text{FeCl}_3 > \text{BiCl}_3 > \text{SbCl}_3 > \text{ZnCl}_2$) the yield of char decreased from 27.0 wt.-% for AlCl_3 to 20.9 wt.-% for ZnCl_2 during a pyrolysis process at 600 °C. The Lewis acids cause a cationic polymerization and thereby a bridging of polyene chains, which lead to a formation of char.

Similar reduction of solid product yields as well as an increasing amount of liquid products could be observed in a co-pyrolysis of PVC with ZnO or Fe_2O_3 . In contrast to ZnO and Fe_2O_3 , significant effects on the yields of liquid and gaseous product were not observed in the case of PbO and the Rare Earth Oxides (REO) La_2O_3 , Nd_2O_3 , and CeO_2 [Masuda et al. 2006].

Further tests regarding the influence of metals and metal oxides on the thermal decomposition of PVC and its decomposition products were conducted by [Blazsó, Jakab 1999] using pyrolysis GC-MS at 350, 450, and 550 °C. They revealed that an addition of Al, Fe, Zn, Fe_2O_3 , or TiO_2 decreased the minimum temperature of dehydrochlorination due to a weakening of the C-Cl bonds in PVC. In the cases of an addition of Fe or Zn to PVC pyrolysis, the evolution of HCl as well as benzene and toluene were depressed compared to pure PVC. Contrary to Fe and Zn, an addition of Al led to a stronger emission of HCl and toluene as well as an earlier completed formation of benzene. The addition of TiO_2 , Fe_2O_3 , and CuO led to a lower yield of benzene at all three temperature levels; however, especially in the case of CuO , the depression was strongly increased by raising the temperature from 450 to 550 °C, while in the case of TiO_2 and Fe_2O_3 the depression decreased. An addition of Al_2O_3 resulted in an increased formation of benzene at all three temperature levels. The evolution of toluene was slightly heightened by Al_2O_3 just at 350 °C and 550 °C; at 450 °C the evolution was suppressed. All other oxides led to a suppressed formation of toluene. Concerning the evolution of HCl, it is interesting to see that by adding TiO_2 at 450 °C roughly two times more HCl is formed than in the case of pure PVC, but at 350 and 550 °C, the amount of HCl is lower than in the case of pure PVC. By adding Fe_2O_3 , the formation of HCl is depressed at all three temperature levels; by adding CuO just at 550 °C. The results by [Blazsó, Jakab 1999] revealed that a formation of benzene is suppressed by the studied additives if a formation of chlorides takes places (Fe, Zn, CuO and TiO_2). Correspondingly, the formation of HCl is depressed as well; it is more depressed in the case of metals compared to metal oxides.

4.2.3 Formation and avoidance of (poly-)halogenated aromatic compounds

Thermal decomposition on halogenated flame retardants can cause the formation of highly toxic and persistent polycyclic aromatic hydrocarbons (PAH), polyhalogenated aromatic hydrocarbons (PXAH), polyhalogenated biphenyls (PXB), as well as dioxins and furans like polyhalogenated dibenzo-*p*-dioxins and furans (PXDD/F) [Reuter et al. 2013]. The chemical structures of PXDD, PXDF, and PXB are shown in Figure 20.

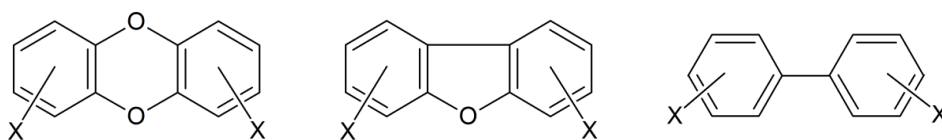


Figure 20: Chemical structures of PXDD, PXDF, and PXB.

Concerning PAH and PXB, [Müller et al. 1997] and [Müller, Dongmann 1998] quantified the amounts of PAH, methyl-PAH, penta-, and hexachlorobenzene, as well as polychlorinated biphenyls (PCB) 206 and 209 during the pyrolysis of PVC without any additives as well as in the presence of Al and metal chlorides AlCl_3 , BiCl_3 , GaCl_3 , FeCl_3 , SbCl_3 , and ZnCl_2 . Concerning penta- and hexachlorobenzene as well as both PCB compounds, no clear correlation could be found. In contrast, with just a small increase of any above listed metal chlorides or Al, the yield of PAH and methyl-PAH such as 1-methyl-naphthalene, 2-methyl-naphthalene, and 2,6-dimethyl-naphthalene decreased greatly. However, contrasts between two groups of metal chlorides had been revealed: metal chlorides with B_p below the temperature of polyene formation from PVC (250 °C), namely AlCl_3 , GaCl_3 , and SbCl_3 , cause that the level of naphthalene decrease much more slightly than those which have higher B_p , which reach a constant level with small portions of metal chlorides. The authors explained this by a partial existence of low boiling metal chlorides in the vapor phase, which cannot react with the PVC any longer. Tests with Cu(I)-halides CuCl, CuBr, and CuI showed similar effects concerning an increase of formed char and the reduction of aromatics. However, just CuCl was able to reduce the yield of chlorobenzenes.

In comparison to PAH, a group of substances with a higher toxicity are dioxins and furans (PXDD/Fs) [Eljarrat, Barceló 2004]. Their formations usually start under presence of halogens and oxygen and are catalytically increased by presence of heavy metals, mainly Cu and its oxides or halides [Dettmer 2001; Müller, Dongmann 1998; Sakai et al. 2001]. During combustion, polychlorinated dibenzo-*p*-dioxins and furans (PCDD/F) are mainly formed in a temperature range between 260 °C and 430 °C (heating phase – in-situ synthesis⁷) and between 250 °C and 450 °C (cooling phase – de-novo synthesis).

⁷ The in-situ synthesis is also known as “precursor theory”, because it needs precursor chemicals like halogenated phenols, benzene, biphenyl, or diphenyl ether for synthesis [Dettmer 2001].

De-novo synthesis of PCDD/F, which is catalyzed by fly ash, takes place if HCl or Cl₂ is present; however, those formations are high in the case of Cl₂ versus HCl [Ni et al. 2012]. Precursor chemicals for the in-situ synthesis of PXDD/Fs cannot be formed from incineration of polymers without additives, however, depending on the polymer itself, aromatic substances can be formed and can become halogenated subsequently [Dettmer 2001].

Due to the presence of many different aromatic substances in WEEE, especially in the form of BFR, a formation of PXDD/F is feasible not only if oxygen is present (combustion), but also in the case of pyrolysis. While under oxidative atmosphere, PCDD/F decompose at temperatures above 800 °C [Dettwiler et al. 1997], formations under pyrolytic conditions could take place at temperatures of 600 °C and, perhaps, even higher [Joung et al. 2006]. Additionally, in contrast to a formation of PCDD/F during combustion, the yield of precursors such as chlorobenzene, which are formed in a pyrolysis of PVC, could increase with an increase of temperature: [Masuda et al. 2006] presented that during a pyrolysis of PVC at 400 °C and a residence time of 30 min and at 800 °C for 10 min, the formation of chlorobenzene was detected only at pyrolysis at 800 °C.

One pathway for the formation of one exemplary polybrominated dioxin and one furan under pyrolytic conditions will be explained in detail: As mentioned above (chapter 4.2), from halogenated compounds such as mono- or di-brominated phenols, or halogenated flame retardants such as TBBPA free radicals could be formed due to thermal stress [Hornung et al. 2003]. As an example, by heating *o*-, *p*-bromophenols or *o*-brominated TBBPA above 250 °C an unstable cyclohexadienone structure via keto-enol tautomerism can be formed. Further heating results in a C(allylic)–Br bond scission by forming an alkoxy radical and generates a Br radical [Wang et al. 1992]. Similar results could be drawn for dibrominated phenols such as 2,4- or 2,6-dibromophenol [Hornung et al. 2003].

In a further reaction, 2,4,6-tribromophenol could be formed from a previously gained phenoxy and Br radical. However, concerning the formation of dioxins, the more interesting reaction is between 2,4- or 2,6-dibromophenol and a phenoxy radical. As an intermediate product, a phenoxyphenol get formed, which could react further to a dibromodibenzo-*p*-dioxin (2,7-dibenzo-*p*-dioxin) under the formation of HBr either directly or via a Smiles rearrangement (Figure 21). Another feasible product is, for instance, tribromodibenzofuran (Figure 22) [Balabanovich et al. 2005b; Hornung et al. 2003].

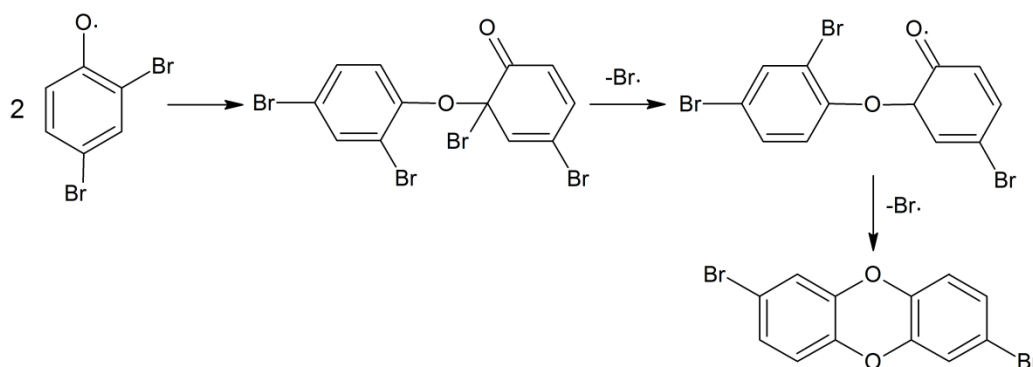


Figure 21: Formation of 2,7-dibenzo-*p*-dioxin on the pyrolysis of 2,4-dibromophenol [Balabanovich et al. 2005b].

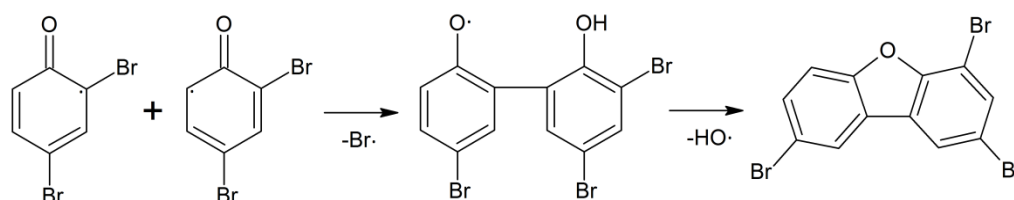


Figure 22: Formation of tribromodibenzofuran on the pyrolysis of 2,4-dibromophenol [Balabanovich et al. 2005b].

[Joung et al. 2006] determined the concentrations of PCDD/F from a pyrolysis of PVC at 600 °C for the different pyrolysis products. It was shown that the major parts of PCDF (85.3 wt.-%) and PCDD (85.8 wt.-%) were found in the oil while just a small amount was left in the char (9.3 wt.-% and 10.8 wt.-%, respectively) or vaporized to the gas (5.4 wt.-% and 3.4 wt.-%, respectively). Similar results were obtained for polychlorinated biphenyls (PCB).

In comparison to PCDD/F, most of the polybrominated dibenzo-*p*-dioxins and furans (PBDD/F) are absorbed by solid products like char (83 wt.-%) and just a small amount can be found in flue gas (17 wt.-%) [Lai et al. 2007]. This may be related to the higher molecular weights and lower vapor pressure of PBDD/F [Birnbaum et al. 2003]. Due to this, the temperature for decreasing the total amount of PBDD/F is higher than those of PCDD/F [Lai et al. 2007].

Concerning the formation of PBDD/F, there are several publications with various results. [Luijk and Govers 1992] investigated the formation of PBDD/F from polybutylene terephthalate (PBT) containing decabromobiphenyl (deca-BB) and ABS containing TBBPA at temperatures between 400 and 700 °C. In the case of PBT + deca-BB, they reasoned that there is no formation of PBDD, but there were formations of PBDF with a maximum at 500 °C. For ABS + TBBPA the maximum yield of PBDF was at temperatures between 600 and 700 °C, while PBDD was formed at a temperature of 600 °C. A former study by [Luijk et al. 1991] quantified the yield of PBDD/F from pyrolysis of HIPS deca-BDE and Sb₂O₃ at temperatures between 275 and 825 °C. There were two main results: (1) just PBDF and no PBDD were detected and (2) the yield of PBDF decreased significantly with an increasing temperature. The highest yields were at 275 °C (4 280 ppm), where no degradation of HIPS is observed, and at 360 °C (1 200 ppm). Similar results were

presented by [Bhaskar et al. 2002], who revealed that HIPS containing both Sb_2O_3 and deca-BDE produces dioxins at a temperature of 275 °C. Depending on the temperature during thermal treatment of halogen containing plastics, various $\text{Me}_x\text{-R}_y\text{-X}_z$ -compounds are formed. In contrast, from low-temperature pyrolysis (290 - 310 °C) of TBBPA-based epoxy resins no PBDD/F were detected by [Balabanovich et al. 2005a]. Additionally, present metals and metal oxides could influence the formation of brominated compounds, which could act as precursors for the generation of PBDD/F [Marongiu et al. 2007; Sakai et al. 2001]. As an example, [Dumler et al. 1989] examined formations of PBDF from pyrolysis of deca-BDE as well as samples of PBT mixed with different ratios of deca-BDE and Sb_2O_3 . As shown in Figure 23, formations of PBDF are significantly higher in the case of any mixture compared to pure deca-BDE. In addition, it is obvious that due to presence of PBT and Sb_2O_3 higher amounts of tri- and tetrabrominated dibenzofurans were formed while from pyrolysis of pure deca-BDE yields of mainly hexa- and heptabrominated dibenzofurans were formed. However, not only due to the presence of Sb_2O_3 , but also from conventional pyrolysis at high temperatures between 700 and 900 °C formations of PXDF with smaller numbers of brominated ligands compared to the flame retardant take place. Tests with PS and PE, both separately mixed with deca-BDE or penta-BDE, revealed that mainly tri-brominated dibenzofurans were formed from plastic mixtures with Penta-BDE while mainly tetra- and penta-brominated dibenzofurans were formed during pyrolysis of plastics mixtures with deca-BDE [Thoma et al. 1987].

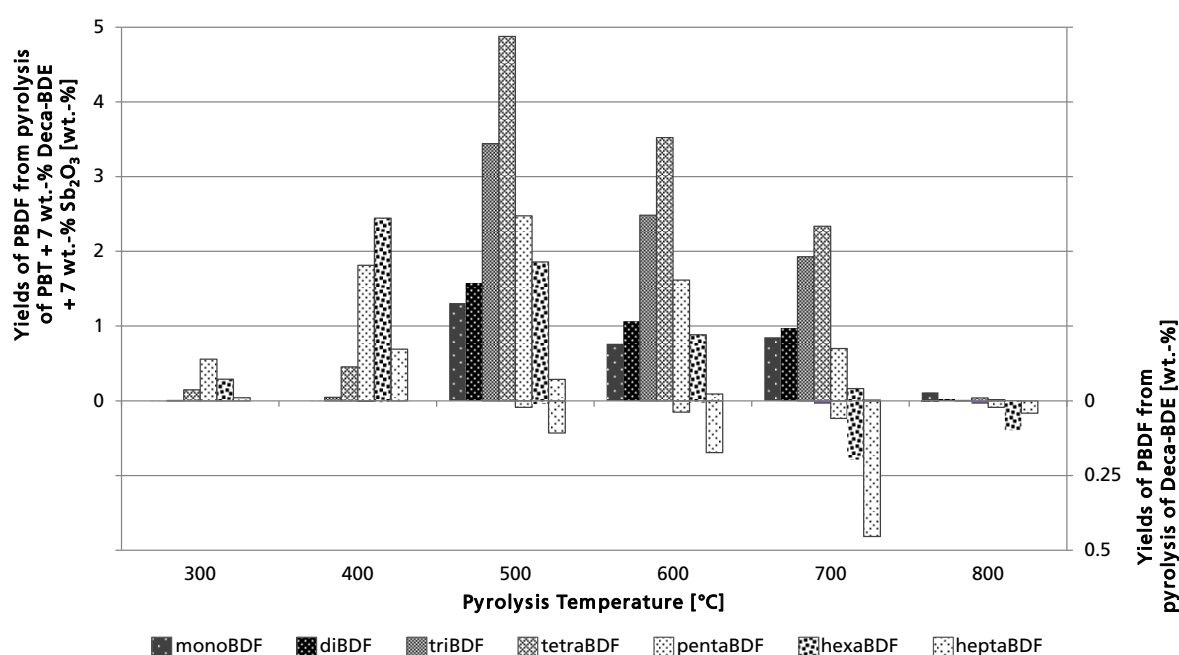


Figure 23: Yields of PBDF from pyrolysis of PBT + 7 wt.-% deca-BDE and 7 wt.-% Sb_2O_3 (primary ordinate) and from pyrolysis of deca-BDE (secondary ordinate) (in wt.-%). Second named yields are shown in reverse order (own diagram based on [Dumler et al. 1989]).

In summary, cause plastics from WEEE could contain both polymers with aromatic compounds (e.g. phenol or epoxy resins) and halogens (e.g. from ABS-Br, HIPS-Br or PVC), a formation is feasible at temperatures of about 200 - 800 °C and a prior quantitative determination of PXDD/F formation is almost impossible due to the high

number of different kind of polymers and additives [Ebert, Bahadir 2003; Luijk et al. 1991]. Additionally, the presence of metals could make a formation of PBDD/F possible up to temperatures of about 1 200 °C. Therefore, in a pyrolysis process, low and medium temperature ranges should be either skipped as fast as possible to prevent the formation of these toxic substances, or the formation of precursor substances should be avoided and halogens vaporized as fast as possible, mainly as hydrogen halides. Although applying a pyrolysis temperature above 850 °C leads to decreased total yields of PXDD/F [Lai et al. 2007], this temperature could cause further challenges and problems like a high energy consumption, melting of metals in the solid residue, and a decrease of pyrolysis oil and gas quality concerning an energetic utilization [Wong et al. 2015]. On this account, pyrolysis solid products and oils from tests with temperatures between 450 °C and 650 °C should be analyzed to determine the yields of PXDD/F.

4.3 Pathways for dehalogenation

Dehalogenation of pyrolysis products is one of the main aims for an eco-friendly pyrolysis process. From the literature, there are several known pathways for dehalogenation. Generally, these could be classified in following three groups [Yang et al. 2013b]:

- 1) First Dehalogenation, followed by decomposition of plastics.
Example: Two-stage pyrolysis
- 2) Dehalogenation and decomposition of plastics at the same time.
Example: Co-Pyrolysis
- 3) First Decomposition, followed by dehalogenation of pyrolysis vapor/oil.
Example: Ad- or Absorption of halogens in vapor phase mode

In the next subsections, dehalogenation by two-stage pyrolysis will be summarized as well as by using different additives.

Previously, with regard to the third mentioned pathway, an industrial process should be described: The process "Pyromaat" was developed in an industrial scale to recover Br from WEEE as combination of pyrolysis and gasification. Pyrolysis was conducted at 550 °C for a minimum of 15 minutes. The produced char-metal mix was used as feedstock for pyrometallurgical processes. The uncondensed gas fraction was lead through a high temperature gasifier at 1 230 °C to crack tars and produce a syngas. The syngas is cleaned by a NaOH-scrubber to remove and recover halogens, in the form of NaBr/NaCl. The remaining syngas is used in a combustion chamber where NH₃ is injected as neutralization agent for remaining halogenated compounds. Halogens from the input material volatilized as HBr/HCl, Br₂/Cl₂, and, in connection with Sb₂O₃, as different halogenated Sb-compounds, which hydrolyze to Sb₂O₃ in the scrubber. In summary, the process was able to recover up to 96 wt.-% of Br and 97 wt.-% of Cl [Boerrigter et al. 2002]. However, both halogens are recovered as HX or NaX and have

to be separated further in order to use both in adequate processes. Besides other aspects, due to the very complex separation (cf. [Coenen et al. 1979]) of such halogens, there are no huge advantages for a recovery.

4.3.1 Two-stage pyrolysis

A two-stage pyrolysis, with or without additives, is one option to reduce the amount of halogens, mainly in the pyrolysis oil. It is based on the different temperature dependencies of thermal degradation of polymers and flame retardants. As mentioned above, [Bockhorn et al. 1998] and [Ma et al. 2002] described this degradation behavior for chlorinated, [Hornung et al. 2003] and [Jakab et al. 2003] for brominated polymers. However, due to the composition of the feedstock and the use of additives, there could be different levels of thermal degradation.

[Bockhorn et al. 1998; 1999] investigated the thermal degradation behavior of halogenated plastics, mainly PVC, and showed that dehydrohalogenation takes place at lower temperatures than the degradation of thermoplastics. Due to this, they estimated that a separation of pyrolysis products in fractions containing halogens and halogen free fractions could be possible, corresponding to the two degradation stages. In a cascade of well stirred reactors, [Bockhorn et al. 1998] were able to separate about 99.6 wt.-% Cl in a mixture of PVC, PS, and PE (1:6:3 by weight) as well as to form separated monomers of the feedstock-polymers. In this case, a cascade of three reactors at temperatures of 330 °C, 380 °C, and 440 °C were used.

Based on investigations about two-stage decomposition reactions of halogen containing polymers like PVC, SAN, or ABS, the patented⁸ and trademark-protected process Haloclean[®] was developed with the aims to produce halogen free oils, which can be used energetically in an engine, as well as to produce HBr for the chemical industry. The Haloclean[®] process was developed in two projects (Halocleanconversion and Haloclean-application⁹) funded by the European Union (EU), as two-stage process for Br containing plastics: in the first stage, at about 350 °C, mainly HBr is formed, while in a second stage, at about 450 °C, pyrolysis products with very small amounts of halogens are formed. The residence time at both stages was 120 minutes. By using these parameters of temperature and residence time, in pyrolysis solid products the lowest values for PBDD/F¹⁰ were detected as 89.47 µg PBDD and 3.23 µg PBDF per kg solid products.

⁸ International Publication Number of Patent: WO 02/50484 A1.

⁹ G1RD-CT-1999-00082 (Process integrated thermal-chemical treatment of halogens containing materials as source of halogens free fuels for steel production and residues for noble metal recovery, Haloclean-conversion) and G1RD-CT-2002-03014 (Waste management and recycling of WEEE – process integrated thermal-chemical treatment of halogens containing materials, Halocleanapplication).

¹⁰ The amounts of PCDD/F were not analyzed [Koch 2007].

These were the lowest values in different combinations of residence time and temperature, but they have been about 4.5 times higher than those values of the feedstock¹¹ [Koch 2007]. Additionally, the aim to produce oil free of halogens was not reached and the concentrations of both PBDD/F and PCDD/F were not analyzed in pyrolysis oils. However, from literature it is known that PBDD/F are formed mainly in a temperature range below 500 °C [Luijk et al. 1991] and allocate mainly to the char [Lai et al. 2007], while PCDD/F can be found mainly in the liquid phase [Joung et al. 2006]. With regard to these aspects, quantification of PXDD/F was incomplete and suggests that selected temperatures could be suboptimal, because PCDD/F are mainly formed in these temperature ranges. In order to decompose PBDD/F in the oil under formation of HBr [Hornung et al. 2007], the process chain was successfully upgraded with a downstream polypropylene reactor. Concerning energy efficiency, a novel approach based on heated metal spheres, which were fed to the process directly with the feed, was used for the implementation of the process. Due to added, hot metal spheres, application of energy was increased and produced char partly grinded, which again, increased the application of energy [Koch 2007]. Nevertheless, a huge amount of energy is necessary in order to heat the process for a residence time of four hours.

In order to analyze the influence of heating rate in combination with two-stage pyrolysis on debromination effectiveness, a series of pyrolysis tests with HIPS-Br (13 wt.-% deca-BDE, 5 wt.-% Sb₂O₃) were conducted by [Grause et al. 2012]. In first test runs, it was shown that approximately the same amount of Br released from HIPS-Br at 330 °C and 360 °C and just a slightly higher amount at 700 °C. Therefore, a debromination of HIPS-Br was successfully tested in two-step pyrolysis at 330 and 700 °C: oil from the first stage contained 23 times higher Br concentrations than those from the second stage. Additionally, in first stage oil 16.3 wt.-% SbBr₃ was found, while the oil from second stage did not contain any SbBr₃. Concerning polybrominated compounds, concentrations of dibromodibenzofurans were 55 times higher in stage one oil than in stage two oil. However, tetra- and pentabromodibenzofurans were 1.6 and 3.6 times higher in stage one oil than in stage two oil. Furthermore, oil from one-stage pyrolysis at 700 °C with a heating rate of 5 °C·min⁻¹ and stage two oil from two-stage pyrolysis at 330 and 700 °C had similar concentrations of brominated dibenzofurans. Additionally, due to a higher heating rate of 50 °C·min⁻¹ in a one-stage pyrolysis, concentrations of all brominated compounds become reduced, which reveals that high heating rates promote efficient debromination. Regarding quantities of pyrolysis products, it has to be mentioned that highest yields of pyrolysis oil (79 wt.-%) were reached from one-stage pyrolysis at 50 °C·min⁻¹ and this becomes reduced due to a lower heating rate (5 °C·min⁻¹) to just 55 wt.-%. From two-stage pyrolysis, just 44 and 36 wt.-% were

¹¹ Used PWB already contained 19.89 µg PBDF and 0.74 µg PBDD per kg PWB.

produced at heating rates of 50 and 5 °C·min⁻¹, respectively. Similar effects from a pyrolysis of a plastic mixture containing PE, PP, PS, and PVC were reported by [Bhaskar et al. 2006].

The effectiveness of two-stage pyrolysis processes for dehalogenation is not only affected by heating rate, but also by the composition of the input material. As shown in pyrolysis experiments (450 and 600 °C for 20 s each) with PWB-samples consisting of brominated phthalic polyester and ceramic fibers, the effectiveness decreased strongly [Blazsó et al. 2002]. The authors recommended that the decomposition of the contained flame retardant bisphenol A was not successful by two-stage pyrolysis. Furthermore, pyrolysis tests with different additives (CaO, ZnO, Na₂CO₃, Na₂SiO₃, NaOH, and two kinds of molecular sieves (5A and 13 X)) were performed to identify relative amounts of CH₃Br as well as Br- and Br₂-phenols. Concerning matters of health, safety, and product utilization, the quantity of these products is crucial. For instance, CH₃Br is potentially explosive, very toxic and classified as water pollutant [DGUV 2016]. An increased yield of CH₃Br occurred after the addition of molecular sieve 5A, ZnO, and NaOH. The addition of CaO or ZnO resulted in an increased yield of Br- and Br₂-phenols, whereas all other kinds of additives, mainly NaOH and Na₂SiO₃, caused a decreased yield. The most significant reduction of CH₃Br, Br-, and Br₂-phenols was observed after the addition of molecular sieve 13X as well as after the addition of Na₂SiO₃. These results revealed that the use of molecular sieve 5A, ZnO, or NaOH is disadvantageous while that of molecular sieve 13X or Na₂SiO₃ seems to be advantageous. Further analyses on the formation of other brominated compounds, mainly HBr, molecular bromine (Br₂), and brominated metals, are necessary to figure out which additives have the most promising effects.

4.3.2 Use of metal-free additives

Another approach for dehalogenation and avoidance of polyhalogenated compounds such as PXDD/F, is an increase of hydrogen concentration in the feedstock in order to form HX. Besides pure hydrogen, hydrogen-rich alkanes such as n-hexane (C₆H₁₄) [Evans et al. 1991] and eicosane (C₂₀H₄₂), or tetralin (1,2,3,4-tetrahydronaphthalene) [Borojovich, Aizenshtat 2002a; Borojovich, Aizenshtat 2002b] could be added to receive a homolytic scission of C-X bonds and a formation of HX (Equation 4.6) [Hornung et al. 2005].



The use of biomass as an additive is another source for hydrogen. [Liu et al. 2013] performed a co-pyrolysis of Br containing plastics from WEEE and biomass in a temperature range between 400 and 600 °C. Adding biomass to the pyrolysis of WEEE seems to prevent the formation of PBDD/F due to high amounts of H₂, which leads to a formation of HX via a homolytic scission of C-X Bonds. Additionally, a higher amount of added hydrogen in the input could deliver better results in the pyrolysis oil concerning the C/H-molar ratio. [Liu et al. 2013] presented that the yield of oil was increased during

the co-pyrolysis (62.3 wt.-%) compared to a pyrolysis of biomass (46.3 wt.-%) or WEEE (53.1 wt.-%). However, due to the co-pyrolysis of WEEE with biomass, additional water could be given to the system, which is often not easy to separate from pyrolysis oil and has to be deposited afterwards. Concerning dehalogenation, an additional effect was observed: with an increase of temperature from 400 to 600 °C, the amount of Br captured in the char increased significantly [Liu et al. 2013]. As mentioned above, a separation of Br from the pyrolysis char is more complex, compared to a separation of HBr from the pyrolysis vapor.

Utilization of hydrogen-rich polyolefins such as PE or PP, is feasible, too. As an example, there is a hydrogen abstraction from PE or PP, which makes a formation of stable molecules (e.g. HBr, 2-bromophenol) under pyrolytic conditions possible (Figure 24), which suppress a formation of PBDD effectively.

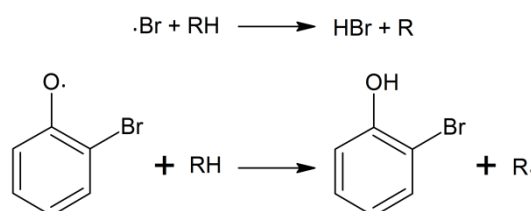


Figure 24: Reductive debromination of Br containing radicals by using PE or PP (RH) [Hornung et al. 2003].

A co-pyrolysis of PP and 2,6-dibromophenol causes, not only changes of the PP concerning chemical composition, but also visual effects: from FTIR it was shown that double bonds and aromatic structures become part of the polymer. Additionally, it becomes black and waxy. From a co-pyrolysis of PP and TBBPA, alkylated aromatics were found in the solid residue as well as HBr and small brominated aliphatic compounds, such as CH_3Br in the gaseous phase. Both products indicate the debromination reactions via hydrogen and alkyl transfer reaction. High debromination effectiveness were reported from pyrolysis of Br containing PWB, in which the yield of bromophenol decreased to approximately 1.3 wt.-% of the initial amount [Hornung et al. 2005]. Other tests with PP as agent for debromination were conducted by [Ma et al. 2015] in a co-pyrolysis of different mixtures with brominated HIPS containing Sb_2O_3 (7.1 wt.-% Br, 4.2 wt.-% Sb) at a temperature of 410 °C. With an increase of PP in the mixture, there was a non-linear effect on the yields of pyrolysis products wax and oil (the yield of char was not influenced significantly): When 10 wt.-% of PP was added, the yield of wax and gas increased while those of oil decreased; however, this effect was reversed, if more than 20 wt.-% of PP was added. Concerning the effect of PP on the pyrolysis products, it was clearly seen that mainly the amount of styrene increased greatly, while aromatic hydrocarbons such as ethylbenzene, 1,3-diphenylpropane, 1,3-diphenylbutane, and 1,3-diphenyl-1-butene decreased slightly. Additionally, due to the presence of PP, the Br content in pyrolysis oil decreased theoretically when PP was added, but even greater in practice: by adding 30 wt.-% of PP, the expected content of Br was 2.94 wt.-% while the measured content was 1.62 wt.-%.

By comparing PE and PP, PP has the positive effect that it needs lower amounts of energy compared to PE. As shown by [Hornung et al. 2003], the effectiveness of debromination by using PP at 350 °C is better than using PE. The authors explained this fact due to the dependency of the above mentioned reaction (Figure 21) on the C-H bond strength of the polyolefin. The energy of the *tert*-H-C bond in PP is lower than those of the *sec*-H-C bond in PE. In order to achieve the same debromination effectiveness of PP by using PE, the temperature has to be set to 400 °C. Additionally, PE and PP show different effects concerning pyrolysis product compositions, mainly pyrolysis gases. Organic gases from tests with HIPS-Br and PP/PE (4:1 by weight) at 430 °C suggest that less C₂H₄, C₂H₆, C₄H₁₀, and C₅H₁₂ got formed in a co-pyrolysis of HIPS-Br with PP compared to a co-pyrolysis with PE. If antimony (as Sb₂O₃,) is present; additionally, no C₄H₁₀ and C₅H₁₂ as well as just a very small amount of C₄H₈ get formed in favor of C₂H₆ and C₃H₈ in a co-pyrolysis with PP. In a co-pyrolysis with PE, the yield of C₄H₁₀ decreased significantly while that of ethene increased [Hall et al. 2007].

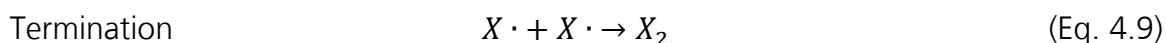
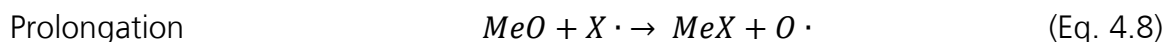
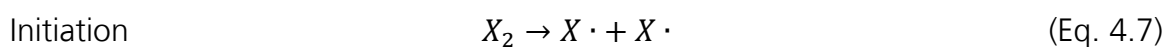
In contrast to the above mentioned results regarding the debromination of different compounds such as TBBPA, 2,6-dibromophenol, or 2,4,6-tribromophenol, using PP for dehalogenation of chlorinated compounds such as 2,4-dichlorophenol is not effective. Tests with PP as dechlorination-agent for 2,4-dichlorophenol revealed that at 450 °C 93 wt.-% of the initial 2,4-dichlorophenol left unreacted [Balabanovich et al. 2005b] and even at 500 °C 2,4-dichlorophenol is the main product [Hornung et al. 2005].

4.3.3 Halogen fixation by metals and metal oxides

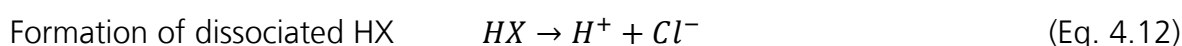
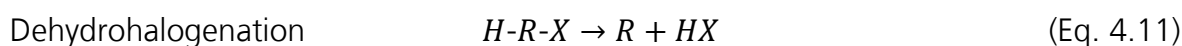
A number of scientific papers deal with the co-pyrolysis of plastics from WEEE with metal compounds, mainly metal oxides. One of the main aims for the application is a dehalogenation by binding halogens as halides (Me_xX_z) or oxyhalogenides (Me_xO_yX_z). Concerning a recycling of critical, chemical ignoble metals, underlying reactions are relevant to understand a loss of these metals from pyrolysis solid products due to vaporization from the solid residue. Therefore, the following section focuses on halogen fixation by metals and metal oxides in pyrolysis processes of chlorinated and brominated plastics.

In the context of reactions between halogens and metals or metal oxides, it is important to have a detailed look on the source of halogens and its pathway of halogenation. A number of studies dealt with the halogenation using Cl₂ or Br₂ as source of halogens. In this case, radicals (Cl· and Br·) are formed, which could react with the metal/metal oxide via radical substitution.

The radical substitution can be divided in three steps: initiation (formation of halogen radicals), prolongation (formation of halides), and termination (formation of different compounds) (Equations 4.7 - 4.10):

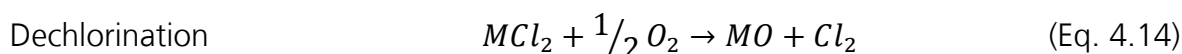
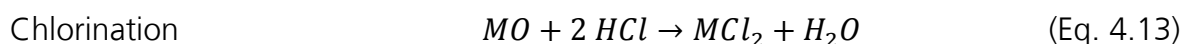


Besides these molecular halogen gases, halogen containing plastics or some other compounds like PVC or TBBPA could act as source of halogens. In this case, HX is formed via dehydrohalogenation. Under typical pyrolytic conditions (e.g. temperature above 300 °C in a pyrolysis of PVC), HX is present in a dissociated form (Equations 3.11 - 3.12).



The knowledge of both reaction types is useful concerning a halogen fixation by metals. Concerning pyrolysis of a halogen containing plastic mixture or WEEE, reactions of dissociated halogens with metals are quantitatively more relevant [Karama et al. 2013]. However, both types of reactions could take place. Additionally, more publications concerning reactions with different metals and metal oxides with halogen gases are present. From these reactions, first estimations can be completed on the fixation ability of metals and metal oxides.

Concerning reactions of halogens with metals or metal compounds, most publications handle investigations regarding reactions of metal oxides with HCl from PVC pyrolysis. Corresponding reactions (Equation 4.13) are exothermic and – with regard to the thermodynamic equilibrium – are enhanced at lower temperatures. A feasible de-chlorination reaction (Equation 4.14) of formed metal chlorides takes place in oxidative atmosphere at higher temperatures and is endothermic [Horikawa et al. 1999].



As mentioned in chapter 4.2.2, Ca compounds are commonly used additives in PVC. Additionally, Ca is an effective additive to capture HX, mainly HCl and HBr, in the solid residue as $CaCl_2/CaBr_2$. [Zhu et al. 2008] examined the decomposition of PVC samples with different Ca-based additives ($CaCO_3$, CaO , $Ca(OH)_2$) by TGA. The degradation of PVC took place between 280 and 400 °C with a maximum at 320 °C as well as between 400 and 560 °C with a maximum at 482 °C. HCl was released in the first stage, hydrocarbons in the second one. Without additives, Cl was completely found as

HCl after degradation. By adding Ca-based additives, the yield of HCl decreased while the yield of CaCl_2 increased. To use the tested Ca-based additives as agents to achieve less HCl in the pyrolysis products, Ca:Cl molar ratios of 1.5 for $\text{Ca}(\text{OH})_2$, 1.5 - 2.5 for CaO and 2.6 for CaCO_3 were recommended. To enhance the efficiency of dehalogenation by a Ca-based additive, [Bhaskar et al. 2002; 2004] formed a Ca-C catalyst by kneading, molding, and calcination of a mixture of CaCO_3 and phenol resin. Pyrolysis tests of a plastic-mixture containing Cl and Br were performed at 430 °C and revealed that the tested catalyst seemed to be very effective: without catalyst, pyrolysis oils contained a minimum of 0.49 wt.-% of Br and 0.12 wt.-% of Cl. In contrast, oils from a pyrolysis test with 20 - 80 wt.-% of Ca-C catalyst contained a maximum of 0.07 wt.-% of Br and 0.01 wt.-% of Cl. Due to the addition of the catalyst, the yield of liquids and solid products decreased while those of gaseous products increased. In addition, the composition of the liquid products changed: the yield of C_6 - C_{10} hydrocarbons increased greatly by 50 wt.-% and the yield of C_{11} - C_{15} hydrocarbons increased slightly, but higher hydrocarbons (C_{16} - C_{20}) decreased significantly. Similar results were published by [Mitan et al. 2007], who tested different catalysts during thermal degradation of HIPS-Br and ABS-Br at 450 °C. It was concluded that a combined catalytic system based on folded sheet mesoporous silica (FSM) and a "calcium to carbon composite" offers low concentrations of Br, N, and O in the oil and the highest quantities of oil and gas with mainly short-chained hydrocarbons.

[Alston et al. 2011] operated pyrolysis tests at 800 °C with two different mixtures of plastics, both typically used in EEE. One of these samples contained an amount of 11.4 wt.-% Cl, mainly from PVC, and 6.7 wt.-% Ca, mainly in form of CaCO_3 , which serves as a filler material in PVC-plastics. The yield of potential fuel was about 72.0 wt.-% (45.5 wt.-% permanent gases and 27.8 wt.-% oils including tars). The authors presented an interesting aspect on Br fixation: the amount of Cl and Ca in the solid residue was much lower than in the input material. In addition, only a small amount of Cl and no Br was detected in the liquid phase. The authors suggested that Cl reacted with CaCO_3 by forming water-soluble CaCl_2 , which could be removed in a water-trap.

Besides pyrolysis tests with added or present Ca compounds, in a number of studies co-pyrolysis tests with different metal oxides were conducted. As mentioned above, due to added metal oxides, the thermal degradation of PVC can be influenced [Gupta, Viswanath 1998; Müller, Dongmann 1998; Sivalingam et al. 2003]. For both stages of PVC thermal degradation (Equations 4.15 - 4.16) and for complete decomposition (Equation 4.17), compensation plot equations as well as corresponding values of frequency factor A and activation energy E were developed by [Sivalingam et al. 2003] and [Gupta, Viswanath 1998], respectively.

$$\text{First stage of decomposition} \quad \ln A = 0.945E - 3.53 \quad (\text{Eq. 4.15})$$

$$\text{Second stage of decomposition} \quad \ln A = 0.703E - 4.29 \quad (\text{Eq. 4.16})$$

$$\text{Complete decomposition} \quad \ln A = 0.221E - 7.17 \quad (\text{Eq. 4.17})$$

For tested metal oxides, the values for E and $\ln A$ are listed in Table 5.

Additionally, in Table 6, the nature of formed metal chlorides is listed. Besides these chlorides, H_2O is formed from PVC decomposition. In order to identify suitable metal oxides as an additive for dehalogenation, knowledge on behaviour of formed metal halides gives access to control the allocation of halogens to the different pyrolysis products. As an example, if metal chlorides volatilize, Cl could become part of formed oil which means an incomplete dehalogenation.

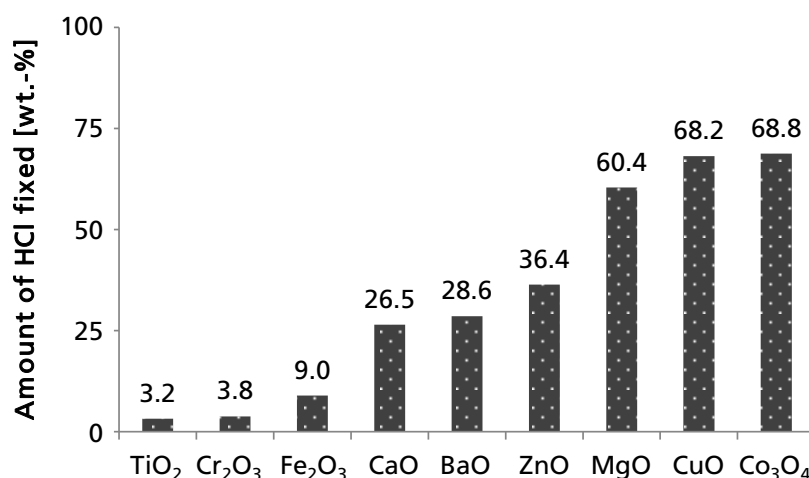
Table 5: Values of activation energy E and frequency factor A for first and second stage of PVC decomposition as well as full decomposition [Gupta, Viswanath 1998; Sivalingam et al. 2003].

Parameter Unit	First stage		Second Stage		Complete degradation	
	E $\text{kJ}\cdot\text{mol}^{-1}$	$\ln A$ min^{-1}	E $\text{kJ}\cdot\text{mol}^{-1}$	$\ln A$ min^{-1}	E $\text{kJ}\cdot\text{mol}^{-1}$	$\ln A$ s^{-1}
Pure PVC	147.79	29.8	177.52	25.4	302.5	59.18
Al_2O_3	110.11	21.0	180.87	26.3	274.1	19.94
CeO_2	105.93	20.9	169.98	24.5	223.1	41.52
Co_3O_4	188.41	39.4	125.19	16.5	n.a.	n.a.
Cr_2O_3	162.03	32.7	139.00	19.0	149.8	25.78
CuO	171.66	35.4	184.64	26.7	366.5	74.76
Cu_2O	n.a.	n.a.	n.a.	n.a.	254.6	49.39
Fe_2O_3	147.38	30.2	257.49	38.8	155.6	27.45
MoO_3	196.36	41.0	154.91	21.7	183.7	32.86
PbO_2	226.51	47.4	206.83	30.3	n.a.	n.a.
Sb_2O_3	n.a.	n.a.	n.a.	n.a.	195.3	36.30
SnO_2	n.a.	n.a.	n.a.	n.a.	90.1	13.63
TiO_2	123.51	24.2	194.27	28.2	190.8	35.34
V_2O_5	n.a.	n.a.	n.a.	n.a.	113.3	17.96
ZrO_2	146.96	29.0	200.13	29.6	132.5	21.81
Reference	[Sivalingam et al. 2003]		[Sivalingam et al. 2003]		[Gupta, Viswanath 1998]	

Table 6: Nature of metal chlorides formed during co-pyrolysis of PVC and metal oxides [Gupta, Viswanath 1998].

Metal Oxide	Metal Chloride	Nature of metal chlorides formed			promotes PVC degradation
		(subsequent) decomposition	volatilization	sublimation	
Al_2O_3	AlCl_3		of AlCl_3		
CeO_2	CeCl_4	to CeCl_3			
Cr_2O_3	CrCl_3	to CrCl_2			
CuO	CuCl_2				X
Cu_2O	Cu_2Cl_2				X
Fe_2O_3	FeCl_3	to FeCl_2			
MoO_3	MoCl_6		of MoCl_6		
PbO_2	PbCl_4				
Sb_2O_3	SbCl_3			of SbCl_3	
SnO_2	SnCl_4				X
TiO_2	TiCl_4	to TiCl_3			
V_2O_5	VCl_5	to VCl_3			
ZrO_2	ZrCl_4		of ZrCl_4		

In order to test the halogen fixation ability of different metal oxides, [Horikawa et al. 1999] conducted tests with BaO , CaO , Co_3O_4 , Cr_2O_3 , CuO , Fe_2O_3 , MgO , TiO_2 , and ZnO (stoichiometric mixtures), which were placed in vapor phase contact mode of PVC pyrolysis at 300 °C. As shown in Figure 25, the highest fixation ability as 68.8 wt.-% was measured for Co_3O_4 under these circumstances. In a further test, it was shown that using 1.75 times or more of Co_3O_4 than the stoichiometric mixture, more than 90 wt.-% of HCl was fixed. Concerning the reactions taking place, the authors revealed that HCl was absorbed before ingressed in the metal oxide crystallizes. The first reaction (absorption) is increased with an increase of surface area; however, the second reaction (ingression) decreases due to lowered space inside crystallizes. Therefore, it was concluded that an intermediate high surface area shows a compromise of both.

**Figure 25:** Amount of HCl fixed by different metal oxides in stoichiometric mixture at 300 °C (in wt.-%) (own diagram based on [Horikawa et al. 1999]).

Further tests were conducted by [Masuda et al. 2006], who analyzed the HCl fixation ability of Al_2O_3 , CaO , CeO_2 , Fe_2O_3 , La_2O_3 , Nd_2O_3 , PbO , and ZnO in a co-pyrolysis with PVC (2:1 for PVC:metal oxide). Temperature and residence time were fixed at 30 min at 400 °C and 10 min at 800 °C. Due to the different additives no significant changes on the pyrolysis products main composition were reported. The most relevant products of the pyrolysis liquids were aromatic hydrocarbons ($\text{C}_6 - \text{C}_{14}$), mainly benzene and toluene, while the gaseous products were mainly CO , CO_2 , and light hydrocarbons ($\text{C}_1 - \text{C}_3$) as well as aromatic hydrocarbons with three to six benzene rings. In the cases of the addition of Al_2O_3 , the formation of benzene and toluene was increased. Besides the main products, relevant changes on the formation of chlorobenzene were detected, which could act as precursor substance on the formation of PCDD/F: an addition of Fe_2O_3 or CeO_2 yielded an increased amount of chlorobenzene, while ZnO decreased that formation. Most relevant changes were obvious as various changes in the yield of different pyrolysis products solids, oil, and gas. For example, due to an addition of ZnO , the amount of char increased while that of liquid products decreased to less than 30 wt.-% compared to pure PVC. Fe_2O_3 and Al_2O_3 showed the most significant changes concerning gaseous products: due to the addition of Fe_2O_3 , the amount increased while under the presence of Al_2O_3 gases are suppressed by more than 70 wt.-%. No significant correlations were obvious in the case of PbO and REO. As mentioned above (chapter 4.2.2), the effects of metal chlorides on the allocation to solid, liquid, and gaseous products can be explained due to the strength as Lewis acid, which cause a cationic polymerization and thereby a bridging of polyene chains, which lead to a formation of char [Müller, Dongmann 1998]. Due to the present Cl from PVC, different chlorinated products such as ZnCl_2 , PbCl_2 , CaCl_2 , CaClOH , as well as chlorides and oxychlorides from REO were formed in the solid products. Nearly all La_2O_3 is converted to LaOCl , while just a small amount of NdOCl and an even smaller amount of CeOCl_2 were detected. In Figure 26, the ratios of trapped Cl at a water trap as part of the gas cleaning are shown for pyrolysis of PVC and the different mixtures at 400 °C (just PVC, + ZnO , + PbO , + Al_2O_3 and + La_2O_3) and 800 °C. The strongest effect on the fixation of Cl was obviously for La_2O_3 , which resulted in a decrease of Cl to just 24 and 3.1 wt.-% at 400 and 800 °C, respectively. All other metal oxides showed lower ratios between 25 wt.-% (Nd_2O_3 at 800 °C) and 89 wt.-% (Al_2O_3 at 800 °C). With the exception of Al_2O_3 and PbO , the effect of metal oxide fixation was significantly stronger at 800 °C than at 400 °C. This could be explained by two different facts: Al_2O_3 has slow kinetics in the reaction with HCl, while the chlorination of PbO seems to be complete at temperatures about 400 °C [Masuda et al. 2006].

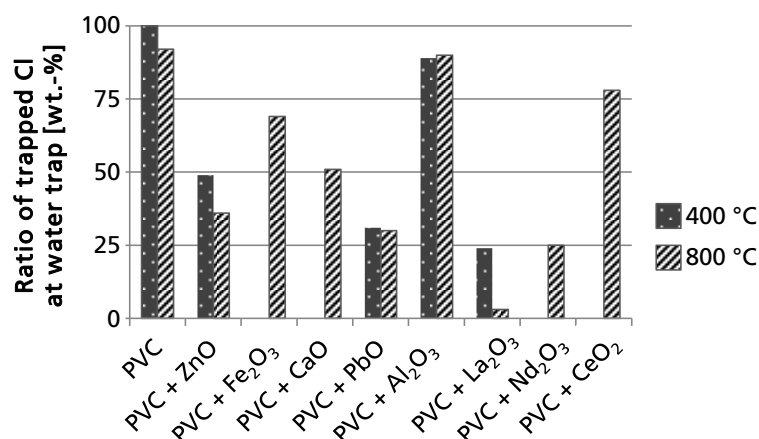


Figure 26: Ratio of trapped Cl at water trap for pyrolysis tests of PVC and different PVC-metal oxide mixtures at 400 and 800 °C (own diagram based on [Masuda et al. 2006]).

As mentioned above, compared to a pyrolysis of PVC without additives, higher amounts of chlorobenzene were formed just in the cases of PVC + Fe₂O₃ (factor 1.6) and PVC + CeO₂ (factor 1.7). This fact could be partially explained due to the catalytic effect of Lewis acids in Friedel-Crafts chlorination. In this case the (strong) Lewis acids FeCl₃ and, probably, CeOCl₂ or CeCl₃ could act as catalyst for the formation chlorobenzene as shown in Figure 27 [Holleman et al. 2007].

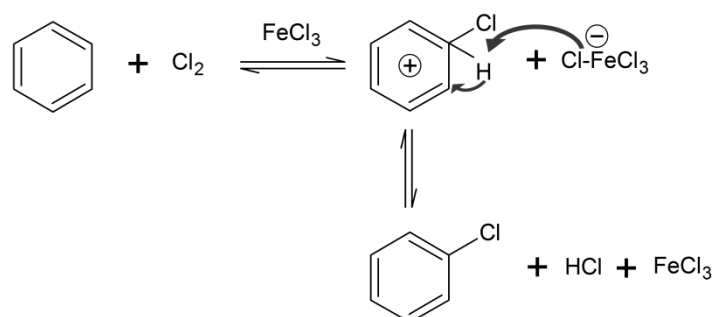
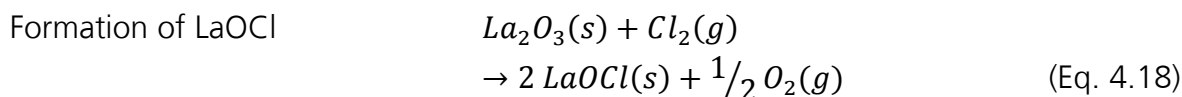


Figure 27: Friedel-Crafts chlorination of benzene with Cl₂ with a Lewis acid (FeCl₃) as catalyst [Holleman et al. 2007; Fels et al. 2016].

With regard to a dechlorination in combination with a recovery or circuitry of the used metal oxide and a suppression of chlorobenzene, La₂O₃ promised beneficial properties: during pyrolysis, La₂O₃ is capturing Cl as LaOCl, which can be converted afterwards back to La₂O₃ by hydrolysis at high temperature [Masuda et al. 2006]. LaOCl shows beneficial aspects concerning its handling, because it is not hygroscopic and stable under air conditions [Gaviría et al. 2012]. Compared to PbO and ZnO, from which water-soluble PbCl₂ and ZnCl₂ get formed, LaOCl do not vaporize at temperatures below 850 °C and start decomposing at 934 °C (in vacuum) [Gaviría et al. 2012], which means – in combination with the strong fixation of Cl during pyrolysis – a very high amount of Cl can be captured before becoming part of pyrolysis oil and/or get solved in it.

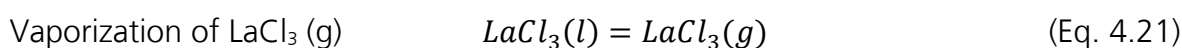
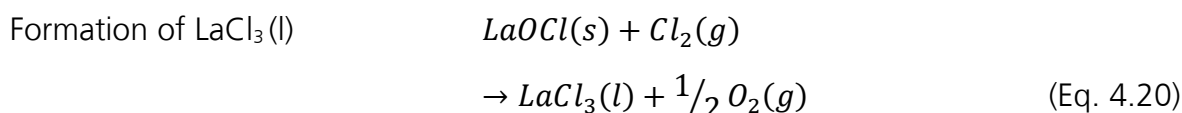
More detailed analyses concerning chlorination of La_2O_3 were conducted by [Gaviría et al. 2012]. From nonisothermal chlorination experiments under Ar-Cl_2 atmosphere, a strong increase of mass by 18 wt.-% at temperatures above 260 °C were obvious, which corresponds to a formation of LaOCl . The corresponding reaction, which is shown in Equation 4.18, was confirmed by tests using X-ray diffraction (XRD) analysis and energy dispersive spectroscopy (EDS).



For the degree of conversion α , a function of Δm was defined (Equation 4.19) with m_0 and $m_{t\text{La}_2\text{O}_3}$ are weights of La_2O_3 at start and time t , respectively; Δm is the measured mass change from the thermo-balance.

$$\begin{aligned} \text{Degree of conversion} \quad & \alpha = \alpha_{\text{La}_2\text{O}_3} = \frac{m_0 - m_{t\text{La}_2\text{O}_3}}{m_0} \\ & = \frac{\left(\frac{\Delta m}{m_0}\right)}{\left(2 \frac{PM_{\text{LaOCl}}}{PM_{\text{La}_2\text{O}_3}} - 1\right)} \cong \left(\frac{\Delta m}{m_0}\right) \cdot \frac{1}{0.169} \end{aligned} \quad (\text{Eq. 4.19})$$

In further tests, isothermal, thermo-gravimetric experiments were conducted, which revealed conversion curves at different temperatures between 325 and 950 °C. From these tests, it was shown that up to a temperature of 600 °C the reaction speed increased and did not increase at higher temperatures. At temperatures above 850 °C two further reactions (Equations 4.20 and 4.21) take place, from which the vaporization of LaCl_3 is faster than the formation of it.

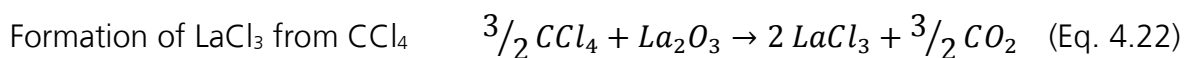


For Equation 4.18, [Gaviría et al. 2012] calculated the activation energy E_a in a temperature range between 260 and 325 °C as $113 \pm 5 \text{ kJ}\cdot\text{mol}^{-1}$. As shown in Table 7, this value is lower compared to other REO. These aspects revealed that using La_2O_3 absorption of Cl_2 at relatively low temperatures/low energy input is feasible.

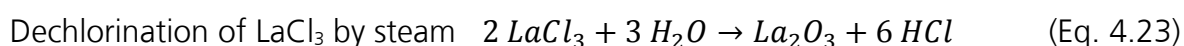
Table 7: Activation energy E_a and its temperature ranges of different REO.

REO	E_a value $\text{kJ}\cdot\text{mol}^{-1}$	Temperature Range of E_a °C	Reference
Sm_2O_3	129 ± 1	270 - 350	[Esquivel et al. 2005]
Gd_2O_3	132 ± 3	350 - 450	[Pomiro et al. 2015a]
Eu_2O_3	154 ± 5	615 - 660	[Pomiro et al. 2015b]
Y_2O_3	187 ± 3	575 - 800	[Gaviría, Bohé 2009]
Ce_2O_3	190 ± 8	800 - 950	[Esquivel et al. 2003]

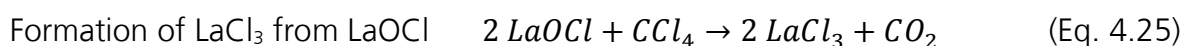
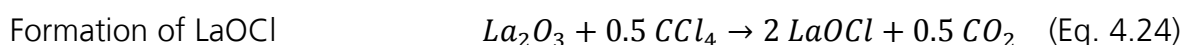
Besides reactions with HCl [Masuda et al. 2006] and Cl₂ [Gaviria et al. 2012], La₂O₃ can adsorb Cl from chlorinated hydrocarbons (CHCs) such as CCl₄, CHCl₃ and CH₂Cl₂, too (e.g. Equation 4.22) [van der Avert, Weckhuysen 2004].



Similar to their results by [Gaviria et al. 2012], La₂O₃ was found to be the most effective adsorption agent compared to other lanthanide oxides such as Pr₂O₃ or Nd₂O₃. Adsorption of Cl from CCl₄ by La₂O₃ starts at a temperature of about 250 °C and its efficiency increased at higher temperatures. Due to an easy dechlorination of LaCl₃ in steam atmosphere (e.g. 300 °C for 4 h), utilization of La₂O₃ as catalyst seems feasible (Equation 4.23).



As mentioned above, during chlorination of La₂O₃ the stable, intermediate form LaOCl is formed (Equation 4.24), which could become chlorinated to LaCl₃ (Equation 4.25).



In order to combine both processes of firstly dechlorination of CHCs (chlorination of La₂O₃) and secondly dechlorination of LaCl₃ or LaOCl under the formation of HCl, [van der Avert et al. 2004] investigated both processes at 350 °C with and without Al₂O₃ as well as in different molar ratios of H₂O and CCl₄. From Raman spectroscopy of reactions between CCl₄ and H₂O (1:61 by molar ratio) they revealed that, firstly, a complete transformation of La₂O₃ into LaOCl (Equation 4.22) takes place followed by formation of LaCl₃ (Equation 4.23). Secondly, it was shown that due to present steam, chlorination is hindered and La₂O₃ is formed. In order to increase the conversion of CCl₄, mixtures of La₂O₃ and Al₂O₃ were prepared. In a ratio of 10 wt.-% La₂O₃ and 90 wt.-% Al₂O₃ conversions rates of 100 wt.-% were reached at 350 °C, which is significantly higher than pure La₂O₃ (62 wt.-%). This effect can be explained by higher rates of La₂O₃-chlorination than dechlorination. The same effect is obvious when steam was missing. Concerning the reaction mechanisms, the authors revealed that reactions take place on a lattice, basic surface oxygen site of La₂O₃ or LaOCl. The findings showed that a full conversion of CCl₄ into CO₂ and HCl is possible and its destruction rates are relatively high (0.289 g CCl₄ · h⁻¹ · g⁻¹). These high destruction rates were reached just in a mixture of Al₂O₃ and La₂O₃, however, addition of Al₂O₃ showed two disadvantages: first, CH₃Cl gets formed from CCl₄ and second, the formation of coke is enhanced, which can theoretically block the catalyst. Concerning destruction of CHCl₃ and CH₂Cl₂, it was shown that catalytic destruction was lowered with decreased amount Cl in CHCs. Figure 28 shows the full corresponding reaction scheme for the catalytically destruction of CHCl₃ and CHCl₂ over La₂O₃ in the presence of steam [van der Avert et al. 2004; van der Avert, Weckhuysen 2004].

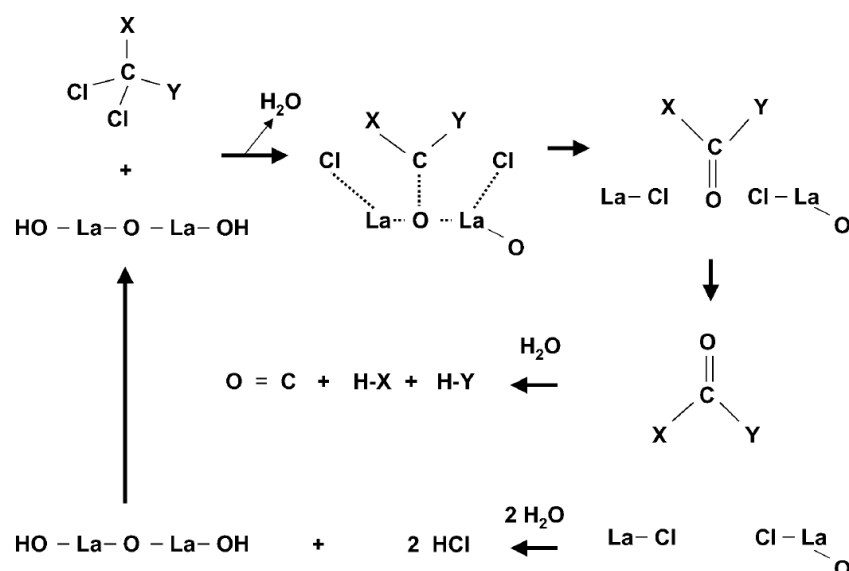


Figure 28: Reaction scheme for the destruction of CCl_2XY (with $\text{X} = \text{H}$ and $\text{Y} = \text{Cl}$ for CHCl_3 and $\text{X} = \text{Y} = \text{H}$ for CHCl_2) over La_2O_3 in the presence of steam [van de Avert et al. 2004].

Besides dechlorination, a small number of studies focused on debromination by metals and metal oxides. Tests with Ca based additives in a fast pyrolysis (at 460 °C) of HIPS-Br using a fluidized bed reactor were conducted by [Jung et al. 2012]. From this study, the effects of adding CaO or $\text{Ca}(\text{OH})_2$ on the pyrolysis product allocation, its composition as well as the debromination effectiveness should be specified.

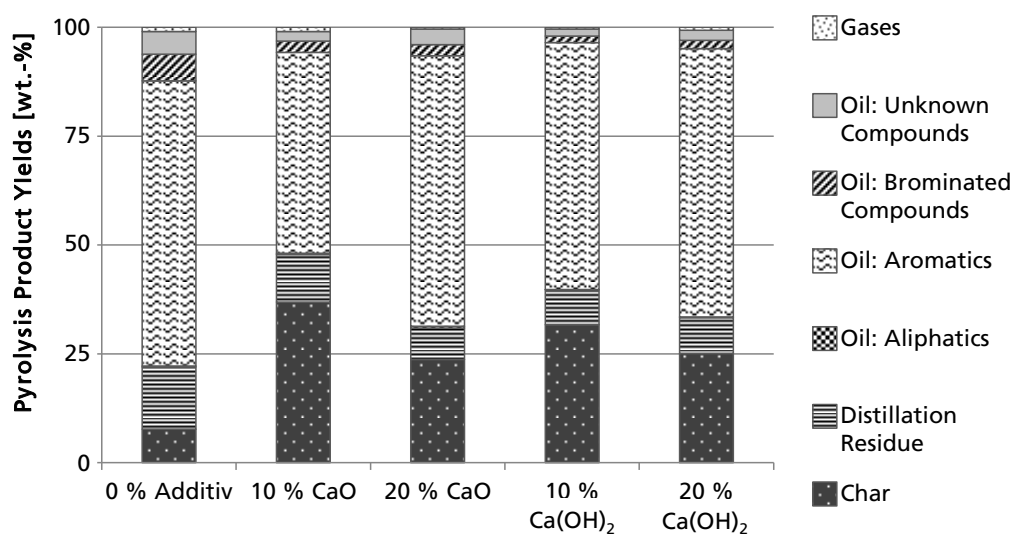


Figure 29: Pyrolysis product yields from fast-pyrolysis of HIPS-Br at 460 °C in a fluidized bed reactor with and without adding $\text{CaO}/\text{Ca}(\text{OH})_2$ (in wt.-%) [Jung et al. 2012].

As shown in Figure 29, due to added Ca compounds the yield of char increased strongly while those of oil (mainly aromatics) and distillation residue decreased. Additionally, the amount of brominated compounds in the oil decreased in the case of CaO by 57.4/59.0 wt.-% (10/20 wt.-% CaO) and in the case of $\text{Ca}(\text{OH})_2$ by 75.4/68.9 wt.-% (10/20 wt.-% $\text{Ca}(\text{OH})_2$). The total amount of Br was decreased by 68.0 and 74.0 wt.-% due to an addition of 20 wt.-% CaO and $\text{Ca}(\text{OH})_2$, respectively. From these results, it can be seen that the effects due to added Ca compounds did not follow linearity by adding more Ca compounds. Therefore, further tests such as those by [Zhu et al. 2008]

with PVC concerning optimal ratios of these additives have to be conducted for brominated plastics. Concerning Sb, which amounts to 2.9 wt.-% in the HIPS-Br feed, 83.6 ppm Sb was found in the oil and 434.6 ppm Sb in the distillation residue from pyrolysis without and 13.9 ppm Sb in the oil and 689 ppm Sb in the distillation residue from the pyrolysis with 20 wt.-% $\text{Ca}(\text{OH})_2$. This reveals that the formation of SbBr_3 was not hindered due to an addition of Ca compounds, but Sb could be separated from pyrolysis oil via distillation very efficiently.

Besides $\text{Ca}(\text{OH})_2$, $\text{Mg}(\text{OH})_2$, NaOH, and KOH show the ability of halogen reduction in pyrolysis oil due to fixation of halogens in pyrolysis solid products. Thereby, strong bases such as NaOH and KOH shows a better fixation ability than weaker bases such as $\text{Ca}(\text{OH})_2$ or $\text{Mg}(\text{OH})_2$ [Luda et al. 2002b]. As an example, an addition of 17 wt.-% NaOH to a pyrolysis of two different PWB showed a fixation ability between 62.1 and 80.5 wt.-% (as inorganic soluble salts) [Luda et al. 2002b].

[Grabda et al. 2011] investigated a stoichiometric mixture of ZnO and TBBPA (3.34:1 by weight). The impact of temperature and process duration on the formation and vaporization of ZnBr_2 has been examined. The tests clearly revealed that the diffusion of ZnBr_2 significantly depends on residence time. At even higher temperatures of 850 °C and above, a deoxidation process of ZnBr_2 into elementary Zn took place with char reacting as reductive while CO and CO_2 were formed.

Further studies on Br-fixation reactions by metal oxides are published by [Terakado et al. 2011; 2013]. In a first examination, they compared the Br-fixation ability of ZnO, Fe_2O_3 , La_2O_3 , CaO and CuO during the thermal degradation of TBBPA. Both TGA and pyrolysis experiments were carried out at 400 °C and 800 °C under He-atmosphere with mixtures of 1:1 for Fe_2O_3 and 1:2 for all other oxides by weight. Similar to those results of [Grause et al. 2008], which have been explained in chapter 3.1, the amount of HBr greatly increased at higher temperatures, regardless of the presence of metal oxides. In the case of pure TBBPA, about 90 wt.-% of Br was formed as HBr at a process temperature of 800 °C. The addition of metal oxides decreased the amount of HBr by minimum 30 wt.-% (CuO) and maximum 99 wt.-% (La_2O_3). To take a look at other WEEE fractions, [Terakado et al. 2013] examined the Br-fixation ability of metal oxides using PWB as feedstock material. Fe_2O_3 showed similar suppressive effects on HBr formation, like with TBBPA as a feedstock. However, the impact of CaO and La_2O_3 decreased while the impact of CuO and ZnO increased these effects. The authors explained the reduced effect of CaO by deactivation reactions with glass fibers contained in PWB, e.g. due to the formation of Ca-silicates. With respect to the yield of precursor compounds of PBDD/F, due to the addition of ZnO, no bromophenols were formed. Furthermore, the addition of metal oxides led to an enhanced yield of CO_2 in the pyrolysis gas and of heavy metals in the solid residue. Heavy metals, especially Cu, act as catalyst during the formation of PBDD/F [Dettmer 2001; Sakai et al. 2001].

[Oleszek et al. 2013a] investigated the distribution of Cu, Ag, and Au in a mixture with TBBPA and TTDE-TBBPA-diglycidyl ether copolymer (TTDE) at different temperatures between 320 and 1 000 °C. Pyrolysis of mixtures with TTDE (TTDE:Cu = 5.16:1 by weight; TTDE:Ag 10:1 by weight) delivered the following results: at 370 °C, about one quarter of Cu had been brominated. At 600 °C, more or less half of the present Cu and Ag was brominated and, in the case of Cu, a very small amount of CuBr/CuBr₂ was vaporized (0.4 wt.-%). Due to a further increase of temperature up to 1 000 °C, more than one third of Cu and Ag was vaporized as MeBr. Gold did not react with Br. The study points towards fixation of Br in form of metal bromides, which explains the translocations of metals in WEEE pyrolysis. Two further studies by [Oleszek et al. 2013b; Oleszek et al. 2013c], dealing with pyrolysis of TBBPA-Fe₂O₃ and TBBA-PbO mixtures, delivered similar results concerning metal bromination. Figure 30 shows these as well as previously mentioned results concerning bromination and vaporization of brominated metals such as Ag, Cu, Sb₂O₃, PbO, ZnO from tests with different TBBPA and TTDE in different mixtures (by weight).

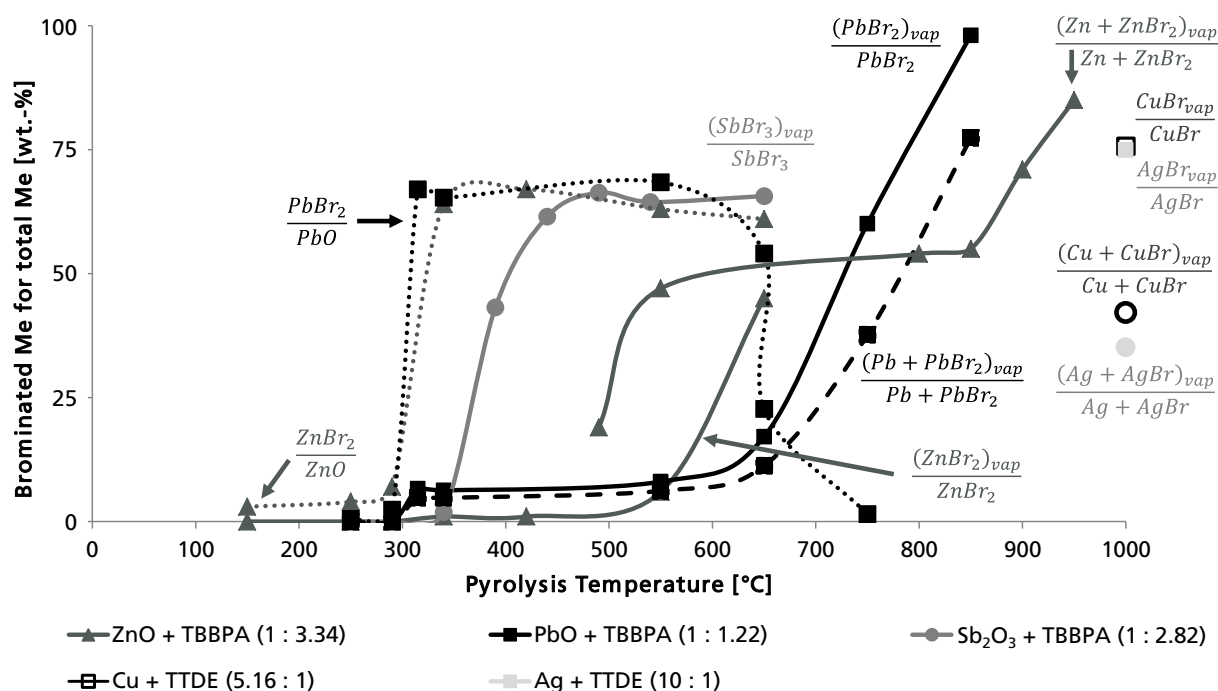


Figure 30: Bromination of different metals and metal oxides with TBBPA and TTDE over temperature (own diagram based on [Grabda et al. 2009; Grabda et al. 2010; Rzyman et al. 2010; Oleszek et al. 2013a; Oleszek et al. 2013b; Oleszek et al. 2013c; Terakado et al. 2011]).

In order to achieve both dechlorination and debromination of Br and Cl containing plastic mixtures, [Uddin et al. 2002] formed a catalyst based on Fe₃O₄ (FeO · Fe₂O₃) and tested it in vapor phase contact mode during co-pyrolysis of HIPS-Br and PVC (4:1 by weight) at 430 °C. Due to addition of this catalyst, yields of liquids decreased slightly, while those of gaseous products decreased greatly (roughly 40 wt.-%). Concerning the liquid products quality, two aspects were obvious: both density and average carbon number decreased due to an addition of the catalyst, which results in cracking of higher molecular weight compounds. In order to determinate the amount of catalyst required for a dehalogenation of pyrolysis oil, 1, 2, 4, and 8 g catalyst was tested during pyrolysis

of a 5 g plastic sample. By adding 1 g catalyst, content of halogens decreased from 55 000 and 4 300 ppm to 910 and 1 870 ppm for Br and Cl, respectively. An addition of 2 g catalyst already effectuated a complete debromination; however, the concentration of Cl was 840 ppm. A complete dehalogenation of pyrolysis oil was obvious due to a minimal addition of 4 g catalyst. Analysis of pyrolysis solid residue revealed that after thermal degradation (without catalyst) 2.4 wt.-% of total Br and 6.9 wt.-% of total Cl were left in the solid residue. Its concentration increased slightly in the presence of a small amount of catalyst, while it decreased slightly with higher amounts of catalyst. XRD analyses revealed that after pyrolysis FeCl_2 and FeBr_2 became part of the catalyst [Uddin et al. 2002]. For a stoichiometric halogenation reaction of FeO forming FeCl_2 , during pyrolysis of used plastic mixture (7.2 wt.-% Br; 11.4 wt.-% Cl) 0.7374 g of FeO is necessary (0.1618 g for Br plus 0.5756 g for Cl). In relation to the above mentioned results, this indicates that the amount of this catalyst should be approximately five times higher than the amount, which is stoichiometric required.

These results by [Uddin et al. 2002] revealed that Fe based catalysts give good results concerning debromination of pyrolysis oil, but show some weaknesses on dechlorination. In similar pyrolysis studies with mixtures of PP, PE, PS, PVC, and ABS-Br, both Fe and Ca based catalysts were added in order to examine their effectiveness of debromination and dechlorination as well as on nitrogen removal [Brebou et al. 2005]. Concerning nitrogen removal, Fe based catalyst revealed a slightly greater efficiency than Ca based ones. With regard to dehalogenation, iron based catalysts had high debromination efficiency while Ca based ones had high dechlorination efficiency. These results reveal that a mixture or cascade of such catalysts could be used for an efficient dehalogenation.

Besides relatively homogenous and pure compounds, many industrial solid wastes such as red mud, natural minerals such as (calcined) limestone, and natural zeolite or synthetic zeolites were tested as catalyst and/or additives in the pyrolysis of biomass and plastics (e.g. [Hall, Williams 2008a; Lee et al. 2002; López et al. 2011; Vasile et al. 2008; Yanik et al. 2001]). Concerning a thermo-chemical treatment of different plastics – especially those plastics from WEEE containing Br – red mud, limestone, and zeolite revealed positive effects on the formation of different brominated compounds. As an example, [Wu et al. 2014] tested red mud, limestone, and zeolite (20 wt.-%) in a co-pyrolysis with HIPS-Br (Br: 9.30 wt.-%; Sb: 3.77 wt.-%) at a temperature of 500 °C. The aim of the study was a debromination of pyrolysis oil and a destroying of organo-brominated compounds in it. Red mud was found as most effective additive, e.g. due to a decrease of brominated compounds by 94.5 wt.-% or a decrease of 3-methylbenzyl bromide from 9.47 wt.-% below the detection limit. In summary, contents of Br and Sb decreased strongly by 90.0 and 81.0 wt.-%, respectively.

4.4 Conclusion: Chemical reactions concerning a thermo-chemical treatment of WEEE

Chapter 4 gave an overview on how pyrolysis processes of polymers, plastics, and mixtures of these materials are influenced by main parameters. As shown in chapter 4.1, based on literature work, there is a good knowledge about the decomposition of different plastics under pyrolytic conditions. Additionally, similar knowledge is given concerning halogen containing plastics (chapter 4.2). However, concerning a pyrolysis of WEEE, as a mixture of several different plastics, metals, and many other components, there are many weaknesses about the pyrolysis of it. In this context it is difficult to conclude all the different parameters, which are relevant in order to reach all aims of a pyrolysis of WEEE. As an example, polymers (in a mixture of different plastics) influence the decomposition of each other (e.g. [Bhaskar et al. 2004; Bhaskar et al. 2005; Blazsó et al. 1995; Czégény et al. 2012; Miskolczi et al. 2009]) and their decomposition products could react with present metal and metal compounds (e.g. [Blazsó, Jakab 1999; Gupta, Viswanath 1998; Masuda et al. 2006; Sivalingam et al. 2003; Terakado, Hirasawa 2005; Terakado et al. 2013; Yoshioka et al. 2005]). With regard to heterogeneous fractions with varying composition from WEEE treatment, such as shredder residues, all influences of different compounds on each other are not predictable.

In spite of this lack of knowledge, some aspects should be highlighted. Table 8 shows some general, linear effects of varied parameters in pyrolysis tests. Besides the changes of these parameters, types of pyrolysis tests can be varied as well. In this regard, there are mainly the following three variations feasible:

- Two-stage instead of one-stage pyrolysis for a production of two different oils with a low and a high halogen concentration while toxic organic halogens are concentrated in first step oil (c.f. [Bhaskar et al. 2006; Grause et al. 2012]);
- Co-Pyrolysis with additives which enables influencing kinetics and mechanisms as well as halogen fixation. Additionally the yield of solids usually increases (c.f. [Buekens 2006; López et al. 2011; Zhu et al. 2008]);
- Pyrolysis with additives, which are in contact as vapor phase mode for an increased fixation of metals, e.g. by halogens (c.f. [Yanik et al. 2001]).

Furthermore, some nonlinear effects were obvious: The yields of pyrolysis liquid products peak at medium temperatures, e.g. in the case of HIPS-Br (containing Sb) at nearly 500 °C [Wu et al. 2014]. Similar to this, peaks of formation are obvious concerning products composition. As an example, the formations of permanent gases, phenol, and its derivatives, light hydrocarbons, as well as aromatics from a pyrolysis of phenol-formaldehyde resin peak at different temperatures [Wong et al. 2015].

Table 8: Effects and feasible opportunities of varied parameters during pyrolysis.

Parameter	Variation	Effect/feasible Opportunity	Exemplary references
Temperature	Increase	Enhanced bond-braking: Increased yield of gas; decreased yield of solids	Buekens 2006
Heating rate	Increase	Enhanced bond-braking: Formation of small molecules; decreased amount of PXDF	Buekens 2006
Residence Time	Increase	Higher volatilization rates of compounds with high B_p ; Increased number of secondary reactions: increased yield of thermally stable products such as char and tar; thermal degradation of organohalides	Buekens 2006; Miskolczi et al. 2008
Purging gas	Increase	Decrease of residence time and therefore secondary reactions; removal of vaporable products	Yanik et al. 2001
Pressure	Decrease	Reduced condensation of reactive fragments: Increased yield of char and high-molecular species	Buekens 2006

With regard to a continuous plant, [Miskolczi et al. 2008] designed a pyrolysis reactor with an extruder as feeding system (chapter 4.2.1). This option for inlet of feedstock shows strong advantages, because it reduces the need for N_2 or other purging gases; however, feedstock has to be crushed and sized as well as free of inert materials such as metals and minerals, which could damage the screw inside the extruder.

In order to reach a successful dehalogenation, different options were discussed. Co-pyrolysis with halogen fixing additives offers an opportunity to decrease the amount of halogens in pyrolysis oil and gas; however, the concentration of halogens in the pyrolysis solid product increases. Additionally, a complete dehalogenation of oil and gas could not be reached due to feasible vaporization reactions of some halides. Two-stage pyrolysis is another option, from which a dehalogenation of pyrolysis solid products as well as a formation of an oil fraction with low concentrations of halogens (oil from the second stage) is possible. However, dehalogenation of this oil is incomplete and halogen-rich oil (from the first stage) is formed additionally, which has to be processed further. Concerning an avoidance of PXDD/F in all pyrolysis products, another weakness is possible for two-stage pyrolysis, because of a feasible formation of PXDD/F at low temperatures. Due to low pyrolysis temperatures at first stage, residence time of the second stage with higher temperatures has to be much longer in order to decompose PXDD/F, which were formed in the first stage previously. Furthermore, with regard to a continuous process, a reactor for a two-stage pyrolysis would need a special, complex design and heat transfer strategy in order to supply an adequate amount of energy at corresponding temperature levels.

From the findings, it can be concluded that a high heating rate as well as fast cooling of pyrolysis products at the end of the residence time is necessary in order to avoid formations of PXDD/F. Additionally, increased pyrolysis temperatures and residence times of volatile products favor a thermal degradation of organohalogens, which causes a formation of HX from those compounds. HX could become absorbed in downstream filter processes, e.g. installed in vapor phase mode (cf. [Uddin et al. 2002]). However, as mentioned above, a small amount of halogens can be part of organic compounds. Therefore, a treatment of vapor in a hydrogen donating substance like a polyolefin can be used in order to form HX from organohalogens.

In order to absorb halogens from HX rich vapor, theoretically, an option for de-halogenation of vapor is a staged condensation at approximately 130 and 100 °C in order to form three different oils: from the first stage, heavy oil with compounds, which B_p are above 130 °C, should not contain any HBr (B_p : 124.3 °C) and HCl¹² (B_p : 108.5 °C). Similar to this, light oil with compounds, which B_p are below 100 °C, can be formed as oil from the third stage. Oil, which is formed between these two stages, should contain more or less all the HBr and HCl. However, in the case vapor halogens are present not only as HX, but also in organic compounds or as molecular halogens, the main weakness of this opportunity is that these compounds become part of the heavy oil (organohalogens, c.f. [Miskolczi et al. 2008]), light oil (Br_2), or gas phase (Cl_2), which makes a further treatment necessary.

Therefore, a halogen absorbing filter should be installed as part of the vapor/gas cleaning system to eliminate both molecular halogens as well as HX. The filter is installed upstream to condensation and has to be heated in order to prevent a condensation of vapor in the filter unit itself and additionally to increase absorption effectiveness. The selection of the filter material should be done on the basis of following properties/requirements:

- the material should have a high reactivity with both HX and molecular halogens,
- it as well as formed products should have low vapor pressures, low water solubility and low impacts concerning human health and environmental risks,
- it should show a good recyclability (and – if possible – established recycling pathways), and
- it should be cheap.

¹² B_p of HBr and HCl are 124.3 °C and 108.5 °C, respectively, in the azeotrope mixtures (HBr: 47.63 wt.-% HBr, 52.37 wt.-% H_2O ; HCl: 20.22 wt.-% HCl, 79.78 wt.-% H_2O) [Holleman et al. 2007].

As shown by [Masuda et al. 2006] (chapter 4.3.3), halogen fixation ability of materials could be increased with an increase of temperature. However, with an increased temperature, vapor pressures of formed products increase as well, which therefore, could vaporize and contaminate pyrolysis oil with halogens at the same time. Hence, it is necessary to select a filter material in which products have low vapor pressures in a wide temperature range. For the same reason, a low water solubility of the filter material and formed products is necessary to prevent a solution of halogen containing materials with water from the pyrolysis vapor.

Taking all the different aspects of dehalogenation into account, La_2O_3 as filter material in vapor contact of a one-stage pyrolysis without additives should be tested. Between the pyrolysis reactor and this filter unit, a tar cracking unit and reactor with molten PP should be installed, too. From all the above mentioned absorbents, La_2O_3 shows higher halogen fixation ability than not only other REO, but also common absorbents such as ZnO or PbO. Additionally, the activation energies for corresponding reactions are smaller than those for other REO. The ability of REO to form stable oxyhalides in a wide temperature range makes it possible to test La_2O_3 as filter material between 325 and 600 °C [Gaviria et al. 2012]. However, similar to many other publications, corresponding test series with bromine (Br_2 and HBr) cannot be found for La_2O_3 .

This process chain seems feasible for a treatment of Br rich feedstock from WEEE. However, in order to dechlorinate corresponding vapor, PP as well as PE are ineffective [Hornung et al. 2005]. Therefore, based on research by [van der Avert et al. 2004], La compounds should be tested not only for absorption, but also as catalyst in the form of $\text{La}(\text{OH})_3$. Pre-tests not only with pure PP, but also with a blend of PP+ $\text{La}(\text{OH})_3$ should be conducted and effects on PXDD/F tested.

5. Material and methods

5.1 Raw materials

5.1.1 Shredder residues from WEEE treatment

In spite of best techniques available, in every treatment of Waste Electrical and Electronic Equipment (WEEE) residual fractions like shredder residues and dust as well as hazardous materials like halogenated plastics are discharged, which are usually incinerated or landfilled (cf. chapter 3.4.1). For the main test series of this thesis, a shredder residue from a German WEEE treatment plant, hereinafter referred as "SR1", was used as feedstock for thermo-chemical treatment in order to analyze influences of varied pyrolysis parameters. The WEEE treatment plant, which spent SR1, is treating WEEE from most relevant categories 1, 2, 3, and 4 (c.f. chapter 3.2) mechanically with the exception of visual display units, which get just dismantled manually.

Mechanical processes in the corresponding company are in accordance with the current German act ("ElektroG") [ElektroG 2005] and the guiding principles number M31, defined by the German "Bund/Länder-Arbeitsgemeinschaft Abfall" (LAGA) [LAGA 2009]. The mechanical treatment corresponding for SR1 consists exclusively of dry processes starting with a smasher followed by manual sorting, a crushing and different separation, as well as sorting techniques. Therefore, also fine particles with potentially high amounts of metals were found in the shredder residue (c.f. [Chancerel et al. 2009; Gagli et al. 2014]).

In general, shredder residues presents not only a major by-product of WEEE treatment, which has to be treated in incineration plants or disposed, but also a mixture of more or less all different components, which could be found in WEEE. Therefore, the developed bench-scale plant as well as corresponding results from pyrolysis tests could be transferred for a number of different kinds of WEEE, too. However, it should be noted that even if the material was crushed and consists of particles with a low size as well as a small particle size distribution compared to other kinds of waste, the material shows a high heterogeneity. In order to lower undesirable effects due to this property, the material was taken from a bigger charge of a few hundred kg, mixed strongly and were filled in the reactor in charges of 250 g. In order to lower effects of one charge additionally, for all tests with shredder residues, four charges were filled in the reactor one by one.

5.1.2 Selected fractions containing scarce and critical metals

Critical metals are used for the production of a number of different components in Electrical and Electronic Equipment (EEE). As mentioned in chapter 3.4.2, thermo-chemical treatment of critical metals containing fractions offers an opportunity to forward such metals to suitable recycling processes in combination with a thermal decomposition of existing polymeric matrixes without any oxidation of target metals.

In general, pyrolysis processes could be used either to extract such metals via halogenation and/or vaporization or to expose it from polymeric matrixes. For both cases tests were conducted additionally to those conducted with shredder residues in order to show process models for utilization of pyrolysis to enable critical and scarce metals recycling.

Additionally, halogenation and subsequent vaporization processes could be conducted in order to depollute different fractions. As an example, some toxic metals such as As or Sb are very reactive with halogens and show low boiling points in halogenated forms [Holleman et al. 2007].

Liquid crystal displays

Liquid crystal displays (LCD) represent a composite material containing not only scarce and critical metals such as In and Ga, but also toxic metals such as As. Due to both low amount of polymeric material as well as low concentrations of metals like In and Ga, three different pathways of thermo-chemical treatment were conducted in order to find the best technique regarding metal extraction: (1) pyrolysis, (2) co-pyrolysis with polyvinyl chloride (PVC), and (3) pyrolysis with PVC plus LCD in vapor-phase mode. For all of these tests, LCD were provided by a WEEE treatment facility, which disassemble flat panel displays from EoL-TVs, -laptops, and -monitors using automated operation devices.

As mentioned in chapter 3.4.2, LCD consist out of a sandwich-structure with two main layers specifiabile due to bright and dark coloration. Elemental composition analyses using energy dispersive X-ray fluorescence spectrometry (EDXRF) were conducted for both sides of the sandwich-structure in order to quantify metal concentration on both layers. Analyses revealed that content of In was nearly four times higher in dark layers¹³ of LCD than in bright ones (Table 9); therefore, dark ones were chosen for pyrolysis tests. Mainly for tests with LCD in vapor-phase mode, material was required, which

¹³ Dark part of LCD represents that side, which is in the direction of an applicant of flat panel displays.

showed free space that vapor from PVC pyrolysis could pass through easily. Therefore, LCD were crushed and sieved in order to separate material with a particle size >1 mm, which was used for all different pyrolysis tests.

Table 9: Concentrations of As, Ga, In, and Sn in both tested LCD layers (in $\text{mg}\cdot\text{kg}^{-1}$).

Element	Bright Layer	Dark Layer	Element	Bright Layer	Dark Layer
As	1 119.0	1 740.0	In	29.0	110.0
Ga	7.3	0.0	Sn	611.6	414.5

* EDXRF with C, H, N, S given and O as missing component

PVC for above mentioned tests as co-pyrolysis or with LCD in vapor-phase mode was taken from waste window frames. These were accurately cleaned using water and ethanol as well as crushed and sieved in order to gain material free of adherences with a particle size of 1 - 10 mm. For vapor-phase mode test, crushed LCD were placed inside a heated, vertical installed pipe¹⁴, which connected the pyrolysis reactor with a cooling unit. Due to a maximum temperature inside the corresponding pipe of 570 °C, this temperature was chosen for pyrolysis and co-pyrolysis, too. Pyrolysis of PVC during vapor-phase mode test was conducted at a lower temperature corresponding to the first stage of PVC decomposition.

Besides tests regarding concentrations of metals in pyrolysis solid products, those in liquid products as well as in NaOH-solution ($6.75 \text{ mol}\cdot\text{l}^{-1}$) were analyzed, too. Therefore, a solid fraction, which becomes precipitated in NaOH-solution during pyrolysis tests, was separated from liquid part and dried at 105 °C for analysis. The liquid phase become thickened by boiling and dried at 105 °C afterwards, too.

Tantalum capacitors

Capacitors for integrated circuits (IC) such as printed wiring boards (PWB) are produced in many different forms, which often make a determination concerning its main component such as Ag, Al, Nb, Mn, Ta, or ceramics impossible without any disruptive analysis. Therefore, seven different capacitors were manually replaced from common PWB and its elemental composition analyzed using wavelength dispersive X-ray fluorescence (WDXRF).

¹⁴ The corresponding pipe is the later mentioned "tar cracking unit" and will be described in chapter 5.4.1.

The different capacitors were previously characterized due to the following parameters:

- mounting technology (Through Hole Technology (THT) or Surface Mounted Device (SMD))
- shape (just for THT capacitors)
- characteristic color of the exterior mold

The concentrations of above mentioned metals as well as Si, which is used as filler (fumed silica) in some resins, are listed in Table 10; corresponding photos of each type of capacitors can be found in the appendix (Figure 87).

Table 10: Concentrations of selected metals in different capacitors (shortly Cap.) (in wt.-%).

Mounting Technology	Through Hole Technology (THT)			Surface Mounted Devices (SMD)			
[wt.-%]	Blue, yellow Disks	Green Drops	Orange, yellow Drops	Brown	Black	Yellow	Orange
Ag	0.4285	<0.10	2.7115	2.8454	1.8529	1.9090	2.6017
Al	0.7907	31.3201	1.1305	<0.10	0.2580	0.1901	0.1871
Mn	4.0947	0.0201	11.5121	0.0506	8.8737	12.4550	13.8375
Nb	<0.001	0.0016	0.0545	0.5629	0.0048	0.0022	<0.001
Si	8.6498	0.5493	17.6712	0.6045	38.8650	34.2911	3.7924
Ta	<0.10	<0.10	18.4276	<0.10	19.2286	24.7981	62.0498

For recovery tests concerning Ta, two most commonly used types of capacitors containing Ta “SMD Yellow” and “SMD Black” were chosen, which, additionally, showed medium levels of Ta concentrations in relation to all Ta containing capacitors.

5.2 Analysis: Instrumentation

For the characterization and specification of different tested feedstocks, a number of analyses were conducted for each feedstock. If particles in samples showed too large sizes for analyses, samples were crushed using a cutting mill SM 300 (Retsch, Haan, Germany) for particles up to 1 mm. Below this size, samples were given to an external laboratory to reduce size using a cryogenic mill. Particle size distributions of solid materials were determined using a sieving tower (Analysette 3, Fritsch, Idar-Oberstein, Germany).

Elementary analysis (C, H, N, S)

Determination of C, H, N, and S were conducted using a Vario MACRO Cube elemental analyzer (Elementar Analysensysteme, Hanau, Germany). Samples of up to 1.5 g gets incinerated under injected oxygen in an integrated oven inside the device and the content of C, H, N, and S of the sample gets analyzed via chromatography after separation in three different columns.

Higher heating value

Higher heating values *HHV* were measured using a bomb calorimeter C 2000 (IKA, Staufen, Germany) with an isoperibol mode of operation for samples of up to 40 000 J according to DIN 51900.

TGA and DSC

Thermal gravimetric analyses (TGA) were carried out using a STA 409 PC *Luxx*[®] thermal analyzer (Netzsch, Selb, Germany). In accordance with DIN EN ISO 11357, a DSC 204 F1 Phoenix (Netzsch, Selb, Germany) was used for Differential Scanning Calorimetry (DSC). In both cases the heating rate was 5 K·min⁻¹ in an Ar flow of 100 ml·min⁻¹ with 14.9 - 70.6 mg of the respective sample.

Dry residue and ignition loss of solid materials

The dry residue from solid materials was determined by drying a sample at 105 °C following DIN EN 12880. In order to analyze the ignition loss of solid materials, samples were placed in a muffle furnace at 550 or 750 °C for a minimum of 12 h following DIN 18128. In both cases (drying and incineration), samples were weighted and the procedure repeated for 3 h. If the weight of each sample differs more than 2 mg, a further drying or incineration, respectively, was conducted.

Metals, metalloids, and nonmetals

Determination of metals, metalloids, and nonmetals were conducted using a benchtop energy dispersive X-ray fluorescence (EDXRF) spectrometer Epsilon 3^{XLE} (PANalytical, Kassel, Germany), which could be used for elemental analyses from C to Am.

Additionally, in some cases tests using inductively coupled plasma mass spectrometry (ICP-MS) according to DIN EN ISO 17294-2 and inductively coupled plasma optical emission spectrometry (ICP-OES) according to DIN EN ISO 11885 were conducted. In these cases, concentrations of Br and Cl were measured with ion chromatography in accordance with DIN 51727. Chemical digestions were done by microwave and aqua regia extraction (DIN EN 13657) as well as alkaline fusion (DIN ISO 14869-2). Analyses based on ICP-MS and ICP-OES were done in specialized laboratories (UCL, Lünen,

Germany; Dorfner Analysenzentrum und Anlagenplanungsgesellschaft mbH, Hirschau, Germany), which are accredited by DAkkS (German accreditation body) in accordance with DIN EN ISO/IEC 17025.

Results from EDXRF and ICP-MS/-OES analyses could differ not only due to the heterogeneous character of the material, but also on some influencing effects of sample matrix. Digestion of metals during preparation for ICP-MS/-OES analyses could be insufficient for metals with high concentrations. In contrast, for analyses conducted with EDXRF no digestion is necessary; however, disadvantage of this method is that used x-rays just analyzed thin layers of samples and/or metals.

Metal phases

X-ray diffraction (XRD) analyses were conducted for qualitative and quantitative analyses of crystalline phases in different pyrolysis solid products. Tests were conducted using either a D500 (Siemens, Munich, Germany) with scintillation counter, increment of 0.01° per step and a measurement time 8 s per step or a D5000 (Siemens, Munich, Germany) with position-sensitive detectors, increment of 0.01° per step and 1 s per step.

Water and total acid number of liquid products

For quantification of water in liquid products such as pyrolysis liquid products, a semi-automatic 915 KF Ti-Touch (Metrohm, Herisau, Swiss) was used. The Total Acid Number *TAN* was determined iteratively, using a 916 Ti-Touch (Metrohm, Herisau, Swiss). In dependency of the expected *TAN*, the sample weight had to be corrected according to Table 11 and the measurement replayed.

Table 11: Sample weight and weighting accuracy for quantification of *TAN*.

TAN [mg KOH · g⁻¹ sample]	Sample weight [g]	Weighting accuracy [mg]
0.05 - 0.9	10 ± 2	100
1 - 4.9	5 ± 0.5	20
5 - 19	1 ± 0.1	5
20 - 99	0.25 ± 0.02	1
100 - 250	0.10 ± 0.01	0.5

Molecular compounds of pyrolysis liquid products

GC-MS analyses were conducted for determination of different compounds present in pyrolysis liquid products. Therefore, samples of liquid products were mixed with acetonitrile as solvent in a ratio of 0.1 wt.-% and spiked with 0.1 ml internal standard solution (100 mg·l⁻¹ 1,3,5-tri-terz-butylbenzene in cyclohexane).

Analyses were performed with a single-channel gas chromatograph (6850, Agilent HP, Santa Clara) connected to a quadrupole mass spectrometer (5975, Agilent HP, Santa Clara) with an electron ionization of 70 eV at a frequency of 1.55 scan s⁻¹ within the 10 - 450 m/z range. Analytes were separated by a HP-5 fused silica capillary column (stationary phase poly [5 wt.-% diphenyl/95 wt.-% dimethyl] siloxane, 30 m, 0.25 mm i.d., 0.25 mm film thickness) using He as carrier gas with the following thermal program: 50 °C with a hold for 5 min, then ramping up with a heating rate of 10 °C·min⁻¹ until 325 °C followed by a column cleaning at 325 °C for 10 min.

Compounds of formed gases

Main gaseous compounds of produced pyrolysis gases were determined using an online multi gas analyzer MGA-12 (Dr. Födisch Umweltmesstechnik AG, Markrandstädt, Germany) according to DIN EN 15267-3. Measurements are based on an infrared photometer¹⁵ for CO, CO₂, CH₄, and C_xH_y as well as an electrochemical cell for O₂. H₂ was measured using a measuring transducer which analyzes the thermal conductivity and temperature of a present gas. In order to segregate side effects on H₂ analyses from other gases, the following correction term was used to quantify the yield of H₂ accurately:

$$H_{2\text{ corr}} = H_{2\text{ crude}} - (-0,00174 * CO_2^2 - 0,13109 * CO_2) \\ - (0,00114 * CH_4^2 + 0,12092 * CH_4)$$

In all tests, a measurement interval of 10 s was chosen.

Heating value and density of formed gases

In addition to the above mentioned measurements of compounds of formed gases, a gas calorimeter CWD 2005 (Union Instruments, Karlsruhe, Germany) was used for measurements and calculations of lower *LHV* and higher heating values *HHV*, specific (ρ), and relative densities (d), as well as corresponding Wobbe indexes W_s and W_i as:

- $d = \frac{\rho_n}{\rho_{n(dry\ air)}} \approx \frac{\rho_n}{1.184} [kg * m^{-3}]$
- $W_s = \frac{HHV}{\sqrt{d}} [MJ * m^{-3}]$
- $W_i = \frac{LHV}{\sqrt{d}} [MJ * m^{-3}]$

¹⁵ Concentrations of CH₄ and C_xH_y were calculated in one cell. If concentration of C_xH_y are >5 vol.-%, measurement of CH₄ was not conductible.

For calculations of d , ρ of dry air was set as $1.184 \text{ kg}\cdot\text{m}^{-3}$ as it is simplified at 25°C (standard conditions). Calculations of Wobbe indexes are necessary in order to classify compatibility of gases from different sources with regard to thermal load [Nitschke-Kowsky et al. 2012]

Polyhalogenated dibenzo-*p*-dioxins and furans

Determinations of polyhalogenated dibenzo-*p*-dioxins and furans (PXDD/F) were conducted in a specialized laboratory (Münster Analytical Solutions, Münster, Germany) following DIN EN ISO 17025:2005 based on high-resolution GC-MS (HR GC-MS). Main steps of analyses were:

- Sample preparation and extraction
 - o Homogenization and determination of dry matter
 - o Addition of polychlorinated dibenzo-*p*-dioxins and furans (PCDD/F) standards to aliquot sample materials
 - o HCl extraction of sample material, filtration of resulting suspension, liquid-liquid extraction of filtrate using toluene
 - o Drying of filtration residue and Soxhlet extraction with toluene for 24 h
 - o Combination of partial extracts
- PXDD/F analysis
 - o Addition of $^{13}\text{C}_{12}$ -marked PCDD/F or polybrominated dibenzo-*p*-dioxins and furans (PBDD/F) as internal standards
 - o Stepwise extract clean-up
 - o Addition of $^{13}\text{C}_{12}$ -marked PCDD/F standards for retrieval of PCDD/F; addition of isotopic marked retrieval standards for PBDD/F.
 - o HR GC-MS analysis
 - o Quantification using former added and marked internal standards

In summary, 17 PCDD/F and 8 PBDD/F according to the German act on restriction of chemicals (GGVSEB) and the German chemicals prohibition ordinance (ChemVerbotsV) as well as 9 further PBDD/F plus sums of tetra-, penta-, hexa-, and heptachlorinated and -brominated dioxins and furans were determined¹⁶.

¹⁶ Assignment of some hexa-BDF and of 1,2,3,4,7,8,9-hepta-BDF were based on comparison of retention indexes due to non-existing commercial standards. In order to quantify such compounds, response factors

For comparability, mainly five different sums of PCDD/F or PBDD/F congeners according to GGVSEB and ChemVerbotsV were shown in the text. A full list of congeners and corresponding sums is shown in the appendix (Table 48).

5.3 Analysis: Statistical methods

Such statistical methods were selected, which are manageable with characteristics of gained results: due to high heterogeneity of feedstock from WEEE as well as medium number of statistical tests, both compared to complex statistical evaluations of tests with population of a few hundred or thousand single values, calculations with basic statistical methods were conducted.

Results from pyrolysis tests under different circumstances were analyzed using a number of different statistical methods. Besides common methods to describe present populations such as arithmetic mean \bar{x} , median \tilde{x} , range R , standard error $\sigma_{\bar{x}}$, standard deviation σ_x , or variance σ_x^2 , some further statistical methods were used, mainly in order to test relations and differences due to changed parameters and corresponding results.

Identification of abnormal extreme values

Before results from pyrolysis tests can be evaluated, e.g. concerning significant differences, all results were tested on abnormal values. Therefore, every single value was compared to a value v :

$$v = \bar{x} - 2 * \sigma_x$$

In the cases of $x < v$, the corresponding value x can be defined as strongly below-average, while x in the case of $x > v$ is strongly above-average. Such values were not used in any further calculation. This kind of test on outliers was repeated as long as no further abnormal value was present in the datasets.

Significance test

In order to analyze, if a difference between two groups of values (as means) is significant, a two-random t-test, shortly "t-test", was conducted:

of 2,3,7,8-substituted congeners of the same homologous groups were used. Therefore, such quantification is just semi-quantitative.

$$\hat{t} = \frac{|\bar{x}_1 - \bar{x}_2|}{\sqrt{\frac{Q_1 + Q_2}{n(n-1)}}} = \frac{|\bar{x}_1 - \bar{x}_2|}{\sqrt{\frac{s_1^2 + s_2^2}{n}}}$$

with Q as sum of all deviances $\sum(x - \bar{x})^2$. The level of significance was set as $\alpha = 0.05$: values for $\hat{t} < 0.05$ implicate significant differences between tested groups. For all tests a bidirectional distribution and a heteroscedastic type (two random samples with different variances) was used.

Analyses regarding relationships

For identification of relations and correlations between different pyrolysis parameters, linear and non-linear regression analyses were conducted. These analyses allows to estimate a dependent command variable y , if the independent factor x is given. For linear regression the general term

$$y = a + bx$$

was used and for non-linear regression either the general polynomic term

$$y = a + bx + cx^2$$

or the general logarithmic term

$$y = a \ln(x) - b.$$

In order to determine regressions quality, residuals $\hat{\epsilon}$ as difference between the given value y and the estimated value \bar{y} were calculated as

$$\hat{\epsilon} = y - \bar{y}$$

For high regression quality, $\hat{\epsilon}$ should be as small as possible. Accuracy of every regression gets expressed as coefficient of determination R^2 with values between 0 (target values cannot be explained with chosen regression) and 1 (all target values can explained). Calculations of R^2 were done as square of the empirical correlation coefficient r :

$$r = \frac{s_{xy}}{s_x s_y} = \frac{\sum_{i=1}^n (x_i - \bar{x})(y_i - \bar{y})}{\sqrt{\sum_{i=1}^n (x_i - \bar{x})^2 \sum_{i=1}^n (y_i - \bar{y})^2}}$$

r is an index for the strength of a given relation with values between -1 and 1. Values below 0 indicate negative relations while those above 0 positive ones. No correlation is given in the cases when r is 0. Additionally, when linear regression is given and r has a value of exactly 1 or -1, all single values are on a line and have proportional character.

For statistical evaluations on significant influences and relationships due to additions or fundamental changes in the pyrolysis system, such as the addition of the PO-reactor, following cascade was conducted: Firstly abnormal values were eliminated in both

compared datasets as described above. Secondly both datasets were tested on significant differences using t-test: if values of both groups showed no significant differences, values of the added group became part of the basic population. Otherwise, corresponding results with significant differences were presented stand-alone. In the cases that both groups could become one population, tests on abnormal values were conducted a second time, followed by a second test on significance regarding the added population.

Test on dependency

In addition to the above mentioned significance test, a further test was used in order to check if categorized data are dependent from each other or not. Therefore, the so called chi-squared test for categorical data was conducted:

$$\chi^2 = \sum_{j=1}^m \sum_{k=1}^r \frac{(n_{jk} - n_{jk}^*)^2}{n_{jk}^*}$$

with m and r as numbers of categorizes j and k , as well as n as summarized number of all observations. For calculation of χ^2 , data will be previously categorized in groups, from which every group have to has a minimum of one observation. Null hypothesis H_0 , as both groups are dependent from each other, gets rejected in the case of

$$\chi^2 > \chi^2_{(1-\alpha; (m-1)(r-1))}$$

with α as level of significance, which was set to 95 %, and $(m - 1)(r - 1)$ as number of degrees of freedom.

5.4 Bench-scale plant

A bench-scale test plant was designed and implemented in the technical center of Fraunhofer UMSICHT in Sulzbach-Rosenberg in order to test different feedstock and construction materials as well as to investigate pyrolysis reactions under different circumstances like varying temperature or residence time.

Due to feasible high temperature levels of pyrolysis processes and the partial corrosive products, most parts of the reactor were made out of austenitic, stainless, weldable, and creep-resistant steel (e.g. 1.4571, 1.4404, 1.4301, 1.6358). The development and optimization of the bench-scale pyrolysis plant was an iterative process in which influences of added or varied components were tested in order to find best parameters for designing a continuous pilot plant.

5.4.1 Structure and components

The complete experimental set-up is shown in Figure 31. A detailed drawing of a special part of the set-up, the so called polyolefin-reactor, is shown in Figure 32. Bold written numbers in the text refers to numbered items in such figures. Detailed drawings are given in the appendix (Figure 88 and Figure 89).

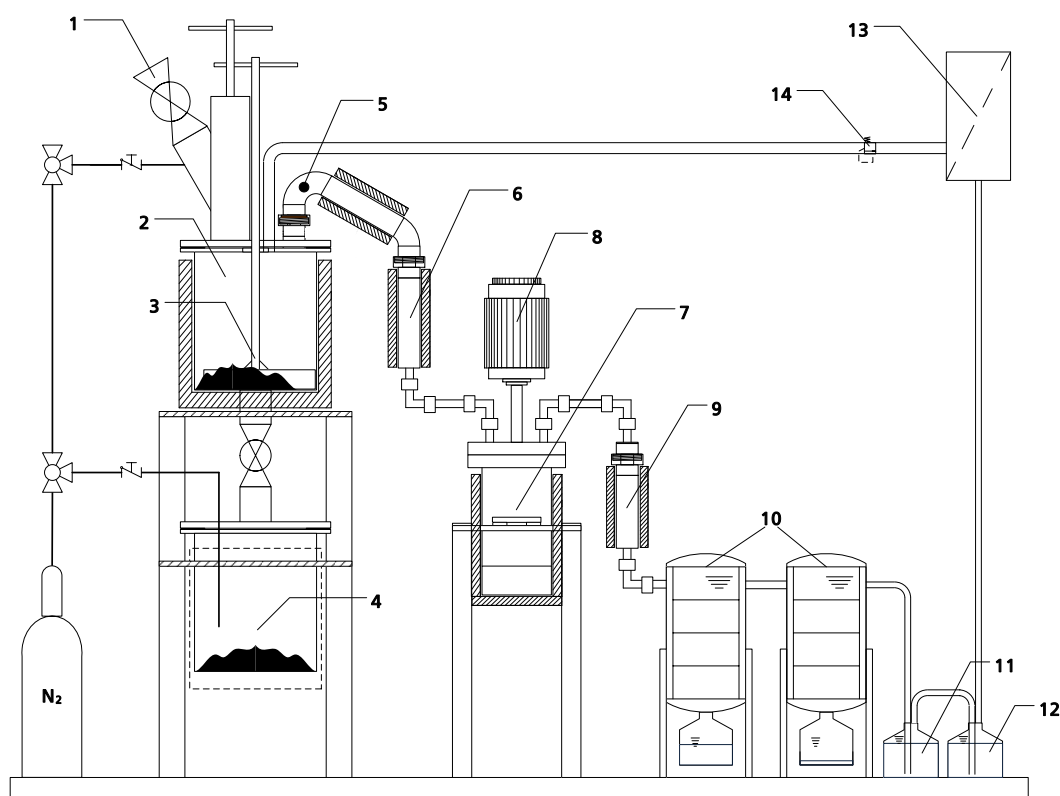


Figure 31: Experimental setup of the bench-scale pyrolysis plant.

1: double door system for feed input; 2: pyrolysis reactor; 3: stirring unit; 4: char pot; 5: lambda sensor; 6: tar cracking unit; 7: polyolefin-reactor; 8: electric spur gear motor; 9: halogen-filter; 10: cooling-units; 11: NaOH scrubber; 12: n-hexan scrubber; 13: activated carbon filter; 14: pressure relief valve.

Pyrolysis reactor and tar cracking unit

As mentioned above, in the bench-scale plant a number of different feedstock were analyzed under pyrolytic conditions. The reactor (**2**) (stainless steel 1.4571) has a cylindrical shape, sized 160 mm in inner diameter and 215 mm in length. It was heated with two panel heatings, one from the shell (KH 210, Ø 162 mm, length 186 mm, 4.5 kW, WEMA, Lüdenscheid, Germany) and one from the bottom (BK 210, Ø 162 mm, 1.0 kW, WEMA, Lüdenscheid, Germany), which were controlled by two thermocouples (NiCrNi, Type K, WEMA, Lüdenscheid, Germany) and a programmable temperature controller (TPR 35/M2, WEMA, Lüdenscheid, Germany). Inside the reactor, there are two more thermocouples (NiCrNi, Type K), one next to the bottom, and one next to the top. Feedstock is given to the reactor through a double door system (**1**), which is installed at the top of the reactor. In order to mix the feedstock during the residence time and to

discharge the produced solid products after that time, a stirring unit (**3**) and a second rotatable bottom with an opening is installed inside the reactor. The solid products fall downwards in a second pot (**4**), which is indirectly cooled by ice cooled water and can be purged with N₂ (≥ 99.8 vol.-%).

From the pyrolysis reactor evolved vapor pass a lambda sensor (**5**) (LSU4, Bosch, Stuttgart) and a tar cracking unit (**6**), heated with four nozzle heater bands (DH400, Ø 35 mm, length 25 mm, 0.14 kW, WEMA, Lüdenscheid, Germany), which are controlled with two clamping band thermocouples (S5420, Ø 32 - 50 mm, WEMA, Lüdenscheid, Germany) and a programmable temperature controller (TPR 35/M2, WEMA, Lüdenscheid, Germany). The tar cracking unit is filled with stainless steel wool in order to decelerate vapors speed through the cracking unit and to form an extended surface. A small piece of pipe (length 120 mm) in between the reactor and the tar cracking unit is heated with four additional nozzle heater bands (DH400, Ø 35 mm, length 30 mm, 0.18 kW, WEMA, Lüdenscheid, Germany), which are controlled with the same temperature controller and an own additional thermocouple (S5420, Ø 32 - 50 mm, WEMA, Lüdenscheid, Germany). The cracking unit is either connected directly to cooling units (**10**) or to a heated polyolefin-reactor (**7**) and a filter unit for halogens (**9**) in order to fulfil further tasks of cleaning. In both cases hot vapor pass two ice-water-cooled units to separate the condensable compounds, followed by two scrubbers of NaOH (**11**) (1 mol·l⁻¹) and n-hexane (**12**) (95 vol.-%). Afterwards, evolved gases were cleaned in an activated carbon filter (**13**). In the unlikely case that the pressure inside the reactor increased to more than 400 mbar, a pressure relief valve (**14**) in a single pipe, which connects the pyrolysis reactor with the activated carbon filter, gets open automatically.

Before conducting any test run, the previously cleaned reactor, char pot, and tar cracking unit including all corresponding seals are installed, the tar cracking unit filled with about 8 - 11 g of stainless wool and all screws as well as connections of the whole system fixed and checked. In order to check tightness of the whole system, pressure air instead of N₂ will be given to the system, while the outlet of the tar cracking unit is locked. After reaching a pressure of 200 mbar inside the reactor, the connection to the pressure air becomes blocked and the pressure drop inside the reactors measured. Only in the case that this drop is very small and close to zero, the pyrolysis test can be started. Therefore, N₂ is connected to the char pot and the cooling units to the tar cracking unit. The whole system is poured with N₂ while the content of O₂ is measured with the lambda sensor inside the vapor pipe at the head of the reactor.

During the heat-up phase and during the test run itself, N₂ is poured constantly into the system, typically with a flow rate of 0.2 l·min⁻¹. The tar cracking unit should be switched on and set to a value of 300 °C, when the pyrolysis reactor reached this temperature, too. After reaching the desired temperature in the pyrolysis plant, a sample is fed to the pyrolysis reactor through a double door system using a cartridge, which was also poured with N₂. After infilling, the sample is held at the desired temperature for the residence

time and become mixed after 15 min with the stirring unit for the first time, followed every additional 5 min by a further mixing. At the end of the residence time, the pyrolysis solid products are led out of the reactor to the second pot by moving the stirring unit in the reverse direction. This opens a hole at the bottom of the reactor.

Due to condensation of vapor in the cold char pot during exhaustion of the reactor, a huge pressure drop can be noticed in some cases. If the pressure falls down to a negative range, the flow of N_2 was increased in order to prevent a vacuum inside the pyrolysis system.

When the reactor is completely empty again, the hole at the bottom of the reactor becomes locked using the stirring unit in order to conduct a next batch test with a further sample. Past the last batch, the reactor becomes emptied a last time and the heating system of the reactor switched off. However, the heating system of the tar cracking unit should be switched off 15 min later to make sure that all condensed products were cracked.

Polyolefin-reactor

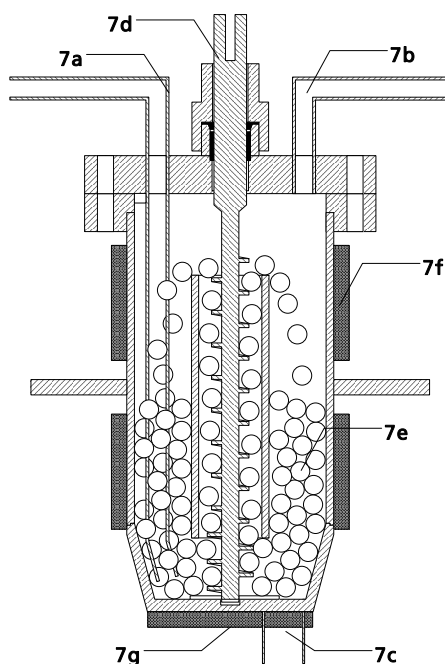


Figure 32: Sectional drawing of the polyolefin-reactor.

7a: vapor inlet; 7b: vapor outlet; 7c: outlet for molten polyolefin; 7d: screw conveyor; 7e: spheres; 7f: panel heating; 7g: bottom heating.

As mentioned in chapters 4.3.2 and 4.4, pyrolysis liquids and vapor containing PBDD can be debrominated using molten polyethylene (PE) or polypropylene (PP), which spends hydrogen for cracking such compounds [Hornung et al. 2003; Hornung et al. 2005]. Additionally, a stirred sphere reactor can be used for efficient decomposition of polymers [Hornung 1997]. Against this background, a new polyolefin-reactor (PO-reactor) was designed and constructed in order to decompose PXDD/F using not only PP,

but also blends with additives. Design and construction of the PO-reactor (Figure 32) was mainly based on developments by [Hornung 1997]. The reactor (**7**) (stainless steel 1.4571) has a cylindrical shape, sized 100 mm in inner diameter and 212 mm in length with a cone-shaped, concentric bottom. In the top cover are three openings (\varnothing 12 mm) for polyolefin inlet as well as vapor in- (**7a**) and outlet (**7b**) as well as different openings for sensors. In the bottom is an outlet (**7c**) for molten polyolefin (\varnothing 22 mm). Inside the reactor, a screw-conveyor (stainless steel 1.6358) is installed, which is linked to an electric spur gear motor (**8**) (Type BG06-31/D06LA4-TF, 0.18 kW, Bauer Gear Motor, Esslingen, Germany). The motor can be driven between 11.0 and 44.5 rpm at a load torque of 43.0 and 51 Nm, respectively. The screw conveyor (**7d**) is installed in order to transport spheres (**7e**) (stainless steel 1.4034, \varnothing 10 mm, KGM, Fulda, Germany) from the bottom of the reactor to its top. In the case those spheres are blocking the screw conveyor, the motor stops at the current load torque, run for a very short time in the opposite direction and starts again. Additionally, a shear pin (brass, \varnothing 4.6 mm) is installed in the shaft, which connects the screw and the spur gear motor. Preliminary tests with shear pins of this material and thickness revealed a maximum load torque of 60 Nm, in order to install a predetermined breaking point to protect the electric spur gear motor as well as the screw-conveyor. Besides two panel heatings (**7f**) (KHK \varnothing 108 mm, length 58 mm, 1.3 kW, Ihne&Tesch, Nuremberg, Germany) at the sides of the reactor, a further heating from the bottom (**7g**) is installed (KA240-B-2000, \varnothing 85 mm, 0.22 kW, Ihne&Tesch, Nuremberg, Germany).

In order to fill the PO-reactor with a molten plastic, an extruder (19/25 D, 3:1 constant taper screw, max. feed rate 3 kg·h⁻¹, heating power 4.7 kW, motor power 1.1 kW, Brabender, Duisburg, Germany) is connected at the top of the reactor. A throttle diverter is installed at the end of the extruder and conveys the molten polyolefin inside the PO-reactor. It is heated with a nozzle heater band (DH400, \varnothing 80 mm, length 40 mm, 0.5 kW, WEMA, Lüdenscheid, Germany) with an integrated thermocouple (Type J, FeCuNi, WEMA, Lüdenscheid, Germany).

Filled with 500 spheres as well as installations such as screw, the free space of the sphere packing is approximately 260 ml, which represents the volume of polyolefin, used for any tests.

For test runs, the water cooling unit of the extruder gets switched on, followed by its nozzle heater bands as well as those of the PO-reactor. The selected temperatures of heater bands from the extruder are 140, 180, 200, and 340 °C for zone 1, 2, 3, and throttle diverter, respectively. The temperature of the heater bands of the PO-reactor are set to 350 °C. In order to obtain a uniform heat distribution in the whole system, approximately 100 K before reaching the desired temperature of 350 °C, the motor of the PO-reactor gets switched on. When the reactor reached this temperature, the screw of the extruder can be switched on to 10 r·min⁻¹ and a polyolefin filled in. After 6.1 min, when the polyolefin achieve the throttle diverter, the rotating speed gets increased to 48 r·min⁻¹ to fill polyolefin inside the reactor fast. After 9 min, rotating speed is set to

0 r·min⁻¹. At this time, the reactor got filled with 260 ml (234 g). In order to ensure impermeability to gas through the extruder, the receiver tank of polyolefin-feedstock must be filled sufficiently to prevent that the extruder gets empty.

After switching off the PO-reactor and at an end of a test run, it should be waited until the polyolefin inside the PO-reactor reaches a temperature of approximately 200 °C. After that, a drain plug at the bottom of the reactor can be unscrewed in order to discharge the polyolefin in a water quench for cooling it down rapidly.

Halogen-filter

Due to the installation of a PO-reactor, it seems feasible to decompose halogenated aromatic compounds under formation of HX. In order to absorb such compounds from pyrolysis vapor, a new filter material (see chapter 5.4.2) was developed and a corresponding filter unit designed. The halogen-filter (**9**) is a fixed bed filter and installed downstream the PO-reactor in order to absorb HCl and HBr. The filter material is placed inside a pipe (stainless steel 1.4571) of 110 mm length and an inner diameter of 27.2 mm, which is heated with two nozzle heater bands (DH600, Ø 35 mm, length 50 mm, 0.5 kW, WEMA, Lüdenscheid, Germany), which are controlled with one clamping band thermocouple (S5420, Ø 32 - 50 mm, WEMA, Lüdenscheid, Germany) and a programmable temperature controller (WTD 35/M-1, WEMA, Lüdenscheid, Germany). In order to prevent release of filter material out of the filter-pipe, a perforated strainer (diameter of holes: 2 mm) is set inside, 10 mm from the bottom. For changing of filter material, the top of the filter can be unscrewed.

For test runs, the halogen-filter is filled with 90 - 100 g of filter material and the nozzle heater bands of the halogen-filter set to a temperature of 450 °C.

5.4.2 Development, optimization, and preliminary tests

The above described system of pyrolysis reactor and its additional components shows the results from a series of preliminary tests. During these tests, not only reported feedstocks, but also further samples from WEEE or other kind of feedstock were tested. All findings were used to optimize the system to the present one.

Pyrolysis reactor and tar cracking unit

Firstly the reactor consisted only out of the reactor pot itself as well as one in- and outlet in the cap for feedstock and produced vapor, respectively. In this case it was not able to discharge the pyrolysis reactor in order to finish a batch after a defined residence time, because the material left in the reactor, which cooled down very slowly. In comparison to a continuous plant, which should be designed, results from these tests concerning product allocation and quality are not comparable. However, first conclusions could be noted concerning materials as well as types of seals and connections. Additionally,

influences of the sample size were tested. Therefore, sample sizes between 100 and 300 g were tested and its impacts on product allocation analyzed. These tests suggest that sample sizes of more than 250 g led to an incomplete pyrolysis.

In order to imitate a moving inside the reactor, comparable to that in a continuous plant, as well as to be able to discharge the reactor and load a new batch, a tar pot became installed below and a stirring unit inside the reactor. Due to these installations some changes concerning the pyrolysis product allocations as well as solid products were noted. On the one hand, the yields of liquids increased while that of solids decreased, which indicate that pyrolysis processes could be incomplete before these parts were installed. On the other hand, ignition loss of pyrolysis solid products increased. This effect could be explained due to a much longer residence time of such products in a hot atmosphere inside the reactor, before these parts were installed. Last but not least a non-quantifiable, but discernible effect concerning odor of pyrolysis solid products could be noted. Before both installations were done, such products have a characteristically odor of phenols, which was absent after stirring unit and char pot were installed.

In test series, small amounts of stiff and highly viscous compounds inside the vapor pipe were accumulated. These amounts were significantly higher in the case of another shredder residue, which shows higher amounts of plastics. In order to prevent an accumulation of and/or to destruct these compounds two different options were tested. On the one hand, the length of the vapor pipe was increased in order to gain a slow cooling of vapor. This installation did not bring up the desired effect, quite the contrary, and the amount of blocking compounds increased. On the other hand, the above mentioned tar-cracking unit was designed and installed instead of this pipe. The tar-cracking unit and the corresponding connection to the pyrolysis reactor are heated on the full length at approximately 310 - 320 °C. In order to decelerate vapor speed inside this unit, it was filled with stainless steel wool. The installation of the tar-cracking unit showed the desired effect: No stiff and just very small amounts of highly viscous compounds were found inside the vapor pipe after pyrolysis tests. Instead of these products, small amounts of char were formed onsite the stainless steel wool as products of further decomposition reactions. As a further, advantageous aspect, the yield of pyrolysis liquid products increased (slightly).

Polyolefin-reactor

For tests in the PO-reactor, PP with a high melt flow rate was used in order to yield low pressurization inside the whole pyrolysis system. The chosen PP (Purell HP 570 U natural, LyondellBasell, Rotterdam, Netherlands) shows a melt flow rate (230 °C/2.16 kg) of 7.5 g·min⁻¹ and a density of 0.90 g·cm⁻³ [LyondellBasell 2013].

Before any tests in the pyrolysis reactor were done, TGA of selected PP was conducted in order to find out optimal process temperatures for the main tests. As shown in Figure 33, the melting point, characterized by a negative peak of DSC-curve, is at a temperature of 174.1 °C. Additionally, the analysis shows that the weight loss of the material starts at 351.6 °C with a peak at 424.1 °C. Therefore, a process temperature of 340 °C was chosen in order not to decompose PP strongly.

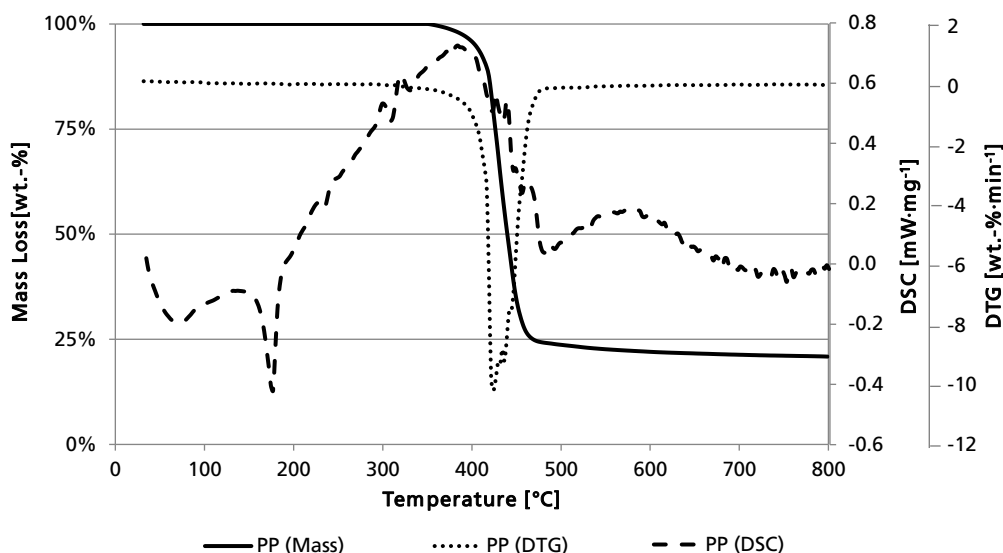


Figure 33: TGA, DTG, and DSC of PP (HP 570 U natural); 5 K·min⁻¹; argon.

Average and minimal residence times of pyrolysis vapor, which pass the PO-reactor, were calculated using formulas for velocity of flow

$$v = \frac{Q}{A} = \frac{Q * 4}{d_i^2 * \pi}$$

and for pressures of gases at various temperatures

$$V(T) = V_0 * (1 + \gamma_0 * (T - T_0))$$

with Q as volume flow rate (in m³·s⁻¹), A as flow cross-section (in m²), d_i^2 as inner diameter (in m) and γ_0 as $\frac{1}{T_0} = \frac{1}{273.15 \text{ K}}$. For purposes of simplification, a high of molten polyolefin accounting for ½ inner length of PO-reactor (= 106 mm) and a temperature of 340 °C were assumed. For calculations, the measured gas volume after cooling (25 °C) was taken into account as well as the theoretical volume of formed pyrolysis liquids at a temperature of 340 °C at the measured pressure inside the PO-reactor.

For this

$$\rho * V = m * R_s * T$$

was used with a specific gas constant $R_s = \frac{R}{M}$ (in J·kg⁻¹·K⁻¹) based on analyzes of main molecular compounds by GC-MS.

Halogen-filter

A new filter material for absorption of halogens was developed, which should be placed in the halogen-filter downstream the PO-reactor. From literature Cl absorption ability of La_2O_3 is well known (chapter 4.3.3). However, that of Br absorption is not reported. Therefore, preliminary tests with HBr and Br_2 were conducted at temperatures between 300 and 600 °C. Due to the future installation position in vapor phase mode between PO-reactor and condensation units, tests at temperatures <300 °C were not conducted in order to prevent a blocking of the filter with high-boiling substances such as tar and waxes.

In order to produce a filter material, which is able get streamered by pyrolysis vapor and which does not lay out of the filter-pipe, a three-dimensional filter material have to be formed. In first tries, $\text{La}(\text{OH})_3 + \text{LaOOH}$ (41:59 by weight) in powder form (99.9 wt.-%, Haines & Maassen, Bonn, Germany) was used for sintering at temperatures up to 1 325 °C. Even after addition of sintering agents such as SiO_2 and H_3BO_3 , formed structures decomposed to fine powder again, due to reactions between formed La_2O_3 and H_2O from air to $\text{La}(\text{OH})_3/\text{LaOOH}$. Due to this reaction and additionally relatively high melting point of La_2O_3 (2 315 °C [Perry, Phillips 1995]) the desired effect forming a stable filter material was not reached.

Against this background a novel approach was successfully developed and tested. In order to fix La powder in a three-dimensional form, tests with glass beads as carrier material were conducted. On the basis of melting point, surface area, and porosity for flow ability of gases, glass beads were selected. Due to the particular property of glass melting in a comparatively wide range, which start could be detected by the glass transition temperature, an agglutination of glass' surface and La powder seemed to be possible. Based on DSC (Figure 34) of selected glass beads (Ø 5 mm, Glaswarenfabrik Karl Hecht, Sondheim vor der Rhön, Germany), in three test series at 570, 770 and 850 °C, coating ability of glass beads with above mentioned $\text{La}(\text{OH})_3/\text{LaOOH}$ powder were conducted.

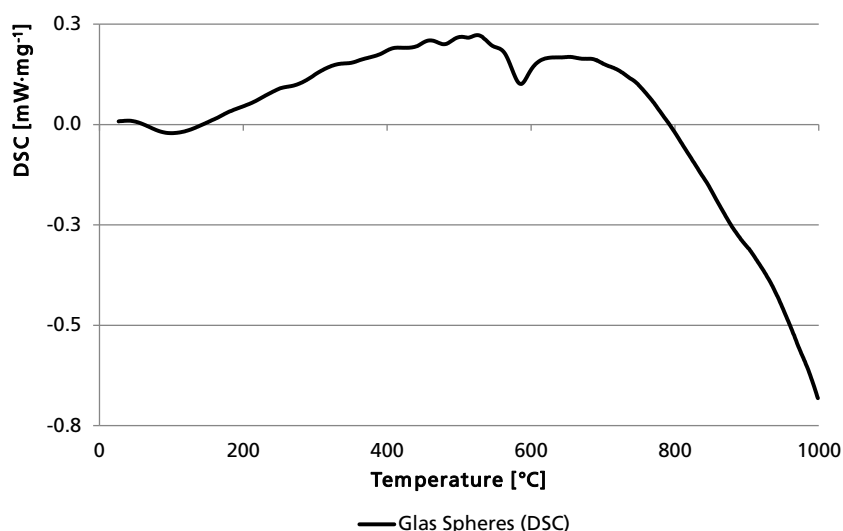


Figure 34: DSC of glass spheres; 20 K·min⁻¹; air.

While at 570 °C no coating on spheres could be conducted, at 770 °C a very small amount of 0.16 wt.-% of La(OH)₃/LaOOH could be set on spheres surface. At 850 °C a solid and comprehensive coating with an average amount of 4.13 wt.-% La were set on spheres. Figures from scanning electron microscope (SEM) confirmed this (Figure 35). A further increase of temperature led to the undesirable effect that the glass spheres agglutinated to each other, which means that indeed a filter material was formed, but its ability for streaming decreased towards zero.

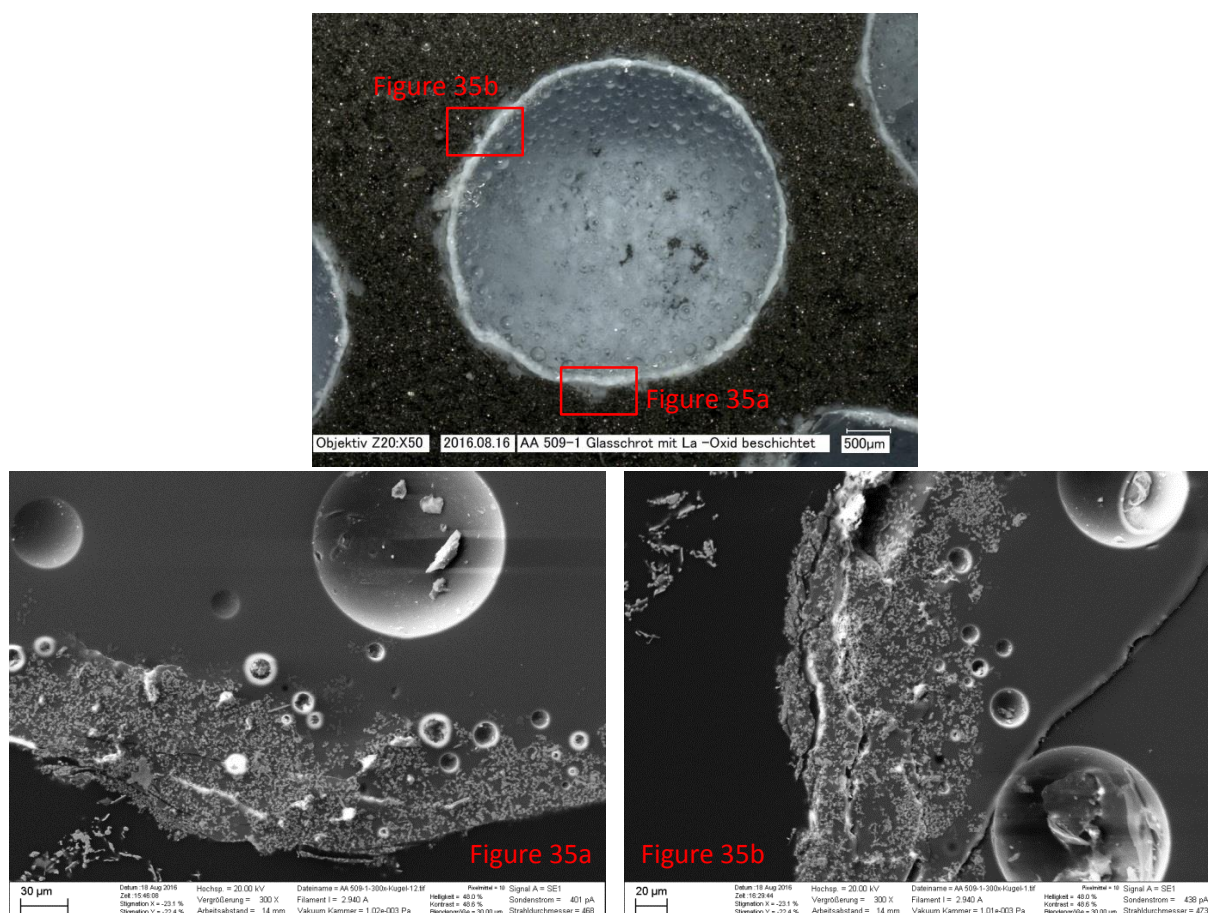


Figure 35: Figures from SEM of coated glass spheres (magnification of 300 for figures 35a and 35b).

In combination with the recordings of figures by SEM, elemental analyses were conducted using EDXRF. From the results (Table 12 and Table 13) it is obvious that the concentration of La on spheres surfaces is comparatively high and that the coating is homogenous. Spectra of both analyses can be found in the appendix (Figure 91 and Figure 92).

Table 12: EDXRF results from La coated glass spheres, spectrum from Figure 35a.

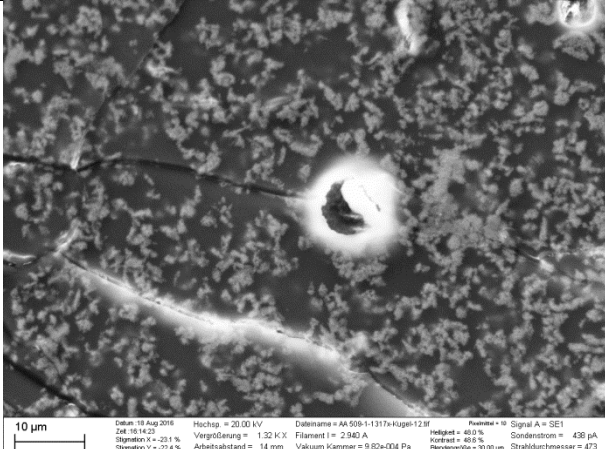
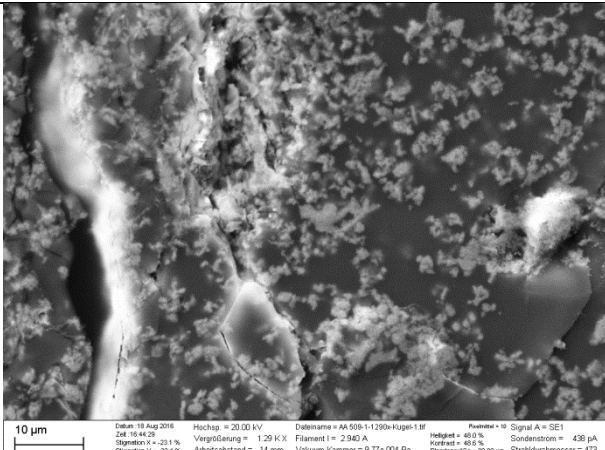
Spectrum of Figure 35a with a magnification of 1317	Element	Concentration [wt.-%]
	Al	1.36 (± 0.09)
	Ca	2.69 (± 0.03)
	Cl	0.34 (± 0.02)
	Br	0.00 (± 0.00)
	K	0.27 (± 0.02)
	La	22.52 (± 0.09)
	Mg	1.60 (± 0.03)
	Na	9.18 (± 0.07)
	O	41.15 (± 0.12)
	Si	19.81 (± 0.07)
	Zn	1.07 (± 0.05)

Table 13: EDXRF results from La coated glass spheres, spectrum from Figure 35b.

Spectrum of Figure 35b with a magnification of 1290	Element	Concentration [wt.-%]
	Al	1.45 (± 0.09)
	Ca	2.24 (± 0.02)
	Cl	0.35 (± 0.02)
	Br	0.00 (± 0.00)
	K	0.28 (± 0.02)
	La	22.35 (± 0.09)
	Mg	1.87 (± 0.03)
	Na	9.62 (± 0.07)
	O	41.04 (± 0.13)
	Si	19.63 (± 0.07)
	Zn	1.15 (± 0.05)

Absorption tests were conducted using approximately 90 g of filter material and either Br₂ (99.8 %, Alfa Aesar, Karlsruhe, Germany) or PBr₃ (98 %, Alfa Aesar, Karlsruhe, Germany) in order to form HBr¹⁷.

Formation of HBr from PBr₃ $PBr_3 + 3 H_2O \rightarrow H_3PO_3 + 3 HBr$ (Eq. 5.1)

The amount of absorbed Br₂ or HBr in the filter was estimated indirectly by gravimetric determination of precipitated AgBr in a downstream solution of AgNO₃:

Reaction of HBr with AgNO₃ $HBr + AgNO_3 \rightarrow AgBr \downarrow + HNO_3$ (Eq. 5.2)

Therefore, vapor of HBr was passed directly into a solution of 120 ml NaOH (1 mol·l⁻¹, Sigma Aldrich, Darmstadt, Germany) and 100 ml distilled H₂O while Br₂ vapor had to become reduced in order to gain Br⁻. Following [Fehér et al. 1953] 8 g of an alkaline solution of H₂O₂ (30 vol.-%, VWR, Darmstadt, Germany) was used to reduce Br₂ to Br⁻ under formation of O₂:

Reduction of Br₂ using H₂O₂ $H_2O_2 + Br_2 \rightarrow 2 HBr + O_2$ (Eq. 5.3)

The formed HBr containing solution was afterwards firstly decoct in order to remove surplus reductive agent followed by neutralization using sulfuric acid (98 %, Merck, Darmstadt) and mixing with AgNO₃ solution for precipitation of AgBr. In both cases (HBr and Br₂), precipitated AgBr was afterwards quantified gravimetrically using a strainer (porosity level 3). Filtered material from strainer was dried and weighted.

Test runs were conducted at 300, 450, and 600 °C each with and without La filter material inside the filter. Test runs without filter material were necessary in order to gain reference values, because it seems possible that highly reactive Br compounds react with parts of the filter case. Table 14 shows the yields of precipitated AgBr from different test runs as well as corresponding efficiencies.

¹⁷ Direct utilization of HBr (48 % solution in water, Acros Organics, Geel) was also tested; however, after heating above its boiling point, an extremely strong corrosion in the filter unit took place, which made determination of filter efficiency impossible.

Table 14: Yields of precipitated and dried AgBr and corresponding efficiencies from test runs with Br₂ and HBr at 300, 450, and 600 °C.

Temperature	Br ₂			HBr		
	Without La	With La	Efficiency	Without La	With La	Efficiency
	AgBr [wt.-%]	AgBr [wt.-%]	[wt.-%]	AgBr [wt.-%]	AgBr [wt.-%]	[wt.-%]
300 °C	60.43	64.75	---*	100.00	63.22	36.78
450 °C	73.15	5.78	92.10	61.70	32.54	47.26
600 °C	32.06	7.84	75.56	98.00	8.82	91.00

* Efficiency seems to be zero due to higher absorption without La instead of with it.

As shown in Table 14 highest efficiency concerning Br₂ was reached at a temperature of 450 °C, while that regarding HBr was at a temperature of 600 °C. XRD analyses of spheres from absorption tests with Br₂ at 450 °C emphasized this (Figure 93 in the appendix). Just a comparatively low amount of LaBr₃ accounting for 2.3 wt.-% were found while 23.9 wt.-% were in the form of LaOBr (%-values after normalization). Additionally, regarding oxides and hydroxides of La it is obvious that much more La₂O₃ is present compared to La(OH)₃ and LaOOH due to production of spheres and heating of it in the filter¹⁸.

5.5 Sustainability assessment of a continuous pilot plant

Before a pilot plant, based on the results of this thesis, will be designed and developed for a treatment of shredder residues, a sustainability assessment will be conducted in order to identify major influences of plants design or changes during operation. Therefore, an ecological as well as economical assessment will be conducted.

5.5.1 Ecological assessment

Goal and scope

Following the method of DIN EN ISO 14040/14044 an ecological assessment was conducted in order to compare a thermal treatment of shredder residues in a municipal waste incinerator (MWI) (option 1, status quo) with a treatment based on a pyrolysis process (option 2).

The goal for the above mentioned comparison was set to “to compare the environmental impacts of pyrolysis (as pretreatment for a pyrometallurgical recycling of metals applicable in an integrated copper smelter) with the alternative of incineration in an

¹⁸ The initial La material consisted out of 41.0 wt.-% of La(OH)₃ and 59.0 wt.-% LaOOH.

MWI (for depollution and reduction of wastes volume as well as thermal energy recovery)". In both cases energy production from vapor or steam using a combined heat and power plant (CHP) or a steam generator is included. Therefore, "1 Mg of shredder residue as input for treatment", shortly "1 Mg Shredder Residue", was set as functional unit. The shredder residue entering the systems as described in chapter 5.1, which means without any pretreatment and including all metals, plastics, and inert material.

Start point of the comparison was already discharged shredder residue onsite a WEEE treatment plant. According to a holistic approach all emissions as well as credits for preservation of primary sources were included in the calculations. In Figure 36 and Figure 37 all emissions and credits are shown as well as credits for substituted raw materials for option 1 and 2 respectively. Credits take place in the assessment for produced energy and recovered metals. These recovered metals substitute those from primary sources in all cases with the exception of Fe¹⁹ in pyrolysis solid products. Following the status quo, just Al, Cu, and Fe with particle sizes >2 mm are recovered from bottom ash formed during treatment in a MWI [Kuchta, Enzner 2015]. Produced power and heat substitute those from the grid, in this case the conventional German electricity and heat production-mix.

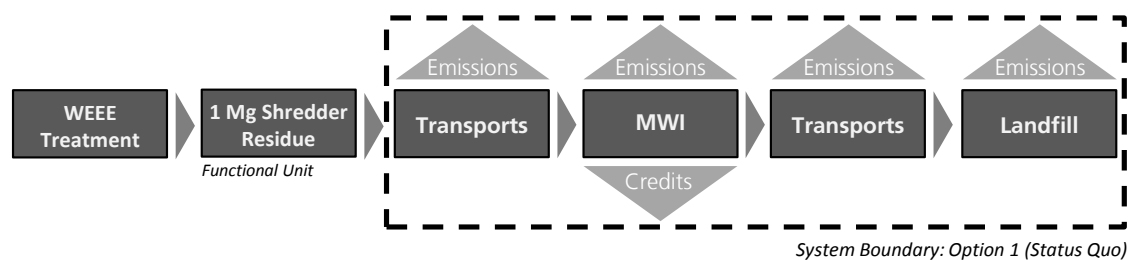


Figure 36: System boundary, direct emissions, and credits in the case of treatment by pyrolysis.

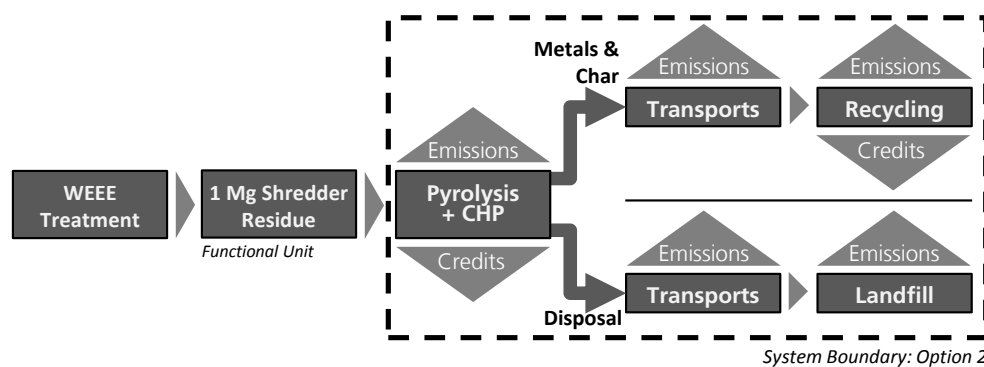


Figure 37: System boundary, direct emissions, and credits in the case thermal treatment in MWI.

¹⁹ Fe does not become recovered as pure metal in copper smelter processes, but in processes such as those from Aurubis AG, it is used as added reductive agent. Therefore, a substitution of secondary steel was assumed.

With regard to emissions, no direct emitted substances from oxidation of pyrolysis products in a CHP (liquid and gaseous products) or smelter processes (solid products) as well as no emissions from incineration of shredder residues in a MWI were taking into account. Based on missing reliable data concerning allocation of different emissions such as CO₂, NO_x, SO₂, or PO₄³⁻ from different processes, it was presumed that after complete conversion of reaction educts the amounts of corresponding products are the same from all different processes.

The functional unit “1 Mg of shredder residue as input for treatment” allows a reduction of allocations as much as possible. All emissions and credits from a formation of by-products can be allocated to the feedstock in sum. However, in general, thermal treatment of residues shows multifunctional systems. As an example, [Finnveden 1999] explained this as follows: main aim of a thermal treatment of waste is disposal and reduction of waste, but recovery of metals and “production” of power and heat become important more and more. In order to compare thermal treatments with systems such as landfilling, which are not able to recover metals and “produce” power and heat, two different approaches can be conducted for an ecological comparison: either an alternative source for metals/energy has to be added (“allocating product system”) or recovered metals/energy has to get diminished (“subtracted-extending”). Figure 38 illustrates these approaches.

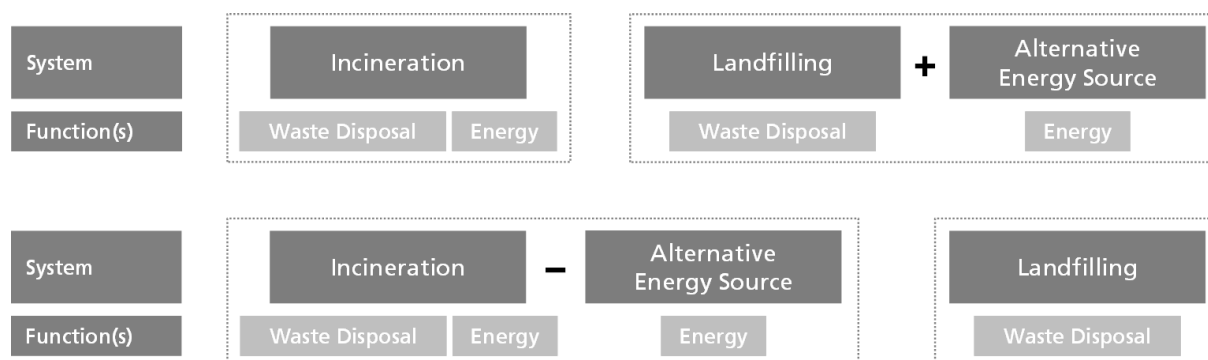


Figure 38: Product systems “allocating” (at the top) and “subtracted-extending” (at the bottom).

In the present case study, a subtracted-extending system was used, which means that credits for substitutions due to recovered metals and gained energy are taking into balance account.

Calculations in the environmental impact assessment were conducted using impact categories shown in Table 15. Concerning impact categories anthropogenic stock extended abiotic depletion potential (AADP) and Areatime some short explanations will be given.

Table 15: Impact categories used for environmental impact assessment.

Impact Category	Abbreviation	Equivalent
Abiotic resource Depletion Potential	ADP	kg Sb
Anthropogenic stock extended Abiotic Depletion Potential	AADP	kg Sb
Acidification Potential	AP	kg SO ₂
Aretime	---	m ² a
Energy as net calorific value	Energy	kWh
Eutrophication Potential	EP	kg PO ₄ ³⁻
Global Warming Potential	GWP	kg CO ₂
Ozone Layer Depletion Potential	ODP	kg R11
Photochemical Ozone Creation Potential	POCP	kg C ₂ H ₄

Besides abiotic resource depletion potential (ADP), AADP shows an additional impact category, which describes the depletion potential of abiotic resources. However, due to two different basics, strong differences between both categories can be obvious. ADP gets calculated as follows [Guinée et al. 2002]:

$$ADP_{i,ultimate\ reserves} = \frac{extraction\ rate\ i}{(ultimate\ reserves\ i)^2} \times \frac{(ultimate\ reserves\ Sb)^2}{extraction\ rate\ Sb}$$

with

$$ADP = \sum ADP_i \times m_i$$

while AADP get calculated as:

$$AADP_{i,resources} = \frac{extraction\ rate\ i}{(resources\ i + anthropogenic\ stock\ i)^2} \times \frac{(resources\ Sb + anthropogenic\ stock\ Sb)^2}{extraction\ rate\ Sb}$$

with

$$AADP = \sum AADP_i \times m_i$$

[Schneider et al. 2011]. m_i is the raw material input of the raw material i . Ultimate resources are defined as “amount of a resources that is ultimately available in the earth’s crust (natural concentration of the resource multiplied by the mass of the crust)” [Schneider et al. 2011], while resources are that amount of a material, which actually can be extracted economically. The anthropogenic stock means that amount of a material, which was already mined and reported in history [Schneider et al. 2011]. Mainly with regard to critical elements, which can be characterized by highly limited resources and high extraction rates such as for the element Co, values of ADP and AADP could show highly divergent results.

The term “Areatime” describes how long a defined area is used for any production or service. Usually this impact category is measured as $m^2 \times a$ or shortly m^2a . As an example, a value of 100 m^2a could be interpreted either that an area of 100 m^2 is used for one year or that an area of one m^2 is used for 100 years.

Further impact categories, mainly those concerning toxicological impacts, were not selected – on the one hand – due to base and fundamental discussions about methodologies basic [Heijungs et al. 2004]. As an example, non-ferrous metals such as Cu and Zn are elements fundamentally important for human beings; however, in the case of many environmental assessment methodologies, emissions of these elements are set as harmful irrespective of emitted masses. On the other hand, incomplete data such as amounts of highly toxic substances like dioxins and furans emitted from both treatment processes makes calculations imprecise and incomplete.

As methodology for impact assessment, the latest version (January 2016) of the CML methodology was used, which is widely applied and was introduced in the year 1992 by the Dutch Institute of Environmental Sciences [Heijungs et al. 1992]. This methodology is valid for Europe and was used on midpoint level, which allows a presentation of the different results from impact categories separately and unweighted, e.g. in order to find out aspects for further optimization.

Determinations and assumptions

Inventory data, which were used for the assessment, was based on both own data (c.f. chapter 6.2.1) and literature. Due to no existing mono-line for the incineration of shredder residues in a MWI, it was assumed that efficiency and overall circumstances of an MWI is not influenced. However, in order to compare both options for treating shredder residues in a MWI or by pyrolysis, all results such as yields of residues or amounts of energy are based on properties of SR1. Concerning incineration, an energy efficiency of the MWI was expected to be 13.0 % and 30.0 % for power and heat, respectively [UBA 2008]. Furthermore, transport distances were assumed, such as between WEEE treatment plant and MWI as well as between MWI and sanitary landfill as 50 km each (c.f. [Dehoust, Christiani 2012]).

Table 16: Determined transport distances for the ecological assessment (in km).

Transport Distance		MWI	Pyrolysis
WEEE Treatment Plant	→ MWI	50	---
Recovered Metals	→ Smelter/Recycling Plant	500	500
Precipitated NaX from Pyrolysis	→ Underground Deposit	---	200
Ashes from Incineration	→ Sanitary Landfill	50	---

Besides data presented above, ecoinvent-database version 3.1 [ecoinvent 2016] and [Nuss, Eckelmann 2014]²⁰ were used. Where applicable, data characterizing the situation in Europe were used to assess recycling and incineration processes, while data for primary materials were mainly on a global scale.

As mentioned above, no direct emitted substances from incineration of shredder residues or pyrolysis products were taken into calculations, due to missing data. Although this simplification affects that quantity and quality of emissions from both different processes are equal, it does not favor one option based on the assumption that after complete conversion, all products shows the same quantity and quality of compounds (e.g. H₂O and CO₂ in case of hydrocarbons).

Regarding recycling of metals, a recycling of Ag, Au, Cu, Ga, Fe, In, Ni, Pb, Sb, Se, Sn, Te, Zn, and platinum group metals (PGM) from both pyrolysis solid products and filtration residue from liquid products in an integrated copper smelter was assumed. Specific recycling process efficiencies were available from literature just in the case of Ag, Au, and PGM, which was accounted as 95 wt.-% [Buchert et al. 2012]. In the case of Fe, substitution of sorted iron scrap was assumed. Therefore, recycling efficiency of Fe was set to 100 %. With regard to all other metals, for which data about recycling efficiencies during pyrometallurgical processes are unavailable, an average loss of 15 % was assumed. Besides substitution of primary metals, it was assumed that carbon from pyrolysis solid products substitute petroleum coke which is used in copper smelters as reductive agent. An alternative substitution of fossil fuels such as oil or gas was not assumed due to the non-volatile character of carbon from pyrolysis solid products.

In the case of metals, which are recovered from bottom ash, data from previous work of Fraunhofer UMSICHT, conducted with the same feedstock, was used [Hense 2013]. As mentioned above, recovery of metals >2 mm was assumed with extraction efficiencies of 96.9, 35.0, and 35.0 wt.-% for Fe, Al, and Cu, respectively [Pretz, Meier-Kortwig 1998]. For recycling in different correspondent pyrometallurgical processes same efficiencies than for metals from pyrolysis residues were assumed. Concerning Al a recycling to cast alloy was assumed.

²⁰ Data for As, Bi, Ir, Rh, and Ru were taken from [Nuss, Eckelmann 2014] due to missing data in ecoinvent database 3.1.

According to DIN EN ISO 14040/14044, a sensitivity analysis was conducted in order to evaluate effects of uncertainties in the assessment. In detail, the corresponding aspects are:

- Scenario I: Influence of enhanced metal recovery in the status quo
 - o Separation and recovery of metals with particle sizes >1 mm from MWI bottom ash instead of >2 mm.
- Scenario II: Recovery of Al and Fe from pyrolysis solid products
 - o Separation and recovery of Al and Fe from pyrolysis solid residues and subsequent recycling in secondary aluminum smelter and steel smelter facilities. Recovery efficiencies are equal to those of a recovery from MWI bottom ash (Al: 35.0 wt.-%; Fe: 96.9 wt.-%)
- Scenario III: Influence of gross energy efficiency in MWI
 - o IIIa: Variation of MWI gross energy efficiency to 10.4 and 27.8 %²¹ [Tanner 2011]
 - o IIIb: Variation of MWI gross energy efficiency to 27.0 and 98.0 %²² [Wood et al. 2013]
instead of 13.0 and 30.0 % for power and heat, respectively.
- Scenario IV: Influence of transports
 - o Variation of transport distances between WEEE treatment plant and MWI as well as between MWI and sanitary landfill to 150 km instead of 50 km.

5.5.2 Economical assessment

Model and methods

For an economical assessment of a pyrolysis pilot plant an accounting of investment costs were conducted. In general, using this method an intended project could be tested if it is worthwhile due to a concentration of forecasted cash flows. As a result of corresponding calculations the rate of return gets formed. In addition, the most relative advantageous option could be proofed by comparing different options.

²¹ MWI Kassel, Germany.

²² Reno Nord, Aalborg, Denmark.

In the economical assessment three different designs of a pyrolysis pilot plant for WEEE and corresponding scenarios should be considered:

- I. A pyrolysis pilot plant with a flow capacity of 70 kg shredder residues per hour. Pyrolysis solid products will be sold to an integrated copper smelter, while vapor get condensed and burned in a combustion unit in order to produce heat.
- II. A pyrolysis plant identical to that of scenario I, but the vapor gets condensed and both fractions are utilized energetically in a CHP in order to produce power and heat.
- III. A pyrolysis plant with CHP identical to those of scenario II, but a reactor filled with molten PP (PO-reactor) and a halogen-filter are installed in order to absorb halogens from vapor before they get utilized in the CHP.

A pyrolysis plant with a flow capacity of 70 kg was chosen mainly due to an actual implementation of a pyrolysis plant with this mass flow by Fraunhofer UMSICHT. Thus, information based on real data instead of estimated ones could be delivered for a number of items. Because a number of data and estimations are influenced by regional and national features such as transport distances or earnings and costs for pyrolysis products, an installation in a selected country should be assumed. Therefore, an installation in Germany was selected based on a more comprehensive data set.

In all scenarios, project duration accounted for 10 years. Operating hours of different devices were determined with 5 500 hours for pyrolysis plant and associated parts²³ while those of the CHP were determined with 6 500 hours²⁴. For operation, one admin labor, who works one hour per week at the plant on average, as well as one technical supervisor and one operational labor, who work each for ten hours per week at the plant, were assumed. As further assumptions 3 960 m³ N₂, 3 614 kg NaOH, 1 540 kg activated carbon, 660 MWh of natural gas, and 45.16 MWh of power are necessary for usual operation per year. These data were either based on existing pyrolysis plants for treating biomass at Fraunhofer UMSICHT (amounts of N₂ and natural gas), on already existing data of parts from the above mentioned pyrolysis plant for WEEE, which is still under construction (amount of power), or stoichiometric calculations plus safety margins (amounts of NaOH and activated carbon).

²³ 5 500 operating hours per year correspond to a capacity of 385 Mg per year.

²⁴ Due to an installation in Germany, higher earnings can be gained in the cases of smaller CHP than larger CHP. In order to gain similar amounts of produced energy from a smaller CHP, higher rates of operating hours were assumed.

Amortization calculation: In order to investigate the risk of an investment, an amortization calculation will be conducted. Because in general, dynamic calculations cause more precise results [Pape 2009], discounting of net returns should be conducted using a discount factor DF :

$$DF_n = (1 + i)^{-n}$$

with n as individual year and i as required rate of return [Wöhe et al. 2016].

Net present value method: For determination of cost-effectiveness, a net present value NPV gets calculated by discounting all net cash inflows with the required rate of return to that year, when all investments have to be done:

$$NPV = \sum_{t=0}^n (E_t - A_t) * (1 + i)^{-t}$$

with E_t and A_t as predicted in- and outflows. The result $NPV < 0$ indicates that the required rate of return will not be reached. If $NPV = 0$, then $NPV = i$ meaning that the required rate gets reached exactly as minimal as wanted. A $NPV > 0$ means that the exceptions of interest yields will be exceeded [Wöhe et al. 2016].

Method of internal rate of return: This method could be used in order to determine any effective interest rate of an investment taking into account when in- and outflows will be done. The internal rate of return IRR can get expressed as:

$$0 = \sum_{t=0}^n (E_t - A_t) * (1 + IRR)^{-t}$$

This means that such interest rate will be determined, when $NPV = 0$ [Wöhe et al. 2016].

Similar to the ecological assessment, a sensitivity analysis was conducted in order to evaluate effects of uncertainties in the assessment. In detail, earnings and expenditures were calculated due to varied values for metals, labor, investments, operating hours, and energy costs by 5 to 10 %

Determinations and assumptions

Basic data: In order to calculate the time value of money, it is necessary to define the required rate of return (i). This rate was determined to be 5 % as sum of following aspects: due to the actual low interest level of an alternative, riskless investment, any investor would be able to earn approximately 1 %. In addition, an inflation rate of 1.5 % as well as an additional charge for risk of 2.5 % was assumed. An inflation rate of 1.5 % represents the average level of the last 10 years [Statista 2016], while the charge for risk was added due to the fact that a new technology will be implemented. The economical assessment should include taxes, which has to pay by the business for

profits. Against this background, it was assumed that a corporate entity represents the operator of the pilot plant. In this case, the corresponding tax rate includes 15 % corporate tax, 0.83 % solidarity surcharge as well as 14 % trade tax with the profit as base. In summary, over tax burdens account for 29.83 %.

Costs: For the economical assessment, investment, and operating costs were determined. According to DIN 276, investment costs of construction projects are classified in seven different groups. For installation of a pyrolysis plant, a container should be used as housing. Therefore, just the groups “construction – structural design (300)” and “construction – technical equipment (400)” will be considered in the economical assessment [DIN 2008a]. Even if recovery periods for these cost groups are usually set as 25 and 15 years for structural designs and technical equipment, respectively [Steinfeld et al. 2002], a linear depreciation of 10 years was assumed. Costs for services of assembly were determined as 10 % of costs for technical equipment. Both, costs for services as well as costs for permissions should be depreciated in the first year of the project. Table 17 summarizes all investments costs relevant for an installation of the pyrolysis pilot plant. With the exception of permissions costs, which are assumed, all investment costs are based on requested offers by Fraunhofer UMSICHT.

Table 17: Investment costs for a pyrolysis pilot plant (in €).

	Scenario I	Scenario II	Scenario III
Constructions			
- Container	1 900	1 900	1 900
Technical Equipment			
- Feeding System	6 060	6 060	6 060
- Pyrolysis Plant	199 990	199 990	199 990
- Combustion Unit	58 410	58 410	58 410
- PO-Reactor	---	---	52 268
- Halogen-Filter	---	---	14 690
- Air Treatment	8 195	8 195	8 195
- Activated Carbon Filter	4 500	4 500	4 500
- Fuel Tanks	---	5 120	5 120
- CHP	---	103 216	90 648
- Char Containers	5 000	5 000	5 000
- Condensor	11 350	11 350	11 350
- NaOH-Scrubber	11 350	11 350	11 350
- Piping	680	680	680
Others			
- Services (10 % of tech. Eq.)	30 554	41 387	54 240
- Permissions	20 000	20 000	20 000
SUM	357 989	477 159	618 535

Besides expenditures for investments in capital assets, a further investment as working capital was assumed for operating materials and similar goods, which has to be paid quickly upon receipt, as well as for liquidity reasons. As working capital, an investment of 15 % was assumed and added to capital assets at projects beginning. This position decreases during projects runtime under release of corresponding capital.

Regarding operating costs, fixed and variable costs were determined. As fixed costs, labor, maintenance, and costs for insurances were taken into account while variable ones comprise such for feedstock, operating materials, energy, disposal and transports.

Calculations for labor costs (Table 18) included gross wage, incidental wage costs (26.8 % of gross wage), and extra charges, which were, for instance, calculated for acquisition, dismissal of health, and safety actions and were assumed as 10 % of gross wage.

Table 18: Calculation of labor costs for different admin labor, technical supervisor, and operational labor (in €·h⁻¹).

Labor costs	Admin Labor	Technical Supervisor	Operational Labor
Gross wage	30.75	12.50	8.50
Wage costs (26.8 %)	8.24	3.35	2.28
Extra charges (10 %)	3.08	1.25	0.85
SUM	42.07	17.10	11.63

Costs for maintenance were calculated as 1 and 4 % of investment costs for technical equipment and constructions, respectively [Steinfeld et al. 2002]. As an exception, costs for maintenance of CHP were assumed to be 20 €·MWh⁻¹ power (10.83 %), e.g. due to feasible higher corrosion from pyrolysis liquid products. For all kind of equipment and construction, costs for insurances were calculated as 1 % [Steinfeld et al. 2002].

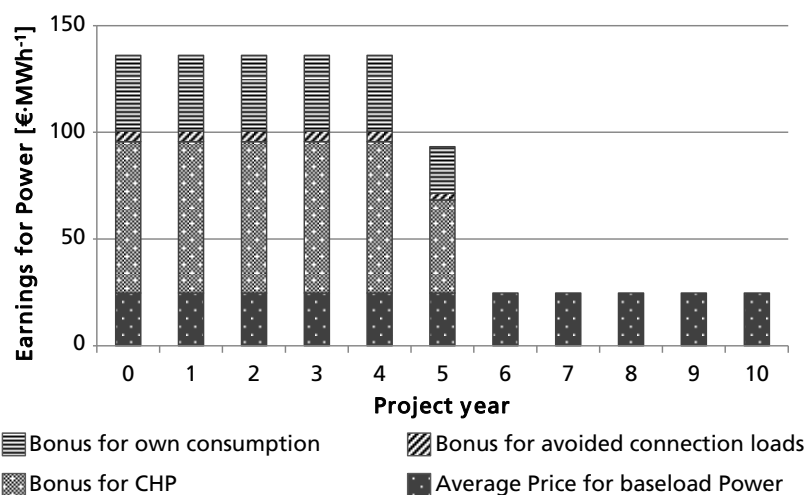
Variable costs depend on actual prices of in- and outputs, which could show high volatilities. Therefore, it is unfeasible to conduct calculations based on real data. Nevertheless, for this assessment actual data from different references were used in order to estimate costs as good as possible. Costs of operating materials, disposal, and energy for the pilot plant are listed in Table 19. Due to a very high volatility of energy products, average prices of the year 2015 were taken, calculated by the German federal statistical office [Destatis 2016]. For transports of pyrolysis solid products to an integrated copper smelter as consumer of this char-metal mixture, an average transport distance of 500 km was assumed.

Table 19: Variable costs of operating materials, disposal, transports, and energy.

Variable Costs	Unit	Costs per Unit [€]	Reference
N ₂ (≥ 99.8 vol. %)	m ³	1.34	[Linde 2016]
PP (K59)	Mg	95.00	[EUWID 40.2016]
La ₂ O ₃ (≥ 99.5 %)	kg	1.79	[MFA 2016]
Activated Carbon	Mg	2 490.00	[Staub et al. 2015]
NaOH (≥ 97.0 %)	kg	4.20	[VWR 2016]
Disposal of hazardous material	Mg	260.00	[GSB 2016]
Transports of solid products (500 km)	Mg	28.00	[Geis 2015]
Light Fuel Oil*	Mg	580.83	[Destatis 2016]
Natural Gas*	MWh	30.75	[Destatis 2016]
Power*	MWh	130.80	[Destatis 2016]

* Prices were calculated as sold to industrial clients

Earnings: As earnings from operation of the pyrolysis plant, sold energy, and pyrolysis products were taken into account. As power and heat, that amount of energy was sold, which was produced less own consumptions and losses. For power, an infeed to the national grid was assumed, while heat was sold to a district heating system. Earnings from produced power are calculated in accordance to the German act on combined heat and power generation ("KWKG"), which allows a bonus for power from CHP for the first 30 000 operation hours, a bonus for avoided connection loads, and a bonus for own consumed power [KWKG 2015]. If 30 000 operation hours were exceeded, just the price for baseload power will be paid. For this price of baseload power the last updated price as EPEX Spot per Quarter were chosen [EEX 2016]. Figure 39 shows the corresponding earnings from sold power per MWh for the project duration. For heat, produced from combustion unit or CHP and delivered to a district heating system, the same price than for natural gas was assumed.

**Figure 39:** Earnings for sold power in accordance with [KWKG 2016].

Following the main task of the pyrolysis plant as formation of pyrolysis solid products, in which metals are accumulated, earnings will be earned due to sale of these products to integrated copper smelters. Unfortunately, real data for corresponding earnings from a copper smelter was not present. Therefore, following assumption was made: based on available, daily price lists for secondary metals a mixed price for all present metals, which

could be recycled in an integrated copper smelter, were calculated. If available, prices for metals in alloys or mixtures were selected instead of pure ones. Additionally, 35 % were discounted on calculated price e.g. due to probably present penalty elements. In summary, earnings accounting for $683.55 \text{ €} \cdot \text{Mg}^{-1}$ metal-char-mixture were calculated [ESG 2016, EUWID 41.2016, Nederkorn 2016].

The feedstock itself could be classified either as part of earnings or without any burdens depending on the following determinations: Usually an operator of a WEEE treatment plant in Germany had to pay about $98.50 \text{ €} \cdot \text{Mg}^{-1}$ on average at the end of 2015 by disposing it in a MWI [Katz 2016]. Due to a treatment of shredder residues in a pyrolysis plant, the operator could save the corresponding amount of money. Therefore, two options will be considered in calculations: on the one hand $95.50 \text{ €} \cdot \text{Mg}^{-1}$ shredder residues are calculated as imputed earnings; on the other hand the feedstock is calculated as free of burdens ($0.00 \text{ €} \cdot \text{Mg}^{-1}$ shredder residues).

6. Results

6.1 Raw material characterization

6.1.1 Shredder residues from WEEE treatment

The feedstock SR1 was characterized on physical as well as chemical characteristics. Particle size distribution shows that most particles have a size between 2 and 4 mm (64.3 wt.-%). Additionally, 7.1 wt.-% can be found between 1 and 2 mm plus 8.8 wt.-% have a size between 4 and 5 mm. In summary, regarding particle size, those particles between 1 and 5 mm are the main components and account for more than 80 wt.-% (Figure 40). Additionally, it should be noted that distinctive amounts of dust were obvious from optical assessment.

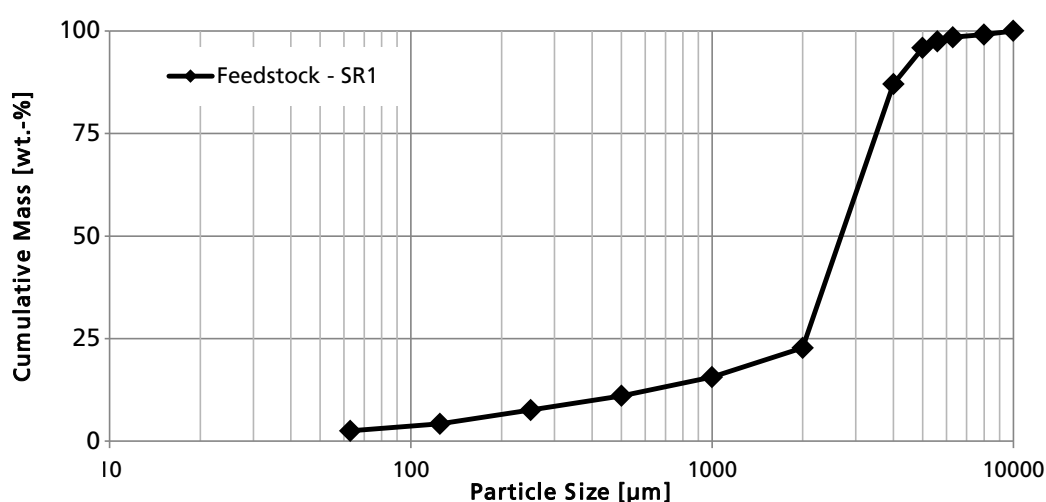


Figure 40: Particle size distribution of SR1.

SR1 was further analyzed concerning basic parameters such as water content, ignition losses, and heating values (Table 20). The content of water was very low corresponding to the dry treatment techniques for SR1. Both heating values as well as ignition losses were relatively low compared to common plastics such as polyethylene (PE) or polypropylene (PP). This indicated a high content of either inorganic mineral material and/or metals.

Table 20: Basic characteristics of SR1.

Parameter	Unit	Value	Parameter	Unit	Value
Dry Residue 105 °C	wt.-%	99.1	Bulk Density	kg·m ⁻³	642
Ignition Loss 550 °C	wt.-%	43.4	LHV	MJ·kg ⁻¹	16.70
Ignition Loss 750 °C	wt.-%	45.2	HHV	MJ·kg ⁻¹	17.54

For accounting the content of nonmetals and metalloids, different analyses were conducted and the results are shown in Table 21. With less than 1 wt.-%, relatively low contents of Br (0.4 - 0.6 wt.-%) and Cl (0.4 - 0.5 wt.-%) were found. The high content of O revealed that many metals could be present as oxide in the feedstock.

Table 21: Content of nonmetals and metalloids in SR1.

Element	Value (wt.-% DM)	Analysis	Element	Value (wt.-% DM)	Analysis
C	34.08	A	P	0.25/0.16	B/C
H	3.71	A	O	39.51	C
N	0.83	A	Br	0.58/0.35	C/D
S	0.17/0.076	A/C	Cl	0.53/0.40	C/D

A: Analyses were conducted using Vario MACRO Cube elemental analyzer.

B: ICP-OES according to DIN EN ISO 11885.

C: EDXRF with C, H, N given and O as missing component.

D: Ion chromatography according to DIN 51727.

Concerning content of nonmetals, metalloids, and metals in SR1, a number of different types of analyses were conducted due to a very inhomogeneous character of SR1. Mainly with regard to the content of metals, some large differences were obvious if analyses were conducted either with energy dispersive X-ray fluorescence (EDXRF) or inductively coupled plasma mass spectrometry (ICP-MS) / inductively coupled plasma optical emission spectrometry (ICP-OES). These differences could be based not only on the heterogeneous character of the material, but also on some influencing effects of sample matrix. Therefore, results from both analyses are shown in Table 22; however, results based on EDXRF were used just for comparable analytics with qualitative aspects (relatively), mainly allocation of metals, while results from ICP-MS/-OES were used for quantitative assessments such as ecological and economical assessment. Therefore, some metal contents determined via ICP-MS/-OES should be highlighted: analyses revealed that there are still high amounts of metals contained in SR1. Mainly bulk metals like Cu (10.53 wt.-%), Fe (1.74 wt.-%), Al (1.57 wt.-%), Pb (0.81 wt.-%), and Sn (0.75 wt.-%) could be found as well as many critical metals, but in much lower concentrations (e.g. Sb (1012 mg·kg⁻¹), Ti (160 mg·kg⁻¹), La (61.5 mg·kg⁻¹), Nd (88.5 mg·kg⁻¹), or Pr (11.5 mg·kg⁻¹). A further analysis for Hg was determined in aqua regia soil extracts with cold-vapor atomic spectrometry (CVAS) according to DIN ISO 16772 with a result of 0.60 mg Hg ·kg⁻¹.

Table 22: Content of metals in SR1 (determination by EDXRF and ICP-MS/-OES).

Element	Value (mg·kg ⁻¹ DM)			Element	Value (mg·kg ⁻¹ DM)		
	EDXRF ¹	ICP-MS ²	ICP-OES ³		EDXRF ¹	ICP-MS ²	ICP-OES ³
Ag			78	Nb			6.0
Al	26 650	15 700		Nd	<1	78	99
As	3		16	Ni	344		555
Au		<10	1.4	Os	95		
Ba	7 640			Pb	9 353	9 240	8 000
Be			<0.1	Pd		<10	7.0
Bi		19		Pr		11.5	
Ca	17 675		12 300	Pt		<10	<0.1
Cd	70		68	Rh		<1	
Ce	62			Ru		<10	
Co			76	Sb	2 003	723	1 300
Cr	702		153	Sc		<10	
Cu	9 073		10 533	Se		3	
Dy		<10		Si	65 545		
Eu	414			Sn	1 700	7 490	
Fe	20 218		17 400	Sr	5 903		250
Ga	<1	104	5.0	Ta		<10	0.6
Ge		<10	1.4	Te	73	<1	32
In		30.7	1.2	Ti	2 363		160
Ir	42	<10		Tl		<0.4	
K	6 608			V			6.5
La		61.5		W		<10	
Li			53	Y		9	
Mg	4 448		3 110	Yb	5		
Mn	1 028		1 355	Zn	5 008		5 310
Mo			17	Zr	902		24
Na	17 120		2 480				

¹ EDXRF with C, H, N given and O as missing component.² ICP-MS according to DIN EN ISO 17294-2.³ ICP-OES according to DIN EN ISO 11885.

Mass changes over temperature, differential thermogravimetric (DTG), and results of differential scanning calorimetry (DSC) for SR1 are shown in Figure 41. Two significant mass losses were obvious between 240 and 270 °C as well as between 330 and 470 °C. Corresponding highest rates of mass losses were at 263.3 °C in the first range as well as 408.3 in the second range. The residual mass of SR1 was 49.36 wt.-% at 800 °C. DSC-curve showed an exothermic reaction at temperatures above 126 °C.

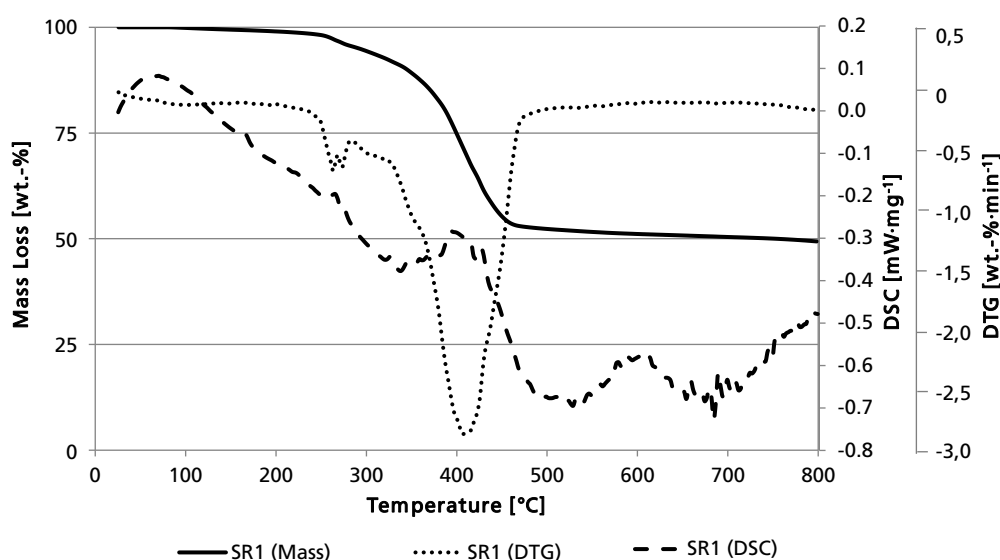


Figure 41: TGA (solid line), DTG (dotted line), and DSC (dashed line) of SR1; 5 K·min⁻¹; argon.

6.1.2 Selected fractions containing scarce and critical metals

Tantalum capacitors

As mentioned in chapter 5.1.2, the most commonly used types of Ta capacitors “SMD Yellow” and “SMD Black” were selected for pyrolysis tests. Both capacitor types were manually separated from common PWB. Elemental analyses concerning C, H, N, and S as well as metal and some further non-metals were conducted using Vario MACRO Cube Elemental Analyzer (Table 24) and EDXRF (Table 25).

Table 23: Basic characteristics of Ta capacitors.

Parameter	Unit	SMD Yellow	SMD Black
Dry Residue 105 °C	wt.-%	99.8	99.8
Ignition Loss 550 °C	wt.-%	5.8	9.7
Bulk Density	kg·m ⁻³	1 967	1 497

Table 24: Content of C, H, and S in “SMD Yellow” and “SMD Black” determined with Vario MACRO Cube elemental analyzer.

Element	Value (wt.-% DM)	
	SMD Yellow	SMD Black
C	5.95	8.88
H	0.25	0.32
N	0.07	0.14
S	0.02	0.05

Table 25: Elemental Composition of "SMD Yellow" and "SMD Black" Ta Capacitors based on EDXRF (in wt.-%).

Element	SMD Yellow	SMD Black	Element	SMD Yellow	SMD Black
Ag	1.676	1.780	Os	0.049	0.029
Al	0.989	1.001	P	0.211	0.194
Ba	0.070	---	Pb	0.054	0.080
Br	0.939	0.417	Sb	1.269	0.191
Ca	---	0.133	Se	0.004	0.006
Cl	0.108	0.136	Si	20.908	24.420
Cr	0.079	0.0759	Sn	0.131	0.268
Fe	0.992	0.367	Sr	0.016	0.008
Mg	---	0.213	Ta	11.502	10.175
Mn	7.306	5.698	Ti	0.500	0.041
Ni	0.119	0.114	Zr	0.015	<0.001

* EDXRF with C, H, N, S given and O as missing component.

From elemental composition differences between both capacitor types were obvious; the results are mainly conspicuous for Ba, Br, Ca, Fe, Mg, Sb, Si, Ti, and Zr. Additionally, large differences are obvious from analyses concerning content of C, H, N, and S (Table 24).

Most of the different highlighted results can be mainly explained due to different amounts of brominated flame retardants (BFR) (Br, Sb), size of contacts (Fe), fillers in the exterior mold type (Ca, Si, Ti), as well as sintering aids for the Ta pellet (Ba, Ca, Mg, N, Si, Sr, Zr). The concentration of Ta is approximately 12 wt.-% lower in the case of black SMD capacitors compared to yellow SMD ones. Similarly, the concentration of Mn is lower in the case of black capacitors due to the function of Mn as electrolyte (MnO_2) for Ta_2O_5 .

The exterior mold of Ta capacitors are often made out of an epoxy resin, which is obvious from the high concentration of Si (filler: fumed SiO_2), Br, and Sb (BFR and corresponding additive) as well as the characteristic peak of DTG analysis (Figure 42): as mentioned in chapter 4.1, the first and main step of thermal decomposition of an epoxy resin is in a temperature range between 330 and 440 °C.

Additionally, by setting ignition loss (Table 23) as well as contents of C and bulk densities of both capacitor types in relation, different amounts of epoxy resins could be assumed: SMD black capacitors had a lower bulk density corresponding to the lower density of epoxy resin compared to Ta_2O_5 (epoxy resin: $1.2 - 1.3 \text{ g}\cdot\text{cm}^{-3}$ [Pang, Gillham 1989]; Ta_2O_5 : $8.2 \text{ g}\cdot\text{cm}^{-3}$ [Perry, Phillips 1995]), a higher concentration of C, and a higher mass loss compared to yellow SMD capacitors.

DSC analyses of both capacitors revealed fundamental differences (Figure 42) while the yellow ones has just small positive values up to 565 °C, followed by increasing negative values, the black capacitor type has negative values up to 125 °C, followed by positive ones. These differences indicate either different structures or different kinds of resins were used.

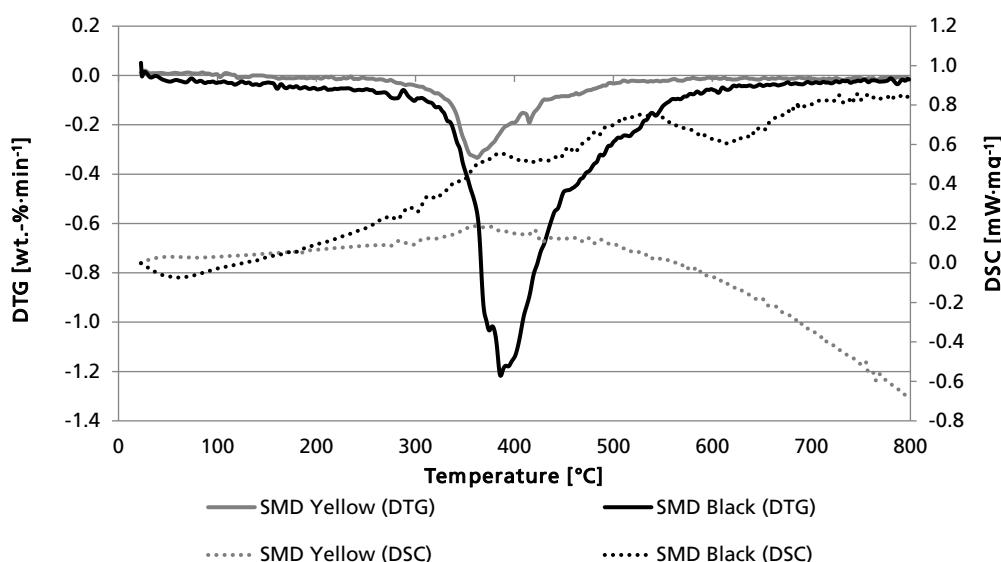


Figure 42: DTG and DSC of Ta Capacitors “SMD Yellow” and “SMD Black”; 5 K·min⁻¹; argon.

Liquid crystal displays

For pyrolysis tests, dark sides of liquid crystal displays (LCD) (“LCD-Dark”) were chosen and characterized. As shown by ignition loss (Table 26) as well as TGA (Figure 43), just low amounts of volatile compounds can be found in the feedstock. Additionally, TGA revealed a mass loss above 300 °C with a maximum rate of mass loss at 313.6 °C, which is a bit lower compared to analyses from literature, which shows maximum weight loss rates at 360 - 365 °C for the polarizing film as main volatile component [Wang, Xu 2016].

Table 26: Basic characteristics and contents of C, H, and S of LCD-Dark.

Parameter	Unit	Value	Element*	Unit	Value
Dry Residue 105 °C	wt.-%	99.5	C	wt.-%	8.73
Ignition Loss 550 °C	wt.-%	15.3	H	wt.-%	0.97
LHV	MJ·kg ⁻¹	3.21	N	wt.-%	0.03
HHV	MJ·kg ⁻¹	3.44	S	wt.-%	0.04

* Quantification determined with Vario MACRO Cube Elemental Analyzer.

In order to quantify contents of metals, metalloids, and non-metals in the LCD sample, analyses using EDXRF were conducted. As shown in Table 27, mainly elements, which are used for the production of glass, can be found with high concentrations (Si, Ca, Sr, Ba) as well as elements from the polarizing film (e.g. P from triphenyl phosphate (TPP)).

Concerning critical and scarce metals, not only In ($178 \text{ mg}\cdot\text{kg}^{-1}$), but also rare earth elements (REE), namely Eu ($43 \text{ mg}\cdot\text{kg}^{-1}$) and Yb ($9 \text{ mg}\cdot\text{kg}^{-1}$) were detected. Contrary to information from literature (e.g. [Chuang et al. 2015]), no Ga was found in the sample.

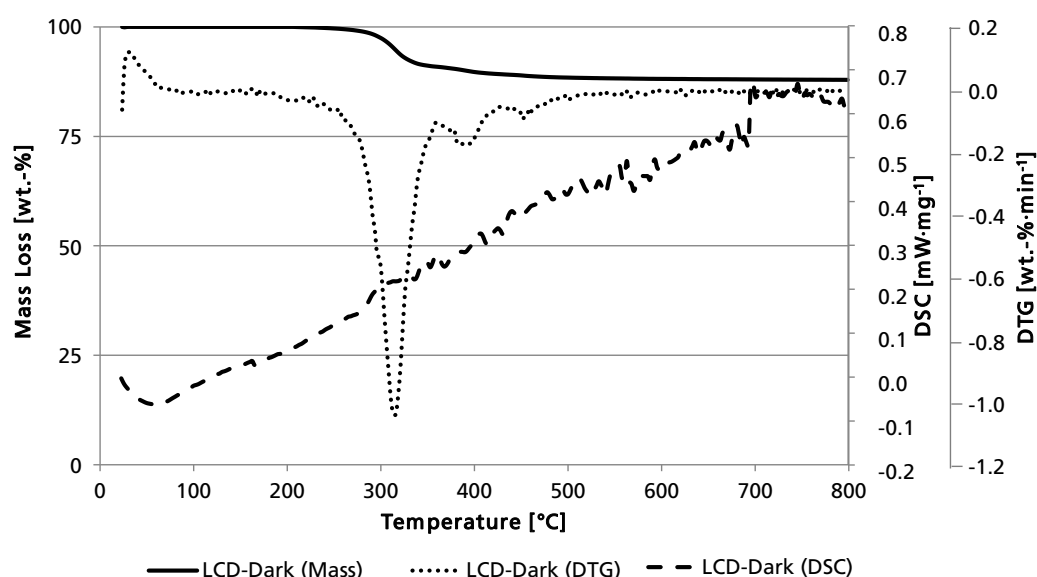


Figure 43: TGA, DTG, and DSC of “LCD-Dark”; $5 \text{ K}\cdot\text{min}^{-1}$; argon.

Table 27: Metals, metalloids, and non-metals found in LCD-Dark based on EDXRF* (in $\text{mg}\cdot\text{kg}^{-1}$).

Element $\text{mg}\cdot\text{kg}^{-1}$	Al 40 335	As 1 770	Ba 8 395	Ca 16 545	Cl 778	Cr 170	Cu 17	Eu 43
Element $\text{mg}\cdot\text{kg}^{-1}$	Fe 663	Ga 0	I 876	In 178	K 135	Mg 1 740	Mn 5	Ni 44
Element $\text{mg}\cdot\text{kg}^{-1}$	P 2 700	Re 13	S 63	Sb 291	Si 104 700	Sn 794	Sr 14 275	Te 103
Element $\text{mg}\cdot\text{kg}^{-1}$	Ti 87	Yb 9	Zn 85	Zr 392				

* EDXRF with C, H, and O as missing components.

Pyrolysis tests with LCD were conducted not only just with LCD as feedstock, but also with polyvinyl chloride (PVC) in co-pyrolysis for instance. Analyses concerning content of metals, metalloids, and halogens revealed that waste-PVC with comparatively high concentration of Cl and low concentrations of metals, such as Ca or Ti, were chosen, which could be used as fillers (Table 28). Figure 44 shows TGA, DTG, and DSC of PVC, which were mainly relevant for defined thermal decomposition with HCl as main product. On the basis of two-stage decomposition of PVC, a temperature of 370°C was chosen for pyrolysis of PVC during vapor-phase mode tests.

Table 28: Metals, metalloids, and halogens found in PVC based on EDXRF* (in $\text{mg}\cdot\text{kg}^{-1}$).

Element $\text{mg}\cdot\text{kg}^{-1}$	Al 1 520	Ba 397.3	Ca 999 0	Cd 1 190	Cl 569 010	Fe 43.0	Ga 0.0	Na 1 620
Element $\text{mg}\cdot\text{kg}^{-1}$	P 279	Pb 11 210	Si 2 750	Sr 50.5	Ti 16 270	V 32.5	Zr 5.8	

* EDXRF with C, H, and O as missing components.

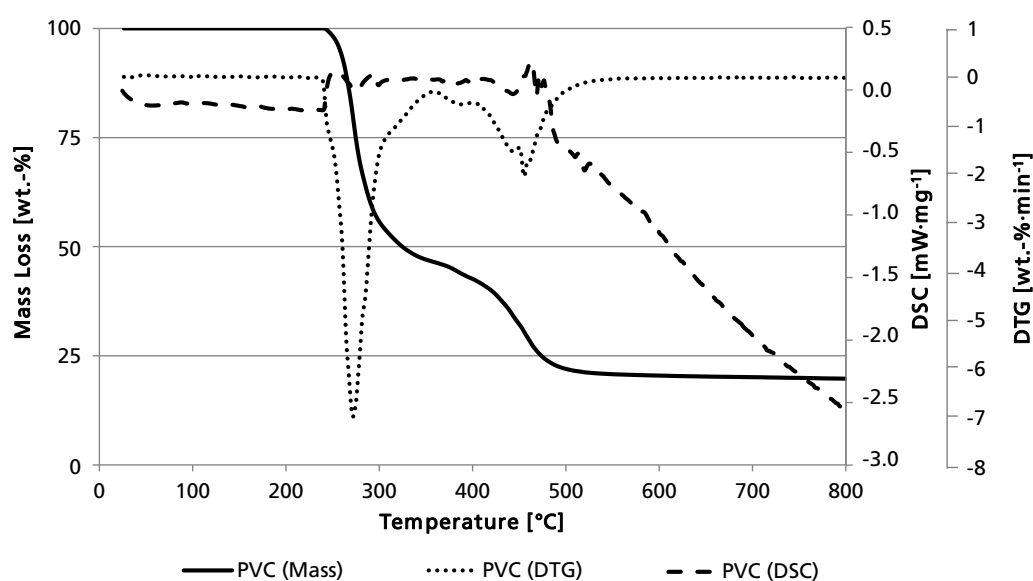


Figure 44: TGA, DTG, and DSC of PVC; 5 K·min⁻¹; argon.

As feedstock for co-pyrolysis, crushed LCD and PVC were mixed accurately in a ratio of 1:11 (by weight). For vapor-phase mode test same amounts were used, but filled in the different parts of the system separately.

6.2 Pilot tests in bench-scale plant

6.2.1 Pyrolysis tests with shredder residues from WEEE treatment

Table 29 shows the number of all conducted test runs in the bench-scale plant with SR1 as feedstock under conventional circumstances. The corresponding test results are contained in later mentioned calculations and results. In addition, a number of tests like preliminary tests were conducted, which were relevant during the iterative development and optimization of the bench-scale plant. Such tests, which are not shown here, were

- with other feedstock than SR1,
- under changed circumstances, e.g. heating rate,
- before the stirring unit was installed or
- with SR1 as feedstock and same circumstances, but the test run was not in line with previously defined requirements.

Table 29: Number of conducted test runs with SR1.

Pyrolysis Temperature	Residence Time	Total number of test runs	Tests with tar cracking unit	Tests with PO-reactor	Tests with Halogen-Filter
°C	Min	n	n	n	n
350	60	1	-	-	-
450	30	5	4	-	-
450	60	4	3	-	-
550	30	5	4	-	-
550	60	5	4	-	-
550	90	1	-	-	-
650	30	15	15	7	3
650	60	7	6	-	-
Sum		43	36	7	3

Based on those tests listed in Table 29, a number of results were gained, which are shown in Figure 45 (product allocation²⁵), Table 30 (quality of pyrolysis solid products), Table 31 (quality of pyrolysis filtered liquids) and Table 32 (quality of pyrolysis gases). All results in this figure and tables are adjusted, which means that they are previously checked on abnormal extreme values.

In general, tests with a pyrolysis temperature <450 °C were conducted just one time in order to prove that thermal decomposition of feedstock was complete. Similar to results of TGA analysis (chapter 5.1), it could be clearly seen that pyrolysis at 350 °C for 60 min was incomplete, indicated by a comparatively high yield of solid products (71.96 wt.-%), high content of C (47.73 wt.-%), as well as high ignition loss (33.58 wt.-%) of this product. Therefore, no further tests with temperatures <450 °C were conducted.

²⁵ A comprehensive list is shown in the appendix (Table 49).

Product allocation²⁶: With an increase of temperature from 450 to 550 °C, the yields of solid products, waxes, and filtration residues from liquids decreased, but stood comparatively stable between 550 and 650 °C. Formation of gases increased steadily with an increase of temperature from a minimum of 11.7 wt.-% (450 °C, 60 min) to a maximum of 22.8 wt.-% (650 °C, 60 min). A nonlinear effect was present for yields of filtered liquids, which had the highest yields at a pyrolysis temperature of 550 °C. An increased residence time had obvious effects, not just on solid products, but also liquid products and only at 450 °C: at this temperature the yield of solid products increased in favour of liquid products with an increase of residence time.

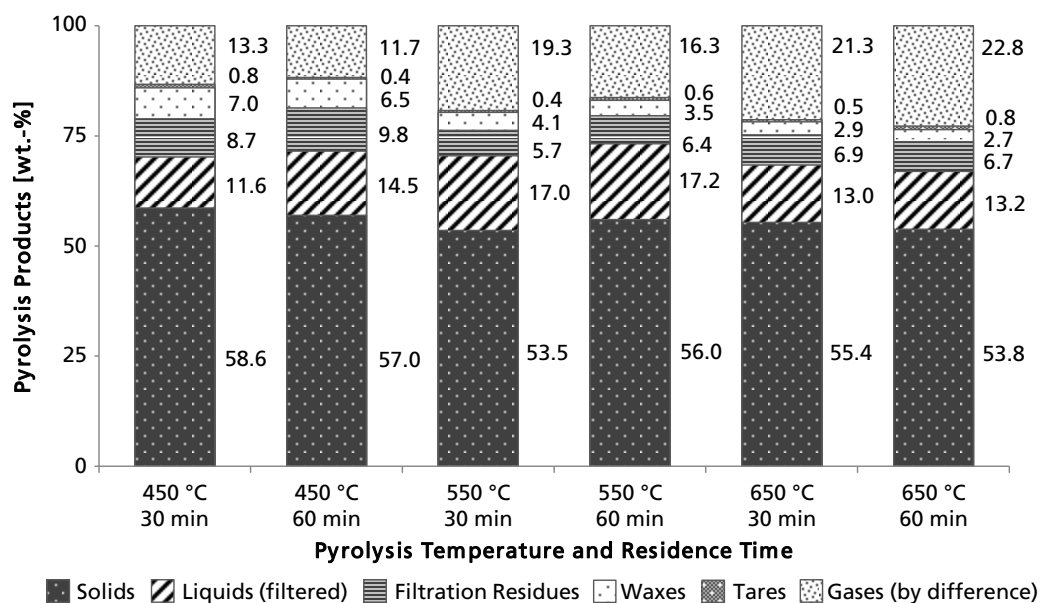


Figure 45: Product allocation from tests with SR1 as feedstock (in wt.-%).

Pyrolysis solid products: Concentrations of C, H, and N decreased clearly with both an increase of temperature or residence time. Mainly the content of H decreased greatly from 1.1 wt.-% at 450 °C to just 0.2 wt.-% at 650 °C (both for 30 min residence time). Regarding S, concentrations are similar at all test conditions. The ignition loss of the solid product from pyrolysis over 30 min decreased greatly with an increase of temperature from 450 to 550 °C; however, it increased slightly from 550 to 650 °C. In contrast, the ignition loss from tests over 60 min revealed that this parameter decreased clearly with an increased temperature. Regarding the higher heating value *HHV*, values from tests with a residence time of 30 min decreased from 6.3 to 4.9 MJ·kg⁻¹ while those values from tests with longer residence time increased from 5.1 to 6.0 MJ·kg⁻¹ (450 → 650 °C).

²⁶ The term “Waxes” describes that amounts of residues, which were left in both cooling units; “Tares” describes that amount of residue, which were left in the tar-cracking unit.

Table 30: Quality of pyrolysis solid products from tests with SR1 as feedstock.

Average Values ±Standard Deviation	Residence Time	Unit	450 °C	550 °C	650 °C
Content of C	30 min	wt.-%	21.3 ±3.9	18.3 ±5.6	14.8 ±1.7
	60 min		20.2 ±1.9	18.3 ±4.1	17.1 ±1.0
Content of H	30 min	wt.-%	1.0 ±0.5	0.5 ±0.4	0.2 ±0.0
	60 min		0.7 ±0.2	0.7 ±0.3	0.3 ±0.2
Content of N	30 min	wt.-%	0.7 ±0.2	0.6 ±0.2	0.5 ±0.1
	60 min		0.8 ±0.1	0.6 ±0.2	0.6 ±0.1
Content of S	30 min	wt.-%	0.3 ±0.1	0.3 ±0.1	0.3 ±0.1
	60 min		0.4 ±0.0	0.3 ±0.0	0.4 ±0.1
Ignition Loss	30 min	wt.-%	17.2 ±1.5	9.8 ±2.0	10.9 ±1.4
	60 min		15.2 ±2.2	11.1 ±1.5	9.0 ±2.4
HHV	30 min	MJ·kg ⁻¹	6.3 ±1.6	5.7 ±0.9	4.9 ±0.9
	60 min		5.1 ±0.9	5.3 ±0.2	6.0 ±0.4

Pyrolysis liquid products (filtered): With two exceptions, clear effects regarding C and H were obvious: on the one hand, with an increased temperature, the concentration of C increased while that of H decreased (exception: 650 °C, 60 min). On the other hand, liquids from tests with longer residence time had lower contents of C and higher contents of H compared to corresponding tests with 30 min (exception 550 °C, 60 min). Additionally, the ratio of C/H showed similar results. Regarding concentrations of N and S no clear effects were obvious. Concerning the energy content of pyrolysis liquids, it is obvious that – with the exception of liquids from tests at 550 °C for 60 min – an increased temperature led to higher heating values. A clear effect was not given regarding liquids from tests with 60 min residence time compared to those with 30 min. The last two parameters content of H₂O and total acid number *TAN*, clearly decreased with increased temperature. Additionally in both cases, but mainly distinctive for values of H₂O, the standard deviation decreased, too.

Table 31: Quality of pyrolysis liquids products (filtered) from tests with SR1 as feedstock.

Average Values ±Standard Deviation	Residence Time	Unit	450 °C	550 °C	650 °C
Content of C	30 min	wt.-%	83.2 ±3.4	83.5 ±1.1	87.4 ±1.6
	60 min		73.4 ±9.7	81.4 ±3.1	79.6 ±4.9
Content of H	30 min	wt.-%	9.6 ±0.5	8.3 ±0.3	7.9 ±0.6
	60 min		8.9 ±1.6	8.7 ±0.4	7.2 ±1.0
Content of N	30 min	wt.-%	2.1 ±0.2	2.5 ±0.2	2.4 ±0.1
	60 min		2.0 ±0.2	2.4 ±0.3	2.8 ±0.3
Content of S	30 min	wt.-%	0.1 ±0.1	0.1 ±0.0	0.1 ±0.0
	60 min		0.1 ±0.0	0.1 ±0.0	0.1 ±0.0
Ratio C/H	30 min	-	8.7 ±0.7	10.1 ±0.4	10.8 ±0.7
	60 min		8.4 ±0.5	9.3 ±0.4	11.1 ±0.4
HHV	30 min	MJ·kg ⁻¹	32.7 ±4.0	36.8 ±1.3	37.7 ±0.9
	60 min		34.0 ±4.0	37.7 ±1.6	36.5 ±2.0
LHV	30 min	MJ·kg ⁻¹	32.5 ±4.1	36.7 ±1.3	37.4 ±1.7
	60 min		33.7 ±4.1	37.6 ±1.6	36.5 ±2.1
Content of H₂O	30 min	wt.-%	10.9 ±7.6	2.9 ±1.7	1.2 ±0.6
	60 min		11.5 ±8.4	3.1 ±2.7	2.1 ±1.6
TAN	30 min	mg KOH ·g ⁻¹	14.9 ±3.4	7.3 ±4.1	3.0 ±1.2
	60 min		17.0 ±4.5	8.5 ±3.3	3.1 ±1.2

Pyrolysis gases: Compositions of formed pyrolysis gases greatly changed by variation of residence time and, mainly temperature. The main components, which are relevant for an energetic utilization of pyrolysis gases (H₂, CO, C_xH_y) greatly increased with an increase of temperature. Concentrations of CO₂ differ very slightly at a residence time of 30 min, but decreased greatly with an increased temperature at a residence time of 60 min²⁷. Concentrations of CH₄ could not be measured at temperatures of 550 °C and 650 °C due to limitations of the used gas analyzer (c.f. chapter 5.2). Densities of pyrolysis gases decreased with an increase of temperature. All parameters which describe energy contents of pyrolysis gases greatly increased with an increase of temperature; in contrast, an increase due to a longer residence time was very small.

²⁷ Regarding CO₂ it could not be ruled out that some values were defective even after replications of tests. For further information see footnote 28 (page 144).

Table 32: Quality of pyrolysis gases from tests with SR1 as feedstock.

Average Values ±Standard Deviation	Residence Time	Unit	450 °C	550 °C	650 °C
Content of H₂ corr	30 min	vol.-%	7.4 ±1.5	14.4 ±2.1	18.3 ±1.3
	60 min		6.6 ±1.2	15.0 ±0.8	18.8 ±0.5
Content of CO	30 min	vol.-%	2.7 ±0.8	10.2 ±1.2	12.0 ±0.9
	60 min		2.8 ±0.8	8.5 ±3.5	12.6 ±1.4
Content of CO₂	30 min	vol.-%	30.5 ±0.0	32.1 ±12.6	33.5 ±1.9
	60 min		68.3 ±2.0	47.4 ±12.8	16.5 ±4.0
Content of CH₄	30 min	vol.-%	5.0 ±0.7	---	---
	60 min		6.8 ±4.1	---	---
Content of C_xH_y	30 min	vol.-%	3.1 ±0.1	8.4 ±0.5	>10
	60 min		2.4 ±0.5	---	>10
Specific Density	30 min	---	1.2 ±0.0	1.1 ±0.1	1.1 ±0.0
	60 min		1.2 ±0.1	1.1 ±0.1	0.9 ±0.1
Relative Density	30 min	kg·m ⁻³	1.6 ±0.0	1.3 ±0.1	1.3 ±0.0
	60 min		1.6 ±0.1	1.3 ±0.1	1.1 ±0.1
HHV	30 min	MJ·kg ⁻¹	13.4 ±0.2	22.2 ±0.8	28.5 ±1.0
	60 min		13.8 ±2.8	20.9 ±2.3	30.0 ±1.5
	30 min	MJ·m ⁻³	19.4 ±10.1	30.5 ±4.1	35.7 ±1.4
	60 min		20.2 ±5.0	27.2 ±5.6	33.0 ±3.4
LHV	30 min	MJ·kg ⁻¹	14.9 ±0.2	24.7 ±0.9	31.8 ±1.2
	60 min		15.3 ±3.1	23.3 ±2.6	33.4 ±1.7
	30 min	MJ·m ⁻³	21.6 ±0.1	34.0 ±4.5	39.8 ±1.5
	60 min		22.5 ±5.6	30.3 ±6.2	36.7 ±3.8
Wobbe index W_s	30 min	MJ·m ⁻³	19.5 ±0.2	32.1 ±3.4	38.7 ±1.4
	60 min		20.2 ±4.6	28.8 ±4.6	38.1 ±2.9
Wobbe index W_i	30 min	MJ·m ⁻³	17.5 ±0.2	28.8 ±3.1	34.7 ±1.3
	60 min		18.2 ±4.1	25.9 ±4.1	34.2 ±2.6

Significance tests

In order to test if differences were significant between means from pair of values, t-tests were conducted. The significance level of 0.05 was set, as well as, for greater certainty, a significance value of 0.01 was used, which means that calculated values, which are below these levels reveal significant difference in the considered pair of values.

Definitions of pairs of values were based either on changed temperatures or changed residence times (Table 33). On the one side, the different temperatures of 450 - 550 °C, 550 - 650 °C, and 450 - 650 °C over 30 min and 60 min were set as well as over both residence times, which indicate that the impact of a residence time of 30 or 60 min is indifferent. On the other side, the impact of residence time was investigated at the different temperature levels 450, 550, and 650 °C.

Table 33: Pairs of values for significance tests.

Pair of Values	1	2	3	4	5	6	7	8	9	10	11	12
Temperature (°C)	450 → 550			550 → 650			450 → 650			450	550	650
Residence Time (min)	30	60	30, 60	30	60	30, 60	30	60	30, 60	30 → 60		

The results from significance tests are shown in Figure 46 to Figure 49. In all figures, both significance levels are integrated as solid (0.05) and dotted lines (0.01) for each difference. If a difference was based on a decreasing change due to an increase of focused parameter, negative values were plotted in the diagrams, while increasing changes are shown by positive ones.

Product allocation: Figure 46 shows the results for the allocation of pyrolysis products. Increases of temperature from 450 to 550 and 650 °C led to (largely) significant decreases of pyrolysis solid products. Only in the case of an increase from 450 to 550 °C at a residence time of 60 min, decrease was not significant. Concerning yields of liquid products, significant decreases are given for unfiltered liquids by changing the temperature from 550 to 650 °C as well as from 450 to 650 °C (just 60 min residence time). The yield of filtered liquids increased (largely) significant with an increase of temperature from 450 to 550 °C. The yields of waxes decreased significantly due to an increase of temperature from 450 to 550 °C as well as from 450 to 650 °C, indicating no or just a relatively low change between 550 and 650 °C.

A changed residence time had no significant influence on any yield of products. This reveals that, concerning product allocation, a residence time >30 min has no significant impact on product allocation at temperatures between 450 and 650 °C.

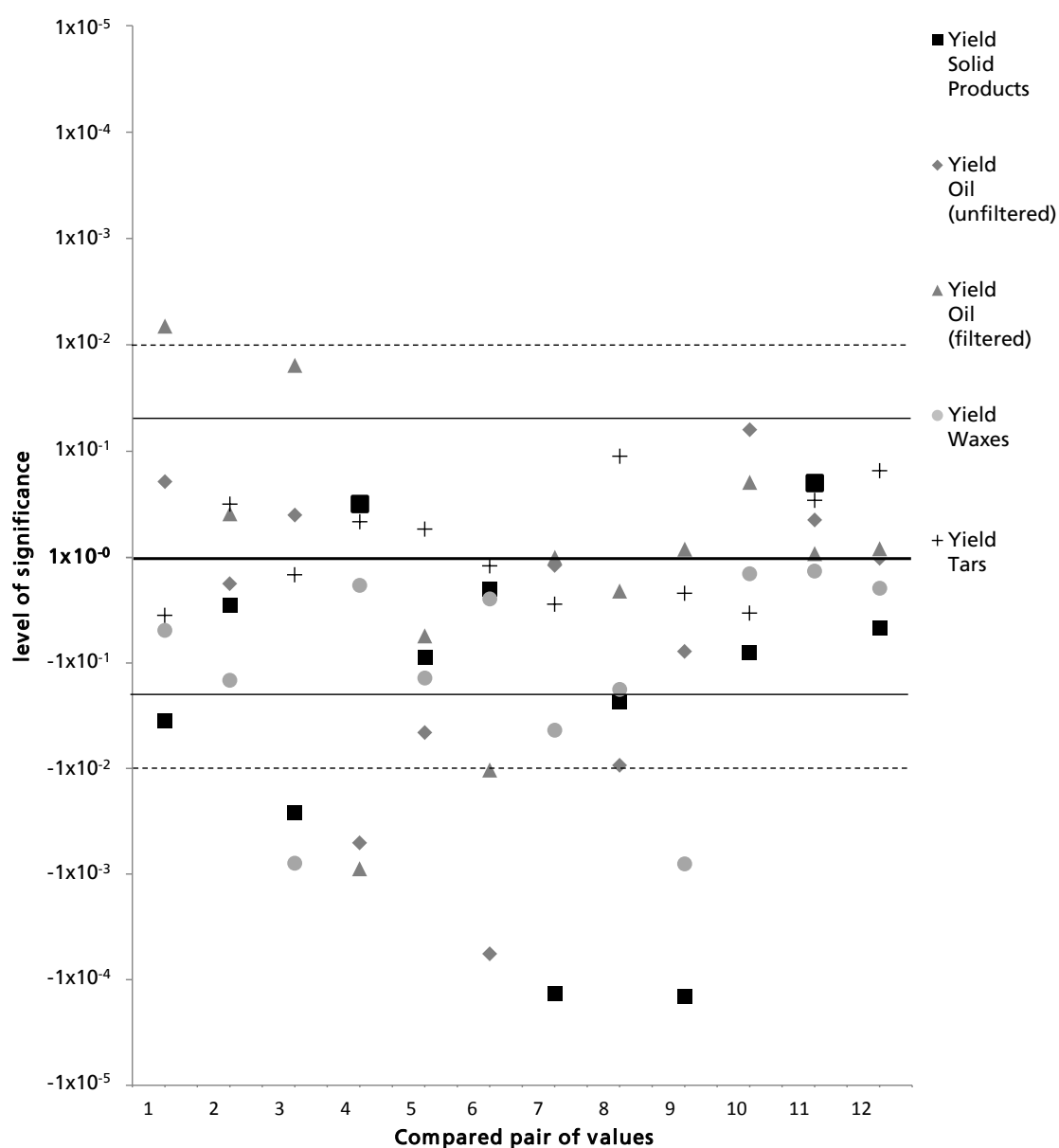


Figure 46: Results of significance tests regarding product allocation.

Pyrolysis solid products: HHV of pyrolysis solid products increased significantly just due to an increase of temperature from 550 to 650 °C (residence time 60 min) as well as due to an increase of residence time from 30 to 60 min at a temperature of 650 °C. Similar results were present for the content of C in the last named constellation of change. In contrast, the ignition loss decreased (greatly) significant due to increases of temperature from 450 to 550 °C as well as to 650 °C with one exception: ignition losses did not decreased significantly due to an increase of temperature from 450 to 550 °C at a residence time of 60 min. This indicates a strong influence of residence time at the low temperature level of just 450 °C. The content of N decreased just due to an increase of temperature from 450 °C to 650 °C at a residence time of 60 min and when both residence times were part of the calculation. The content of H decreased due to a temperature increases from 450 and 550 to 650 °C when both residence times were taken into account. For S no significant changes were obvious.

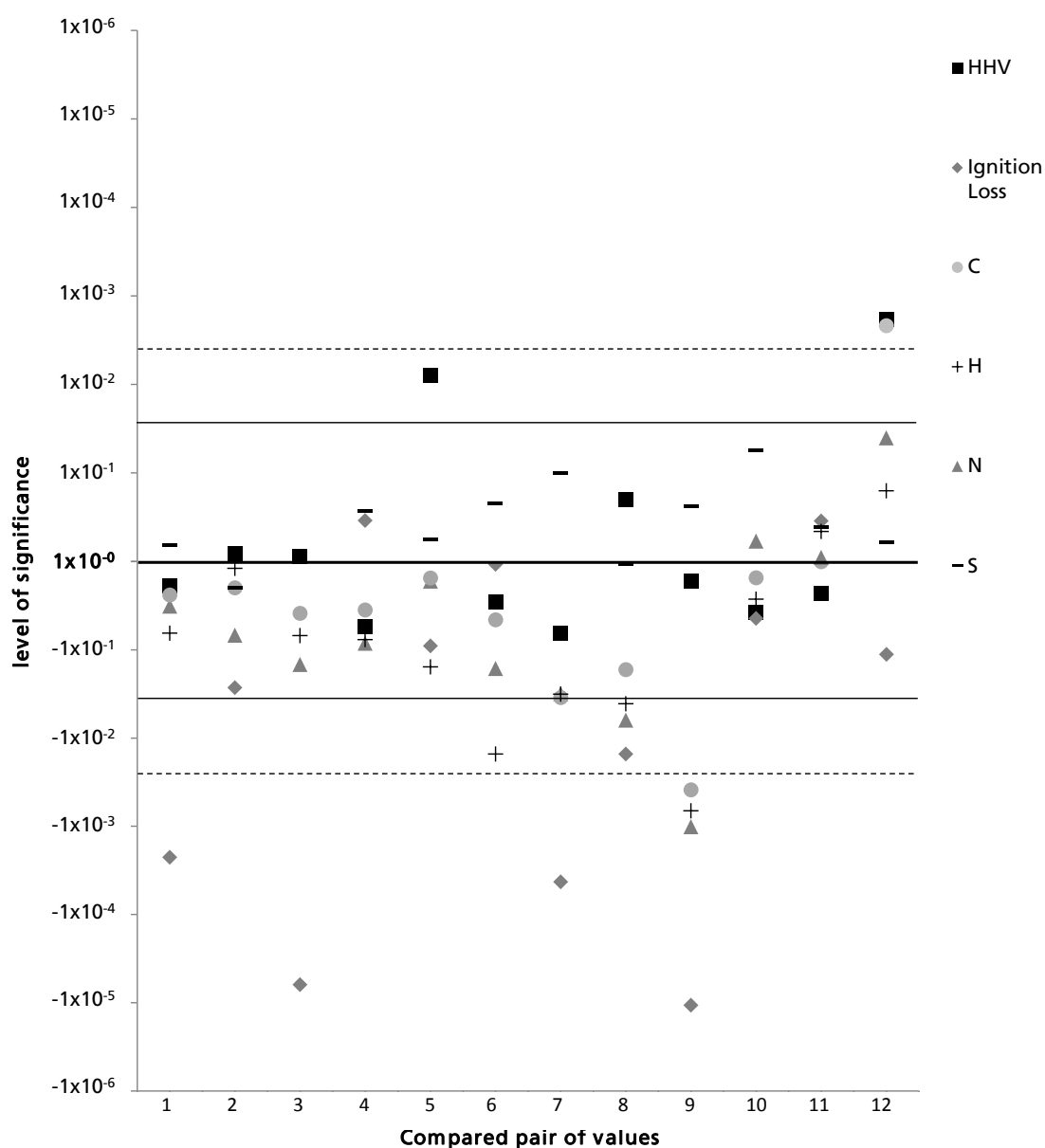


Figure 47: Results of significance tests regarding pyrolysis solid products.

Pyrolysis liquid products (filtered): Parameters *HHV*, content of H_2O , as well as content of S in filtered pyrolysis liquid products did not change significantly due to any varied conditions. Parameter *TAN* showed a significant change (decrease) just due to an increase of temperature from 450 and 550 to 650 °C. In contrast, a number of significant changes were obvious for content of H, content of N, as well as the quotient of C and H: the content of H decreased due to an increased temperature from 450 to 650 °C at 30 min. In addition, when both residence times were part of the calculation, (great) significant decreases were obvious due to changed temperature from 450 to 550 °C, from 550 to 650 °C and from 450 to 650 °C. The content of N increased just due to an increase of temperature from 450 to 650 °C. At least, the quotient C/H increased (great) significantly due to all temperature changes. In contrast to changes due to variations of temperature, variations of residence time had no significant effect on the quality of pyrolysis filtered liquids.

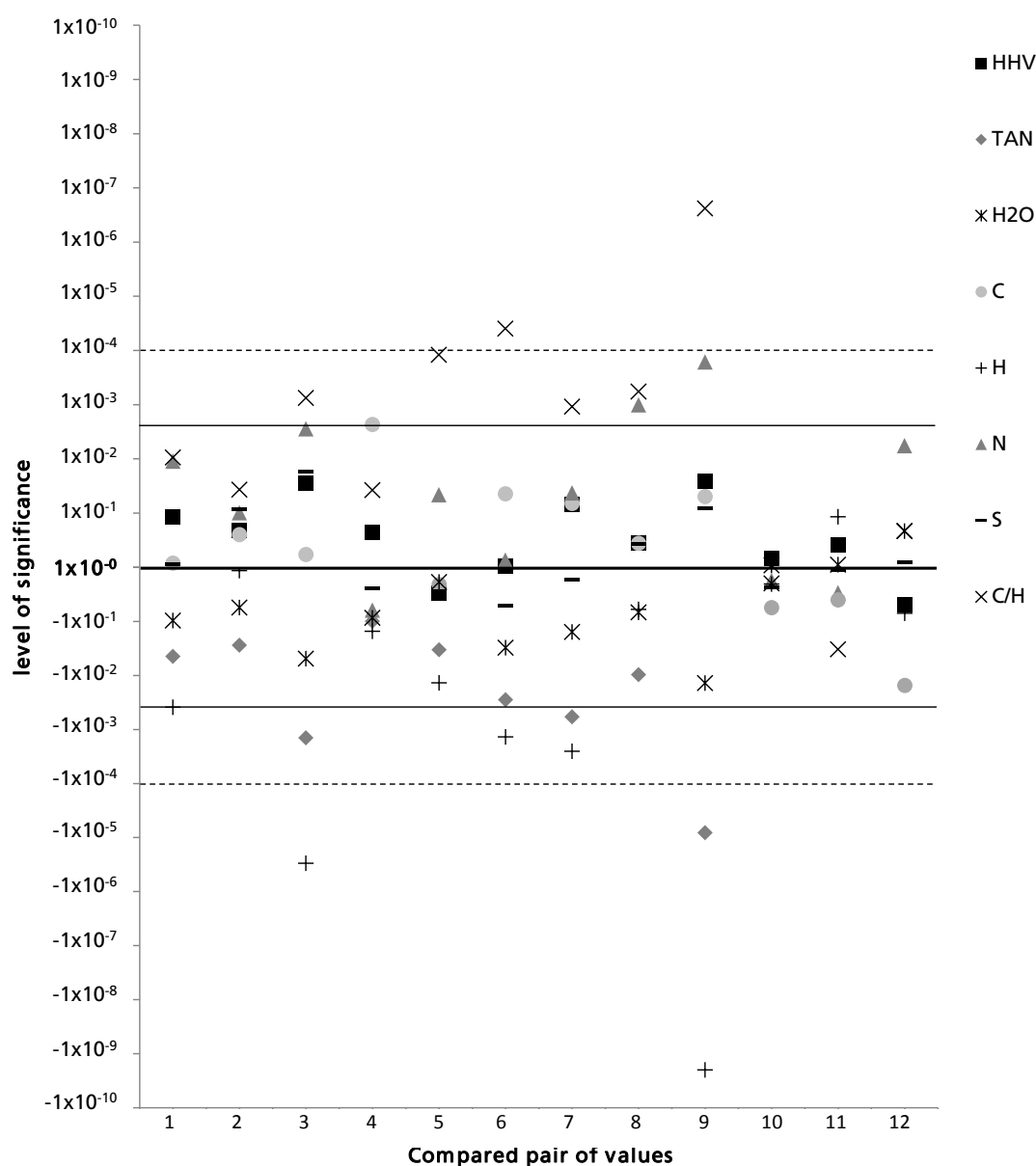


Figure 48: Results of significance tests regarding pyrolysis liquid products (filtered).

Pyrolysis gases: Compared to all other significance tests, those regarding pyrolysis gases showed the greatest differences. Additionally, in all investigated parameters, large significant changes were obvious. Due to any increase of temperature, the content of H_2 _{corr} increased significantly. Similar to this, content of CO as well as both heating values increased significantly. As mentioned above, calculations for content of C_xH_y could be examined not for every constellation. Therefore, significance tests were investigated for just six constellations, from which four results indicated significant increases due to increased temperatures. Only with an increase of temperature from 550 to 650 °C, when both residence times were taken into account, C_xH_y increased insignificant. In contrast, such values of CO_2 content indicated mainly great significant decreases due to increases of temperature with the exceptions of 450 to 550 °C when both residence times were part of the calculation and due to an increase of temperature from 550 to 650 °C at 30 min.

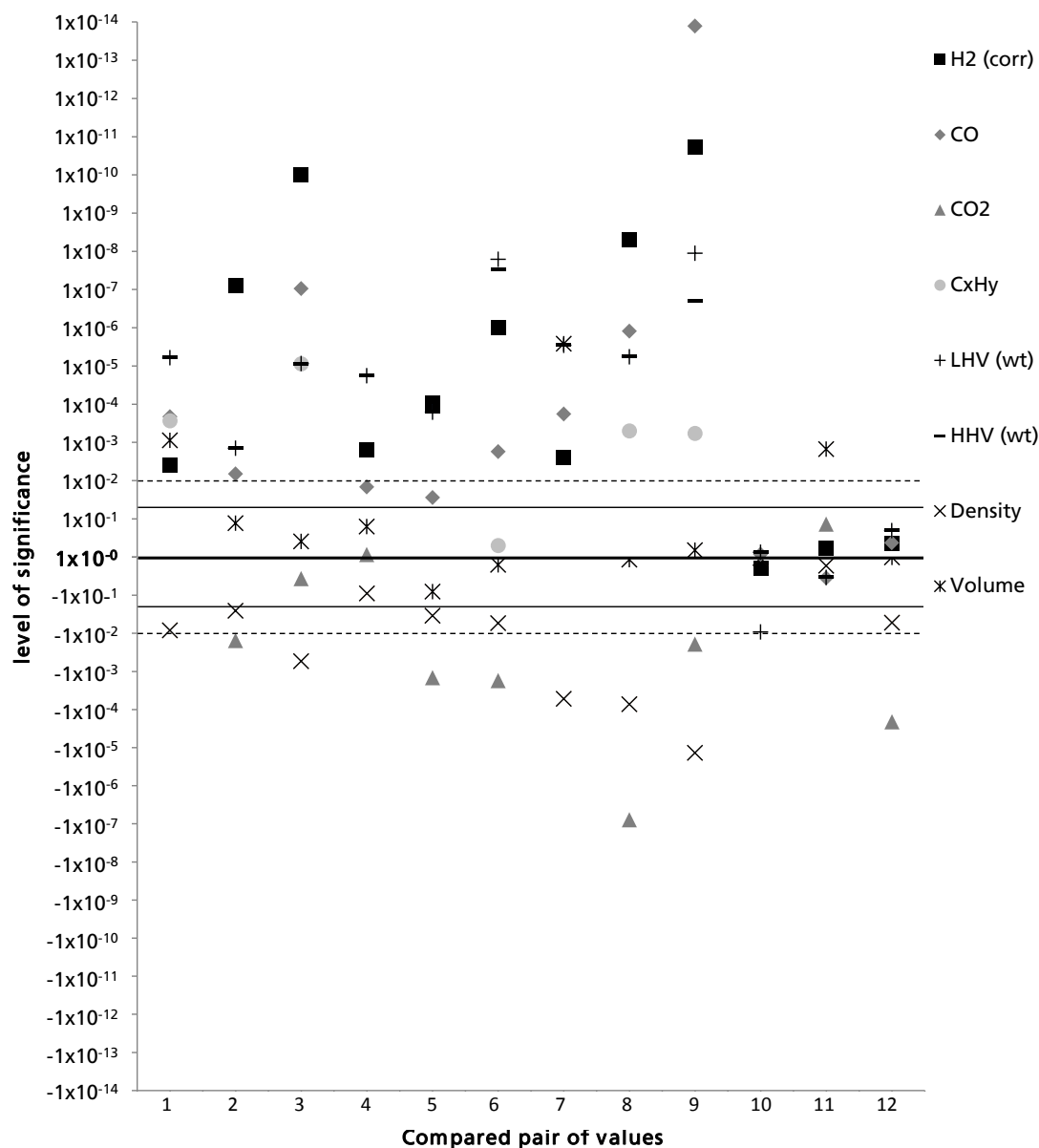


Figure 49: Results of significance tests regarding pyrolysis gases.

Densities of formed gases decreased significantly with increases of temperature with the exception of 550 to 650 °C at 30 min residence time. Volume of pyrolysis gases increased with increases of temperature from 450 to 550 °C as well as to 650 °C at a residence time of 30 min. Variation of residence time from 30 to 60 min significantly decreased the effect on the content of CO₂ at 650 °C. Likewise, lower heating value *LHV* and density decreased significantly due to an increase of residence time at 450 and 650 °C, respectively. In contrast, at 550 °C the produced volume of gases increased strong significantly at 550 °C.

Regression analyses

In order to show correlations between different values of product allocation and quality by a change of pyrolysis temperature, the above mentioned statistical methods were used (see chapter 5.3). Regression analyses regarding residence time were not conducted, because just two values (30 and 60 min) were analyzed.

Regression analyses revealed that in all cases polynomial regressions showed the best results, indicated by a high coefficient of determination R^2 . Due to a high number of analyzed relations, just a number of these should be highlighted: therefore, on the one hand just examples are shown based on both residence time levels and on the other hand, significant differences are shown due to changed temperatures.

Product allocation: Yields of waxes, filtered, as well as unfiltered liquid product over the three temperature levels are shown in Figure 50. For waxes, a great decrease was shown with an increase of temperature from 450 to 550 and 650 °C with a relatively high coefficient of determination ($R^2 = 78.6 \%$). Regarding pyrolysis liquid products, a peak was obvious at a pyrolysis temperature at 550 °C, while that of filtered liquid product was distinctively stronger than those of unfiltered one.

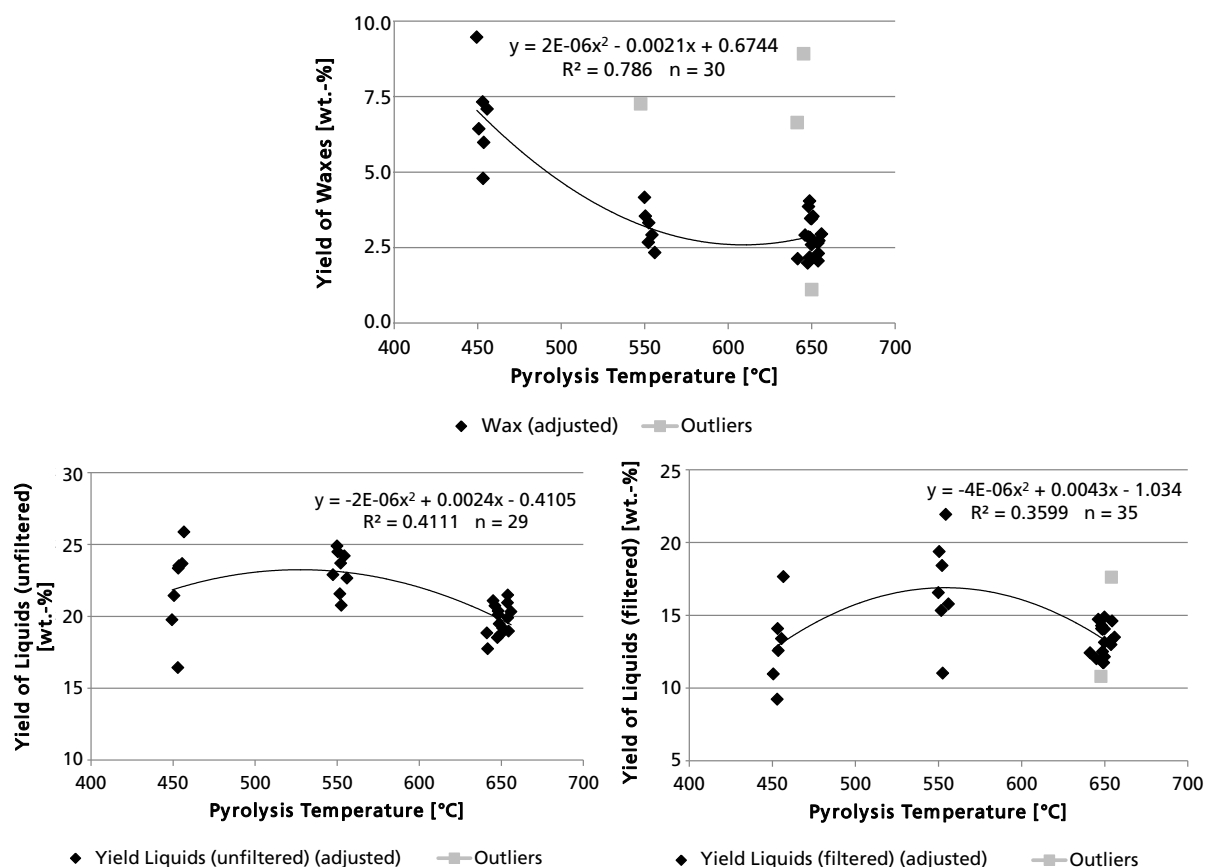


Figure 50: Yields of waxes, unfiltered, and filtered liquid product over temperature.

Pyrolysis solid products: Very similar to the above mentioned relationship between temperature and yield of waxes, the ignition loss decreased greatly from 16.3 wt.-% at 450 to 10.5 wt.-% at 550 °C, but nearly stagnated from 550 to 650 °C (10.4 wt.-% at 650 °C) (Figure 51) ($R^2 = 64.1$ %). The second example concerning quality aspects of pyrolysis solid products regards content of H, which decreased greatly from 0.88 to 0.14 wt.-% (450 to 650 °C) ($R^2 = 52.9$ %). Additionally, it could be clearly seen that the variance decreased too: expressed as standard deviation, it decreased from 0.44 wt.-% at 450 °C to just 0.03 wt.-% at 650 °C.

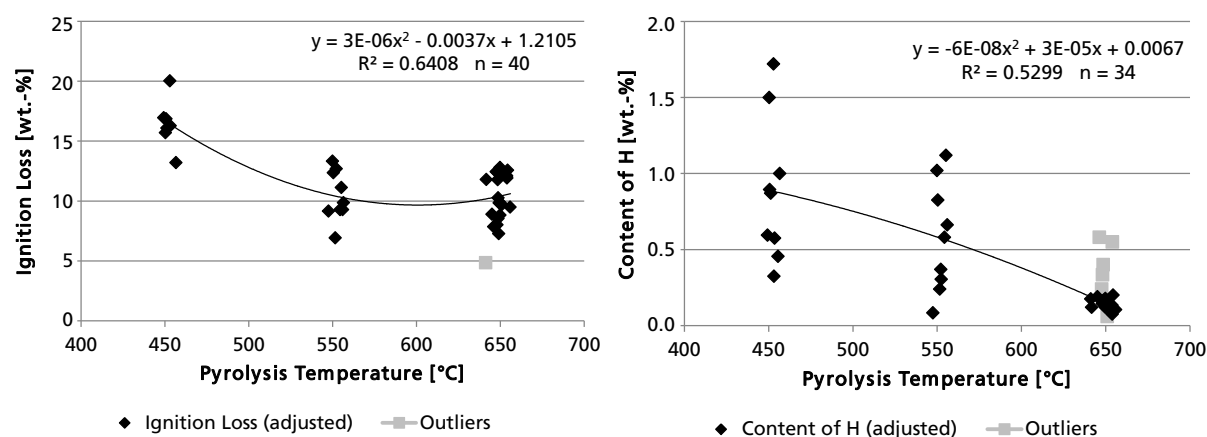


Figure 51: Ignition loss and content of H of pyrolysis solid products over temperature.

Pyrolysis liquid product (filtered): *TAN* decreased greatly with increased temperature from 15.8 at 450 °C to 7.9 and 3.0 mg KOH · g⁻¹ at 550 and 650 °C ($R^2 = 72.0\%$), respectively. Contrary to this, the ratio of C/H increased with an increase of temperature due to an increase of H and a decrease of C in the pyrolysis liquid products ($R^2 = 72.9\%$). Regarding the content of N, an increase from 2.03 wt.-% to 2.44 wt.-% was obviously due to an increase of pyrolysis temperature from 450 to 550 °C, but there was just a very slight increase of 0.04 wt.-% due to a further increase to 650 °C ($R^2 = 33.1\%$). The last shown parameter content of H₂O decreased similar to the values of *TAN* very strongly from 450 to 650 °C ($R^2 = 46.5\%$) (Figure 52).

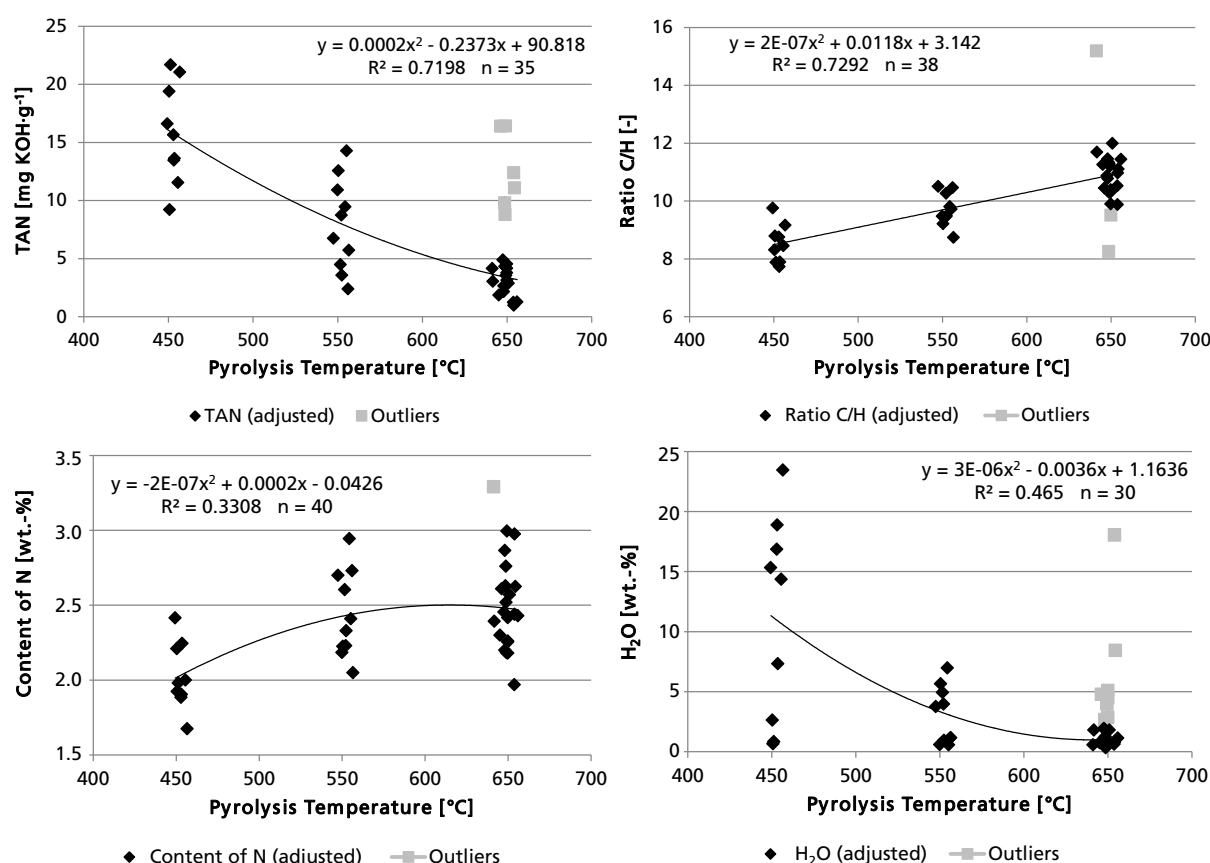


Figure 52: *TAN* value, Ratio of C/H, as well as contents of N and H₂O of filtered liquid pyrolysis products over temperature.

Pyrolysis gases: As mentioned above, the concentration of different components in pyrolysis gases differed greatly over temperature (Figure 53). While the content of CO₂ was more than halved from 54.0 (±15.2) to 24.3 (±9.0) vol.-% with a temperature increase from 450 to 650 °C, both contents of H₂_{corr} and CO decreased due to same temperature changes: at 650 °C the content of H₂_{corr} and CO reached 18.9 (±0.5) and 12.3 (±1.2) vol.-%, respectively. In contrast, the concentration of C_xH_y increased from 2.7 (±0.5) to 8.4 (±0.5) vol.-% within the first temperature step, but nearly stagnated during the second step (8.8 ±0.9 vol.-% at 650 °C). In addition high coefficients of determination, mainly for H₂_{corr} and C_xH_y, could be presented by polynomic regressions as R^2 was 0.94 and 0.96 for H₂_{corr} and C_xH_y, respectively.

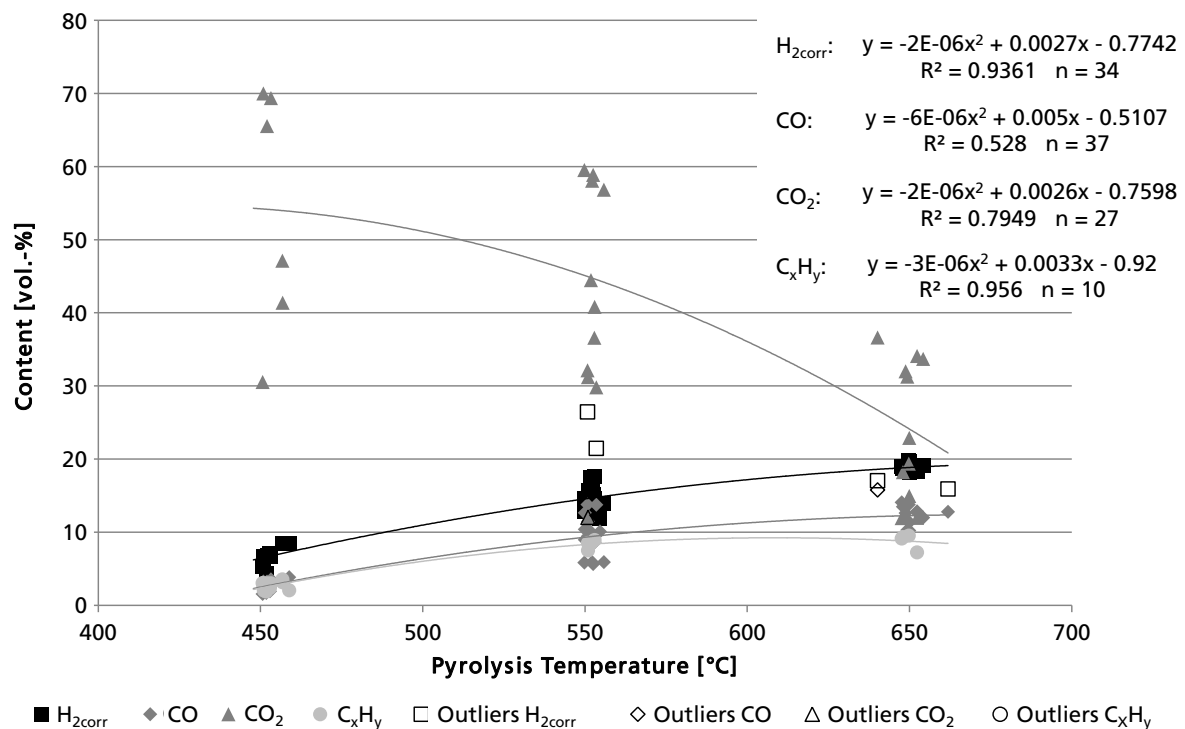


Figure 53: Contents of H_{2corr} , CO , CO_2 , and C_xH_y in pyrolysis gases over temperature.

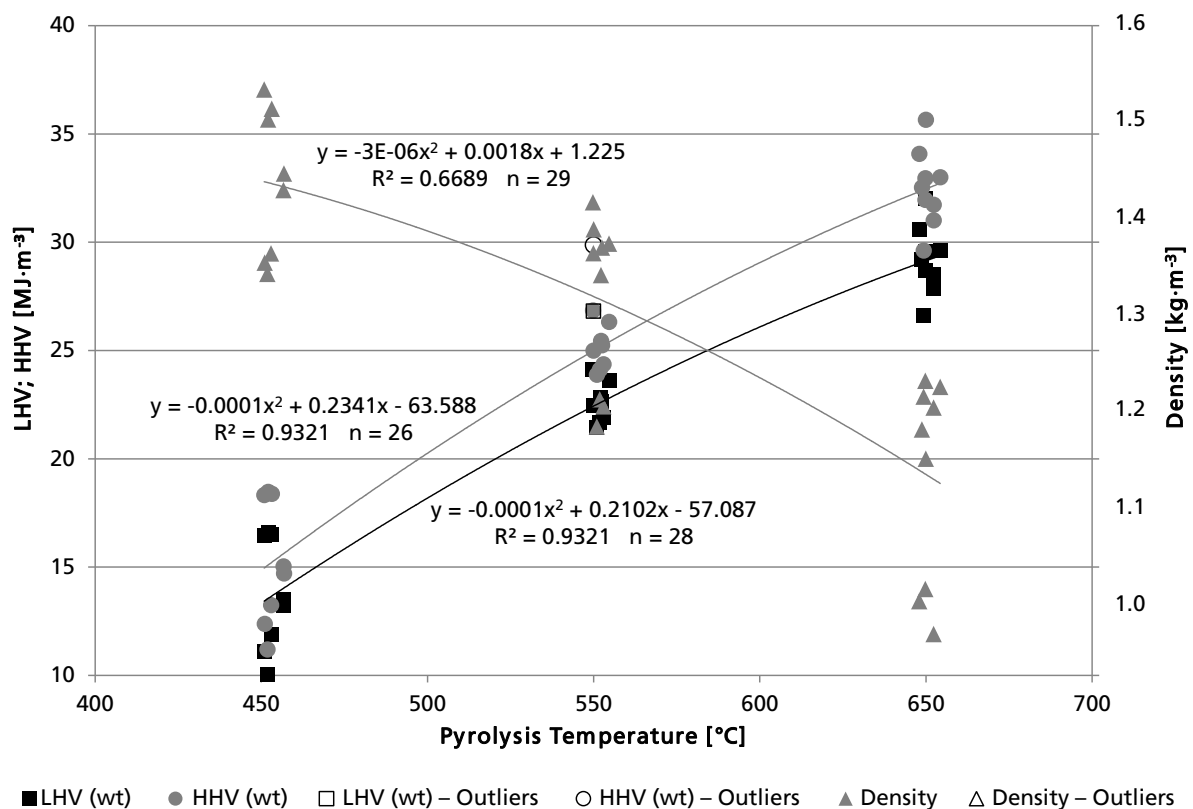


Figure 54: LHV (wt), HHV (wt), and (relative) density of pyrolysis gases over temperature.

Regarding CO_2 it is obvious that its variance is comparatively large. Percentages of CO_2 increased very slightly at residence times of 30 min, but decreased strongly at 60 min. These different strong formations of CO_2 during tests of different residence times could not be explained accurately, even after replications of tests: in general, formations of

gases during different tests usually decreased strongly after 20 - 30 min, therefore, just slight differences of gas concentrations regarding residence time were expected. However, mainly formation of CO₂ was significantly higher in tests at 450 and 550 °C with residence times of 60 min compared to those of 30 min. This unaccountable aspect changed contrary at a temperature of 650 °C²⁸.

Due to the changed compositions of pyrolysis gases, lower and higher heating values increased very significantly with an increased temperature; even while the density of gases decreased (Figure 54). Coefficients of determination were very high for *LHV* and *HHV* ($R^2 = 93.2\%$) and in a medium level for density ($R^2 = 66.9\%$). In order to check dependencies between the main components of pyrolysis gas and the heating value, chi-squared tests were conducted. Results of these tests (Table 54 to Table 57 in the appendix) confirmed clear dependencies between all different components and *HHV*.

Formation and avoidance of polyhalogenated dibenzo-*p*-dioxins and furans

Concerning formation of polyhalogenated dibenzo-*p*-dioxins and furans (PXDD/F) under conventional circumstances, in summary, seven analyses (solid products: 5; liquid products: 2) were conducted. Additionally, the feedstock and pyrolysis solid products from a test with a low heating rate (description see below) were tested on PXDD/F concentrations. The entire data set (Table 58 - Table 60) can be found in the appendix.

Results of high-resolution GC-MS (HR GC-MS) analyses for determination of PXDD/F concentrations are shown in Table 34. Compared to values of polybrominated dibenzo-*p*-dioxins and furans (PBDD/F) sums in feedstock, all sums in conventional pyrolysis tests (450 °C, 550 °C, 650 °C each for 60 min) are much lower; however, sums of polychlorinated dibenzo-*p*-dioxins and furans (PCDD/F) increased compared to the feedstock. In general, amounts of dioxins were either below detection limit, or just very low compared to furans. Concerning the impact of temperature, sums of PCDD/F decreased with an increase of temperature from 450 to 550 to 650 °C, while those of PBDD/F showed lowest values at 550 °C. Besides influence of pyrolysis temperature on PXDD/F concentrations in solid products, two additional analyses were conducted with the aim to prove the impact of residence time. Therefore, tests of solid products at 650 °C for 30 min and at 550 °C for 90 min were analyzed. The results did not show clear effects, because on the one hand, concentrations of PXDD/F decreased due to an elongated residence time as expected due to vaporization, and on the other hand, due to this it was expected that PXDD/F concentrations are higher in the case of a shorter

²⁸ An inlet of excess air during these tests was clearly avoided (like also in all other tests) and could be ruled out due to values of other parameters such as ignition loss of pyrolysis solid products.

residence time (650 °C, 30 min) than in the case of a longer time (650 °C, 60 min). However, values of that test at 650 °C for 30 min showed the second lowest values after that test at 550 °C for 90 min.

Table 34: PXDD/F concentration in SR1 as well as six different pyrolysis solid products (in $\mu\text{g}\cdot\text{kg}^{-1}$).

Pyrolysis	Feed-stock		Pyrolysis solid products				
Temperature [°C]	---	550	450	550	550	650	650
Residence Time [min]	---	60*	60	60	90	30	60
PCDD/F							
Tetra- to OctaCDD	0.369	---	---	---	0.003	---	---
Tetra- to OctaCDF	0.245	117.112	88.361	55.252	0.146	2.804	33.888
Tetra- to OctaCDD/F	0.614	117.112	88.361	55.252	0.149	2.804	33.888
PBDD/F							
Tetra- to OctaBDD	90.240	1.440	0.131	0.040	---	0.029	0.048
Tetra- to OctaBDF	658.500	891.150	78.083	40.984	1.333	38.891	45.078
Tetra- to OctaBDD/F	748.740	892.590	78.214	41.024	1.333	38.920	45.126
PXDD/F							
Tetra- to OctaXDD	90.61	1.44	0.13	0.04	0.003	0.03	0.05
Tetra- to OctaXDF	658.74	1 008.26	166.44	96.24	1.48	41.69	78.97
Tetra- to OctaXDD/F	749.35	1 009.70	166.57	96.28	1.48	41.72	79.01

* Pyrolysis test with a low heating rate.

Additionally to these tests on pyrolysis solid products and feedstock, the influence of a significantly decreased heating rate on PXDD/F concentration in pyrolysis solid products was tested with the aim to prove that formation of PXDD/F decrease with an increase of heating rate and to evaluate effects of a test run with a very low heating rate. Therefore, feedstock SR1 was loaded into the cool reactor. After purging the reactor with N_2 , the reactor was heated up slowly with an approximately linear heating rate of $2.7 \text{ K}\cdot\text{min}^{-1}$ on average²⁹. After reaching the desired temperature of 550 °C, the test run was conducted as usual over a residence time of 60 min. After that time, the pyrolysis solid products were removed from reactor to the char pot. Measured temperatures and pressures of the corresponding test are shown in Figure 55. The average temperature after reaching the target temperature was 549.1 °C with a standard deviation of 8.1 °C.

Compared to pyrolysis tests with same parameters but conventional procedures of heating and filling, a significantly lower yield of solid products (43.79 wt.-%) and higher yields of gases (33.79 wt.-%) were found (Figure 56). These results could indicate that a lower heating rate supports a more comprehensive evaporation of volatile components

²⁹ For comparison: In conventional pyrolysis tests with a temperature of 650 °C, heating rates accounted for 150 - 200 $\text{K}\cdot\text{min}^{-1}$.

from pyrolysis solid products; however, the ignition loss of the solid pyrolysis product was 19.29 wt.-%, which was significantly higher than those of the corresponding tests (11.08 ± 1.53 wt.-%).

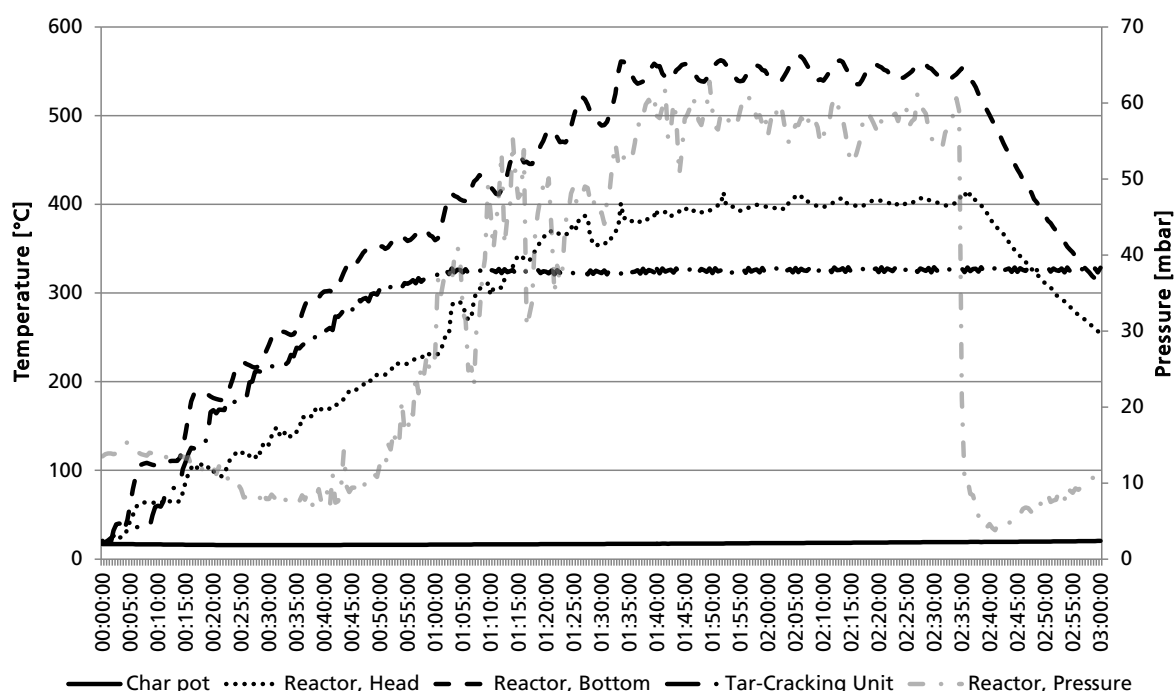


Figure 55: Pyrolysis temperature and pressure during test "low heating rate".

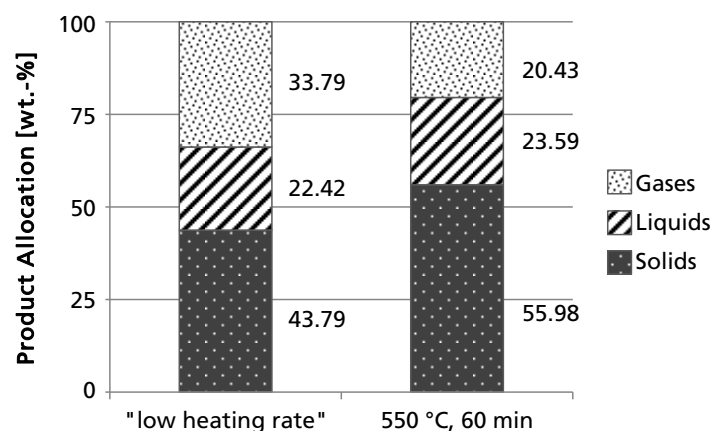


Figure 56: Product allocation from pyrolysis test "low heating rate" and the average values for tests at 550 °C and 60 min.

As shown in Table 34, all sums of PXDD/F concentrations in pyrolysis solid products had the highest values in the case of a low heating rate compared to those under conventional circumstances (high heating rate). These analyses clearly reveal that formations of PXDD/F are effectively suppressed due to a high heating rate.

Figure 57 shows the results of pyrolysis solid products more comprehensively as sums according to the German act on restriction of chemicals (GGVSEB) and the German chemicals prohibition ordinance (ChemVerbotsV) (in $\mu\text{g}\cdot\text{kg}^{-1}$). In these acts on restrictions of chemicals, mainly for the transport sector, different limit values for

PXDD/F sums are set as $1 \mu\text{g}\cdot\text{kg}^{-1}$ for 4 PCDD/F, $5 \mu\text{g}\cdot\text{kg}^{-1}$ for 12 PCDD/F, and $100 \mu\text{g}\cdot\text{kg}^{-1}$ for 17 PCDD/F as well as $1 \mu\text{g}\cdot\text{kg}^{-1}$ for 4 PBDD/F and $5 \mu\text{g}\cdot\text{kg}^{-1}$ for 8 PBDD/F. The full list of congeners and corresponding sums is shown in the appendix (Table 48).

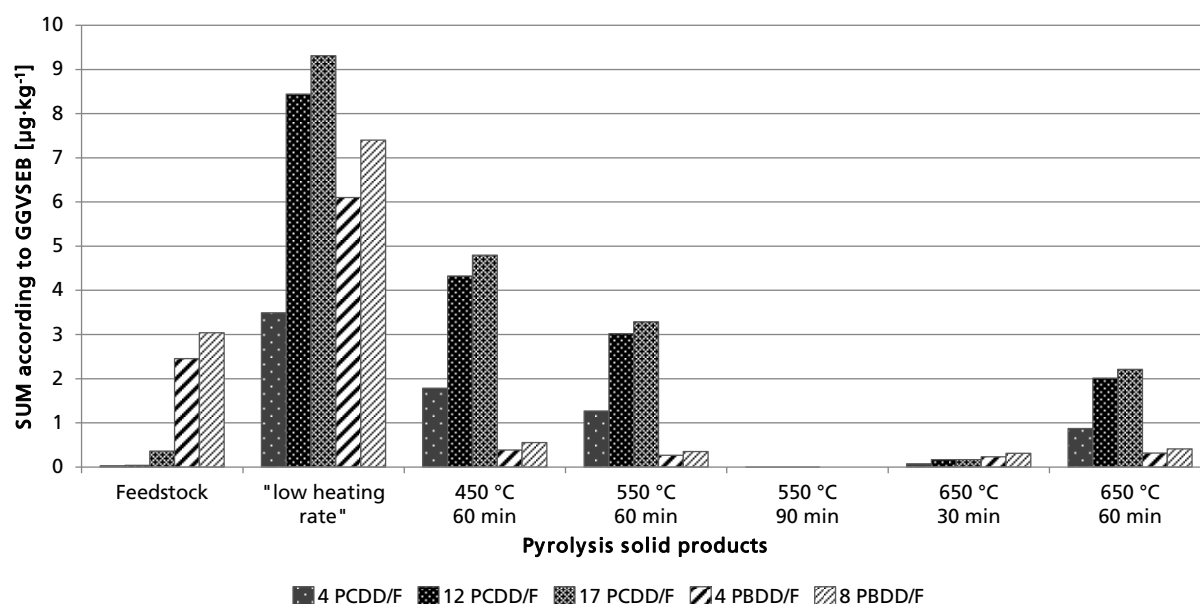


Figure 57: Sums of PXDD/F according to GGVSEB / ChemVerbotsV of feedstock SR1, solid products from conventional tests, as well as from a test with a low heating rate.

The sum of 4 PBDD/F in the feedstock exceed the limit value of $1 \mu\text{g}\cdot\text{kg}^{-1}$ with more than $2.457 \mu\text{g}\cdot\text{kg}^{-1}$ clearly; all other sums were lower than the corresponding limit values. As mentioned, sums of PCDD/F decreased with an increase of temperature from 450 to 550 to 650 °C, but they were lower than all limit values just in the case of 550 °C and 90 min as well as at 650 °C. Solid products from tests at 450 and 550 °C (60 min) exceed the limit value for the sum of 4 PCDD/F with $1.785 \mu\text{g}\cdot\text{kg}^{-1}$ and $1.270 \mu\text{g}\cdot\text{kg}^{-1}$.

In addition to pyrolysis solid products, pyrolysis liquids from five different process constellations were tested on PXDD/F concentrations (Figure 58). Besides two conventional pyrolysis tests at 550 and 650 °C (both with a residence time of 60 min), a number of tests with PO-reactor were conducted. From these tests three different liquid products were analyzed regarding its content of PXDD/F:

- 1) 650-30-PP: liquid product from a pyrolysis with a temperature of 650 °C and a residence time of 30 min; PO-reactor was filled with pure PP (340 °C).
- 2) 650-30-PP+La1.5: pyrolysis was the same than in 1) but the PO-reactor was filled with a mixture of PP + La(OH)₃/LaOOH (100:0.468 by weight), and the halogen-filter was installed afterwards. The mixture ratio of PP and La represented a stoichiometric ratio between X and La of nearly 1.5.
- 3) 650-30-PP+La4.5: pyrolysis was the same than in 1) and 2) but the PO-reactor was filled with a mixture of PP + La(OH)₃/LaOOH (100:1.412 by weight; stoichiometric ratio between X and La of nearly 4.5); halogen-filter was installed, too.

From the first test, the effectiveness of PP got tested regarding its decomposition effectiveness on PXDD/F in pyrolysis liquids. Additionally, as mentioned in chapters 4.3.3 and 4.4, La compounds seem feasible to decompose (poly-)chlorinated aromatic compounds. Therefore, two blends of PP and $\text{La}(\text{OH})_3/\text{LaOOH}$ were prepared in order to test if decomposition using La is also effective regarding brominated compounds³⁰.

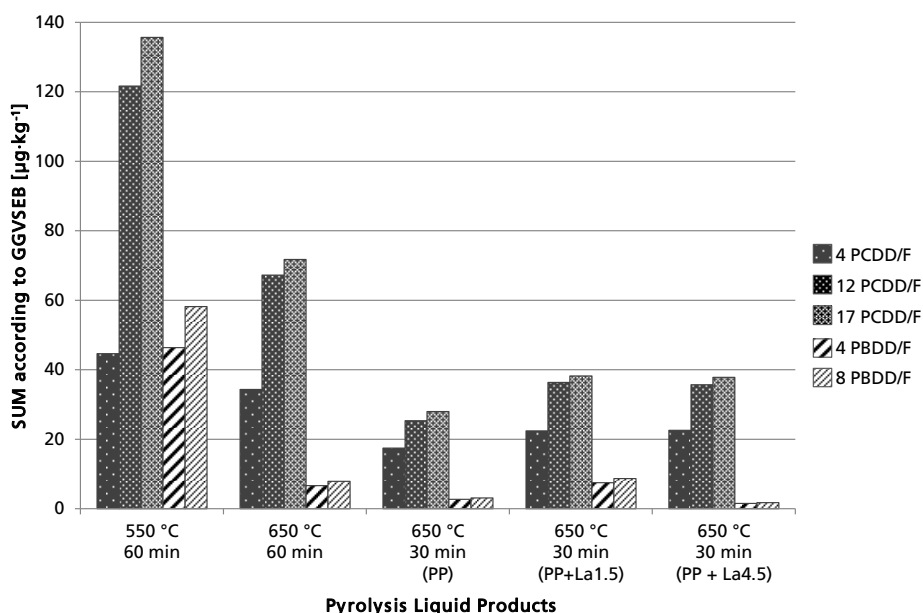


Figure 58: Sums of PXDD/F in different pyrolysis liquid products, according to GGVSEB / ChemVerbotsV.

Due to the strong impact of component's residence times in molten PP on decomposition of PXDD/F, residence times from three different tests, in which the PO-reactor was installed, were calculated. Based on the results of gas chromatography/mass spectrometry (GC-MS) analyzes for liquid products from 650 °C, 30 min tests (see below), a specific gas constant R_s for the pyrolysis liquid product of $73.64 \text{ J} \cdot \text{kg}^{-1} \cdot \text{K}^{-1}$ was estimated. The volume flow rate and flow velocity of vapor through the PO-reactor was calculated as $0.07 \text{ l} \cdot \text{s}^{-1}$ and $0.86 \text{ m} \cdot \text{s}^{-1}$. Based on this data, the residence time of vapor in the molten PP at 340 °C was 0.123 s. It should be noted that any decelerating (and thusly advantageous) effects on the velocity of flow due to present PP or spheres were not taken into account.

Similar to pyrolysis solid products, concentrations of dioxins are considerably lower than those of furans in liquid products. However, in contrast to the solid products, in all cases all sums of PXDD/F were considerably higher, which indicates that most PXDD/F vaporized after formation. However, due to higher temperature (650 °C vs. 550 °C, both for 60 min) more PXDD/F were destructed or its formation suppressed.

³⁰ From literature, just decomposition of chlorinated aromatic compounds is reported [van der Avert, Weckhuysen 2004; van der Avert et al. 2004].

As shown in Table 35, due to the addition of the PO-reactor with PP, amounts of PXDD/F significantly decreased. The highest rate of decrease was obvious for PBDF, which decreased from 1437.10 to 327.65 $\mu\text{g}\cdot\text{kg}^{-1}$ corresponding to 77.2 wt.-%. As a distinctive aspect, it should be highlighted that just due to the addition of La to PP, formations of PXDD are completely suppressed, while such formations are just (significantly) decreased due to the addition of pure PP. Otherwise, concentrations of PCDF increased due to an addition of La to PP.

Table 35: PXDD/F concentrations in four different pyrolysis liquid products (in $\mu\text{g}\cdot\text{kg}^{-1}$).

Pyrolysis	Pyrolysis liquid products				
Temperature [°C]	550	650	650	650	650
Residence Time [min]	60	60	30	30	30
PO-Reactor	---	---	PP	PP+La1.5*	PP+La4.5**
PCDD/F					
Tetra- to OctaCDD	2.10	1.35	0.59	---	---
Tetra- to OctaCDF	2 461.31	2 080.28	788.73	1 067.54	1326.34
Tetra- to OctaCDD/F	2 463.41	2 081.63	789.32	1 067.54	1326.34
PBDD/F					
Tetra- to OctaBDD	9.01	1.02	---	---	---
Tetra- to OctaBDF	7 817.10	1 437.10	327.65	1 255.90	200.17
Tetra- to OctaBDD/F	7 826.11	1 438.12	327.65	1 255.90	200.17
PXDD/F					
Tetra- to OctaXDD	11.11	2.37	0.59	---	---
Tetra- to OctaXDF	10 278.41	3 517.38	1116.38	2 323.44	1526.51
Tetra- to OctaXDD/F	20 289.52	3 519.75	1116.97	2 323.44	1526.51

* Blend of PP and La(OH)₃/LaOOH (100:1.412 by weight).

** Blend of PP and La(OH)₃/LaOOH (100:0.468 by weight).

Allocations of C, H, N, and S under pyrolytic conditions

As compilation of analyses regarding pyrolysis product qualities and influences of PO-reactor on it, allocations of C, H, N, and S were calculated. Therefore, concentrations of C, H, and N in different pyrolysis products were determined using Vario MACRO Cube elemental analyzer, while concentrations of S were analyzed using EDXRF with previously determined concentrations of C, H, and N (O as missing component). For allocation calculations, normalization was conducted. Content of mentioned elements in gases were calculated by difference.

Figure 59 shows a flow diagram of C, H, N, and S. It is obvious that a marginal amount of H (0.4 wt.-%) and just small amounts of C (10.8 wt.-%) and N (19.1 wt.-%) allocated to pyrolysis solid products while 89.6 wt.-% of S was concentrated in this. Majorities of C and H were allocated to pyrolysis gases while the majority of N allocated to the liquid phase. The added PP in the PO-reactor decomposed partly under formation of C and H mainly in pyrolysis gases, while less than a half allocated to the corresponding PP-residue.

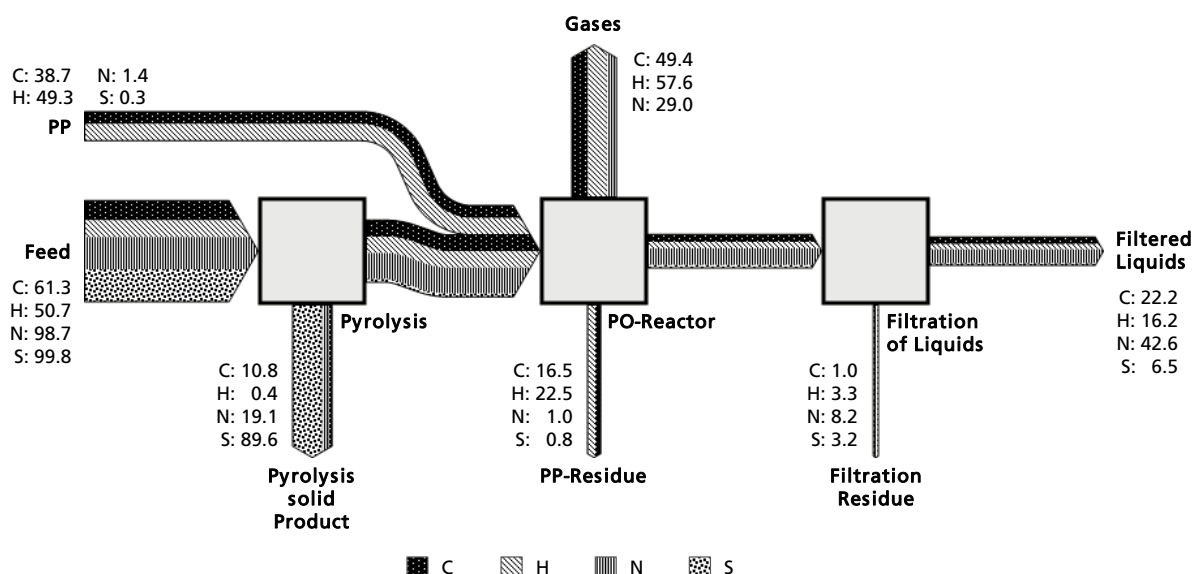


Figure 59: Allocation of C, H, N, and S from pyrolysis at 650 °C for 30 min with PO-reactor based on analyses using Vario MACRO Cube elemental analyzer.

Allocations of metals and its volatilization via halogenation under pyrolytic conditions

In order to enhance metal recycling from shredder residues using pyrolysis technology, analyses concerning concentrations of metals in different pyrolysis products are necessary in order to calculate allocations of metals to it. Additionally, concentrations of halogens, namely Br and Cl, have to be determined, which could affect corrosion or formation of toxic compounds in downstream recycling processes. Therefore, elemental analyses regarding metals, P, Br, and Cl were conducted using ICP-MS/-OES analyses and ion chromatography (Table 36). Results revealed that the main part of metals stay stable in the solid residue. However, some metals, namely As, Cu, Ga, In, Mg, Mn, Ni, Sb, Sn, Ti, and Zn were detected in unfiltered liquid products, too. Even after filtration, As, Sb, Sn, and Zn were detected in filtered liquid products.

Table 36: Content of metals, P (determination by ICP-MS/-OES^{1,2}), Br, and Cl (determination by ion chromatography³) in products from pyrolysis at 650 °C for 30 min with SR1 as feedstock.

Element	Value (mg·kg ⁻¹ DM)			Element	Value (mg·kg ⁻¹ DM)		
	Solid Product	Filtered Liquids	Filtration Residue		Solid Product	Filtered Liquids	Filtration Residue
Ag	97	<1	<1	Nd	96	<10	<10
Al	21 400	<100	<100	Ni	2 260	<1	1.8
As	17	1.3	2.3	P	1 980	340	240
Au	<10	<10	<10	Pb	17 900	5.2	320
Be	0.11	<0.1	<0.1	Pd	18	<10	<10
Bi	63.7	<0.1	<1	Pr	17	<10	<10
Br	4 600	590	580	Pt	<10	<10	<10
Ca	20 700	<100	<100	Rh	<1	<1	<1
Cl	8 100	<1 000	1 400	Ru	<10	<10	<10
Co	300	<1	<1	Sb	1 960	22.9	505
Cr	760	<1	<1	Sc	<10	<10	<10
Cu	81 933	<1	28	Se	5.2	<1	1.1
Dy	<10	<10	<10	Sn	11 400	20.6	169
Fe	79 500	<100	140	Sr	1 720	<1	1.4
Ga	339	<1	1.9	Ta	<10	<10	<10
Ge	<10	<10	<10	Te	2.2	<1	<1
In	46.9	<1	2.3	Ti	410	<1	6.8
Ir	<10	<10	<10	Tl	<0.4	<0.4	<0.4
La	35	<10	<10	W	n.d. ⁴	<10	<10
Mg	5 930	<10	31	Y	12.2	<1	<1
Mn	5 200	<1	6.4	Zn	13 500	21	410
Mo	150	<1	<1	Zr	73	<10	<10
Na	3 320	<200	110				

¹ ICP-MS according to DIN EN ISO 17294-2.² ICP-OES according to DIN EN ISO 11885.³ Ion chromatography according to DIN 51727.⁴ n.d.: not determinable.

In comparison with concentrations of metals in feedstock (chapter 6.1.1), strong degrees of enrichment could be detected for a number of metals such as Mo, Sr, Mn, Fe, Ni, as well as a very low ones for Cu and La. Figure 60 shows all calculated degrees of enrichment for metals not only in pyrolysis solid products, but also in filtration residues and filtered liquid product, based on ICP-MS/-OES analyses. Additionally, a horizontal dashed line at a degree of enrichment of 1.82³¹ for pyrolysis solid products indicates that enrichment of metals correlates directly with the yield of solid products. Due to the much lower amounts of filtration residue and filtered liquid product, corresponding lines are not shown in the figure because they reached values of 14.92 and 8.02 for filtration residue and filtered liquid product, respectively.

³¹ The yields of the pyrolysis solid products, which were analyzed by ICP-MS/-OES for this calculations accounted for 54.83 wt.-%. By division with the input (100 wt.-%) a factor of 1.82 can be calculated.

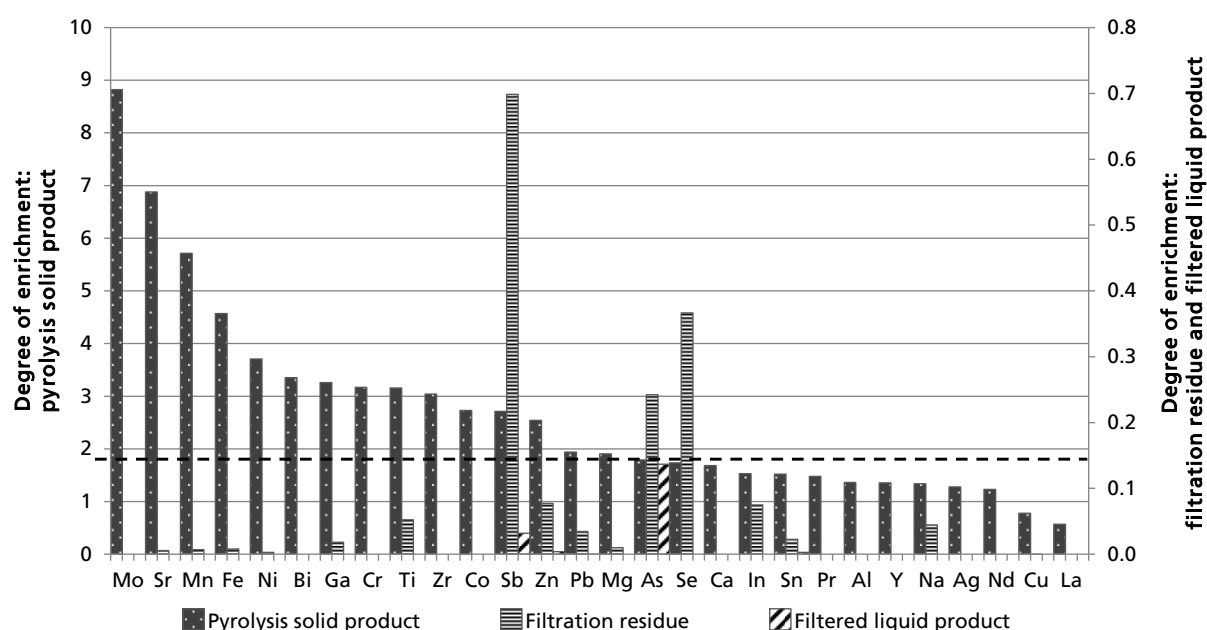


Figure 60: Degrees of enrichment for metals in pyrolysis solid products, filtration residue, and filtered liquid product; calculations based on ICP-MS/OES analyses.

As mentioned, some metals had significantly below and significantly above average degrees of enrichment. Reasons for these abnormal values could have manifold characters: on the one hand, due to heterogeneity of the material as well as matrix effects during measurements³², mainly for metals with very small (e.g. La, Mo, Ni) and very high concentrations (e.g. Cu, Fe), corresponding contents could be calculated wrong; additionally, in preparation for ICP-MS/OES analyses metals with high concentrations could be digested insufficient (c.f. chapter 5.2), and on the other hand, enrichment could not be identical for all metals due to depletion/mobilization of mainly reactive and volatile elements such as H and N, which had partly high concentrations in feedstock but low ones in the solid product (Figure 61).

In contrast, S mainly allocated to pyrolysis solid products. In order to study present chemical bindings of S, a XRD analysis was conducted for the sieve fraction <63 µm, which contained 91.83 wt.-% S of all sieve fractions; the corresponding concentration was measured as 0.219 wt.-% by EDXRF. The XRD pattern (Figure 100 in the appendix) revealed that mainly sulfates of Na, K, and Ca were present and just small amounts of sulfides and sulfites. Besides these S containing compounds with alkaline (earth) metals, sulfates and sulfites containing Fe in addition to Na or K were detected.

³² As an example: measured concentrations of Cu in pyrolysis solid product were between 60 300 mg·kg⁻¹ and 112 000 mg·kg⁻¹ (mean: 81 933 ±21 933 mg·kg⁻¹).

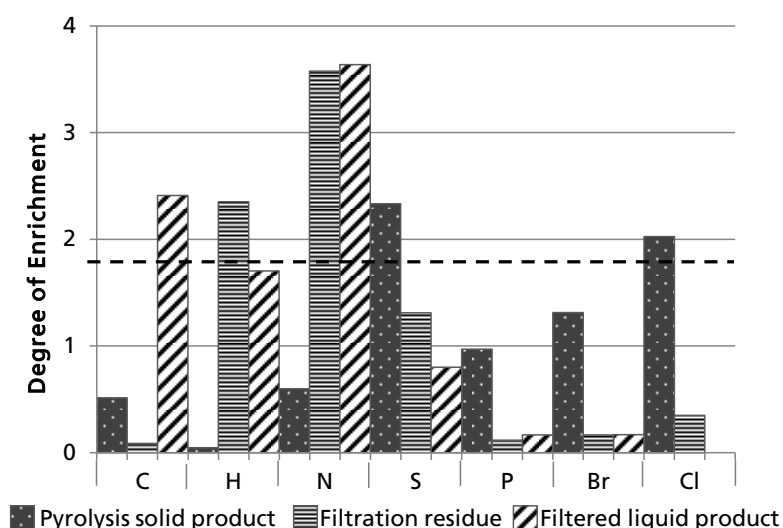


Figure 61: Degrees of enrichment for non-metals, P, and halogens in pyrolysis solid products, filtration residue, and filtered liquid product; calculation of C, H, N, and S based on analyses using Vario MACRO Cube elemental analyzer, of P by ICP-MS/OES, of Br and Cl by ion chromatography.

In addition, Figure 60 already adumbrates mobilization of metals from solid products to filtration residue and filtered liquid product. However, corresponding degrees of enrichment are significantly lower than those of metals in pyrolysis solid products. In general, metals, which showed any allocation to filtration residues or pyrolysis liquid products, could indicate different ways of mobilization:

- mobilization as particles, which became part of the vapor;
- mobilization via bonding to particles, which became part of the vapor;
- exceeding of boiling points of metals and/or its corresponding compounds.

In the last mentioned case, corresponding boiling points have to be between temperature of liquid pyrolysis products after cooling units (approximately 25 °C) and those of pyrolysis (650 °C). Such metals, which were part of the liquid product, were either in solution (e.g. in form of salts) or were present as smaller particles than the filter, which was used (2 µm).

In order to illustrate allocations of metals, Figure 62 shows a flow diagram for metals, which allocations to pyrolysis solid products were less than 99 wt.-% after normalization. As base for conducted calculations, a test with PO-reactor was chosen, in which the PO-reactor was filled with PP and La(OH)₃/LaOOH (100:0.468 by weight). Elemental analyses were conducted using EDXRF with C, H, N, given and O as missing component. A full list of allocations of all metals and P is shown in Table 61 in the appendix.

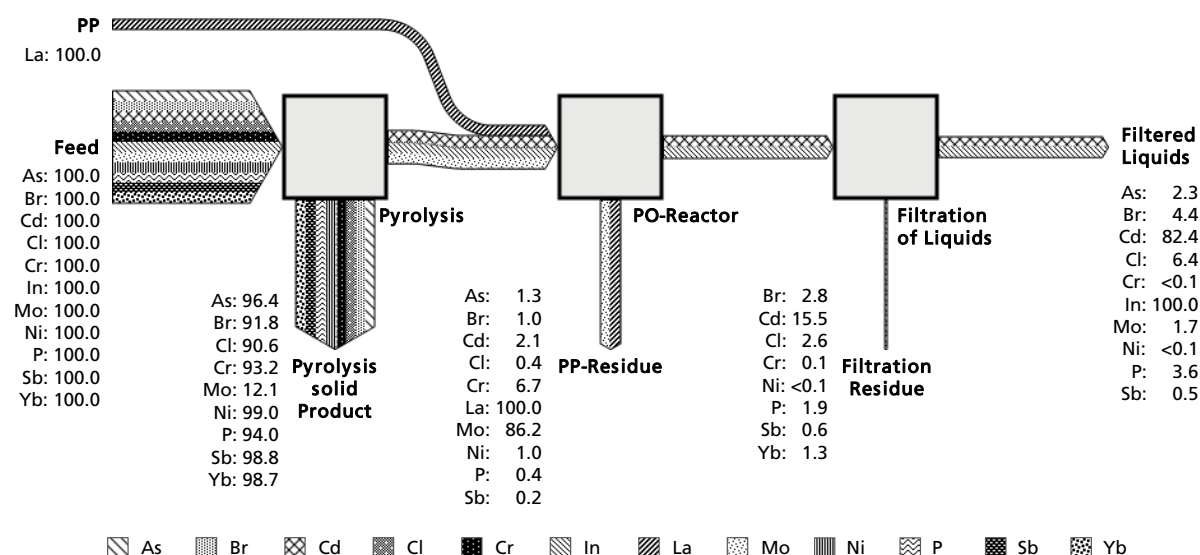


Figure 62: Allocation of metals, halogens, and P with <99 wt.-% allocation to solid product from pyrolysis at 650 °C for 30 min with PO-reactor. Analyses were conducted using EDXRF with C, H, N given and O as missing component.

As shown in Figure 62, even if just metals with allocations <99 wt.-% were illustrated, majority of such elements still allocated to pyrolysis solid products. However, allocation of Mo to pyrolysis solid product was comparatively low (12.1 wt.-%) and those of Cd and In did not exist. The main part of Mo (86.2 wt.-%) allocated to PP-residue, while Cd allocated mainly to filtered liquid products (82.4 wt.-%) and slightly to PP-residue (2.1 wt.-%) and filtration residue (15.5 wt.-%). In contrast, In were detected just in filtered liquids. La, which was an additive to PP, was not mobilized, which means that it was detected just in PP-residue. Besides these metals, mobilization of halogens accounted for 8.2 and 9.4 wt.-% for Br and Cl, respectively. Nearly half of mobilized Br became filtered out by PO-reactor (1.0 wt.-%) and filtration of liquids (2.8 wt.-%), leaving 4.4 wt.-% in filtered pyrolysis liquid product. In contrast, just 32 wt.-% of mobilized Cl was filtered out this way leaving 6.4 wt.-% in the filtered liquids.

As mentioned above, with some exceptions, majority of metals were allocated to pyrolysis solid products. In order to investigate accumulation and depletion of metals and halogens at different temperature levels, solid products from pyrolysis tests at 450, 550, and 650 °C (residence time 30 min) were selected and fine materials analyzed using EDXRF after pre-treatment³³. Figure 63 shows values for some selected metals as well as Br and Cl. With the exception of Ca, Cd, Cr, Sb, and halogens, all metals were enriched in the solid products due to increased temperatures from 450 to 550 and 650 °C. It was obvious that enrichment already took place due to a temperature

³³ Previous to analysis using EDXRF, solid products were grinded (300 rpm, 5 min) and sieved. For analyses particles with sizes <250 µm were conducted.

increase to 550 °C and was continued for most metals due to a further increase of temperature. The strongest depletion was obvious for Cd which is in good correlation with above mentioned results regarding overall allocation to different pyrolysis products.

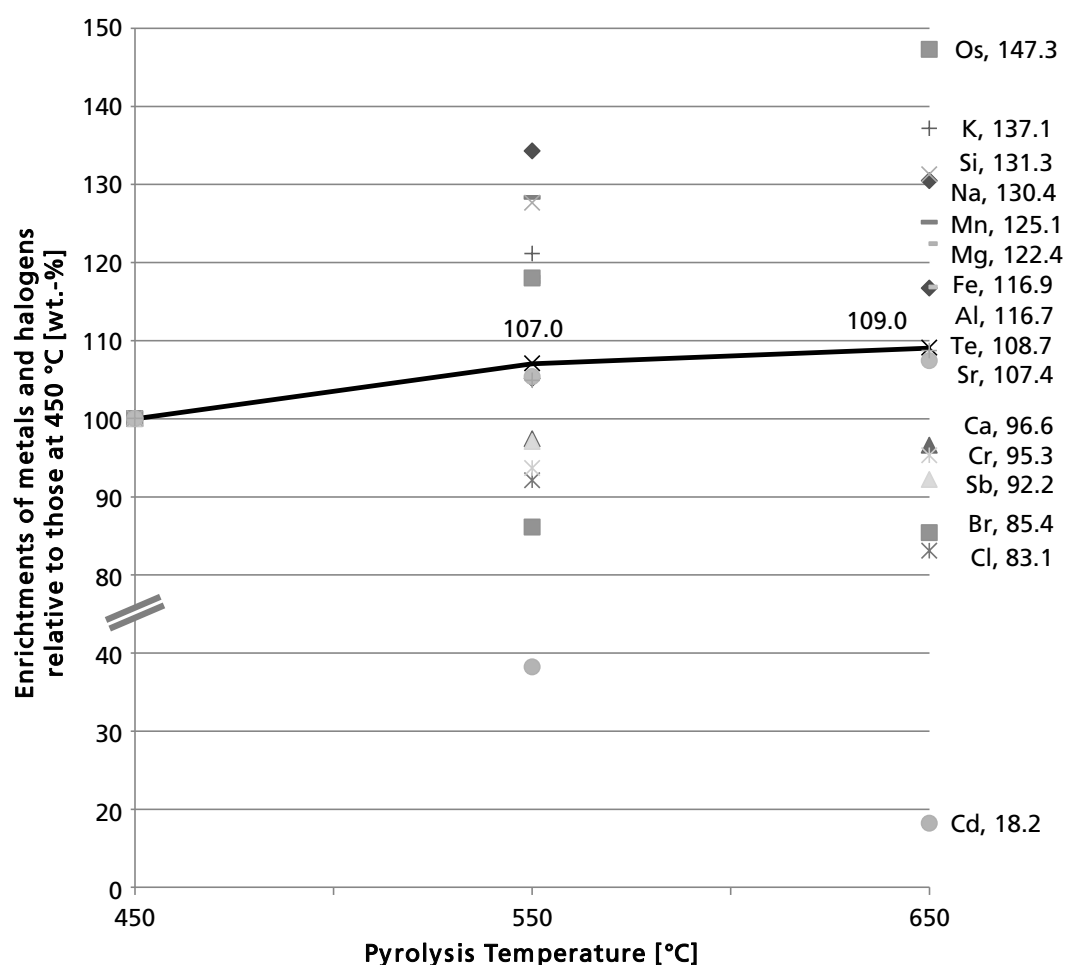


Figure 63: Enrichments of halogens and selected metals in pyrolysis solid products relative to those at 450 °C (residence time 30 min); black line = enrichment due to decreased solid products yields (in %). Analyses were conducted using EDXRF with C, H, N, and S given.

Further analyses were conducted in order to investigate if a fractionation of this heterogeneous solid product could bring up advantages concerning a (selective) recovery of metals. Therefore, the pyrolysis solid product from the above mentioned test with PO-reactor was grinded using a planetary ball mill for 5 min at 300 rpm. The grinded product was afterwards sieved into seven fractions from 0 - 63 µm up to >2 mm and the content of metals in separated fractions was analyzed using EDXRF with C, H, and N given plus O as missing component. A full list of allocations of all metals and P is shown in Table 62 in the appendix.

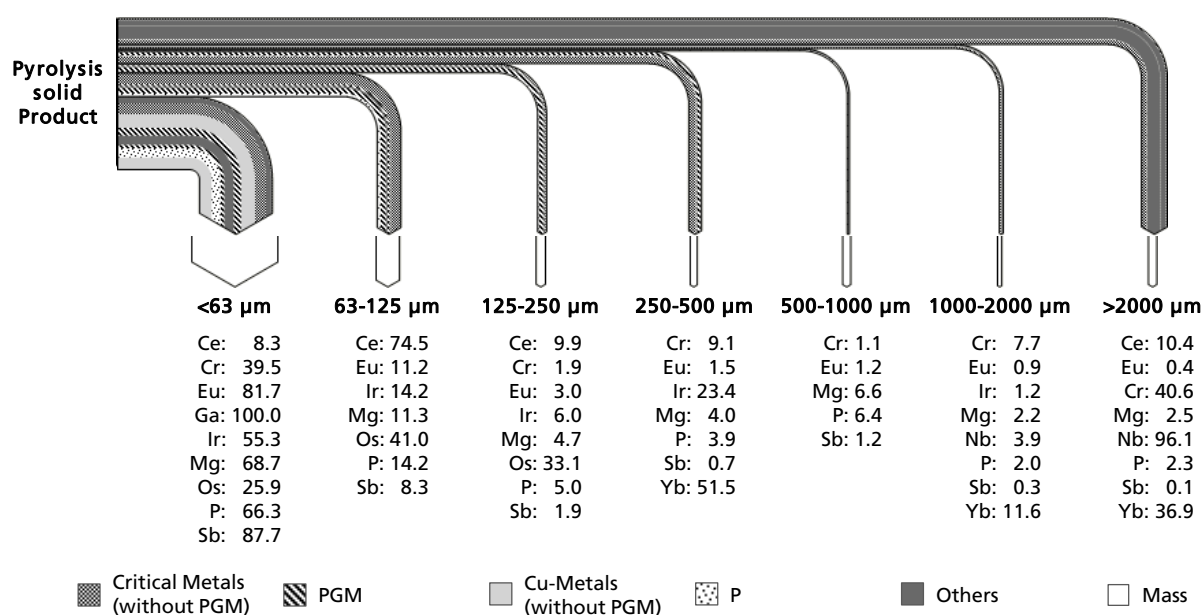


Figure 64: Allocations of Critical Metals from pyrolysis solid product to sieve fractions. Analyses were conducted using EDXRF with C, H, N given and O as missing component.

Figure 64 shows allocations of critical metals from pyrolysis solid product to the different sieve fractions. Additionally, blank flows to the different fractions represent the mass shares of it³⁴. First of all, it is obvious that the general allocations of all metals followed the mass shares strongly; however, mainly for fractions 250 - 500 μm and >2 000 μm a greater allocation and for fraction <63 μm a weaker allocation was obvious compared to mass shares. In particles <63 μm all detected Ga and highest allocations of Eu (81.7 wt.-%), Ir (55.3 wt.-%), Mg (68.7 wt.-%), P (66.3 wt.-%), and Sb (87.7 wt.-%) were found. In the next bigger sized fraction with particles up to 125 μm , those of Ce (74.5 wt.-%) and Os (41.0 wt.-%) were found. Elements which were detected in all sieve fractions are Eu, Mg, P, and Sb, while allocations of other metals were limited to some fractions: Nb was found in fractions >1 000 μm (96.1 wt.-% >2 000 μm), Yb just in fractions >250 μm , and Os in fractions <250 μm . With regard to a formation of concentrates of metal groups, PGM were found mainly in particles <500 μm while REE were detected in all different sieve fractions.

³⁴ Mass shared of the sieve fractions: <63 μm : 58.8 wt.-%; 63 - 125 μm : 16.1 wt.-%; 125 - 250 μm : 6.3 wt.-%; 250 - 500 μm : 4.8 wt.-%; 500 - 1000 μm : 5.5 wt.-%; 1000 - 2000 μm : 2.9 wt.-%; >2000 μm : 5.7 wt.-%.

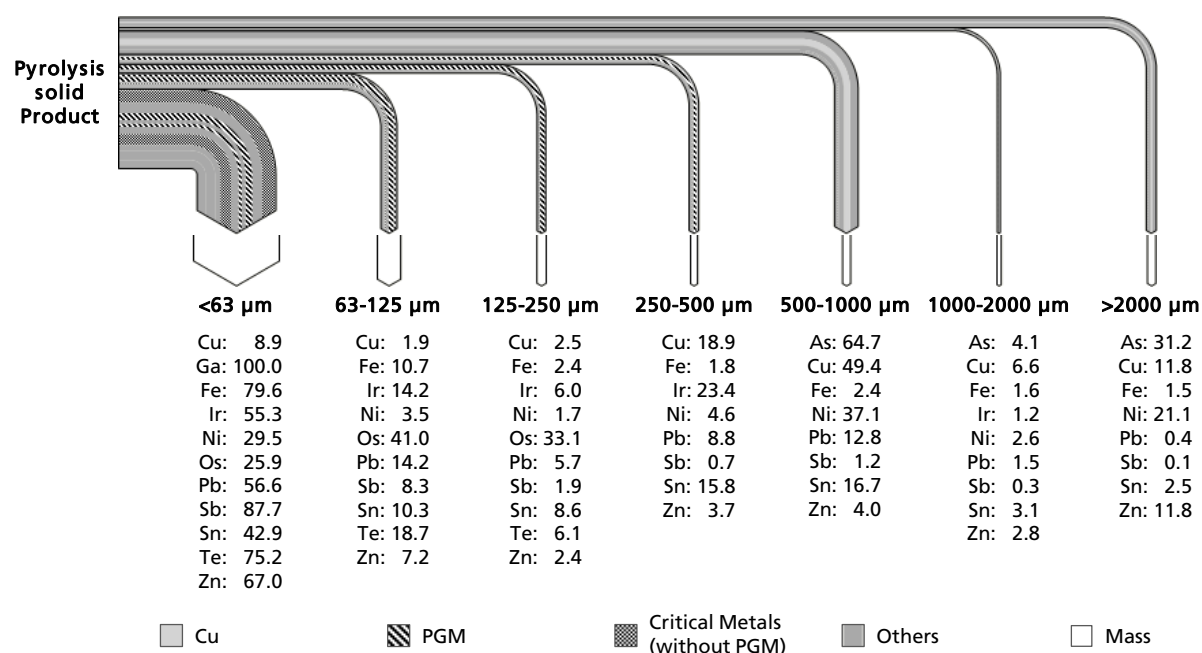


Figure 65: Allocations of metals, which are applicable for a recycling in an integrated copper smelter, from pyrolysis solid product to sieve fractions. Analyses were conducted using EDXRF with C, H, N given and O as missing component.

In addition to allocations of critical metals, calculations for those metals were conducted, which are applicable in an integrated copper smelter (Figure 65). In this case, an above-average allocation of metals to different sieve fractions was obvious for particles with a size of between 500 and 1000 μm . Since critical metals and PGM were already described above, just highlights of non-mentioned elements should be given: similar to critical metals, majorities of a number of metals applicable in a copper smelter were found in fraction <63 μm (Ga, Fe, Ir, Pb, Sb, Sn, Te, Zn). Ubiquity distribution was found for Cu, Fe, Ni, Pb, Sb, Sn, and Zn. In contrast, As was detected just in fractions with particle sizes >500 μm . Concerning the main metal Cu, 86.7 wt.-% were allocated to fractions with particle sizes >250 μm . On this account, separation of corresponding fractions seems to be advantageous; however, due to a complex pricing of revenues from copper smelters e.g. due to discounts for so called penalty elements such as As [Agorhom et al. 2015; Lane et al. 2016], subdivision of pyrolysis solid products could be done at 500 μm , too.

As extensively shown in chapter 4.3.3, a number of metals contained in the feedstock, react easily with halogens mainly at higher temperatures. In addition, these reactions seem to be responsible for a number of volatilizations of metals, too, depending on melting/boiling points (M_p/B_p) of corresponding halides. In order to proof this presumption, relationships between melting/boiling points of halides and its volatilization was investigated based on elemental analyses using ICP-MS/OES and regressions. Additionally, for the purpose of comparison, logarithmic regression analyses for corresponding metals and oxides were conducted, too. Table 37 shows the results of all

regression analyses and Figure 66 two selected examples. A comprehensive list with forms of halides and oxides as well as corresponding melting and boiling points is given in the appendix (Table 65).

Table 37: Terms of logarithmic regression lines for filtration residues, and filtered liquid product with halides, metals, and oxides (determination of metal concentrations were conducted by ICP-MS/OES).

		Filtration residue	Filtered liquid product
Me_xCl_y	M_P	$y = -146.9 \ln(x) - 44.612$ $R^2 = 48.64 \%$	$y = -90.66 \ln(x) - 223.1$ $R^2 = 95.58 \%$
	B_P	$y = -204.7 \ln(x) + 50.086$ $R^2 = 47.07 \%$	$y = -157 \ln(x) - 232.1$ $R^2 = 94.98 \%$
Me_xBr_y	M_P	$y = -147.2 \ln(x) - 80.289$ $R^2 = 58.22 \%$	$y = -66.08 \ln(x) - 99.83$ $R^2 = 77.66 \%$
	B_P	$y = -259.1 \ln(x) - 66.124$ $R^2 = 47.53 \%$	$y = -129.5 \ln(x) - 99.004$ $R^2 = 96.15 \%$
Me	M_P	$y = -131.9 \ln(x) + 196.41$ $R^2 = 20.76 \%$	$y = 82.81 \ln(x) + 865.4$ $R^2 = 64.94 \%$
	B_P	$y = -218.9 \ln(x) + 1060.3$ $R^2 = 24.27 \%$	$y = -206 \ln(x) + 516.28$ $R^2 = 30.17 \%$
Me_xO_y	M_P	$y = -198.5 \ln(x) + 733.35$ $R^2 = 30.62 \%$	$y = -187.4 \ln(x) + 181.07$ $R^2 = 34.36 \%$
	B_P	$y = -545.1 \ln(x) - 11.397$ $R^2 = 52.36 \%$	$y = -176.6 \ln(x) + 457.94$ $R^2 = 56.40 \%$

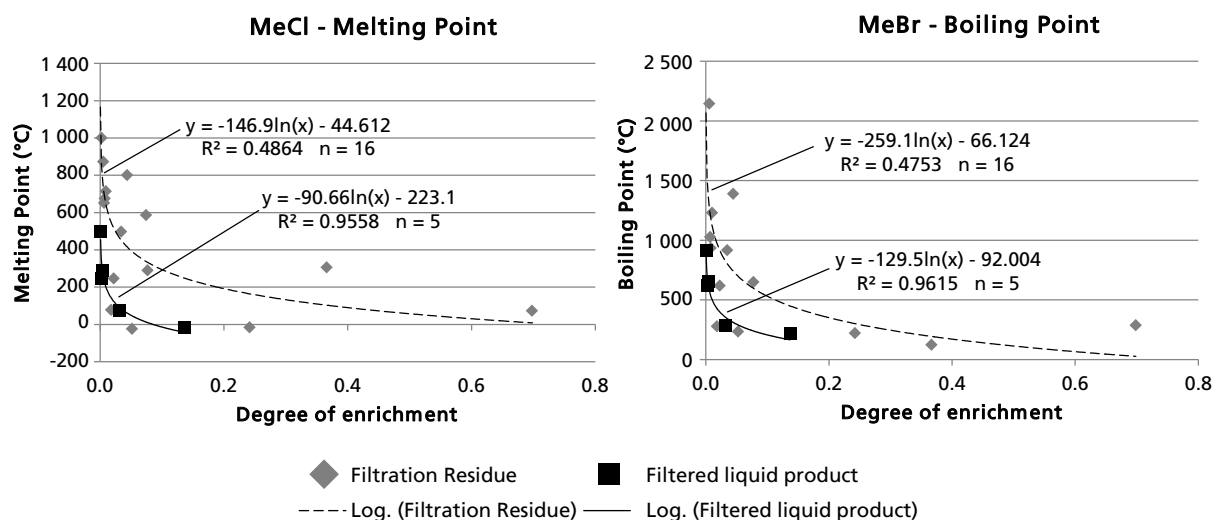


Figure 66: Degree of enrichment vs. **M_P** of metal chlorides (left) and **B_P** of metal bromides (right).

Calculated regressions could not show distinctively that mobilization of metals happened just due to halogenation of it. However, they could show that a strong correlation between those metals, which were enriched in the vapor (mainly in the filtered liquids) were given in form of halides. Coefficients of determinations R^2 are considerably higher in the case of halides compared to those of metals or oxides. In the case of the regression of metals and boiling points in filtered liquids, the term is even positive, which shows a contrary situation than assumed. However, it should be noted that just a small number of metals was found in pyrolysis liquids and that the concentrations of halogens were comparatively low in the feedstock.

Quality of pyrolysis liquid products

GC-MS analyses were conducted for pyrolysis liquid products from different temperature levels in order to investigate amounts of present compounds qualitatively and quantitatively (Table 38).

Table 38: Relative abundances and origins of compounds detected in pyrolysis liquid products from tests at 450, 550, and 650 °C (residence time 30 min) by GC-MS.

Compounds	450 °C 30 min	550 °C 30 min	650 °C 30 min	Origin
	Relative Abundance (wt.-%)			
Styrene	27.09	31.78	29.07	PS, ABS, SAN, SBS, SBR
Isopropenylbenzene	6.50	n.c. ³	4.79	PS, ABS, SAN, SBS
1,2-dimethylbenzene	5.66	6.68	1.13	PVC, PVA
Alkene	5.23	2.66	3.42	
1,3-diphenylpropane	4.54	1.64	1.52	PS, SBS
Phenol	3.79	n.c. ³	4.79	PF Resin
Benzenebutanenitrile	3.24	2.01	0.51	ABS
Ethylbenzene	2.61	4.73	8.84	All
Isopropyl Phenol	1.72	1.31	0.34	
2,4,6-triphenyl-1-hexene ²	1.41	---	0.53	PS
Ethyl dimethoxy benzene	1.40	1.96	1.64	
Dihydronaphthalene	1.31	0.34	0.14	PVC, PVA
Methylstilbene	1.25	0.58	0.19	
2,4-diphenyl-1-butene ¹	1.12	0.28	0.78	PS, SBS
2-phenylnaphthalene	1.04	1.76	0.90	
Benzonitrile	1.02	1.50	1.45	ABS, SAN
Trimethyl benzene	0.96	0.99	0.34	
1-phenyl-1,2,3,4-tetrahydro-naphthalene	0.87	0.27	0.22	
2,4-dimethylphenol	0.77	0.96	0.52	PF Resin
1,4-diphenylbenzene	0.76	0.27	0.17	
2-benzylinnaphthalene	0.70	0.33	0.60	
1-phenylnaphthalene	0.67	0.47	0.39	
1,1-diphenyl-2-methylpropane	0.51	0.20	---	
Naphthalene	0.50	0.77	2.96	PVC, PVA, PE
2-methylstyrene	0.49	0.54	0.33	
Biphenyl	0.42	0.62	1.00	PVC

¹ Styrene dimer

² Styrene trimer

³ Co-elution of phenol + isopropenylbenzene

ABS: Acrylonitrile butadiene styrene, PE: Polyethylene, PF Resin: Phenol-Formaldehyde resin, PS: Polystyrene, PVA: Polyvinyl acetate, PVC: Polyvinyl chloride, SAN: Styrene acrylonitrile, SBR: Styrene-Butadiene Rubber, SBS: Styrene-Butadiene-Styrene block copolymer.

The most abundant compound was styrene accounting for between 27.09 (450 °C) and 31.78 wt.-% (550 °C) (relative abundances). Further compounds with high yields were isopropenylbenzene, 1,2-dimethylbenzene, 1,3-diphenylpropane, phenols, benzene

butanenitrile, and ethylbenzene. Origin of most compounds could be styrene containing compounds such as PS, ABS, SAN, SBS, and SBR as well as PVC, PVA, or phenol-formaldehyde resins [Fabbri 2001; Hall, Williams 2006; Koch 2007].

Due to increased temperature levels, an extraordinary strong increase was obvious for naphthalene from 550 to 650 °C, strong increases for ethylbenzene and biphenyl between 450 and 650 °C, and a slight increase for benzonitrile between 450 and 550 °C. 1,2-dimethylbenzene and trimethyl benzene decreased strongly with an increase of temperature just between 550 and 650 °C while compounds such as isopropyl phenol, methylstilbene or benzenebutanenitrile decreased constantly with an increase of temperature.

In addition, the influence due to the addition of the PO-reactor and halogen filter was tested. Therefore, corresponding liquid products from pyrolysis tests with a temperature of 650 °C and a residence time of 30 min were selected, when PO-reactor was filled with PP, PP+La1.5, and PP+La4.5. Table 39 shows semi-quantitative changes on pyrolysis liquid products due to these changes. Additionally, it should be noted that quantification of some compounds such as methylstilbene or the styrene dimer 2,4-diphenyl-1-butene was not feasible because signals of alkenes were higher due to fragmentation and influence of PP, which were present in the PO-reactor. In these cases, alkenes covered the (dimer) signals in GC-MS analyses.

Table 39: Semi-quantitative changes of compounds in pyrolysis liquid products due to addition of PP and La.

Compound	+ PP	+ La (in PP)	Compound	+ PP	+ La (in PP)
1,2-dimethylbenzene	++	0	Benzonitrile	0	0
Trimethyl Benzene	+	0	Isopropyl phenol	–	0
Styrene	+	–	2,4,6-triphenyl-hexene	– –	0
Isopropenylbenzene	+	–	1,3-diphenylpropane	– –	0
Benzenebutanenitrile	0	0	Ethylbenzene	– –	0

++ strong increase; + slight increase; 0 no significant change; – slight decrease; – – strong decrease

A comprehensive list of all results from GC-MS including also chromatograms is shown in the appendix (Table 63 ff., Figure 94 ff.).

Besides GC-MS analyses for identification and quantification of compounds, quality aspects of pyrolysis liquid products regarding an energetic utilization in a combined heat and power plant (CHP) were analyzed. As mentioned above, some basic parameters such as *TAN* or proportion of C and H contents changed significantly with changed pyrolysis temperatures. From these results, best properties of pyrolysis liquids were found for liquids from pyrolysis with a temperature of 650 °C and a residence time of 30 min. Under these conditions, *HHV* showed the highest values, while those of *TAN* and H₂O-content were at the lowest level.

In addition to tests of pyrolysis liquid products from conventional pyrolysis, analyses of those from tests at 650 °C over 30 min with PO-reactor and halogen-filter³⁵ were conducted. Results presented in Table 40 revealed that the addition of PO-reactor and halogen-filter shows slight changes in density and kinematic viscosity of pyrolysis liquids while the content of ash (at 775 °C) decreased by 22 wt.-%. The greatest change of any parameter tested was present as cetane index, which increased from 10.8 from (basic) pyrolysis tests to 30.1 due to addition of PO-reactor and halogen-filter. From elemental analyses, it was obvious that the halogen contents as Br and Cl decreased significantly, due to the added PP+La and halogen-filter (Figure 67): The addition of PP+La decreased the contents of Br by 26.1 wt.-% and of Cl by 35.4 wt.-%. Due to the addition the halogen-filter, a further strong decrease of Cl concentration by 63.1 wt.-% compared to initial liquid product was obvious, while those values of Br decreased by 58.1 wt.-%. The content of S increased, due to present S from used PP.

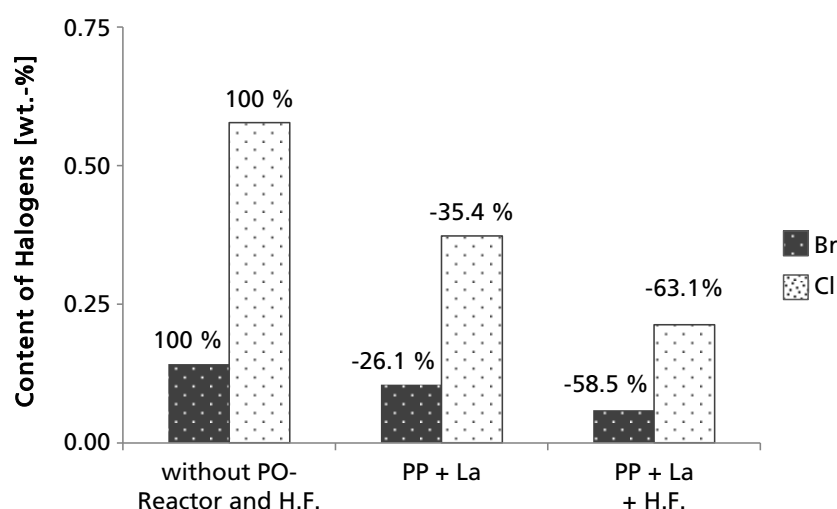


Figure 67: Content of halogens in pyrolysis liquid products from pyrolysis tests (650 °C, 30 min) with and without PP+La, and halogen-filter (H.F.) (in wt.-%). Analyses were conducted using EDXRF with C, H, N given and O as missing component.

³⁵ Polyolefin reactor was heated at 340 °C and filled with PP and La (100:0.468 by weight), halogen-filter was heated at 450 °C.

Table 40: Parameters of pyrolysis liquid products regarding energetic utilization.

Parameter	Test standard	Unit	SR1	SR1 PP + La + H.F.
Density (15 °C)	DIN EN ISO 12185	$\text{g}\cdot\text{cm}^{-3}$	0.9478	0.9268
Kinematic Viscosity (40 °C)	DIN EN ISO 3104 ASTM D 7042	$\text{mm}^2\cdot\text{s}^{-1}$	1.159	1.202
Ash content (775 °C)	DIN EN ISO 6245	wt.-%	0.121	0.094
Corrosiveness to Cu	DIN EN ISO 2160	-	1b	1
Cetane index	DIN EN ISO 4264	-	10.8	30.1
Br content*	---	$\text{mg}\cdot\text{kg}^{-1}$	1 420	589
Cl content*	---	$\text{mg}\cdot\text{kg}^{-1}$	5 770	2 130
S content*	---	$\text{mg}\cdot\text{kg}^{-1}$	397	586

* determination using EDXRF with C, H, N given and O as missing component.

Distillation ranges of both liquids were tested and compared to conventional fuels [Luo et al. 2016], which results are shown in Figure 68: Distillation ranges of pyrolysis liquid products from test without PO-reactor are very similar to those of gasoline. Due to the addition of PO-reactor and halogen-filter, distillation volume increased significantly at distillation temperatures above approximately 150 °C. This effect was also reflected by the increased cetane index, which indicates higher yields of high-boiling compounds.

With regard to an energetic utilization of formed pyrolysis liquids in a CHP, blending tests with conventional fuels and hydrocarbons were conducted in mixtures of 50:50 by weight. With the exception of blending with ethanol, heavy precipitation of particles were obvious for diesel fuel and n-hexane while just a slight and very slight precipitation was given for gasoline (E95) and fatty acid methyl ester (FAME). All influences were obvious immediately and did not change after 24 hours or 14 days. In addition, no two- or multi-phase system became obvious.

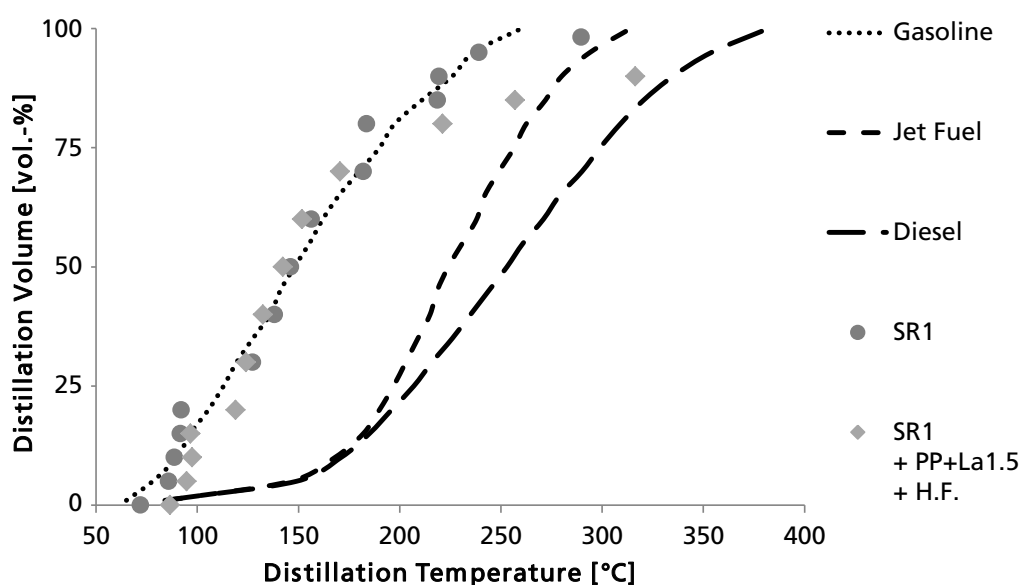


Figure 68: Distillation ranges of pyrolysis liquid products from tests with SR1 and with SR1 with polyolefin-reactor and halogen-filter (SR1 + PP+1.5 + H.F.) in comparison to those of conventional fuels (modified according to [Luo et al. 2016]).

6.2.2 Pyrolysis tests with selected fractions containing scarce and critical metals

A number of different pyrolysis tests were conducted with Ta capacitors and LCD in order to test pyrolysis concerning recovery efficiencies for valuable metals such as Ta, Ga, or In as well as efficiencies concerning depletion of toxic metals such as As. Therefore, different pyrolysis experiments at different temperatures as well as under changed fundamental circumstances like co-pyrolysis were conducted.

Tantalum capacitors

Pyrolysis experiments with regard to an extraction of Ta were tested using “SMD Yellow” and “SMD Black” capacitors. In main tests, different pyrolysis temperatures were tested in order to optimize concentration of Ta in a pyrolysis solid product. For these tests, Ta capacitors “SMD Yellow” were used. Additionally, “SMD Black” capacitors were tested at best conditions, previously determined with Ta capacitors “SMD Yellow”, in order to confirm pyrolysis conditions for both most commonly used kinds of Ta capacitors. Residence time of all tests was set to 30 min.

Pyrolysis tests with Ta capacitors “SMD Yellow” were conducted at temperatures between 450 and 650 °C in steps of 50 °C. Following [Fujita et al. 2014], decomposition of Ta pellets and interrelated allocation of Ta to fine particle fraction <500 µm usually takes place just at temperatures above 600 °C. However, from conducted tests a first significant allocation of Ta to this fraction was obvious at a temperature of 500 °C. In order to accumulate and allocate most Ta as possible to an announced fraction, a pyrolysis temperature of 550 °C showed best results with an allocation of 86.5 wt.-% to sieve fraction <500 µm (Figure 69).

In addition, allocation of Ag, Mn, and Si was investigated. Similar to Ta, highest allocation of Ag to sieve fraction <500 µm was found at 550 °C; however, a much bigger part (65.8 wt.-%) is allocated to fraction >500 µm. Regarding Mn and Si, highest allocation to the smaller sized fraction was found at a temperature of 600 °C as 59.6 wt.-% and 14.4 wt.-% for Mn and Si, respectively. Additionally, results for Si revealed that pyrolysis under all tested conditions had low ability for an allocation of Si to the aim fraction. This shows a further positive effect in order to separate Ta from other materials used in capacitors. Against same background, pyrolysis at 650 °C would enable a considerably very low allocation of Mn to fraction <500 µm.

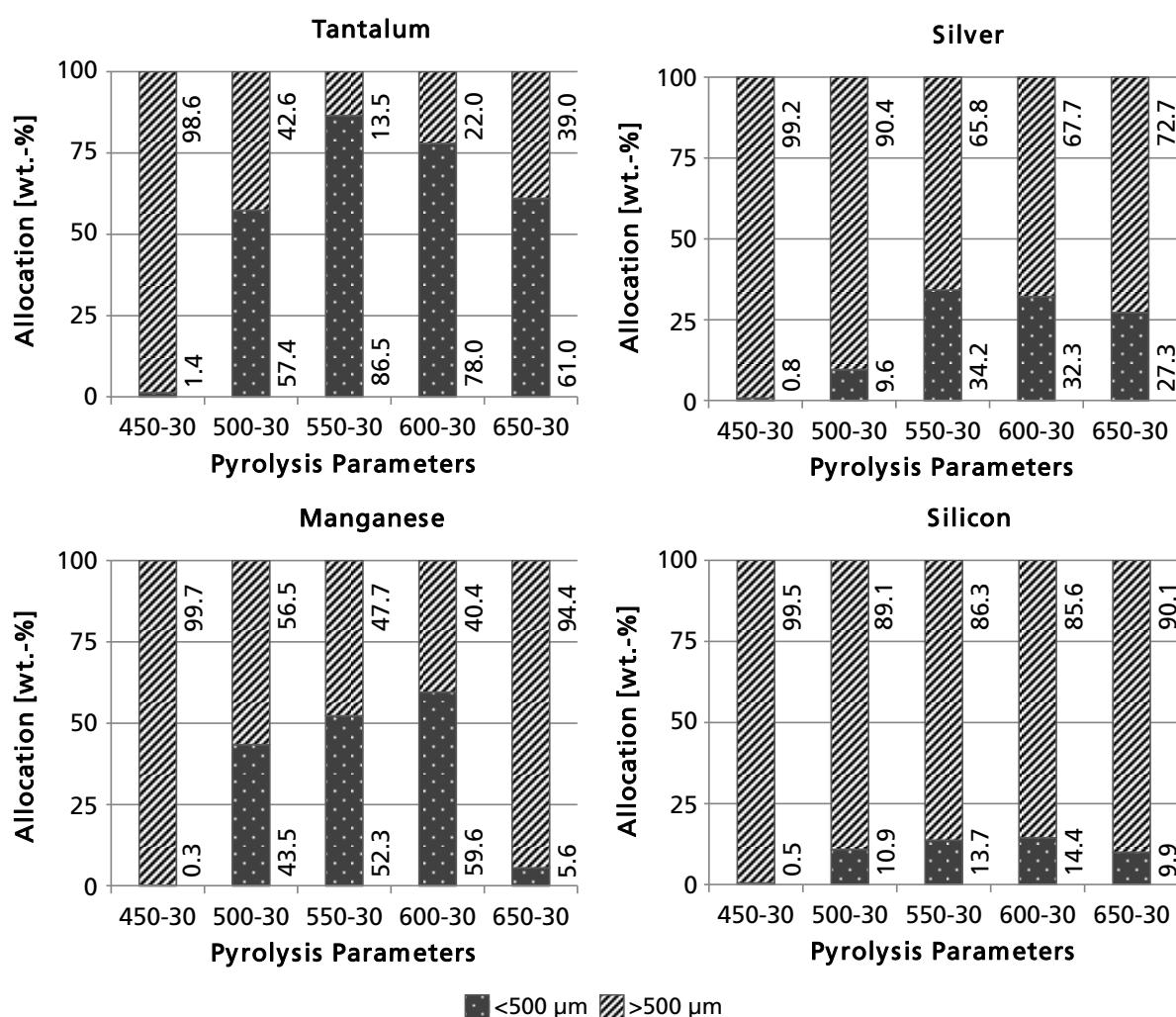


Figure 69: Allocation of Ta, Ag, Mn, and Si to sieve fraction >500 and <500 μm from different pyrolysis tests with Ta capacitors “SMD Yellow” as feedstock. Analyses were conducted using EDXRF with C, H, N, S given and O as missing component.

Figure 70 shows main components of feedstock as well as sieve fractions <500 and >500 μm from pyrolysis tests at 550 °C. Compared to the feedstock, concentrations of Ag, Mn, and Ta in the fraction <500 μm increased to 1.75, 13.64 and 55.69 wt.-%, while that of Si decreased from 20.91 to 18.87 wt.-%. The corresponding accumulation factor for Ta amounted to 4.84 compared to the feedstock. Regarding further elements with low amounts, in general, concentrations of P and Cl increased while all other shown metals and halogens (Sb, Br, Ti, and Sn) decreased.

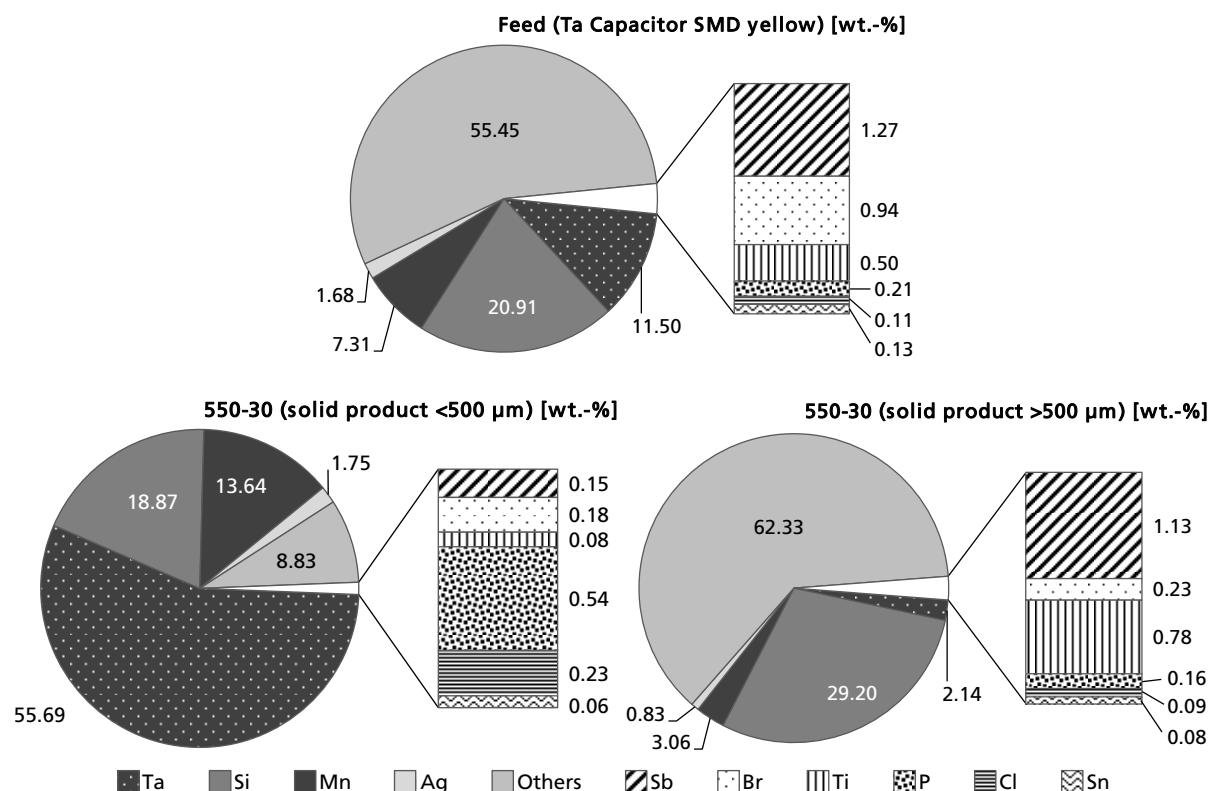


Figure 70: Main components of Ta capacitors "SMD yellow", solid products <500, and >500 µm from pyrolysis test at 550 °C, 30 min (in wt.-%). Analyses were conducted using EDXRF with C, H, N, S given and O as missing component.

Pyrolysis tests with Ta capacitors "SMD Black" as feedstock at a temperature of 550 °C revealed considerably lower allocation of Ta to sieve fraction <500 µm (59.8 wt.-%). As shown during characterization of these capacitors (see chapter 6.1.2), this difference could be based due to another kind of resin, used for the production of Ta capacitors "SMD Black", which did not decomposed as strong as that used for "SMD yellow".

Liquid crystal displays

Three different types of pyrolysis tests were conducted with LCD-Dark as feedstock in order to evaluate recovery efficiencies and mobilizations of valuable metals Ga, In, and Sn as well as toxic metal As. As different pyrolysis types, (1) conventional pyrolysis, similar to those reported for shredder residues or Ta capacitors, (2) co-pyrolysis with PVC as well as (3) pyrolysis of PVC with LCD in vapor-phase mode were conducted. Figure 71 shows the yield of products gained from the different pyrolysis tests. As expected, the yield of solid products from conventional pyrolysis was significantly higher compared to co-pyrolysis and vapor-phase mode due to higher inert material content in LCD compared to blends of LCD and PVC. Analogous, the yield of gases (by difference) are significantly lower in the case of conventional pyrolysis. Yields of waxes are similar in the case of conventional and vapor-phase mode pyrolysis; however, those from co-pyrolysis showed a distinctive yield, which accounted for approximately a quarter of all products,

while the yield of liquid products was just 0.50 wt.-%. Those yields of liquid products from other tests were considerably higher and accounted for 4.19 and 14.54 wt.-% for vapor-phase mode and conventional pyrolysis, respectively.

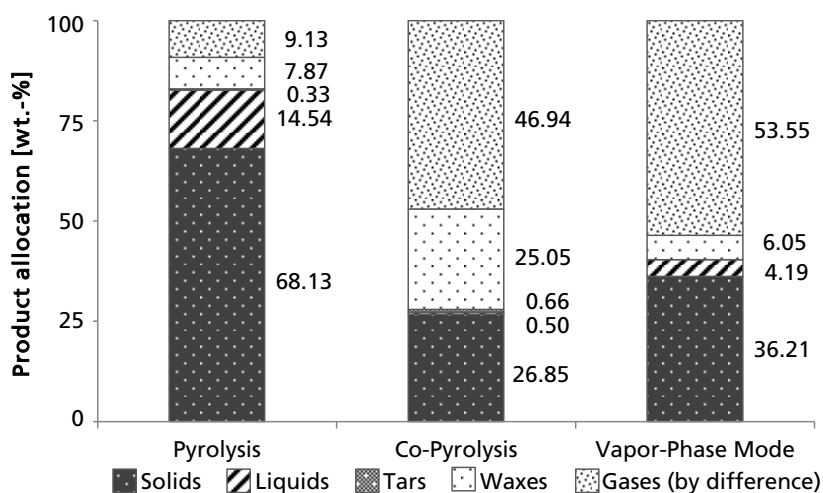


Figure 71: Product allocation from pyrolysis tests with LCD (in wt.-%). Analyses were conducted using EDXRF with C, H, O as missing components.

All products from pyrolysis tests were analyzed concerning its concentrations of As, Ga, In, and Sn, from which corresponding allocations were calculated (Figure 72). During pyrolysis, no significant allocation of any metal to pyrolysis liquid products or NaOH was found. Just a very small allocation of 0.3 wt.-% to pyrolysis liquids was calculated for As.

In contrast, during co-pyrolysis a strong mobilization of As and Sn could be observed: As was found just in pyrolysis liquid products while Sn was found in NaOH in solution (38.8 wt.-%), in precipitated NaOH (23.2 wt.-%), and additionally very slightly in pyrolysis liquid products (0.004 wt.-%). The non-mobilized part accounted for 38.2 wt.-%. Ga was mainly found in pyrolysis solid (97.5 wt.-%) and just very slightly in pyrolysis liquid products (2.5 wt.-%). In could not be detected in any product; however, due to low concentrations of In in LCD and its blending with PVC, concentration of In in pyrolysis solid product could be below detection limit. Therefore, In could be still part of the non-mobilized fraction.

From vapor-phase mode, no mobilization could be found for As, which is in strong contrast to co-pyrolysis. Regarding In, 64.0 wt.-% allocated to pyrolysis liquid product while the remaining part stood stable in pyrolysis solid ones. A bit less than the half of Sn allocated to liquid products (14.8 wt.-%) and was detected in the dissolved part of NaOH (30.0 wt.-%). Ga was not detected in any product, which could be caused due to the very low concentration corresponding to the feedstock (c.f. chapter 6.1.2).

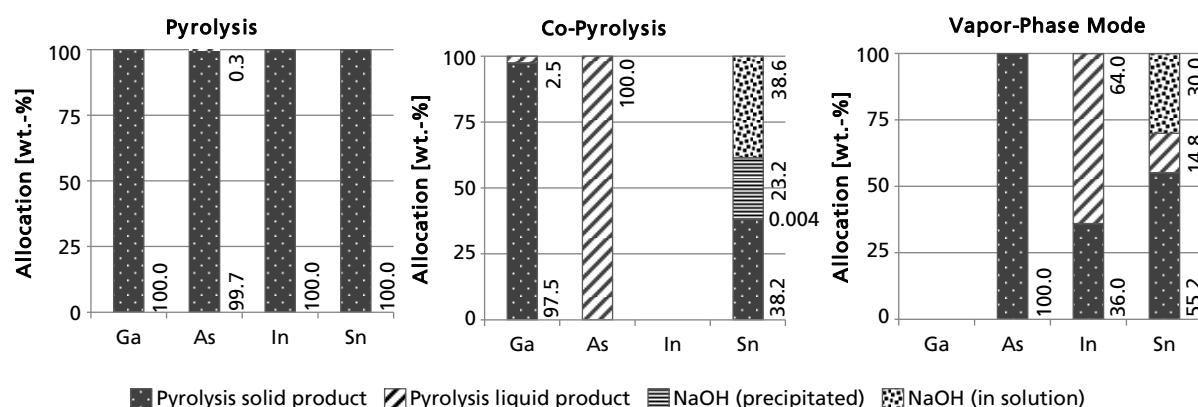


Figure 72: Allocation of Ga, As, In, and Sn to pyrolysis solid and liquid products as well as NaOH (precipitated and in solution) from different pyrolysis tests with LCD and PVC as feedstocks (in wt.-%). Analyses were conducted using EDXRF with C, H, O as missing components.

6.3 Sustainability assessment of a continuous process

6.3.1 Ecological assessment

Inventory analysis

For the ecological assessment, yields and properties of pyrolysis products offered from conducted pyrolysis tests (chapter 6.2.1) were used (Table 41). Yields and properties of pyrolysis products, which were taken into the ecological assessment, are shown in Table 41. With regard to metals recovered from pyrolysis char, total recycled amounts are listed in Table 42; metals, which are not listed, were not found in pyrolysis solid residues using ICP-MS/-OES (c.f. chapter 6.2.1). The amount of each metal listed was calculated by its amount in pyrolysis char and filtration residue (from liquid product) of 1 Mg shredder residue multiplied with its corresponding recycling process efficiency.

Table 41: Yields and Properties of pyrolysis products for the ecological assessment.

Parameter	Unit	Solids		Liquids*		Gases	
Yield	wt.-%	55.35		13.03		24.74	
Content of C; H	wt.-%	14.81	0.15	87.42	7.89	---	---
Content of N; S	wt.-%	0.46	0.33	2.37	0.10	---	---
Content of Br; Cl	wt.-%	0.46	0.81	0.06	0	---	---
LHV	MJ·kg ⁻¹	---		37.38		28.52	

* Liquids = Pyrolysis filtered liquid products.

As mentioned above, pyrolysis liquid and gaseous products are used energetically in a CHP to produce power and heat. The energy efficiency of the CHP was assumed as 36 % and 50 % for power and heat, respectively. Therefore, using pyrolysis liquid and gaseous products from treating 1 Mg shredder residue, 1 217 kWh of power and 1 690 kWh of heat were gained. Taking the own consumption of the whole system into account, 1 148 kWh of power and 833 kWh of heat can be exported.

Table 42: Amount of metals recycled from pyrolysis solid products and filtration residue in copper smelter processes.

Metal	kg Metal recycled per Mg Feedstock	Metal	kg Metal recycled per Mg Feedstock	Metal	kg Metal recycled per Mg Feedstock
Ag	0.0510	Ga	0.1597	Sb	0.9519
As	0.0081	In	0.0222	Se	0.0025
Bi	0.0300	Ni	1.0638	Sn	5.3753
Cu	38.5479	Pb	8.4433	Te	0.0010
Fe	44.0293	Pd	0.0095	Zn	6.3777

In the case of option one (incineration of shredder residues in a municipal waste incinerator (MWI), just Al, Cu, and Fe >2 mm were recovered (Table 43). Non-recovered metals as well as bottom ash account for 0.5453 Mg per Mg shredder residue, which are transported to a sanitary landfill. With a gross energy efficiency of 13.0 and 30.0 % for power and heat, respectively, 603 kWh power and 1 392 kWh heat were gained from incineration.

Table 43: Content of Al, Cu, and Fe in bottom ash >2 mm and those amounts as well as recovered amounts in bottom ash >2 mm.

	Content of metals in bottom ash >2 mm	Amount of metals in bottom ash >2 mm	Amount of metals recovered from bottom ash >2 mm
	wt.-%	kg per Mg Feedstock*	kg per Mg Feedstock **
Al	11.82	6.5	2.3
Cu	47.32	26.0	9.1
Fe	19.78	10.9	10.5

* $\frac{\text{kg metals in bottom ash} > 2 \text{ mm}}{1000 \text{ kg shredder residue}}$

** $\frac{\text{kg metals recovered from bottom ash} > 2 \text{ mm}}{1000 \text{ kg shredder residue}}$

Impact assessment

Impacts of a treatment in a MWI or using pyrolysis technology were calculated in nine categories, which results are shown in Figure 73. From all investigated categories two following main results were obvious:

- In all impact categories both options of treatment (MWI, pyrolysis) had exonerative effects concerning ecological aspects.
- These effects had lower values, indicating stronger exonerative effects, in the case of pyrolysis compared to a treatment in a MWI.

With regard to the last mentioned main result, strong differences between both treatment options were obvious. Factors, which indicate how many times effects are stronger in the case of pyrolysis compared to MWI, had values between 1.4 (ozone layer depletion potential (ODP)) and 55.5 (abiotic resource depletion potential (ADP)) for balances (c.f. also Figure 74).

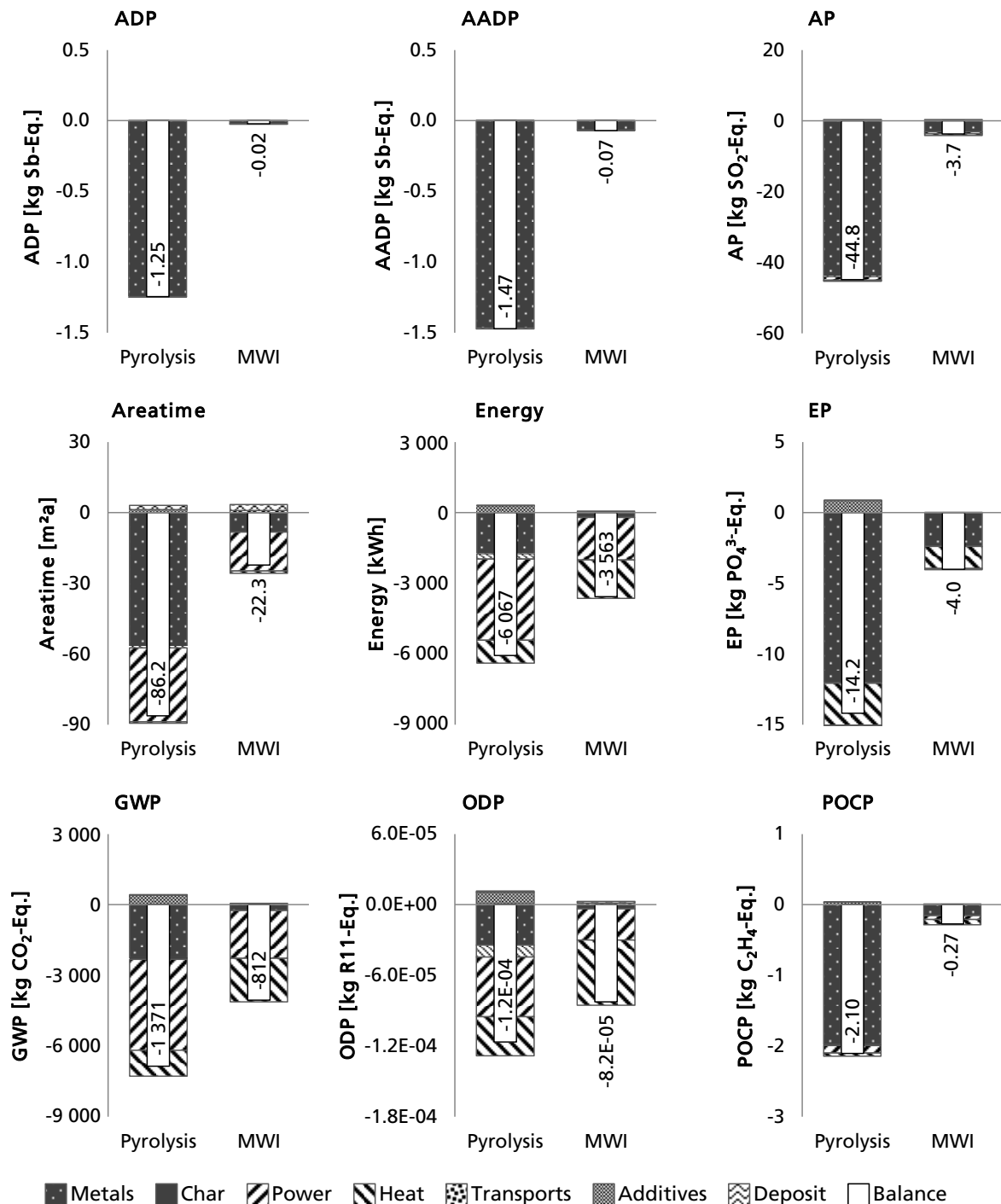


Figure 73: LCA-Results in impact categories ADP, AADP, AP, Areatime, Energy, EP, GWP, ODP, and POCP for a treatment of 1 Mg shredder residues.

A more detailed view on single calculations of the balances revealed influences of the different pyrolysis products such as metals, power, or heat or burdens such as transports, additives, or deposits. In categories ADP, anthropogenic stock extended abiotic depletion potential (AADP), acidification potential (AP), eutrophication potential (EP), photochemical ozone creation potential (POCP), as well as areatime, recovery of metals are key impacts. Regarding both resource depletion categories ADP and AADP, these results are generally based due to much stronger influences of metals in these categories compared to influences from energy. With regard to AP, EP, and POCP,

strong influences of metals could be explained due to avoided emissions of primary metal winning. As an example, acidic emissions, which are relevant for impact category AP, become emitted to the environment during refining of metals such as Cu, which are mainly extracted from ores with copper sulfides. Similar relationships could be found for AP and POCP, too. Other products with partly strong influences were given as power and heat, produced from pyrolysis liquid and gaseous products. Influences of these products are relevant not only – as expected – in categories energy and global warming potential (GWP), but also in ozone depletion potential (ODP) and areatime. All further educts and products, which are required for operation of pyrolysis or produced from it, played a minor role: burdens due to deposits from pyrolysis operations are significant just in the case of areatime, based on area used for underground deposition of waste NaX for a long period of time. Additionally, burdens from required additives for pyrolysis have minor effects in categories energy, EP, GWP, and ODP.

Sensitivity analysis

As mentioned above, besides the basic scenario a sensitivity analysis with five different further scenarios (I, II, IIIa, IIIb, IV) was conducted in order to evaluate effects of uncertainties in the assessment. Therefore, a dimensionless factor was calculated as

$$factor = \frac{Balance_{Pyrolysis}}{Balance_{MWI}}$$

Results of corresponding calculations are shown in Figure 74. With exception of GWP, ODP, and Energy in Scenario IIIa (Variation of MWI gross energy efficiency to 27.0 and 98.0 % instead of 13.0 and 30.0 % for power and heat, respectively), pyrolysis has still stronger exonerative effects concerning all ecological aspects. Three mentioned exceptions indicate that a comparison between pyrolysis with an MWI with best available techniques concerning energetic utilization shows higher exonerative effects for MWI instead of pyrolysis. This could be relevant for regions or countries where such categories are more relevant compared to all other investigated ones.

In addition, scenario I, for which the metal recovery in the status quo was enhanced, showed indirectly significant influences on the exonerative effects of metal recovery in a MWI. However, due to the small number of metals recovered in a MWI (Al, Cu, Fe), recovery of metals using pyrolysis had much greater exonerative effects. From other scenarios, no significant influences were obvious, which means that a recovery of Al and Fe from pyrolysis solid products (scenario I) would have no great influences similar to changed transport distances (scenario IV).

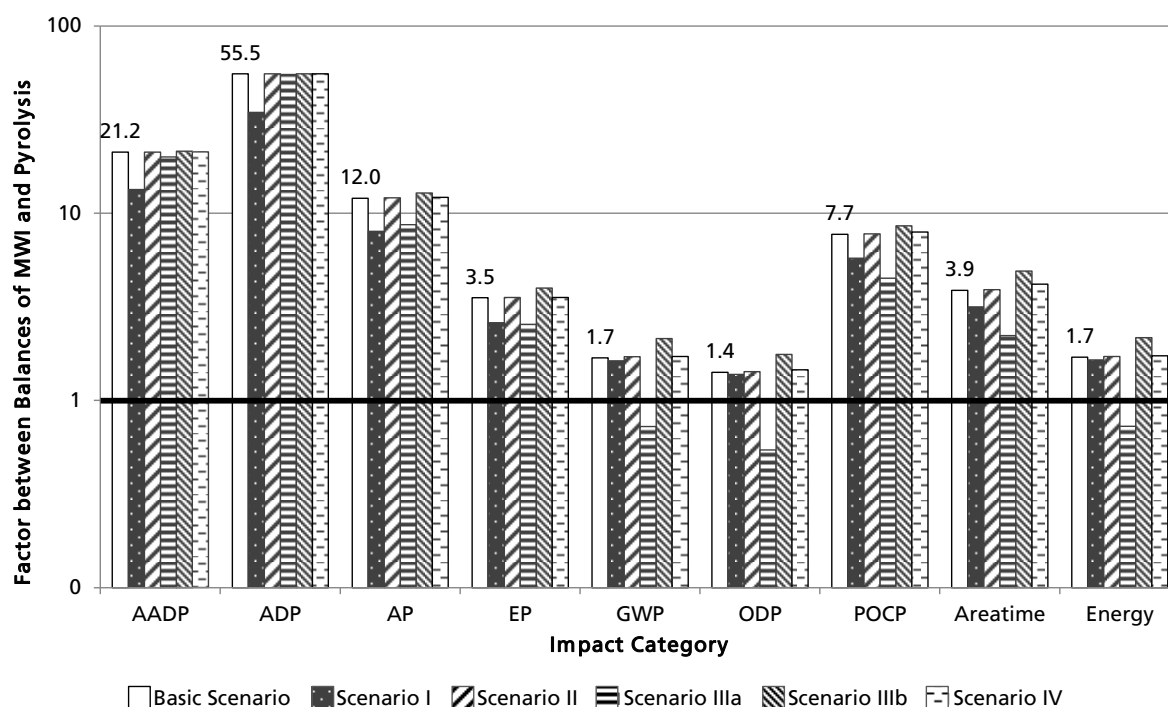


Figure 74: Results of sensitivity analysis from ecological assessment expressed as dimensionless factor between balances of pyrolysis and MWI.

6.3.2 Economical assessment

Within the economical assessment, three different scenarios for a continuous pilot plant with a mass flow capacity of $70 \text{ kg}\cdot\text{h}^{-1}$ were calculated. In the first scenario a combustion unit was added to the pyrolysis pilot plant for energetic utilization of liquid and gaseous products. The corresponding sums of capital expenditure and cash flow accounted for -357 989 € and -370 795 € in project year 0. Even during comparatively high depreciations in the first year, a positive net profit could be achieved during the whole project duration of 10 years (Figure 75).

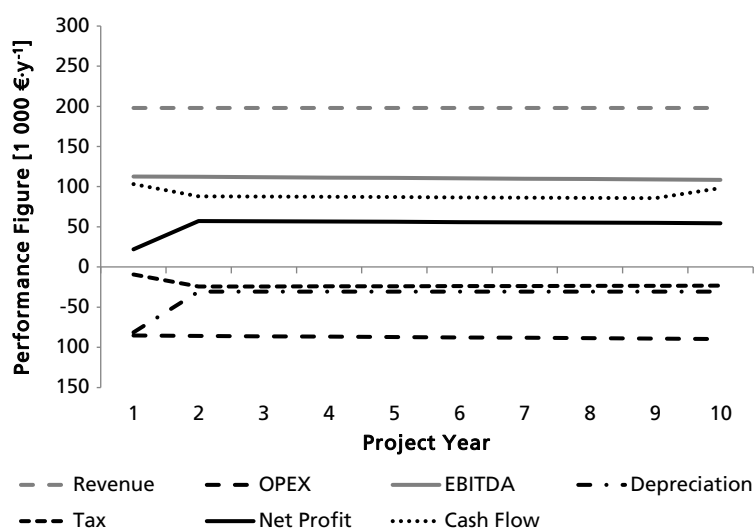


Figure 75: Performance figures for scenario I (in 1 000 €·y⁻¹).

Due to the added investments of a CHP in scenario II, capital expenditure and cash flow increased to -477 159 and 492 132 € at the beginning of the project. In contrast to very linear trends of performance figures in the first scenario, some changes take place within in the project duration during the second (and third) scenario: Due to above mentioned discontinuation of bonuses for electricity, which get sold to the grid, a decrease of revenues and correspondingly of cash flow, net profit, and taxes take place within the fifth project year. Nevertheless, the net profit is positive during the whole project duration (Figure 76).

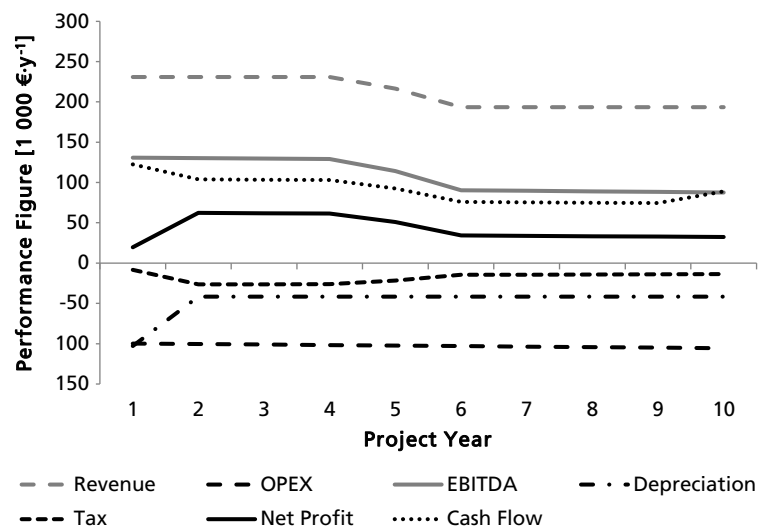


Figure 76: Performance figures for scenario II (in 1 000 €·y⁻¹).

In scenario III, not only a CHP, but also a PO-reactor and a halogen-filter become installed together with the pyrolysis plant. Therefore, a further increase of capital expenditure and cash flow to 618 535 and 638 131 € are present for the project year 0. Also in scenario III, similar changes than in scenario II are obvious, which are influenced by lower earnings from produced power. Due to the added PP in the PO-reactor, additional expenditures have to be spent; however, thusly higher amounts of power and heat could be generated.

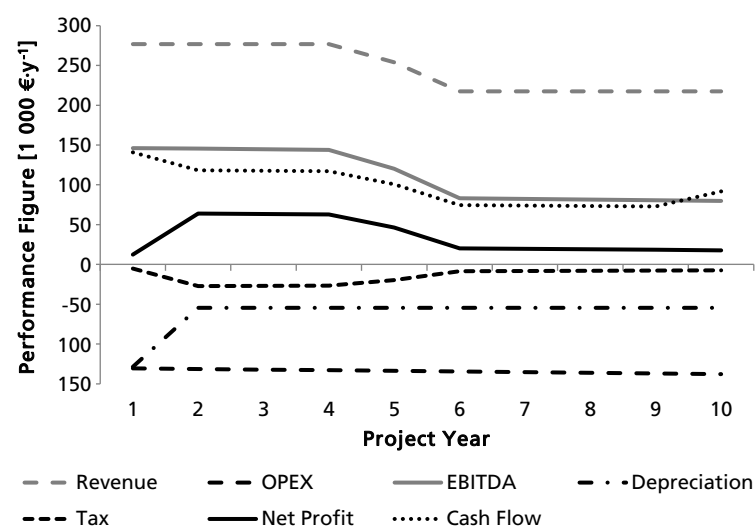


Figure 77: Performance figures for scenario III (in 1 000 €·y⁻¹).

In order to receive a more comprehensive view for all scenarios, cumulative cash flows (Figure 78) and net present values (Figure 79) for the whole project duration were calculated. In these cases also impacts of imputed earnings for the feedstocks of $98.50 \text{ €} \cdot \text{Mg}^{-1}$ are shown. Depending on the selected performance parameters, corresponding payback periods free of burdens accounting for between 4.05 and 4.64 years (scenario I), 4.66 and 5.61 years (scenario II) as well as 5.61 and 7.23 years in static and dynamic calculations, respectively. In the case that imputed earnings are taken into calculations, these values could be decreased to a minimum value of 2.73 years in the case of a static calculation of the payback period for scenario I (Table 44).

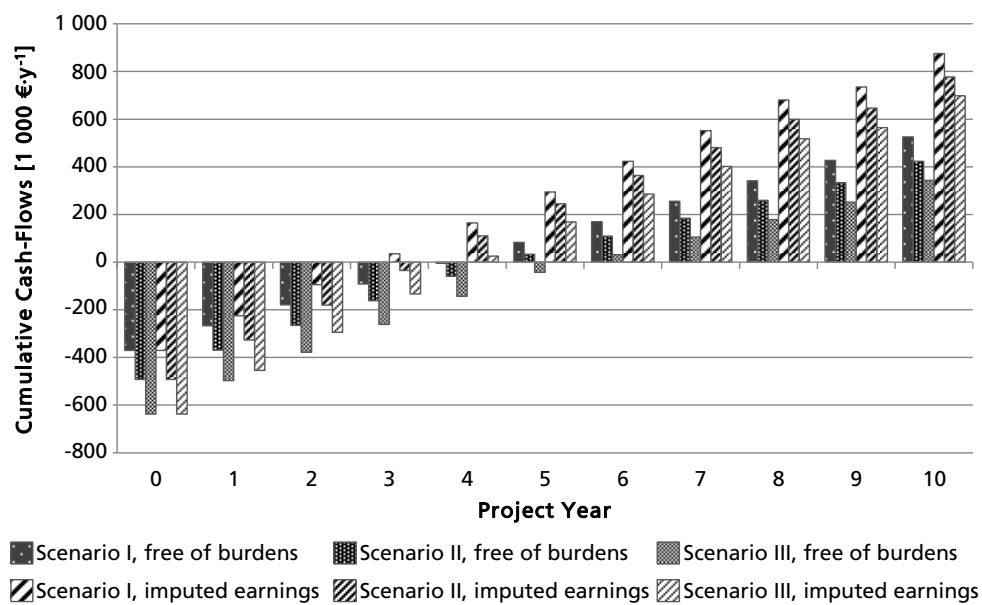


Figure 78: Cumulative cash-flows of all scenarios (in $1\,000 \text{ €} \cdot \text{y}^{-1}$).

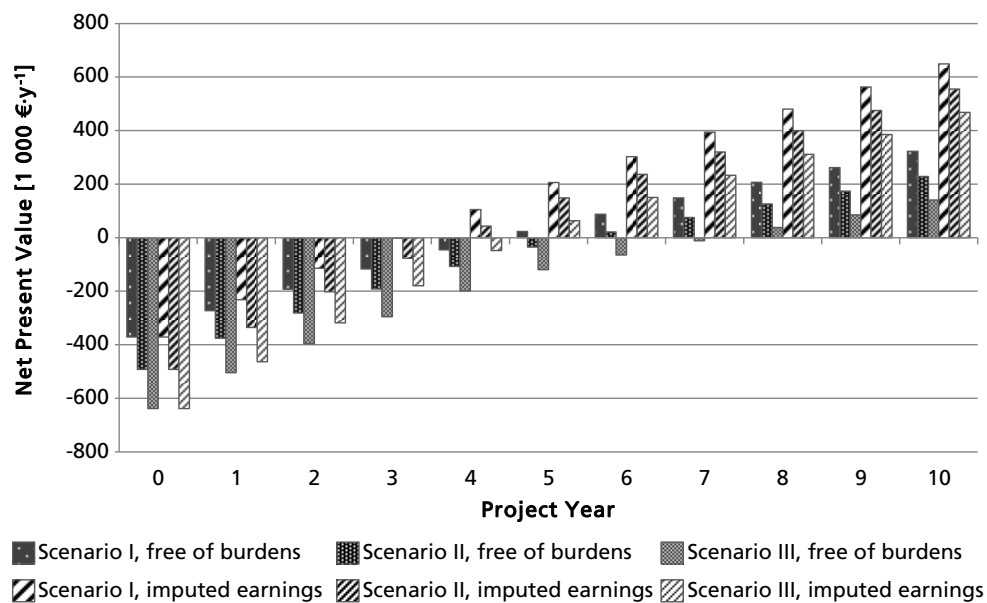


Figure 79: Net present value (*NPV*) of all scenarios (in $1\,000 \text{ €} \cdot \text{y}^{-1}$).

Table 44: Internal rates of return (**IRR**, in %) and payback periods (in years) of the economical assessment in the different scenarios (Sc).

Parameter	Unit	Free of burdens			Imputed earning		
		Sc I	Sc II	Sc III	Sc I	Sc II	Sc III
IRR	%	20.78	14.68	9.96	34.28	26.20	19.78
Payback Period	Static	4.05	4.64	5.58	2.73	3.24	3.84
	dynamic	4.66	5.61	7.23	3.02	3.64	4.43

Sensitivity analysis

Similar to the ecological assessment, a sensitivity analysis was conducted in order to evaluate effects of uncertainties in the assessment and show feasible effects due to volatilities in the market. Therefore, impacts of changes by +5 and +10 % of earnings for metals, labor costs, investments costs, operating hours, and energy costs were analyzed.

Sensitivity results revealed that conducted changes have stronger influences in scenarios free of burdens than those with imputed earnings. These effects confirmed that imputed earnings have a strong influence on economic efficiency of the pyrolysis process. As shown in Figure 80, strongest influences were obvious due to changed earnings for metals, investment costs, and operating hours, while those of labor costs are minor. Regarding energy costs, high influences were obvious mainly in the case of scenario III, slightly in scenario II, and just very slightly in scenario I, because of the different amounts and types of sold energy (power, heat).

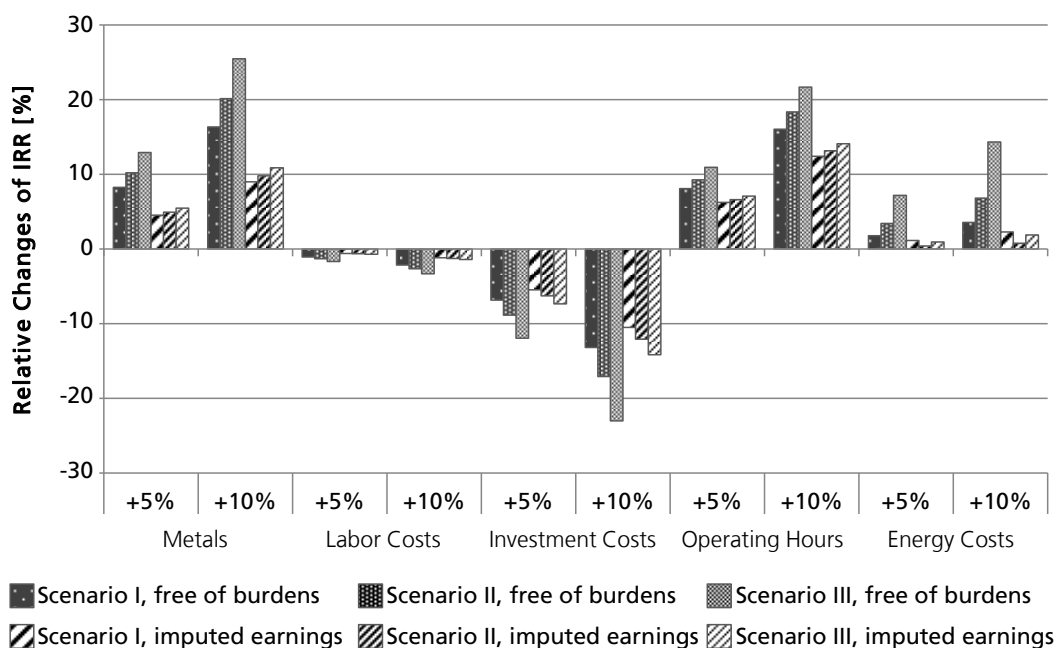


Figure 80: Results of sensitivity analysis from economical assessment as relative change of **IRR** (in %).

7. Discussions

7.1 Pyrolysis tests with shredder residues from WEEE treatment

With the aim to define optimal adjustments of main parameters like temperature and residence time for designing a continuous plant, a number of pyrolysis tests with shredder residues from mechanical treatment of Waste Electrical and Electronic Equipment (WEEE) were conducted. In general, optimal results were found at a temperature of 550 °C regarding pyrolysis products yields: at this temperature lowest yields of pyrolysis solid products but highest ones for liquids were found; yields of gases were nearly unchanged. Additionally, a more detailed view on yields of unfiltered and filtered liquids revealed that the maximum yield of liquids was at 550 °C for filtered ones, but values for unfiltered liquids decreased from 450 to 650 °C constantly. This shows that the filtration residue as unwanted product had highest yields at 450 °C. Any direct comparison to yields of pyrolysis liquids reported in literature is complex, because no differentiation was given with exception of distillation products, from which yields of solid residues in the distillation sump could be estimated (c.f. [Jung et al. 2012]).

Pyrolysis solid products as concentrate of metals for a recycling in (pyro-) metallurgical processes, should have low ignition losses and heating values in order to concentrate metals as strong as possible and not to limit a feed to smelters (c.f. [Brusselaers et al. 2006]). Against this background, optimal results were found at 650 °C and residence times of 30 and 60 min for high heating value *HHV* and ignition loss, respectively. In contrast, those heating values of pyrolysis liquid products should have high values of *HHV*. Additionally, H₂O contents and total acid number *TAN* should be low. For all of these parameters, best results were gained from tests at 650 °C for 30 min.

Regarding *TAN*, which gets measured as mg KOH per g of liquid, three reactions of KOH are generally feasible: reactions with fatty acids, reactions with mineral acids, regarding WEEE mainly HBr and HCl, and reactions with hydroxyl groups or aromatic compounds. In general, gas chromatography/mass spectrometry (GC-MS) analyzes revealed that pyrolysis liquid products did not contain any fatty acids. Concentrations of mineral ones should be similar at all temperature levels: as an example, according to [Grause et al. 2008] HBr gets formed at temperatures above 450 °C. Additionally, formation of HX from aromatic compounds at higher temperatures should play a minor role, due to low concentrations of Br and Cl in the feedstock SR1. Therefore, the leading part of KOH reactions are based on those with hydroxyl groups of aromatic compounds. As source for these compounds, thermoplastics such as polyethylene (PE), polystyrene (PS), or acrylonitrile butadiene styrene (ABS) are implausible as reported in chapter 4.1 by [Suzuki, Wilkie 1995] for instance. In contrast, main products of a thermal decomposition of phenolic or epoxy resins are phenols, cresols, as well as di- and trimethylphenols [Trick et al. 1995; Wong et al. 2015]. [Wong et al. 2015] reported that formations of these compounds peaked at temperatures of about 490 for aromatics and

535 °C for phenols and its derivatives, while all formations nearly reached zero at temperatures >580 °C. Against this background, it would be feasible that the comparatively high *TAN* values of liquid products from pyrolysis are mainly based on decomposition of resins. In this case high *TAN* values do not indicate a high addiction to corrosion, but they strongly indicate the amount of aromatics with hydroxyl groups. Additionally, estimations of resin amounts in different feedstocks could be possible, if all other parameters held constant. However, taking results from GC-MS analyses into account, these argumentation could not be confirmed or declined: yields of those compounds containing hydroxyl groups, namely phenol, isopropyl phenol, and 2,4-dimethylphenol, did not show clear changes due to an increase of temperature: while concentrations of isopropyl phenol continuously decreased from 450 to 650 °C, those of 2,4-dimethylphenol peaked at 550 °C. Unfortunately, values for phenol could not be defined at a temperature of 550 °C due to co-elution with isopropenylbenzene, but were at comparatively high levels of 3.79 wt.-% at 450 °C and 4.79 wt.-% at 650 °C (relative abundance).

High yields of styrene, isopropenylbenzene, 1,3-diphenylpropane, benzenebutanenitrile, and benzonitrile in pyrolysis liquid products suggest that PS, ABS, styrene acrylonitrile (SAN), styrene-butadiene-styrene block copolymer (SBS), and styrene-butadiene rubber (SBR) are the main polymers in SR1. These results are in good accordance to reported results by for ABS mixtures [Bhaskar et al. 2003b; Hall, Williams 2006; Koch 2007] and brominated high-impact PS (HIPS-Br) [Brebü et al. 2007]. Additionally, amounts of 1,2-dimethylbenzene, phenols, dihydronaphthalene, 2,4-dimethylphenol, naphthalene, and biphenyl suggest the existence of polyvinyl chloride (PVC), polyvinyl acetate (PVA), and phenol-formaldehyde resins. However, due to the smaller amounts of phenol-formaldehyde resin derivatives compared to those containing styrene, the amount of corresponding compounds in the feedstock such as printed wiring boards (PWB) had to be small, too (c.f. [Koch 2007]). With the exception of PVA, SBS, and SBR, all suggestions are in good correlation with the reported amounts of polymers in chapter 3.2, which confirm that the analyzed feedstock SR1 is representative for many kinds of WEEE. In addition, TGA of SR1 (see chapter 6.1.1) in comparison to corresponding ones of ABS, HIPS, PVC, and PP (Figure 81) additionally confirm that such polymers could be the main organic compounds in feedstock SR1.

In general GC-MS analyses did not show any decomposition products of brominated polymers. Taking into account that the concentration of Br in the feedstock was comparatively small and that most Br allocated to pyrolysis solid products, it is very likely that corresponding concentrations were too small for conducted GC-MS analyses.

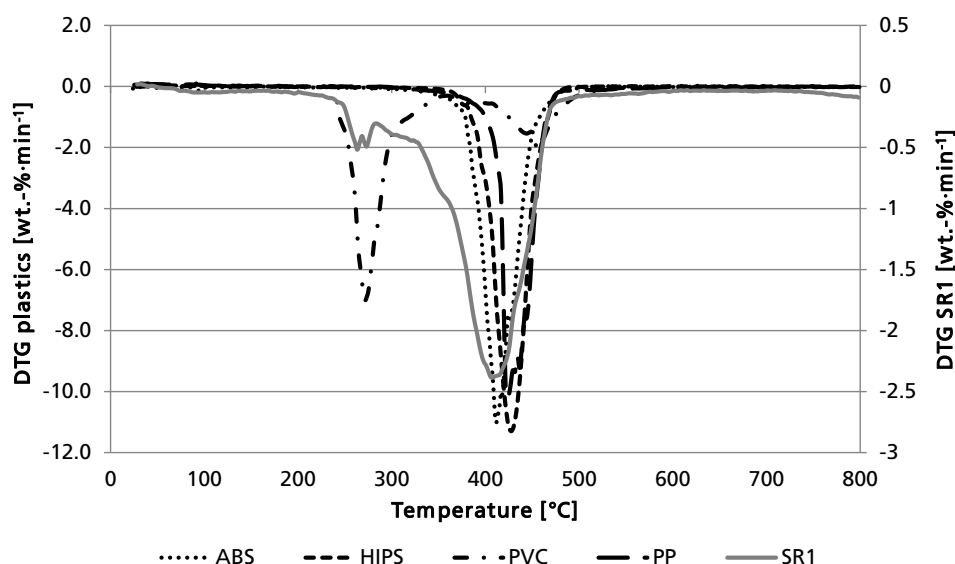


Figure 81: DTG curves of SR1 (solid line) and selected polymers (dotted, dashed lines); 5 K·min⁻¹; argon.

Considering aspects regarding concentrations of H₂O in pyrolysis liquid products as well as CO, CO₂, and H₂ in pyrolysis gases, a further effect could be obvious: the strong and significant decrease of H₂O with an increase of temperature could indicate presence and increase of steam reforming. This assumption was confirmed by (strongly) decreased values of CO₂ in favor of H₂ and CO with an increase of temperature.

From significance tests and regressions analyses different relationships between pyrolysis temperature and products were obvious. Besides the above mentioned differences mainly about pyrolysis liquid products, a strong significant decrease of wax yields were obvious due to an increased temperature from 450 to 550 °C. This could indicate that at 450 °C thermal decompositions of some compounds were not completed and just a vaporization of compounds took place and/or products of these decompositions have medium boiling points. Nevertheless, yields did not change significantly due to a further increase of temperature indicating that thermal decomposition was completed at 550 °C.

Examination of pyrolysis product qualities offered a further aspect besides in- or decreases of quality parameters. Due to an increase of temperature, standard deviations of some parameters decreased. As examples, the standard deviations of H content in pyrolysis solid products as well as the H₂O content in pyrolysis liquid products decreased strongly. A decrease of standard deviation is an additional important aspect for a continuous plant, due to more predictable quantities and qualities.

With regard to the process' energy efficiency, an energy balance was calculated. Figure 82 shows an energy-flow diagram for an exemplary pyrolysis test with SR1 as feedstock at a pyrolysis temperature of 650 °C and a residence time of 30 min plus PO-reactor with PP+La4.5 and halogen-filter. It is obvious that the main part of the energy previously contained in feed and PP allocated to pyrolysis gases (41.79 %), while considerably lower amounts can be found in the pyrolysis liquid (18.79 %) or the solid products (11.07 wt.-%). 38.20 % of the energy given to the process as material, was

PP; the corresponding residue accounted for 27.65 % of the energy in the products. On this, it should be accounted that in future implemented, continuous processes much lower amounts of PP are necessary; additionally, PP-residue could be mixed with the feedstock and given to the pyrolysis process in order to recover all included energy. These both aspects will increase the energy efficiency of the whole process very strongly.

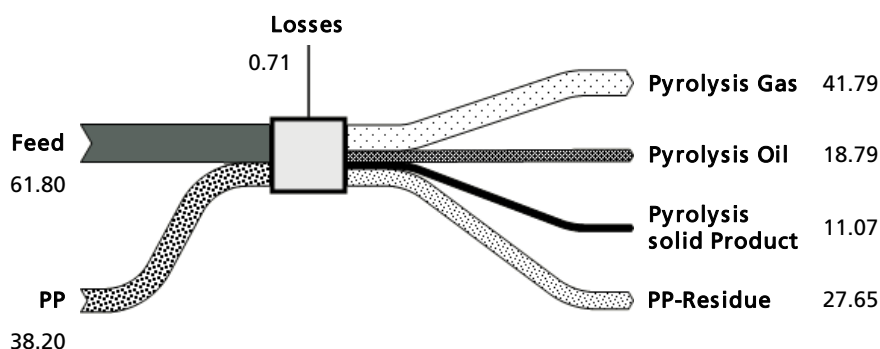


Figure 82: Energy-flow diagram for a pyrolysis-test with SR1 + PP+La4.5 + H.F. (650 °C; 30 min).

Formation and avoidance of (poly-)halogenated aromatic compounds

Allocation of PXDD/F: As shown in chapter 6.2.1, concentrations of polyhalogenated dibenzo-*p*-dioxins and furans (PXDD/F) were considerably higher in pyrolysis liquid products compared to solid products, which indicates that most PXDD/F vaporized after its formations. Due to the observation that PXDD/F concentrations in both types of products decreased due to an increase of temperature, it could be concluded that PXDD/F were destructed or its formation suppressed due to higher temperature.

From literature it is known that polybrominated dibenzo-*p*-dioxins and furans (PBDD/F) allocate mainly to the char [Lai et al. 2007], while polychlorinated dibenzo-*p*-dioxins and furans (PCDD/F) can be found mainly in the liquid products [Joung et al. 2006]. While these results were clearly confirmed for PCDD/F, allocations of PBDD/F as reported in this thesis were not in accordance with [Lai et al. 2007]. The reason could be that [Lai et al. 2007] conducted pyrolysis tests at a temperature of 850 °C. Taking into account that concentrations of PBDD/F in pyrolysis liquid products decreased strongly due to an increase of temperature, while those in solid products increased slightly, it seems feasible that there is a reversal point of PBDD/F allocation to solid and liquid products. Therefore, conclusions by [Lai et al. 2007] could not be confirmed or disproved.

PXDD/F in pyrolysis solid products: High-resolution GC-MS (HR GC-MS) analyzes regarding PXDD/F concentrations in pyrolysis solid products clearly revealed influences of temperature and residence time on such compounds. It was obvious that it is necessary to run a pyrolysis process at 550 °C for at least 90 min or at 650 °C for 30 min in order to go below maximum concentrations as defined by the German act on restriction of chemicals (GGVSEB) and the German chemicals prohibition ordinance (ChemVerbotsV). Only in these cases, no threshold values of the GGVSEB / ChemVerbotsV were exceeded. Besides others, this is necessary to be allowed to transport the pyrolysis solid

products on streets, by train, or on inland waterways. Against economic reasons, the higher temperature of 650 °C compared to 550 °C could compensate three times higher residence times (30 vs. 90 min) easily and hence bring up much more benefits. However, if PXDD/F concentrations in solid products from proposed, later installed pyrolysis processes exceed threshold values of the GGVSEB / ChemVerbotsV, it could be necessary to increase pyrolysis temperature or residence time.

Additionally, contrasts to other processes using mixed fractions from WEEE as feedstock were obvious: As shown by [Koch 2007], there was a strong increase of PBDD/F in pyrolysis solid products compared to feedstock, even after a residence time of four hours in sum. These increases could be reasoned due to the fact that all pyrolysis experiments were conducted in temperature ranges of PBDD/F formation. Differences between samples were based just due to residence times, which enabled a vaporization of PBDD/F. In contrast, tests in this thesis revealed that on the one hand concentrations of PBDD/F decreased with an increase of temperature while on the other hand no enhanced vaporization was obvious within this increase. Additionally, a residence time of 30 min at a temperature of 650 °C was long enough for a strong decomposition of PBDD/F.

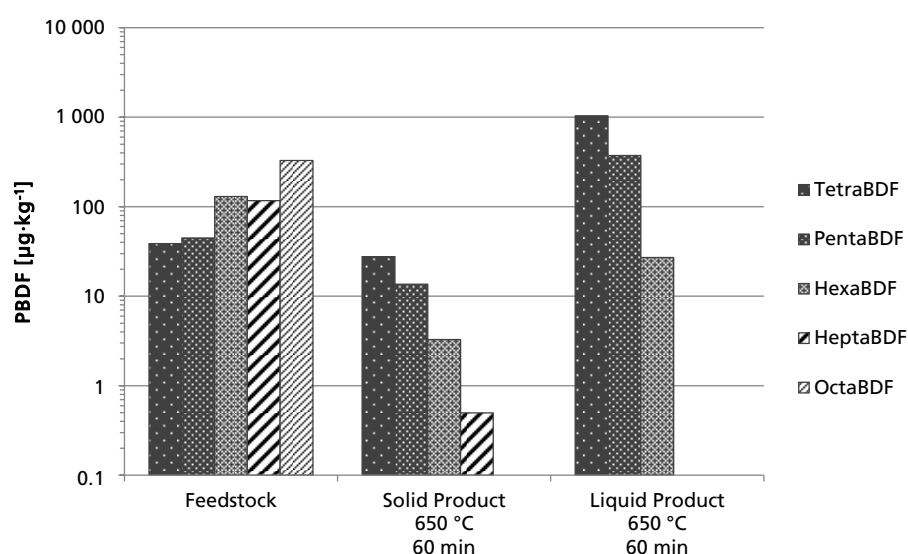
Thermal decomposition of PXDD/F: In addition to results shown in chapter 6.2.1, a more detailed list of PXDF concentrations is shown in Table 45. It is obvious that an increased temperature caused lower PCDF concentrations in pyrolysis solid products, but slightly higher ones regarding PBDF. In contrast, concentrations of both groups decreased in liquid products; however, in liquids, the decreases of PBDF were distinctly higher. Therefore, the impact of an increased temperature is higher on brominated furans than on chlorinated ones. Additionally, it is obvious that mainly such molecules containing more brominated ligands decomposed stronger, which means that the impact of an increased temperature is higher on these compounds. This last mentioned effect was also reported for mixtures or different plastics with flame retardants with or without Sb_2O_3 [Dumler et al. 1989; Thoma et al. 1987]. Therefore, it seems feasible that the present feedstock SR1 contained mainly the very common brominated flame retardants (BFR) decabromodiphenyl ether (deca-BDE) [UBA 2007]. Even when some authors reported that they did not detect any deca-BDE, but mainly penta- and hexa-BDE, by testing PWB and different plastics from WEEE [Chen et al. 2012], it seemed very feasible that mainly this highly brominated flame retardant was present. Different aspects indicated such assumption (Figure 83): PXDD/F analyses of feedstock revealed very high amounts of octa-BDF ($328 \mu\text{g}\cdot\text{kg}^{-1}$), hepta-BDF ($117 \mu\text{g}\cdot\text{kg}^{-1}$), and hexa-BDF ($130 \mu\text{g}\cdot\text{kg}^{-1}$) and significantly lower ones of penta-BDF ($44.7 \mu\text{g}\cdot\text{kg}^{-1}$) and tetra-BDF ($38.8 \mu\text{g}\cdot\text{kg}^{-1}$), which is comparable to analyses by [Ren et al. 2011], who analyzed deca-BDE as BFR additive for new EEE which could still contain different kinds of PBDF. In addition, deca-BDE could be degraded by photolytic debromination due to natural sunlight and PBDF formed before any treatment (pyrolysis, mechanical treatment), which brings thermal energy into the feedstock and could cause PBDF formation [Kajiwara et al. 2008; Weber, Kuch 2003].

Table 45: PXDF concentrations in pyrolysis solid and liquid products (in $\mu\text{g}\cdot\text{kg}^{-1}$).

Pyrolysis	Pyrolysis solid products		Pyrolysis liquid products				
	550	650	550	650	650	650	650
Temperature [°C]							
Residence Time [min]	60	60	60	60	30	30	30
PO-Reactor					PP	PP+La 1.5*	PP+La 4.5**
PCDF							
TetraCDF	40.10	23.80	1 758	1 649	645	860	1096
PentaCDF	11.50	7.63	554	358	122	170	196
HexaCDF	3.20	2.14	128	65.8	18.6	33.3	30.9
HeptaCDF	0.45	0.32	19.78	6.99	2.25	4.24	2.87
OctaCDF	---	---	1.53	0.49	0.88	---	0.57
PBDF							
TetraBDF	26.0	27.7	4 628	1 036	230	935	154
PentaBDF	12.5	13.6	2 732	374	90.4	296	42.7
HexaBDF	2.21	3.28	433	27.1	7.3	24.9	3.5
HeptaBDF	0.27	0.50	24.1	---	---	---	---
OctaBDF	---	---	---	---	---	---	---

* Blend of PP $\text{La}(\text{OH})_3/\text{LaOOH}$ (100:0.468 by weight).

** Blend of PP $\text{La}(\text{OH})_3/\text{LaOOH}$ (100:1.412 by weight).

**Figure 83:** PBDF concentrations in feedstock plus solid and liquid products from pyrolysis at 650 °C, 60 min (in $\mu\text{g}\cdot\text{kg}^{-1}$).

PXDD/F analyses of pyrolysis liquid products confirmed that dehalogenation using PP (+La) is possible and very effective. In contrast to [Hornung 2005], not only decomposition of PBDD/F, but also of PCDD/F took place. Although concentrations of PXDF decreased, there were still high concentrations of it. In general, it should be noted that the residence time of pyrolysis vapor in the molten PP was comparatively short (0.123 s). Main parts of the PO-reactor were constructed mainly on the basis of [Hornung 1997], which means that the PO-reactor was not redesigned against the mass flows of the present pyrolysis process. However, as shown in Table 45, a distinctive effect on PXDF was present even though liquids were not free of PXDF after treatment with molten PP.

Taking into consideration that mainly PXDF and just very low or even no yields of PXDD were detected, formation of PXDF could take place mainly by different pathways, which are shown in Figure 84, exemplary for deca-BDE [Weber, Kuch 2003]. The overall larger amounts of furans could be explained due to intra-molecular ring closure reactions of brominated aromatic compounds via abstraction (intra-molecular elimination) of Br_2 and/or HBr , which both are enhanced by Sb_2O_3 . Abstractions could take place either directly (mainly Br_2) or in a cascade starting with a previous debromination in favor of PBDE, supported by H-donors and/or Br-acceptors such as H_2O , metals, and metal oxides. Due to the high amount of present metals and metal oxides in the feedstock SR1 mainly the last mentioned way of debromination and secondary abstraction of HBr and/or Br_2 seems mostly feasible. Additionally, the high amounts of Br and Cl in the pyrolysis solid products indicated that metals and metal oxides strongly reacted with Br containing compounds compared to plastic mixtures containing just Sb_2O_3 as additive for BFR. Besides formation reactions of PBDF, degradation of previously formed PBDE is feasible in favor of polybrominated biphenyls (PBB) and polybrominated phenols (PBP).

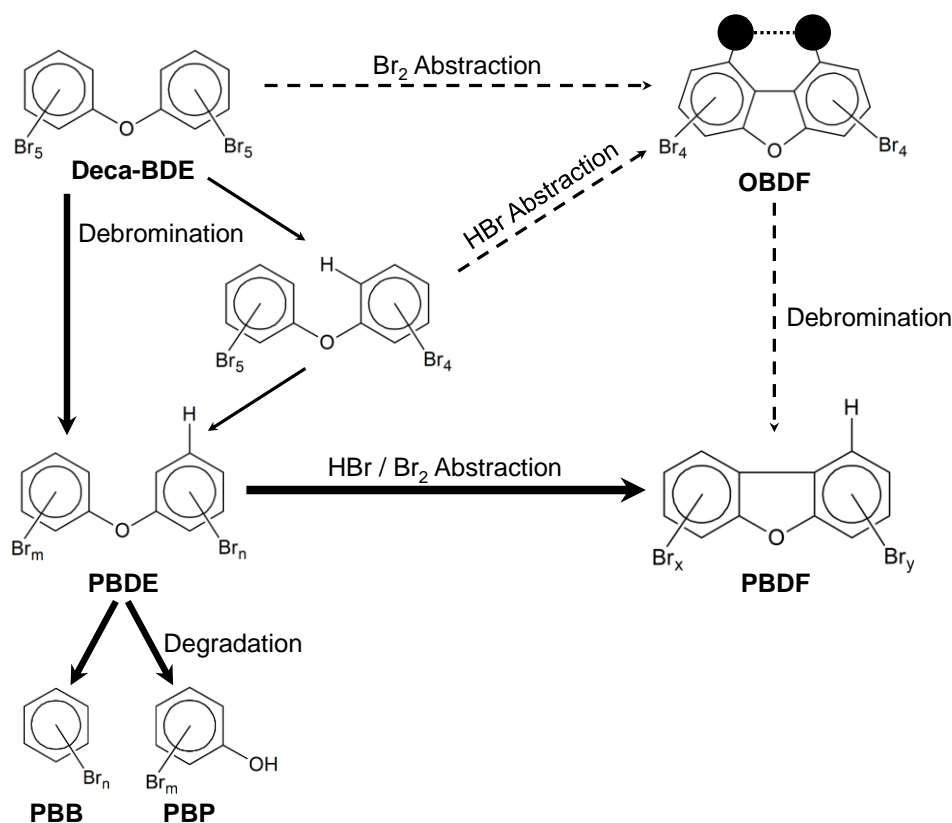


Figure 84: Formation pathways of PBDF during thermal degradation of deca-BDE (modified according to [Weber, Kuch 2003]).

Sums of PXDD/F concentrations in liquid products exceeded three of five threshold values of the GGVSEB / ChemVerbotsV. However, in contrast to pyrolysis solid products, liquid products do not represent a final product from the pyrolysis process, which has to be transported (for final treatment). Due to the proposed energetic utilization, it will be more important to conduct measurements of PXDD/F in the offgases of corresponding

thermal processes. In this case, threshold values could be defined in dependency on the 17. German federal immission control ordinance („17. Verordnung zur Durchführung des Bundes-Immissionsschutzgesetzes“) [BMUB 1990].

Besides threshold values as defined in GGVSEB / ChemVerbotsV, which are mainly relevant for products quality aspects and transports, a number of threshold values for human health with a character of recommendations are defined. As an example, the German environment agency UBA defined maximum values for different kind of areas, which indicate when actions should be conducted [UBA 2014]. These values are expressed as an toxic equivalency factor (TEQ) in the form of 2,3,7,8-TCDD according to the Committee on the Challenges of Modern Society (CCMS) of the North Atlantic Treaty Organization (NATO) in 1990 [Kutz et al. 1990]. The values accounted for $0.1 \mu\text{g}\cdot\text{kg}^{-1}$ in case of children's playgrounds, $1.0 \mu\text{g}\cdot\text{kg}^{-1}$ for housing areas, parks, and leisure facilities, and $10.0 \mu\text{g}\cdot\text{kg}^{-1}$ for industrial grounds [UBA 2014]. As shown in Table 58 (appendix), no pyrolysis solid products exceeded a summarized value of $0.5 \mu\text{g}\cdot\text{kg}^{-1}$ (650 °C, 30 min), while the feedstock reached nearly $1.5 \mu\text{g}\cdot\text{kg}^{-1}$. A comparison to the maximum values defined by the UBA shows the low rates of PXDD/F in pyrolysis solid products.

In order to receive a higher added value from the treatment of shredder residues using a pyrolysis process in combination with the PO-reactor, a further improvement should be taken into considerations: Due to an installation of a sink-flow separation (see chapter 3.3.1) PP and PE could be separated from shredder residues for utilization in the PO-reactor. However, due to comparatively low prices of such polymers, a detailed economical assessment should be calculated previously.

Influence of La in PP: As shown in chapter 6.2.1 (Table 35), just due to the use of $\text{La}(\text{OH})_3/\text{LaOOH}$ as additive in PP, a complete decomposition of all PXDD were achieved. This fact is in good correlation with findings by [van de Avert et al. 2004] about dechlorination of, for instance CCl_4 . Although all tests with PP and La were conducted with a mixture of $\text{La}(\text{OH})_3$ and LaOOH , mainly LaOOH must be present in the PO-reactor, due to corresponding formation from $\text{La}(\text{OH})_3$ as shown by [Gaviría et al. 2012]. Therefore, it was expected that LaOOH reacted directly without any formation of H_2O as shown by [van de Avert et al. 2004]. However, very similar, H_2O is necessary for catalytically dehalogenation. Both expected reaction schemes are shown in Figure 85. Such reaction scheme is valid up to a temperature of 850 °C; at higher temperatures LaOOX is halogenated to LaX_3 , which evaporates immediately [Gaviría et al. 2012].

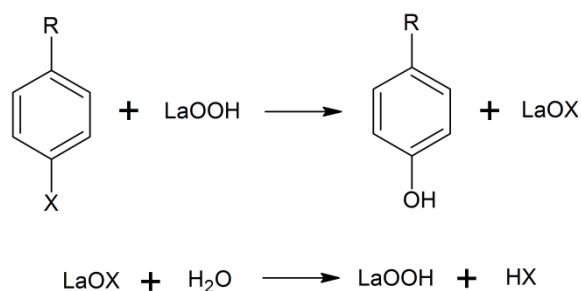


Figure 85: Expected reaction schemes for halogenation and dehalogenation of aromatic compounds using LaOOH in the presence of steam.

In contrast to the complete decomposition of PXDD using $\text{La}(\text{OH})_3/\text{LaOOH}$ as additive in PP, addition of such La compounds impaired the effect of PP on the decomposition of PXDF (Table 45).

In general, reasons for the uncomplete decomposition could have manifold sources:

- as mentioned above, residence time of pyrolysis vapor in the molten PP was comparatively short (0.123 s) and could be too small for complete decomposition,
- concentration of LaOOH was inadequately, e.g. due to further reactions of La with other compounds than halogens (see below) and/or
- the amount of H_2O was too small for dehalogenation of LaOX.

It seems feasible that LaOOH reacted not only with halogens, but also with further substances such as As(III), As(IV), Cr(VI), F, NH_4^+ , NO_3^- , and PO_4^{3-} [Ahmed 2004; Shi et al. 2013; 2015; Wang et al. 2015b; Wang et al. 2016], which slightly corresponds to metal amounts, found in PP-residue from PO-reactor.

According to the reaction schemes (Figure 85), dehalogenation of LaOX seemed to be incomplete mainly due to the too small amount of H_2O to dehalogenate LaOX for a catalytic cycle. In order to increase the amount of H_2O or -OH, respectively, either H_2O could be added to the feedstock or a H_2O donating substance could be added to PP. The first option could show strong disadvantageous due to an unpredictable strength of steam reforming during pyrolysis (see above) and, therefore, an unpredictable amount of H_2O in pyrolysis liquid products. In contrast, adding a H_2O /-OH donating substance to PP would not influence the strength of steam reforming during pyrolysis and deliver a predictable amount of H_2O , which could be therefore lowered. As an example, a blend of PP (+La) and PVOH could be used: as described in chapter 4.1, a pyrolysis of PVOH delivers high yields of H_2O in the liquid (58.2 wt.-%) and gaseous phase (20.9 wt.-%). Additionally, the starting point of decomposition (364 °C) is in a very similar range to that of PP [Shie et al. 2002]. As a further benefit, formation of -OH would take place in a very physical proximity to PP and LaOX.

In general it should be noted that PXDD/F concentrations in liquid products from pyrolysis with PO-reactor were analyzed just for tests with residence times of 30 min, while those without PO-reactor were analyzed for liquids products from tests with 60 min. Liquids from tests without PO-reactor were analyzed before residence time of pyrolysis was optimized to 30 min, while those with PO-reactor were analyzed afterwards. On the one hand it seems feasible that elongated residence times could increase a vaporization of PXDD/F in favor of an allocation to pyrolysis liquid products, but on the other hand, corresponding values in solid products were many times smaller than those in liquids. Additionally it should be noted that formation of liquids mainly took place during the first 20 - 30 min. Therefore, a direct comparison between such values from tests with 30 and 60 min residence times should be allowed.

Volatilization and allocation of elements

Corresponding to the aim to use a pyrolysis process to form concentrates of metals for downstream recycling, allocations of metals were investigated. In general, analyses revealed that most metals allocated with more than 99 wt.-% to the solid phase; however, strong differences regarding these metals and mainly those metals, which did not allocated to solid products, were obvious by comparing results from inductively coupled plasma mass spectrometry (ICP-MS) / inductively coupled plasma optical emission spectrometry (ICP-OES) and energy dispersive X-ray fluorescence (EDXRF) analyses. Fundamental different results were obvious for Cu, Cr, and Mo. Differences for Cu could be explained due to matrix effects or insufficient digestions (c.f. chapter 5.2). In contrast, explanations for Co and Mo are more complex. Differences like these could be explained more general (1) due to different samples, e.g. from different pyrolysis trials, (2) due to changed circumstances or constellations, e.g. with or without PO-reactor, (3) due to corrosion of parts of the plant, e.g. via halogenation and vaporization of metals, and/or (4) due to the measuring methods as already described in chapter 5.2. Following the third mentioned feasible reason, metals such as Mo, Cr, Ni, or Ti, which are alloying elements in the mainly used stainless steel 1.4571, could be found in PP-residue, filtration residue, or liquid product, but did not originate from feedstock. Regarding Mo, the different results should be considered in special: using ICP-MS/OES, Mo was found just in solid residues, while it was found mainly in PP-residue using EDXRF. Test trials, from which products were analyzed by ICP-MS/OES, were conducted without PO-reactor installed. Because in products of this trial Mo was found just in pyrolysis solid product but not in filtration residue or filtered liquid product, either no Mo was mobilized or it allocated to the wax phase, which got collected in the cooling

units³⁶. Due to the upstream position of the PO-reactor a capturing of Mo in the PP-residue could be possible, which could enable a selective recovery of Mo. More general, the PO-reactor seems to be able to filter out particles, as mentioned in chapter 6.2.1 as well as metals. Both effects show fundamental advantages regarding any utilization of pyrolysis liquids as well as to lower the amounts of unwanted filtration residues. Not only Mo, but also a significant amount of Cr was filtered out of the pyrolysis vapor using the molten polyolefin. In the cases that feedstocks, with higher amounts of dust and/or metals and halogens should be treated using pyrolysis, higher amounts of Mo, Cr, and further metals could be present in pyrolysis vapor. If so, a PO-reactor could bring up the positive effect to lower metal contents in pyrolysis liquids, besides its main task to decompose halogenated aromatic compounds. Although a PO-reactor is part of a pyrolysis process, a small amount of filtration residue will be filtered out of formed pyrolysis liquid products. In order not to dispose this material and contained metals, it could be mixed up with the feedstock and given back to the process. Nevertheless, a small amount of metals can be found in the liquids with or without PO-reactor. In this context, allocation of In should be noticed, which was found just in the pyrolysis liquids indicating a very strong mobilization affinity. Feasible reaction mechanism should be discussed later in chapter 7.2.

Besides investigations about allocations of metals, those of C, H, N, S, and halogens were conducted, too. Aspects regarding C and H should be discussed below in the part "utilization of conversion products". N showed a strong volatilization, which is in accordance with reported ones in literature [Bhaskar et al. 2003b]. In contrast, S mainly allocated to solid pyrolysis products (89.6 wt.-%) while pyrolysis liquids from other feedstock often contain high amounts of S (c.f. [Neumann et al. 2016]). As shown by a XRD-analysis, mainly sulfates of Na, K, and Ca were present. This strong fixation of S enables a receiving of liquid products with low sulfur contents. Main parts of halogens were detected in the solid products, which is in strong contrast to allocations reported in literature. As an example, [Bhaskar et al. 2003] revealed that Br from ABS-Br pyrolysis at 450 °C mainly allocated to wax phase, while just 1.8 - 2.9 wt.-% did not become mobilized and was found in the solid residue. Usually, due to the higher temperature a higher amount of Br should be allocated to the vapor and corresponding products such as waxes or liquid products; however, as shown in chapter 6.2.1, from pyrolysis of SR1 at 650 °C 91.8 wt.-% Br did not become mobilized. These strong differences between pyrolysis of ABS-Br and SR1 could be explained either due to a much higher amount of Br in ABS-Br (9.59 wt.-% Br) or due to reactions of Br in the solid phase in favor of compounds with low volatility. Additionally, it seems feasible that mobilization of Br was hindered due to the kind of plastics, which were present in the feedstock. As shown in

³⁶ Due to very small amounts of waxes and just a hardly feasible extraction out of the cooling unit, no analyses were conducted.

chapter 4.2.1, [Miskolczi et al. 2008] revealed that from pyrolysis of HIPS-Br (7.1 wt.-% Br) at 440 °C nearly one third of Br allocated to the char, which is significantly higher than those results by [Bhaskar et al. 2003] but lower than results from this thesis. Therefore, halogenation reactions of metals and mobilization of corresponding halides were analyzed statistically (chapter 6.2.1). Even if calculated regressions with high coefficients of determinations (R^2) showed that mobilization of metals via halogenation seems very feasible, distinctive conclusions were not possible. As an example, due to the high number of various metals and compounds present, further reactions such as formations of complexes could take place or decompositions of compounds enhanced. For instance, as shown by various authors dealing with pyrolytic treatment of chromated copper arsenate treated wood, As could volatilize by different ways such as (1) volatilization of As_2O_3 >200 °C, (2) decomposition of As_2O_5 supported by activated carbon >300 °C, (3) volatilization of As_2O_5 supported by H_2 and CO >425 °C, or (4) volatilization of As due to reaction of Cr_2O_3 and As_2O_5 forming chromium arsenate ($CrAsO_4$), which decompose quickly [Helsen, van den Bulck 2005; Kim et al. 2012]. In summary, volatilization of metals and allocation to pyrolysis liquids or other interrelated fractions should be considered for a recycling of metals from shredder residues.

Utilization of conversion products

Pyrolysis solid products: Results revealed that a utilization of pyrolysis solid products in integrated copper smelters enables a recovery of nearly all metals, which could be technically recovered in corresponding plants. On this account, volatilizations of C and H had a positive side effect with regard to a recycling of metals from solid products in a copper smelter: on the one hand, due to the lowered content of H, mainly the heating value of the solid products decreased, which enables a higher amount as feed in smelters³⁷. On the other hand, due to thermal decomposition of organic material, mainly non-volatile carbon is present in the solid product. Therefore, it could be assumed that the residual amount of carbon in this pyrolysis product could substitute pet-coke, which is used in smelter processes as reduction agent, usually. In addition, a previous recovery of Al and Fe would be also feasible using magnetic and eddy-current or spiral separators. However, an exception is given for In, which was completely allocated to pyrolysis filtered liquid product. In addition, 100 wt.-% of Cd and 87.9 wt.-% of Mo allocated to pyrolysis vapor phase. In order also to enable a recovery of these metals, precipitation or electrolytic winning should be investigated in further process constellations.

³⁷ Due to the often high amounts of components from WEEE, mainly PWB, in the feedstock of integrated copper smelters, additional feed should have low heating values in order not to exceed the maximum energy input and corresponding heat release in the smelter.

Pyrolysis liquid and gaseous products: Pyrolysis liquid and gaseous products represent by-products of high quality with regard to an energetic utilization. However, any energetic utilization of these fuels has to be conducted in adapted engines, because the fuels do not meet the requirements for modern engines, yet. Table 46 shows a comparison between pyrolysis liquids from tests with and without PO-reactor and halogen-filter, and conventional fuel gasoline E5 and diesel fuel according to DIN 51626 and DIN EN 590, respectively. It is obvious that there are a number of differences between conventional fuels and those from a pyrolysis of WEEE. Pyrolysis liquid products showed *HHV* lower than those of conventional fuels (gasoline E5: 43.9 MJ·kg⁻¹; diesel fuel: 43.1 MJ·kg⁻¹) but still in a similar range and even higher than those of bio fuels (bioethanol: 26.7 MJ·kg⁻¹; fatty acid methyl ester (FAME): 37.14 MJ·kg⁻¹) [BDBe 2016].

Table 46: Comparison between pyrolysis liquid products, fuel E5 and diesel fuel.

Parameter	Unit	Pyrolysis liquid products		Gasoline E5 ³	Diesel Fuel ⁴
		SR1 ¹	SR1 + PP + H.F. ²		
HHV	MJ·kg ⁻¹	37.39	38.26	---	---
Cetane index	---	10.8	30.1	---	>46.0
Density (15 °C)	g·cm ⁻³	947.8	926.8	720 - 775	820 - 845
Kinematic viscosity	mm ² ·s ⁻¹	1.159	1.202	---	2.00 - 4.50
Ash content (775 °C)	wt.-%	0.121	0.094	---	<0.01
Corrosiveness to Cu	---	1b	1	1	1
Content of S	mg·kg ⁻¹	396.5	585.5	<10.0	<10.0
Content of Pb	mg·l ⁻¹	33.1	13.8	5	---
Content of Mn	mg·l ⁻¹	---	---	---	<2
Content of H₂O	mg·kg ⁻¹	10 000	6 800	---	<200
Distillation temperature at 95 vol.-% residue	°C	239.1	---	---	<360

¹ Average values for pyrolysis liquid products from tests at 650 °C and 30 min residence time.

² Average values from two pyrolysis tests at 650 °C and 30 min residence time with PO-reactor (PP at 340 °C) and halogen-filter (450 °C).

³ according to DIN 51626-2 [DIN 2008b].

⁴ according to DIN EN 590 [DIN 2010].

Upgrade of pyrolysis liquid products: The addition of the PO-reactor seems feasible not only to decompose PXDD/F in pyrolysis liquid products, but also to enable a selective formation of two different kind of liquid fuels. Due to the addition of the PO-reactor more long-chained hydrocarbons as decomposition products of PP are formed, which increased the cetane index. The cetane index is a fundamental parameter regarding the applicability of a fuel either on a gasoline or diesel fuel engine. While from pyrolysis tests at 650 °C without PO-reactor a fuel was produced, which is very similar to gasoline (low cetane index), that liquid product from tests with PO-reactor (and halogen-filter) could be used on a diesel fuel engine due to its comparatively higher cetane index. This observation is also indicated by changed distillation ranges, mainly in the sector of high-boiling products (see chapter 6.2.1). However, in order to meet the requirements of conventional fuels a further increase of the cetane index (>46.0) is necessary. Concerning this matter, it seems feasible that due to some adaptations of the PO-reactor

like a small increase of temperature, the vapor pressure of long-chained hydrocarbons increases, too. However, the rise of temperature should increase the (simultaneous) decomposition of PP as low as feasible in order not to depropagate PP forming monomers.

Regarding further requirements of ash and metal contents, which are listed in Table 46, it should be noted that the liquid products were just filtered with paper filters at 2 μm in conventional suction strainers. In order to receive better results regarding contents of metals or ash, more efficient filter options, a distillation, or condensation of pyrolysis liquid products could be conducted. As an example, as shown in chapter 6.2.1, analyses regarding allocations of metals revealed that some metals, mainly As, Cd, In, Mo, and Sb were found in filtered liquid products. Considering that these metals could show negative aspects regarding an energetic utilization in engines or harmful emissions from ignition, distillation or condensation, respectively, for instance at 200 °C, could show a further positive aspect: all named metals could be separated due to high boiling points even as halogenated agents, with the exception of AsCl_3 , which has a boiling point of just 130.2 °C [Holleman et al. 2007].

In order to reach further quality aspects as gasoline, blending with ethanol is also possible (see chapter 6.2.1). Nevertheless, further aspects have to be tested in order to meet requirements of conventional fuels: for instance, to utilize pyrolysis liquid products in a diesel fuel engine, aspects such as inflammability and ability of lubricating are important, too.

Besides any energetic utilization of pyrolysis liquid products onsite a WEEE treatment plant, it seems also feasible to use such products as bulk chemical instead of fossil based naphtha in a number of petrochemical processes due to high amounts of aromatic compounds such as styrene, 1,2-dimethylbenzene, phenol, and isopropenylbenzene (c.f. results from GC-MS analyses; Table 63 and Table 64). Regarding this option, the achievements regarding dehalogenation, plays a fundamental role; however, dehalogenation efficiency has to be improved, as described later.

Not only due to economic reasons, but also due to maintainability, it should be tested if reactions, which take place in the tar-cracking unit, also take place in the PO-reactor, which means that any installation of a single tar-cracking unit would be unnecessary. Nevertheless, in the case of a continuous operation further equipment assemblies such as a heated cyclone or an electrostatic precipitator should be taken into considerations for improving qualities of pyrolysis liquid and gaseous products.

Comparison to the status quo: In order to compare the achievements with other pyrolysis processes, which aimed to produce liquid products for an energetic utilization, values regarding the content of H_2O and halogens should be set into relation to such processes. As an example [Koch 2007], who conducted two-stage pyrolysis at 350 and 450 °C gained not only considerably higher concentrations of Br (1.19 wt.-%) and Cl (0.55 wt.-%), but also significantly higher yields of pyrolysis water. Pyrolysis liquid

products consisted out of 32.2 wt.-% H_2O and even after separation an amount of 8.4 wt.-% H_2O was detected. In contrast, from pyrolysis at 650 °C, which were conducted during tests of this thesis, concentrations of just 0.7 - 1.0 wt.-% were gained. This effect could be basically originated from different feedstock; however, due to the above mentioned aspect, steam reforming could be present at high temperature pyrolysis, too.

Dehalogenation of pyrolysis liquid products

EDXRF-Analyses for determination of Br and Cl in pyrolysis liquid products revealed that not only due to addition of the halogen-filter, but also just due to addition of the PO-reactor with PP (+La), concentrations of Br and Cl decreased in pyrolysis liquids. Decreases due to the addition of pure PP could be explained with allocation of halogens and halides to the PP-residue. With the addition of the halogen-filter decreasing amounts of Br and Cl in pyrolysis liquid products were obvious; however, absorption of halogens in the halogen-filter did not reached 100 %, which can be mainly explained due to halogen-filters operation temperature at 450 °C during pyrolysis tests. Pre-tests (chapter 5.4.2) revealed that the highest efficiency regarding Br_2 was at 450 °C while that of HBr was at 600 °C. Taking into account that hydrogen halides, as reported by [Karama et al. 2013] in the form of HCl , is formed a several times more often than molecular halogens, in case of [Karama et al. 2013] as Cl_2 , it seems very likely that the halogen-filter was not operated at the optimal temperature regarding the whole amount of halogen compounds.

In general it should be noted that due to limited test conditions in present labs, absorption tests were conducted just with Br_2 and HBr . In addition to this, further tests with halogens, mainly Cl_2 and HCl , should be done. More general, it should be tested if the developed filter material could be used not only in pyrolysis applications, but also in plastics industry and mainly in exhaust gas treatments of incineration plants.

Reutilization of halogen-filter material: Two options should be discussed regarding reutilization of halogen loaded glass spheres: On the one hand, glass spheres could be heated up to a temperature of 850 °C. At this temperature X_2 gets formed from LaOX or LaX_3 , which could be afterwards captured as NaX in a wet NaOH scrubber. The advantages of this option are that the corresponding NaOH scrubber could be designed comparatively small due to the small amount of formed gases, and the process is very similar to the manufacturing process, which could enable a combination of both. However, this option of desorption needs energy at a high temperature-level, which have to be delivered from secondary energy sources. On the other hand, glass spheres could get streamed with hot steam as described in [van der Avert, Weckhuysen 2004] as second option of desorption. HX gets formed and can be separated in NaOH similar to the above mentioned system. However, disadvantage of this process will be that the scrubber has to be comparatively large due to the high amount of vapor/steam. In contrary, two advantages of this process are that steam could be provided from energy

delivered by a combined heat and power plant (CHP) or combustion unit and that it is not necessary to deconstruct the halogen-filter: In this case, two filters are installed from which one absorb halogens while the other one get desorbed from it. Nevertheless, it has to be clarified if the La coating on the spheres surfaces stays stable during steam desorption.

7.2 Pyrolysis tests with selected fractions containing scarce and critical metals

Tantalum capacitors

Aims of pyrolysis tests with Ta capacitors were a concentration of Ta in a defined fraction as well as decomposition of organic matter. In contrast to [Fujita et al. 2014], who revealed a decomposition of sintered pellet structures at temperatures $>600\text{ }^{\circ}\text{C}$ under air atmosphere, a decomposition under pyrolytic conditions was obvious at temperatures $>500\text{ }^{\circ}\text{C}$. At this temperature, the exterior molds started decomposing, but were still present in form of relatively large particles. Therefore, sieving of pyrolysis solid products ended up in a fine fraction, which contained large amounts of Ta, but comparatively low amounts of SiO_2 . The developed process not only consists out of just two process steps instead of four, which means much more easier treatment and saving of energy and time, but also formations of PBDD/F could significantly avoided: As shown by [Ortuño et al. 2014], in the present temperature range formations of PBDD/F could be up to 85 times higher in the case of combustion than in pyrolysis.

With regard to an industrial approach of a thermo-chemical treatment of Ta capacitors, the described decomposition of Ta capacitors, mainly its sintered Ta structure, could be utilized in a process chain: mounted parts from PWB, which contain Ta capacitors, become solved from PWB mechanically. The separated parts can be used as feedstock for pyrolysis in order to receive a solid pyrolysis product, which can be separated by sieving. From pyrolysis tests at $550\text{ }^{\circ}\text{C}$ (residence time 30 min), it was obvious that 86.5 wt.-% of Ta becomes part of the fine fraction. The corresponding strong accumulation is obvious taking into account that concentration of Ta increased from 11.5 wt.-% in the feed to 55.6 wt.-% in product fraction $<500\text{ }\mu\text{m}$. Although Ta concentration in fine fractions increased with higher temperatures, such concentrations in fractions $>500\text{ }\mu\text{m}$ also increased leading to worse allocation and accompanying loss of Ta. In order to separate Ta from remaining other metals in this fine fraction such as Mn or Si, separation by density could be conducted. Afterwards Ta could be given to specialized metallurgical processes in order to recover it as pure metal. Aiming at a separation by density, e.g. using sedimentation or flotation techniques, a XRD analysis was conducted, mainly in order to examine the form of Mn oxides. A corresponding XRD pattern of sieve fraction $<500\text{ }\mu\text{m}$ from pyrolysis tests with $550\text{ }^{\circ}\text{C}$ and a residence time of 30 min is shown in Figure 101 in the appendix. It shows that mainly Mn_2O_3 (25.3 wt.-%) and Mn_3O_4 (51.7 wt.-%) are present, but also just small amounts of MnO

(8.3 wt.-%) and MnO_2 (14.7 wt.-%) (%-values after normalization). Therefore, separation by density should be conducted between $5.37 \text{ g}\cdot\text{cm}^{-3}$ (MnO) and $8.2 \text{ g}\cdot\text{cm}^{-3}$ (Ta_2O_5) [Perry, Phillips 1995]).

Combining the results of allocation investigations regarding metals in pyrolysis solid products from shredder residues (chapters 6.2.1 and 7.1) and those results about the decomposition of Ta capacitors, an interesting aspect especially for the critical metal Nb was obvious. Nb is mainly used in EEE for small capacitors, very similar to those containing Ta. Because Nb was found just in such pyrolysis solid product fractions from shredder residues, which sizes were $>1 \text{ mm}$, it seems feasible that the structure of these capacitors stays stable after pyrolysis, milling, and sieving, which is in contrast to Ta capacitors. Therefore, a process combination of pyrolysis, milling, and sieving seems to be able to separate the different capacitor types or the metals in it, respectively. A further sieving fraction (besides those $<0.5 \text{ mm}$ for Ta) with sizes between 0.5 and 4 mm , for instance could enable a selective separation of Nb besides Ta, too. All sieve fractions with larger sizes could be given directly to common recycling pathways such as integrated copper smelters.

Liquid crystal displays

In order to analyze volatilization of As, Ga, and In via halogenation, co-pyrolysis of liquid crystal displays (LCD) with PVC as well as LCD in vapor-phase mode of a pyrolysis of PVC was conducted. In addition, a conventional pyrolysis of LCD was conducted as reference. Comparison of both non-conventional process conditions revealed that for a recovery of In, LCD in vapor-phase mode showed clearly higher efficiency. Similar to this, [Yanik et al. 2001] conducted co-pyrolysis and vapor-phase reaction tests in order to compare the effectiveness of dehalogenation in the different contact modes. They could show that vapor-phase mode reactions had higher efficiency concerning fixation of HCl. Likewise results were shown by [Horikawa et al. 1999] or [Uddin et al. 2002] for instance (see chapter 4.3.3).

Allocation of In from vapor-phase mode tests to pyrolysis liquid products accounted for 64.0 wt.-%, which was very similar to [Park et al. 2009], who reached 66.7 wt.-%. In order to increase mobilization, either temperature could be increased to $800 \text{ }^\circ\text{C}$ or even more (c.f. [Park et al. 2009]) or pyrolysis of PVC could be conducted in several charges to receive reactions between Cl and In more often. In comparison to such chlorination processes using chlorination agents like CaCl_2 , NaCl , or NH_4Cl an energy-intensive milling preliminary to chlorination is unnecessary [Ma, Xu 2013].

Regarding As and Ga, a depollution of LCD concerning As seems feasible using co-pyrolysis while no clear conclusion could be done concerning Ga. In order to investigate pyrolysis behavior of Ga from LCD in almost the same manner, bright sites of LCD could be tested, which showed higher concentrations of Ga compared to dark sites. Nevertheless, relating to a later industrial process, an optimization of ratios between

LCD and PVC as well as of temperature levels should be done. As Cl containing feedstock, further feedstocks such as PVC floorings or residues from cable treatment could be used in order to dehalogenate such feedstocks, receive Cl for a treatment of LCD, as well as to concentrate minerals (feedstock: PVC floorings) or metals (feedstock: cable residues) in a solid pyrolysis product for further treatment/recycling.

7.3 Sustainability assessment

7.3.1 Interpretation of results from ecological assessment

During the sustainability assessment, ecological impacts of a continuous pyrolysis process were analyzed and compared to the status quo. In the status quo, shredder residues from WEEE treatment are utilized energetically in a municipal waste incinerator (MWI), which is able to recover energy from organic matter but just comparatively small amounts of metals from slags and ashes. For pyrolysis, it was assumed that formed liquids and gases are also utilized energetically but in a CHP with higher efficiencies compared to those in a MWI. In addition, gained pyrolysis solid products are treated further in an integrated copper smelter for a recovery of contained metals.

As shown, in all considered impact categories higher exonerative effects were found for pyrolysis compared to combustion in a MWI. The highest differences were obvious in such categories, in which metals had a significant influence, such as categories regarding resources (abiotic resource depletion potential (ADP), anthropogenic stock extended abiotic depletion potential (AADP)), acidification and eutrophication potential (AP, EP), areatime, and photochemical ozone creation potential (POCP). In impact categories regarding energy, global warming potential (GWP), and ozone layer depletion potential (ODP), recovered forms of energy showed higher impacts than metals. Both findings indicate that regarding ecological aspects, metal and energy recovery are relevant in order to receive strong exonerative effects compared to the status quo. These findings were proofed and confirmed by a sensitivity analyses. The sensitivity analysis as method for checking quality of used data clearly confirmed above mentioned conclusions. Additionally, it was obvious that just in the case that a MWI in the status quo has significantly higher gross energy efficiency, those impact categories with high impacts from energy could show negative effects of pyrolysis compared to MWI (energy, GWP, ODP).

Nevertheless, no impact assessment was conducted with regard to toxic emissions from both options due to base and fundamental discussions about methodologies basic as mentioned in chapter 5.5.1 [Heijungs et al. 2004]. However, these emissions could be relevant for an overall ecological assessment especially regarding highly-toxic emissions such as PXDD/F. Though these emissions are widely discusses in literature, adequate database is given just for PCDD/F but not for PBDD/F (c.f. [Ecoinvent 2016]).

7.3.2 Economical assessment

The economical assessment was conducted in order to detect strengths and weaknesses for designing a continuous plant. For the assessment, a number of assumptions were proposed, due to actually not existing real data. Nevertheless, even for main influencing parameters such as earnings for metals, power, and heat, clear results could be gained as proofed by the sensitivity analyses.

The economical assessment revealed clear economic benefits for all three scenarios; however, it could be clearly seen that for the proposed design (pyrolysis plant with a capacity of 70 kg·h⁻¹) and the chosen circumstances, burning pyrolysis liquids and gases in a combustion unit is the most economically profitable option. Only in that case, that power cannot be sold and imputed earnings from feedstock are not taken into account, a combination of the pyrolysis plant with a CHP (scenario II) is economically more profitable (Table 47). However, as soon as a PO-reactor and a halogen-filter are necessary, scenario I becomes most profitable again.

Table 47: Internal rates of return (*IRR*, in %) with and without earnings for the sale of heat in the different scenarios (Sc).

<i>IRR</i> [%]	Free of burdens			Imputed earning		
	Sc I	Sc II	Sc III	Sc I	Sc II	Sc III
Sale of Heat (31.6 €·MWh⁻¹)	20.78	14.68	9.96	34.28	26.20	19.78
No Earnings for Heat	4.93	6.72	-2.31	20.72	19.63	10.49

Notwithstanding the results clearly revealed the economic benefits of scenario I, it should be considered that for an installation the actual situation in Germany was presumed. Mainly regards imputed earnings and earnings for power and heat, results could be strongly changed under different circumstances such as the country, where the system will be installed. Additionally, in the cases of smaller systems, an installation of a CHP could bring proportionately more earnings.

8. Conclusions

With the aim to develop and to optimize a thermo-chemical process in order to enable metal recycling from shredder residues of WEEE, liquid crystal displays (LCD), and tantalum (Ta) capacitors as well as to dehalogenate corresponding products, the following conclusions can be made from the experiments.

Bench scale plant: Due to a very modular and adaptive design of the developed bench scale plant not only conventional pyrolysis tests, but also co-pyrolysis and vapor-phase mode tests can be conducted. Additionally, an optimized design of a polyolefin-reactor (PO-reactor) and a new development of a halogen-filter enable a continuous dehalogenation of pyrolysis vapor simultaneously to its formation from pyrolysis tests.

Metal concentrates from shredder residues: In order to obtain valuable metal concentrates from shredder residues, it is necessary to depollute solid products. Statistical evaluations of pyrolysis tests confirmed the well known facts that temperature, residence time, and heating rate are the most influencing parameters on the formation of highly-toxic polyhalogenated dibenzo-*p*-dioxins and furans (PXDD/F). In addition, an iterative experimental approach revealed that a heating rate of $>150 \text{ K} \cdot \text{min}^{-1}$, a temperature of $650 \text{ }^{\circ}\text{C}$, and a residence time of 30 min are the optimum process conditions enabling safe decontamination. These make it possible to receive a solid product, which does not exceed any PXDD/F threshold values of the relevant German act on restriction of chemicals (GGVSEB) and the German chemicals prohibition ordinance (ChemVerbotsV). Therefore, a safe downstream recycling of metals from shredder residues could be enabled for the first time. Allocation analyses revealed that cadmium (Cd), indium (In), and molybdenum (Mo) were mobilized with up to 100 wt.-% to pyrolysis vapor. This can be used to enable selective recovery of these metals from WEEE fractions in order to enable adequate, subsequent metal recycling. Statistical evaluations revealed that these mobilizations are mainly based on halogenation reactions and subsequent vaporization of halides.

Separation and recovery of critical metals: Tests concerning the recovery of critical metals from WEEE have shown that pyrolysis at temperatures of $550 \text{ }^{\circ}\text{C}$ in combination with sizing at $500 \text{ }\mu\text{m}$ enable an efficient separation of niobium (Nb) and Ta from corresponding capacitors, because up to 86.5 wt.-% of sintered Ta pellets decomposed to fine powder ($<500 \text{ }\mu\text{m}$) while Nb particles stood unchanged above $1\,000 \text{ }\mu\text{m}$.

Halogenation and mobilization of metals from LCD: Tests with LCD and waste polyvinyl chloride (PVC) as chlorine donator for halogenation and subsequent mobilization of metals revealed the potential of halogenation reactions: While co-pyrolysis of LCD and PVC can be used to completely depollute LCD regarding arsenic (As), vapor-phase mode tests enabled a selective mobilization of In. In both cases metals allocated to pyrolysis liquid products, from which they can be recovered using precipitation and/or electrolytic winning.

Dehalogenation of pyrolysis liquid products: High-resolution gas chromatography/mass spectrometry (HR GC-MS) analyses for quantification of PXDD/F in pyrolysis liquid products have shown that an increase of pyrolysis temperature decreases PXDD/F concentrations significantly; however, that also even at a temperature of 650 °C four of five threshold values of the GGVSEB / ChemVerbotsV are exceeded. Therefore, polypropylene (PP) was successfully used as hydrogen donating substance in the PO-reactor in order to decompose PXDD/F. HR GC-MS analyses evidenced the first time that in such a combination PP is not only able to decompose polybrominated dibenzo-*p*-dioxins (PBDD) (-100 %), but also corresponding brominated furans (-77.2 %) as well as chlorinated dioxins (-56.3 %) and furans (-62.1 %). To enable a further or even complete decomposition of PXDD/F, PP was blended with LaOOH, which shows superior characteristics regarding ability of halogenation and as catalyst: LaOOH was halogenated by hydrocarbons like PXDD under formation of LaOX, which was afterwards dehalogenated with steam under formation of HX. Thus, a complete decomposition of polyhalogenated dibenzo-*p*-dioxins (PXDD) was achieved the first time.

In order to develop a three-dimensional filter material, which can be streamed by gases, glass spheres were coated with La_2O_3 . Laboratory tests represented that more than 90 wt.-% of Br_2 and HBr can be absorbed from hot vapor. Further tests revealed that even for pyrolysis vapor a depletion of 58.5 wt.-% of Br and 63.1 wt.-% of Cl can be achieved. These findings revealed that the combination of PO-reactor and halogen-filter enables the formation of pyrolysis by-products which could be either processed as bulk chemical in the petrochemical industry and/or could be used energetically.

From tests with both PO-reactor and halogen-filter it can not only be concluded that the quality of pyrolysis liquid products were improved concerning an energetic utilization in a combined heat and power plant (CHP), but also that due to decomposition of PP a flexible and selectable fuel production is feasible: the controllable thermal decomposition of PP due to variation of the process temperature enables an enrichment of long-chained hydrocarbons in the liquid product. Thus, relevant parameters and characteristics of the potential fuel, mainly cetane-index and distillation-ranges, can be adapted to the operator's application. Therefore, the developments show the first process combination, in which WEEE could be treated safely, while quality aspects of the fuel are adapted simultaneously, but independent.

Sustainability assessment: An economic and ecological assessment of the pyrolysis process in a pilot plant scale revealed that the positive effects created by a treatment of shredder residues using pyrolysis exceed a treatment in a municipal waste incinerator (MWI) by factors of up to 55.5. From the view of a WEEE treatment plant operator, a pyrolysis process – even with a capacity of just $70 \text{ kg} \cdot \text{h}^{-1}$ – could reach an internal rate of return *IRR* between 9.96 and 34.28 % depending on the type of energetic utilization and calculations regarding imputed earnings. Corresponding payback periods even from dynamic calculations showed values between 3 and 7 years.

9. Outlook

In the present thesis, main parameters for a construction of a continuous plant for treating WEEE were defined. In this way it has been possible to design a pilot plant with a capacity of $70 \text{ kg}\cdot\text{h}^{-1}$. Furthermore, a heat exchanging system, which allows achieving superior heating rates in order to avoid PXDD/F formations was developed, designed, and patented. Based on these achievements, the machine building company Kautz Technologies GmbH (Willstätt-Legelshurst, Germany) was won as a partner in order to construct the first continuous pilot plant.

The reactor of the pilot plant shows an externally and internally heated screw conveyor with a length of approximately 3 900 mm and an inner diameter of approximately 500 mm (Figure 86). The entire work on this pilot plant is part of a project called "gagendta+"³⁸, which is founded by the German Federal Ministry of Education and Research (BMBF) between June 2015 and May 2018. In combination with the pyrolysis pilot plant, a stirred sphere reactor with three inner screw conveyers will be installed for decomposition of polyhalogenated aromatic hydrocarbons (PXAH) in pyrolysis vapor.

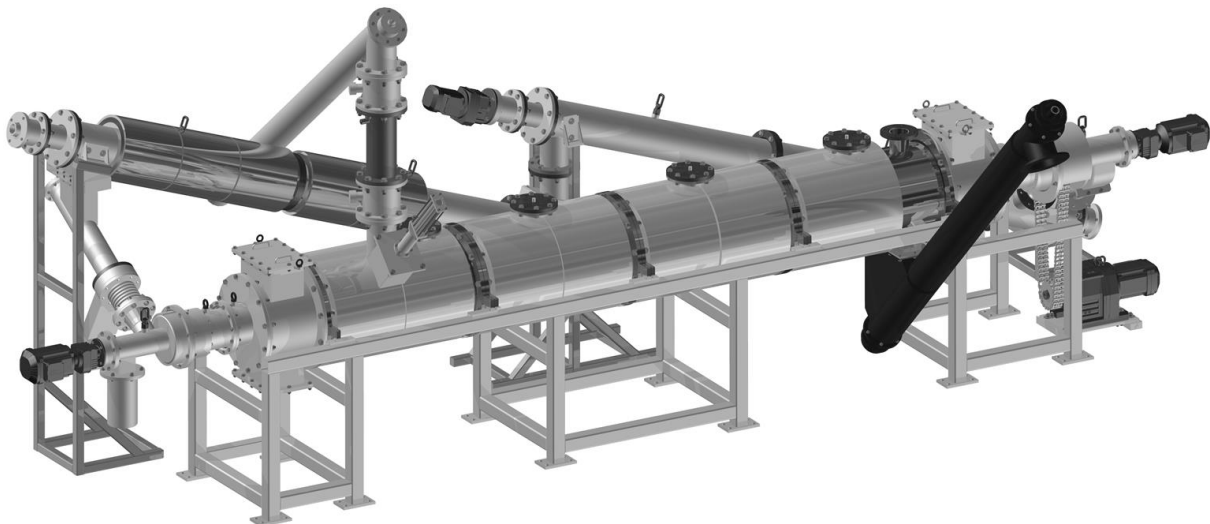


Figure 86: CAD drawing of a pyrolysis pilot plant for 70 kg shredder residues per hour [Kautz 2016].

Not only due to an increasing percentage of sophisticated mechanical treatment of WEEE, but also due to the steadily increasing miniaturization of electrical and electronic equipment (EEE), the unique point of the developed process is to liberate and accumulate metals simultaneously to a formation of valuable by-products. Therefore, the thermo-chemical process will be a key-technology for future decentralized WEEE treatment operators.

³⁸ Support code: 033R146; founding directive: "r⁴ - Innovative Technologien für Ressourceneffizienz – Forschung zur Bereitstellung wirtschaftsstrategischer Rohstoffe".

Overall, a thermo-chemical treatment could be used to enable recycling of not yet treated WEEE and special parts of it to increase end of life recycling rates (EoL-RR) of WEEE. Taking different situations of WEEE treatment in various states and regions world-wide into account, specific pyrolysis plants and designs should be considered. For instance, in industrial nations such as Italy or Germany, a thermo-chemical treatment could enable a recycling of metals and a recovery of energy from mainly shredder residues and some mechanically separable components containing critical metals. In contrast, in regions with low labor costs and/or low levels of mechanical treatment, pyrolysis plants could be installed in order to treat different manually disassembled fractions such as printed wiring boards (PWB) in order to ship highly concentrated metal fractions to copper smelters while organic matter could be used locally to produce power and heat. Additionally, fractions with harmful substances such as plastics with BFR, which could not be sold, could be treated similar to produce power and heat as well as to capture halogens safely. Furthermore, in countries such as emerging markets with low labor costs but good levels of education, a separation of very special fractions such as Ta capacitors could be conducted. These can be afterwards treated locally in pyrolysis plants to produce marketable concentrates for recycling.

Besides treatment of fractions from WEEE for a recovery of metals and energy, the developed and optimized processes also show much promise in processing other waste fractions such as shredder light materials from automotive recycling. Additionally, a selective mobilization and recovery of materials containing either harmful substances, such as As, or scarce and valuable metals, such as In, seems feasible by halogenation similar to those reactions described for LCD.

References

- Agorhom et al. 2015 Agorhom, E. A.; Lem, J. P.; Skinner, W.; Zanin, M. (2015): Challenges and opportunities in the recovery/rejection of trace elements in copper flotation-a review. In: Minerals Engineering, 78, pp. 45 - 57.
- Ahmed 2004 Ahmed, Y. M. (December 2004): Removal of hazardous oxyanion pollutants by Lanthanum (III) hydroxide and Lanthanum (III) -loaded ion exchangers. Master Thesis. Putra Malaysia.
- Alston et al. 2011 Alston, S. M.; Clark, A. D.; Arnold, J. C.; Stein, B. K. (2011): Environmental Impact of Pyrolysis of Mixed WEEE Plastics Part 1: Experimental Pyrolysis Data. In: Environmental Science & Technology, 45(21), pp. 9380 - 9385.
- Andersson et al. 2012 Andersson, M.; Knutson Wedel, M.; Forsgren, C.; Christéen, J. (2012): Microwave assisted pyrolysis of residual fractions of waste electrical and electronics equipment. In: Minerals Engineering, 29, pp. 105 - 111.
- Angerer et al. 2009 Angerer, G.; Erdmann, L.; Marscheider-Weidemann, F.; Scharp, M.; Lüllmann, A.; Handke, V.; Marwede, M. (2009): Rohstoffe für Zukunftstechnologien. Einfluss des branchenspezifischen Rohstoffbedarfs in rohstoffintensiven Zukunftstechnologien auf die zukünftige Rohstoffnachfrage. Stuttgart (ISI-Schriftenreihe "Innovationspotenziale").
- Bakas et al. 2014 Bakas, I.; Fischer, C.; Haselsteiner, S.; McKinnon, D.; Milios, L.; Harding, A.; Kosmol, J.; Plepys, A.; Tojo, N.; Wilts, H.; Wittmer, D. (November 2014): Present and potential future recycling of critical metals in WEEE. Copenhagen.
- Bakas et al. 2016 Bakas, I.; Herczeg, M.; Veä, E. B.; Fråne, A.; Youhanan, L.; Baxter, J. (2016): Critical metals in discarded electronics. Mapping recycling potentials from selected waste electronics in the Nordic region. Copenhagen (2016). Last time checked: 2016, September 23. <http://norden.diva-portal.org/smash/record.jsf?pid=diva2%3A936670&dswid=9407>.

-
- Balabanovich et al. 2004 Balabanovich, A.I.; Hornung, A.; Merz, D.; Seifert, H. (2004): The effect of a curing agent on the thermal degradation of fire retardant brominated epoxy resins. In: *Polymer Degradation and Stability*, 85(1), pp. 713 - 723.
- Balabanovich et al. 2005a Balabanovich, A. I.; Luda, M. P.; Operti, L. (2005): GC/MS Identification of Pyrolysis Products from Fire-retardant Brominated Epoxy Resin. In: *Journal of Fire Sciences*, 23(3), pp. 227 - 245.
- Balabanovich et al. 2005b Balabanovich, A. I.; Hornung, A.; Luda, M. P.; Koch, W.; Tumiatto, V. (2005): Pyrolysis Study of Halogen-Containing Aromatics Reflecting Reactions with Polypropylene in a Posttreatment Decontamination Process. In: *Environmental Science & Technology*, 39(14), pp. 5469 - 5474.
- BDBe 2016 BDBe Bundesverband der deutschen Bioethanolwirtschaft e.V. (BDBe) (2016): Umrechnungsformeln für Biokraftstoffe. Last time checked: 2016, October 30. <https://www.bdbe.de/daten/umrechnung-und-formeln>.
- Bhaskar et al. 2002 Bhaskar, T.; Matsui, T.; Kaneko, J.; Uddin, Md. A.; Muto, A.; Sakata, Y. (2002): Novel calcium based sorbent (Ca-C) for the dehalogenation (Br, Cl) process during halogenated mixed plastic (PP/PE/PS/PVC and HIPS-Br) pyrolysis. In: *Green Chemistry*, 4(4), pp. 372 - 375.
- Bhaskar et al. 2003a Bhaskar, T.; Matsui, T.; Uddin, Md. A.; Kaneko, J.; Muto, A.; Sakata, Y. (2003): Effect of Sb_2O_3 in brominated heating impact polystyrene (HIPS-Br) on thermal degradation and debromination by iron oxide carbon composite catalyst (Fe-C). In: *Applied Catalysis B: Environmental*, 43(3), pp. 229 - 241.
- Bhaskar et al. 2003b Bhaskar, T.; Murai, K.; Matsui, T.; Brebu, Mihai Adrian; Uddin, Md. A.; Muto, A.; Sakata, Y.; Murata, K. (2003): Studies on thermal degradation of acrylonitrile–butadiene–styrene copolymer (ABS-Br) containing brominated flame retardant. In: *Journal of Analytical and Applied Pyrolysis*, 70(2), pp. 369 - 381.
- Bhaskar et al. 2004 Bhaskar, T.; Kaneko, J.; Muto, A.; Sakata, Y.; Jakab, E.; Matsui, T.; Uddin, Md. A. (2004): Pyrolysis studies of PP/PE/PS/PVC/HIPS-Br plastics mixed with PET and dehalogenation (Br, Cl) of the liquid products. In: *Journal of Analytical and Applied Pyrolysis*, 72(1), pp. 27 - 33.

-
- Bhaskar et al. 2006 Bhaskar, T.; Negoro, R.; Muto, A.; Sakata, Y. (2006): Prevention of chlorinated hydrocarbons formation during pyrolysis of PVC or PVDC mixed plastics. In: Green Chemistry, 8(8), pp. 697 - 700.
- Birnbaum et al. 2003 Birnbaum, L.; Staskal, Daniele F.; Diliberto, Janet J. (2003): Health effects of polybrominated dibenzo-*p*-dioxins (PBDDs) and dibenzofurans (PBDfFs). In: Environment International, 29(6), pp. 855 - 860.
- Blaser et al. 2011 Blaser, F.; Castelanelli, S.; Wäger, P.; Widmer, R. (23.12.2011): Seltene Metalle in Elektro- und Elektronikaltgeräten. Vorkommen und Rückgewinnungstechnologien. Bern.
- Blazsó et al. 1995 Blazsó, M.; Zelei, B.; Jakab, E. (1995): Thermal decomposition of low-density polyethylene in the presence of chlorine-containing polymers. In: Journal of Analytical and Applied Pyrolysis, 35(2), pp. 221 - 235.
- Blazsó, Jakab 1999 Blazsó, M.; Jakab, E. (1999): Effect of metals, metal oxides, and carboxylates on the thermal decomposition processes of poly (vinyl chloride). In: Journal of Analytical and Applied Pyrolysis, 49(1-2), pp. 125 - 143.
- Blazsó et al. 2002 Blazsó, M.; Czégény, Z.; Csoma, C. (2002): Pyrolysis and debromination of flame retarded polymers of electronic scrap studied by analytical pyrolysis. In: Journal of Analytical and Applied Pyrolysis, 64(2), pp. 249 - 261.
- BMUB 1990 Federal Ministry for the Environment, Nature Conservation, Building and Nuclear Safety (BMUB) (23.11.1990): Siebzehnte Verordnung zur Durchführung des Bundes-Immissionsschutzgesetzes (Verordnung über die Verbrennung und die Mitverbrennung von Abfällen - 17. BImSchV).
- Bockhorn et al. 1998 Bockhorn, H.; Hornung, A.; Hornung, U. (1998): Stepwise pyrolysis for raw material recovery from plastic waste. In: Journal of Analytical and Applied Pyrolysis, 46(1), pp. 1 - 13.
- Bockhorn et al. 1999 Bockhorn, H.; Hornung, A.; Hornung, U.; Jakobströer, P.; Kraus, M. (1999): Dehydrochlorination of plastic mixtures. In: Journal of Analytical and Applied Pyrolysis, 49(1-2), pp. 97 - 106.

-
- Boerrigter et al. 2002 Boerrigter, Harold; Oudhuis, André B. J.; Tange, Lein (01.02.2002): Bromine Recovery from the Plastics Fraction of Waste of Electrical and Electronic Equipment (WEEE) with stages Gasification. Brussels.
- Boliden 2016 Boliden Group (2016): Copper. Last time checked: 2016, October 30. <http://www.boliden.com/Products/Copper/>.
- Borojovich, Aizenshtat 2002a Borojovich, E. J. C.; Aizenshtat, Z. (2002): Thermal behavior of brominated and polybrominated compounds I. Closed vessel conditions. In: Journal of Analytical and Applied Pyrolysis, 63(1), pp. 105 - 128.
- Borojovich, Aizenshtat 2002b Borojovich, E. J. C.; Aizenshtat, Z. (2002): Thermal behavior of brominated and polybrominated compounds II. Pyro-products of brominated phenols as mechanistic tools. In: Journal of Analytical and Applied Pyrolysis, 63(1), pp. 129 - 145.
- Brebu et al. 2005 Brebu, M.; Bhaskar, T.; Murai, K.; Muto, Akinori; Sakata, Y.; Uddin, Md. A. (2005): Removal of nitrogen, bromine, and chlorine from PP/PE/PS/PVC/ABS-Br pyrolysis liquid products using Fe- and Ca-based catalysts. In: Polymer Degradation and Stability, 87(2), pp. 225 - 230.
- Brebu et al. 2007 Brebu, M.; Jakab, E.; Sakata, Y. (2007): Effect of flame retardants and Sb₂O₃ synergist on the thermal decomposition of high-impact polystyrene and on its debromination by ammonia treatment. In: Journal of Analytical and Applied Pyrolysis, 79(1-2), pp. 346 - 352.
- Brumby et al. 2006 Brumby, A.; Hagelüken, C.; Lox, E.; Kleinwächter, I. (2006): Edelmetalle. In: Winnacker, Karl; Küchler, Leopold (Eds.): Chemische Technik. Prozesse und Produkte. 5th edition. Weinheim: Wiley-VCH, pp. 209 - 276.
- Brusselaers et al. 2016 Brusselaers, J.; Mark, F. E.; Tange, L. (November 2016): Using metal-rich WEEE plastics as feedstock / fuel substitute for an integrated metals smelter. A Technical Report produced by: PlasticsEurope in cooperation with Umicore and EFRA. Brussels.
- Buchert et al. 2012 Buchert, M.; Manhart, A.; Bleher, D.; Pingel, D. (2012): Recycling kritischer Rohstoffe aus Elektronik-Altgeräten. LANUV-Fachbericht 38. Recklinghausen.

-
- Buekens 2006 Buekens, A. (2006): Introduction to Feedstock Recycling of Plastics. In: Scheirs, J.; Kaminsky, W. (Eds.): Feedstock recycling and pyrolysis of waste plastics. Converting waste plastics into diesel and other fuels. Chichester, UK, Hoboken, NJ: J. Wiley & Sons, pp. 3 - 41.
- LAGA 2009 Bund/Länder-Arbeitsgemeinschaft Abfall (September 2009): Anforderungen zur Entsorgung von Elektro- und Elektronik-Altgeräten. Mitteilung der Bund/Länder-Arbeitsgemeinschaft Abfall (LAGA) 31. Altgeräte-Merkblatt. Stuttgart.
- Cal-Chip 2016 Cal-Chip Electronics Inc. (2016): Tantalum Capacitor. Material Declaration Data Sheet. Ivlyand. Last time checked: 2016, August 9. www.calchip.com.
- Castro et al. 2012 Castro, A.; Soares, D.; Vilarinho, C.; Castro, F. (2012): Kinetics of thermal de-chlorination of PVC under pyrolytic conditions. In: Waste Management, 32(5), pp. 847 - 851.
- CDC RAEE 2008 CDC RAEE (Centro di Coordinamento RAEE) (2008): Rapporto Annuale 2008. Sul Sistema di ritiro e trattamento dei rifiuti da apparecchiature elettriche ed elettroniche in Italia. Milano.
- CDC RAEE 2009 CDC RAEE (Centro di Coordinamento RAEE) (2009): Rapporto Annuale 2009. Sul Sistema di ritiro e trattamento dei rifiuti da apparecchiature elettriche ed elettroniche in Italia. Milano.
- CDC RAEE 2010 CDC RAEE (Centro di Coordinamento RAEE) (2010): Rapporto Annuale 2010. Sul Sistema di ritiro e trattamento dei rifiuti da apparecchiature elettriche ed elettroniche in Italia. Milano.
- CDC RAEE 2011 CDC RAEE (Centro di Coordinamento RAEE) (2011): Rapporto Annuale 2011. Ritiro e trattamento dei rifiuti da apparecchiature elettriche ed elettroniche in Italia. Milano.
- CDC RAEE 2012 CDC RAEE (Centro di Coordinamento RAEE) (2012): Rapporto Annuale 2012. Ritiro e trattamento dei rifiuti da apparecchiature elettriche ed elettroniche in Italia. Milano.
- CDC RAEE 2013 CDC RAEE (Centro di Coordinamento RAEE) (2013): Rapporto Annuale 2013. Ritiro e trattamento dei rifiuti da apparecchiature elettriche ed elettroniche in Italia. Milano.

-
- CDC RAEE 2014 CDC RAEE (Centro di Coordinamento RAEE) (2014): Rapporto Annuale 2014. Ritiro e trattamento dei rifiuti da apparecchiature elettriche ed elettroniche in Italia. Milano.
- Chancerel et al. 2009 Chancerel, P.; Meskers, C. E. M.; Hagelüken, C.; Rotter, V. S. (2009): Assessment of Precious Metal Flows During Preprocessing of Waste Electrical and Electronic Equipment. In: *Journal of Industrial Ecology*, 13(5), pp. 791 - 810.
- Chen et al. 2012 Chen, Y.; Li, J.; Chen, L.; Chen, S.; Diao, W. (2012): Brominated Flame Retardants (BFRs) in Waste Electrical and Electronic Equipment (WEEE) Plastics and Printed Circuit Boards (PCBs). In: *Procedia Environmental Sciences*, 16, pp. 552 - 559.
- Chiang et al. 2007 Chiang, H.-L.; Lin, K.-H.; Lai, M.-H.; Chen, T.-C.; Ma, S.-Y. (2007): Pyrolysis characteristics of integrated circuit boards at various particle sizes and temperatures. In: *Journal of Hazardous Materials*, 149(1), pp. 151 - 159.
- Chien et al. 2005 Chien, Y.-C.; Shih, P.-H.; Hsien, I.-H. (2005): Pyrolysis Kinetics of Liquid Crystal Wastes. In: *Environmental Engineering Science*, 22(5), pp. 601 - 607.
- Chuang et al. 2008 Chuang, C.-S.; Fung, T.-C.; Mullins, B. G.; Nomura, K.; Kamiya, T.; Shieh, H.-P. D.; Hosono, H.; Kanicki, J. (2008): P-13. Photosensitivity of Amorphous IGZO TFTs for Active-Matrix Flat-Panel Displays. In: *SID Symposium Digest of Technical Papers*, 39(1), p. 1215 - 1218.
- Coenen et al. 1979 Coenen, A.; Kosswig, K.; Wienhofer, E. (22.06.79): Verfahren zur Trennung von Chlorwasserstoff und Bromwasserstoff, (0008330).
- Czégény et al. 2012 Czégény, Z.; Jakab, E.; Blazsó, M.; Bhaskar, T.; Sakata, Y. (2012): Thermal decomposition of polymer mixtures of PVC, PET and ABS containing brominated flame retardant: Formation of chlorinated and brominated organic compounds. In: *Journal of Analytical and Applied Pyrolysis*, 96, pp. 69 - 77.

-
- Dehoust, Christiani 2012 Dehoust, G.; Christiani, J. (May 2012): Analyse und Fortentwicklung der Verwertungsquoten für Wertstoffe. Sammel- und Verwertungsquoten für Verpackungen und stoffgleiche Nichtverpackungen als Lenkungsinstrument zur Ressourcenschonung. Im Auftrag des Umweltbundesamts. Dessau-Roßlau (40/2012).
- Destatis 2016 Statistisches Bundesamt (09/27/2016): Preise. Daten zur Energiepreisentwicklung. Wiesbaden (- Lange Reihen von Januar 2000 bis August 2016 -). Last time checked: 2016, October 30.
<https://www.destatis.de/DE/Publikationen/Thematisch/Preise/Energiepreise/Energiepreisentwicklung.html>.
- Dettmer 2001 Dettmer, F. T. (2001): Bromorganische Flammschutzmittel. Analytische Anforderungen und thermische Bildung von polybromierten Dibenzo-*p*-dioxinen und Dibenzofuranen. Dissertation. Braunschweig.
- Dettwiler et al. 1997 Dettwiler, J.; Karlaganis, G.; Studer, C.; Joss, S.; Chambaz, D. (1997): Dioxine und Furane. Standortbestimmung Beurteilungsgrundlagen Massnahmen (Schriftenreihe Umwelt - Umweltgefährdende Stoffe, 290).
- DGUV 2016 Deutsche Gesetzliche Unfallversicherung (DGUV) e.V. (2016): GESTIS-Stoffdatenbank. Last time checked: 2016, October 30. [http://gestis.itrust.de/nxt/gateway.dll?f=templates\\$fn=default.htm\\$vid=gestisdeu:sdbdeu\\$3.0](http://gestis.itrust.de/nxt/gateway.dll?f=templates$fn=default.htm$vid=gestisdeu:sdbdeu$3.0).
- DIN 2008a Deutsches Institut für Normung e.V. (2008): Kosten im Bauwesen - Teil 1: Hochbau, (DIN 276-1:2008-12). December 2008. Berlin: Beuth Verlag.
- DIN 2008b Deutsches Institut für Normung e.V. (2008): Kraftstoffe für Kraftfahrzeuge – Anforderungen und Prüfverfahren – Teil 2: Ottokraftstoff E5 / Automotive fuels – Requirements and test methods – Part 2: Petrol E5, 75.160.20 (DIN 51626-2). January 2008. Berlin: Beuth Verlag.
- DIN 2010 Deutsches Institut für Normung e.V. (2010): Kraftstoffe für Kraftfahrzeuge - Dieselkraftstoff - Anforderungen und Prüfverfahren / Automotive Fuels - Diesel - Requirements and test methods, 75.160.20 (DIN 590). May 2010. Berlin: Beuth Verlag.

-
- Dumler et al. 1989 Dumler, R.; Lenoir, D.; Thoma, H.; Hutzinger O. (1989): Thermal formation of polybrominated dibenzofurans from decabromodiphenyl ether in a polybutylene-terephthalate polymer matrix. In: Journal of Analytical and Applied Pyrolysis, 16(2), pp. 153 - 158.
- EAR 2016 EAR Stiftung Elektro-Altgeräte Register (2016): Verzeichnis der Betreiber von Erstbehandlungsanlagen. Last time checked: 2016, October 30. <https://www.ear-system.de/ear-verzeichnis/eba.jsf>.
- Ebert, Bahadir 2003 Ebert, J.; Bahadir, M. (2003): Formation of PBDD/F from flame-retarded plastic materials under thermal stress. In: Environment International, 29(6), pp. 711 - 716.
- Ecoinvent 2016 ecoinvent Association (2016): ecoinvent. Last time checked: 2016, October 30. www.ecoinvent.org.
- EFRA 2007 The European Flame Retardants Association (EFRA) (January 2007): Flame Retardants. Frequently Asked Questions. Brussels.
- ElektroG 2005 ElektroG (2005): Gesetz über das Inverkehrbringen, die Rücknahme und die umweltverträgliche Entsorgung von Elektro- und Elektronikgeräten. Elektro- und Elektronikgerätegesetz – ElektroG (16.03.2005).
- Eljarrat, Barceló 2004 Eljarrat, E.; Barceló, D. (2004): Toxicity Potency Assessment of Persistent Organic Pollutants in Sediments and Sludges. In: Barceló, D. (Ed.): Series anthropogenic compounds. Emerging organic pollution in waste waters and sludge. Berlin, Heidelberg: Springer, pp. 99 - 140.
- ESG 2016 Edelmetall-Service GmbH & Co. KG (ESG) (2016): ESG Edelmetalle Scheideanstalt. Last time checked: 2016, October 30. <https://www.scheideanstalt.de/>.
- Esquivel et al. 2003 Esquivel, M. R.; Bohé, A. E.; Pasquevich, D. M. (2003): Chlorination of cerium dioxide. In: Thermochimica Acta, 398(1-2), pp. 81 - 91.
- Esquivel et al. 2005 Esquivel, M. R.; Bohé, A. E.; Pasquevich, D. M. (2005): Chlorination of samarium sesquioxide. In: Journal of Materials Processing Technology, 170(1-2), pp. 304 - 309.

-
- EC 2014 European Commission (May 2014): Report on critical raw materials for the EU. Report of the Ad hoc Working Group on defining critical raw materials.
- Eurostat 2016 European Commission (2016): Waste electrical and electronic equipment (WEEE) by waste operations. Last time checked: 2016, October 30. http://appsso.eurostat.ec.europa.eu/nui/show.do?dataset=env_waselee&lang=de.
- Eurostat 2017 European Commission (2017): Waste electrical and electronic equipment (WEEE) by waste operations. Last time checked: 2017, February 2. http://appsso.eurostat.ec.europa.eu/nui/show.do?dataset=env_waselee&lang=de.
- EEX 2016 European Energy Exchange AG (EEX) (2016): KWK Index - Download. Üblicher Strompreis gemäß KWK-Gesetz. Last time checked: 2016, October 30. <http://www.eex.com/de/marktdaten/strom/spotmarkt/kwk-index/kwk-index-download>.
- Eionet 2013 European Topic Centre on Sustainable Consumption and Production (2013): What is waste? Last time checked: 2015, June 15. <http://scp.eionet.europa.eu/themes/waste/#6>.
- EU 2003a The European Parliament and the Council of the European Union (13.02.2003): Directive 2002/96/EC of the European Parliament and of the Council of 27 January 2003 on waste electrical and electronic equipment (WEEE).
- EU 2003b The European Parliament and the Council of the European Union (13.02.2003): Directive 2002/95/EC of the European Parliament and of the Council of 27 January 2003 on the restriction of the use of certain hazardous substances in electrical and electronic equipment.
- EU 2011 The European Parliament and the Council of the European Union (01.07.2011): Directive 2011/65/EU of the European Parliament and the Council of 8 June 2011 on the restriction of the use of certain hazardous substances in electrical and electronic equipment.
- EU 2012 The European Parliament and the Council of the European Union (24.07.2012): Directive 2012/19/EU of the European Parliament and of the Council of 4 July 2012 on waste electrical and electronic equipment (WEEE).

-
- EU 2015 The European Parliament and the Council of the European Union (04.06.2015): Commission delegated Directive (EU) 2015/863 of 31 March 2015 amending Annex II to Directive 2011/65/EU of the European Parliament and of the Council as regards the list of restricted substances.
- EUWID (40.2016) EUWID-Preisspiegel: Altkunststoffe Deutschland. September 2016. In: Katz, Casimir (Ed.): EUWID Recycling und Entsorgung. Gernsbach, p. 22.
- EUWID (41.2016) Preisbericht für Altmetalle. 05.10.2016 . In: Katz, Casimir (Ed.): EUWID Recycling und Entsorgung. Gernsbach, p. 17.
- EUWID (43.2016a) EUWID-Preisspiegel: Standard-Kunststoffe Deutschland (Neuware). In: Katz, Casimir (Ed.): EUWID Recycling und Entsorgung. Gernsbach, p. 25.
- EUWID (43.2016b) EUWID-Preisspiegel: Technische Kunststoffe Deutschland (Neuware). Oktober 2016. In: Katz, Casimir (Ed.): EUWID Recycling und Entsorgung. Gernsbach, p. 20.
- Evans et al. 1991 Evans, D. H.; Pirbazari, M.; Benson, S. W.; Tsotsis, T. T.; Devanny, J. S. (1991): Pyrolytic destruction of polychlorinated biphenyls in a reductive atmosphere. In: Journal of Hazardous Materials, 27(3), pp. 253 - 272.
- Fabbri 2001 Fabbri, D. (2001): Use of pyrolysis-gas chromatography/mass spectrometry to study environmental pollution caused by synthetic polymers. A case study: the Ravenna Lagoon. In: Journal of Analytical and Applied Pyrolysis, 58-59, pp. 361 - 370.
- Fehér et al. 1953 Fehér, F.; Hecht, H.; Herr, W.; Schneider, A. (1953): Elemente der Siebenten Gruppe. Fluor · Chlor · Brom · Jod · Mangan · Technetium · Rhenium. Berlin, Heidelberg: Springer.
- Fels et al. 2016 Fels, G.; Kamp, O.; Biele, C. (2016): Reaktionen an Aromaten (gesamt). Halogenierung. Last time checked: 2016, October 30.
- Finnveden 1999 Finnveden, G. (1999): Methodological aspects of life cycle assessment of integrated solid waste management systems. In: Resources, Conservation and Recycling, 26(3-4), pp. 173 - 187.

-
- Fujita et al. 2014 Fujita, T.; Ono, H.; Dodbiba, G.; Yamaguchi, K. (2014): Evaluation of a recycling process for printed circuit board by physical separation and heat treatment. In: Waste Management, 34(7), pp. 1264 - 1273.
- Gaggl et al. 2014 Gaggl, M.; Müller, W.; Bockreis, A. (2014): Pyrolyse ausgewählter Metallmischabfälle. Ein wertstofforientierter Ansatz. In: Deutsche Gesellschaft für Abfallwirtschaft e.V. (DGAW) (Ed.): 4. Wissenschaftskongress Abfall- und Ressourcenwirtschaft, pp. 45 - 49.
- Gaviría, Bohé 2009 Gaviría, J. P.; Bohé, A. E. (2009): The Kinetics of the Chlorination of Yttrium Oxide. In: Metallurgical and Materials Transactions B, 40(1), pp. 45 - 53.
- Gaviría et al. 2012 Gaviría, J. P.; Navarro, L. G.; Bohé, A. E. (2012): Chlorination of lanthanum oxide. In: The journal of physical chemistry. A, 116(9), pp. 2062 - 2070.
- Geis 2015 Geis, Hans GmbH + Co KG (27.08.2015): Telefonische Preisauskunft vom 27.08.2015. Bad Neustadt.
- Goosey 2012 Goosey, M. (2012): The materials in WEEE. In: Goodship, Vanessa; Stevels, Ab (Eds.): Waste electrical and electronic equipment (WEEE) handbook. Cambridge, UK, Philadelphia: Woodhead Publishing, pp. 123 - 144.
- Grabda et al. 2011 Grabda, M.; Oleszek-Kudlak, S.; Shibata, E.; Nakamura, T. (2011): Vaporization of zinc during thermal treatment of ZnO with tetrabromobisphenol A (TBBPA). In: Journal of Hazardous Materials, 187(1-3), pp. 473 - 479.
- Graedel et al. 2011 Graedel, T. E.; Allwood, Julian; Birat, Jean-Pierre; Buchert, Matthias; Hagelüken, Christian; Reck, Barbara K.; Sibley, Scott F.; Sonnemann, Guido (2011): Recycling rates of metals. A status report. A report of the Working Group on the Global Metal Flows to the International Resource Panel. Nairobi, Kenya.
- Grause et al. 2008 Grause, G.; Furusawa, M.; Okuwaki, A.; Yoshioka, T. (2008): Pyrolysis of tetrabromobisphenol-A containing paper laminated printed circuit boards. In: Chemosphere, 71(5), pp. 872 - 878.

-
- Grause et al. 2012 Grause, G.; Karakita, D.; Kameda, T.; Bhaskar, T.; Yoshioka, T. (2012): Effect of heating rate on the pyrolysis of high-impact polystyrene containing brominated flame retardants. Fate of brominated flame retardants. In: *Journal of Material Cycles and Waste Management*, 14(3), pp. 259 - 265.
- Green 1996 Green, J. (1996): Mechanisms for flame retardancy and smoke suppression – a review. In: *The Fire Retardant Chemicals Association (Ed.): Flame retardants 101: Basic dynamics past efforts create future opportunities. Past efforts create future opportunities*, pp. 13 - 30.
- GSB 2016 Sonderabfall-Entsorgung Bayern (GSB) GmbH (08.06.2016): Preisabfrage vom 08.06.2016. Baar-Ebenhausen.
- Guinée et al. 2002 Guinée, J. B.; Gorée M.; Heijungs, R.; Huppes, G.; Kleijn, R.; Koning A. de; Oers L. van; Wegener S., A.; Suh. S.; Udo de H., H. A.; Bruijn H. de; van Duin, R.; Huujbregts, M. A. J. (May 2002): *Handbook of Life Cycle Assessment. Operational Guide to the ISO Standards*. Dordrecht: Kluwer Academic Publishers.
- Gupta, Viswanath 1998 Gupta, M. C.; Viswanath, S. G. (1998): Role of Metal Oxides in the Thermal Degradation of Poly(vinyl chloride). In: *Industrial & Engineering Chemistry Research*, 37, pp. 2707 - 2712.
- Hagelüken 2010 Hagelüken, C. (2010): Edelmetallrecycling - Status und Entwicklungen. In: *Fachausschuss für Metallurgische Aus- und Weiterbildung der GDMB (Ed.): Sondermetalle und Edelmetalle*, pp. 163 - 178.
- Hagelüken, Corti 2010 Hagelüken, C.; Corti, C. W. (2010): Recycling of gold from electronics: Cost-effective use through 'Design for Recycling'. In: *Gold Bulletin*, 43(3), pp. 209 - 220.
- Haig et al. 2012 Haig, S.; Morrish, L.; Morton, R.; Wilkinson, S. (October 2012): Electrical product material composition. Overview of updated data within the Market Flows Model of Electronic Products. Overview. Oxon. www.wrap.org.uk.
- Hall, Williams 2006 Hall, W. J.; Williams, P. T. (2006): Fast Pyrolysis of Halogenated Plastics Recovered from Waste Computers. In: *Energy & Fuels*, 20(4), pp. 1536 - 1549.

-
- Hall et al. 2007 Hall, W. J.; Mitan, N. M. M.; Bhaskar, T.; Muto, A.; Sakata, Y.; Williams, P. T. (2007): The co-pyrolysis of flame retarded high impact polystyrene and polyolefins. In: *Journal of Analytical and Applied Pyrolysis*, 80(2), pp. 406 - 415.
- Hall, Williams 2007a Hall, W. J.; Williams, P. T. (2007): Analysis of products from the pyrolysis of plastics recovered from the commercial scale recycling of waste electrical and electronic equipment. In: *Journal of Analytical and Applied Pyrolysis*, 79(1-2), pp. 375 - 386.
- Hall, Williams 2007b Hall, W. J.; Williams, P. T. (2007): Separation and recovery of materials from scrap printed circuit boards. In: *Resources, Conservation and Recycling*, 51(3), pp. 691 - 709.
- Hall, Williams 2008 Hall, W. J.; Williams, P. T. (2008): Removal of organo-bromine compounds from the pyrolysis oils of flame retarded plastics using zeolite catalysts. In: *Journal of Analytical and Applied Pyrolysis*, 81(2), pp. 139 - 147.
- Hall et al. 2008 Hall, W. J.; Miskolczi, N.; Onwudili, J.; Williams, P. T. (2008): Thermal Processing of Toxic Flame-Retarded Polymers Using a Waste Fluidized Catalytic Cracker (FCC) Catalyst. In: *Energy & Fuels*, 22(3), pp. 1691 - 1697.
- Heijungs et al. 1992 Heijungs, R.; Guinée, J. B.; Huppes, G.; Lankreijer, R. M.; Udo de H., H. A.; Wegener S., A. (1992): Environmental life cycle assessment of products. Leiden: Centre of Environmental Science.
- Heijungs et al. 2004 Heijungs, R.; Koning, A. de; Ligthart, T.; Korenromp, R. (August 2004): Improvement of LCA characterization factors and LCA practice for metals. Apeldoorn (TNO-Report, R 2004/347). Last time checked: 2016, October 30. <http://media.leidenuniv.nl/legacy/final%20report%20metals.pdf>.
- Helsen, van del Bulk 2005 Helsen, L; van den Bulck; E. (2005): Review of disposal technologies for chromated copper arsenate (CCA) treated wood waste, with detailed analyses of thermochemical conversion processes. In: *Environmental Pollution*, 134, pp. 301 - 314.
- Hense 2013 Hense, P. (18.09.2013): Erstellung eines ökologischen Bewertungsmodells zur Metallgewinnung aus mineralischen Rückständen. Master Thesis. München.

-
- Hense et al. 2015a Hense, P.; Reh, K.; Franke, M.; Aigner, J.; Hornung, A.; Contin, A. (2015): Pyrolysis of waste electrical and electronic equipment (WEEE) for recovering metals and energy: Previous achievements and current approaches. In: Environmental Engineering and Management Journal, 14(7), pp. 1637 - 1647.
- Hense et al. 2015b Hense, P.; Reh, K.; Franke, M.; Aigner, J.; Mayer, D.; Hornung, A.; Contin, A. (2015): Pyrolysis - A Key Component for the Recovery of Metals and Energy. In: Cossu, R.; He, P.; Kjeldsen, P.; Matsufuji, Y.; Reinhart, D.; Stegmann, R. (Eds.): 15th International WWaste Management and Landfill Symposium. Sardinia 2015, p. 323.
- Hense et al. 2016 Hense, P.; Reh, K.; Franke, M.; Hornung, A. (2016): Dezentrale Rückgewinnung von Hightech-Metallen. In: Teipel, Ulrich; Reller, Armin (Eds.): 4. Symposium Rohstoffeffizienz und Rohstoffinnovationen. Stuttgart: Fraunhofer Verlag, pp. 89 - 99.
- Holleman, Wiberg 2007 Holleman, Arnold F.; Wiberg, Egon; Wiberg, Nils (2007): Lehrbuch der anorganischen Chemie, 102nd edition. Berlin, New York: de Gruyter.
- Horikawa et al. 1999 Horikawa, S.; Takai, Y.; Ukei, H.; Azuma, N.; Ueno, A. (1999): Chlorine gas recovery from polyvinyl chloride. In: Journal of Analytical and Applied Pyrolysis, 51(1-2), pp. 167 - 179.
- Hornung 1997 Hornung, A. (1997): Entwicklung eines Verfahrens zur fraktionierten thermischen Zersetzung von Kunststoffgemischen. Dissertation. Kaiserslautern.
- Hornung et al. 2003 Hornung, A.; Balabanovich, A. I.; Donner, S.; Seifert, H. (2003): Detoxification of brominated pyrolysis oils. In: Journal of Analytical and Applied Pyrolysis, 70(2), pp. 723 - 733.
- Hornung et al. 2005 Hornung, A.; Donner, S.; Balabanovich, A. I.; Seifert, H. (2005): Polypropylene as a reductive agent for dehalogenation of brominated organic compounds. In: Journal of Cleaner Production, 13(5), pp. 525 - 530.

-
- Hornung et al. 2007 Hornung, A.; Schöner, J.; Seifert, H.; Tumiatti, V. (2007): Pyrolyse von Elektronikschrott. In: Thomé-Kozmiensky, Karl; Versteyl, Andrea; Beckmann, Michael (Eds.): Produktverantwortung. Verpackungsabfälle Elektro- und Elektronikaltgeräte Altfahrzeuge, pp. 367 - 372.
- Huisman et al. 2015 Huisman, J.; Botezatu, I.; Herreras, L.; Liddane, M.; Hintsa, J.; Di Luda Cortemiglia, V.; Leroy, P.; Vermeersch, E.; Mohanty, S.; van den Brink, S.; Ghenciu, B.; Dimitrova, D.; Nash, E.; Shryane, T.; Wieting, M.; Kehoe, J.; Baldé, C. P.; Magalini, F.; Zanasi, A.; Ruini, F.; Bonzio, A. (30 August 2015): Countering WEEE Illegal Trade (CWIT) Summary Report. Market Assessment, Legal Analysis, Crime Analysis and Recommendations Roadmap. Lyon. 978-92-808-4559-4.
- Huseman et al. 2010 Husemann, K.; Peuker, U. A.; Simon, F.; Reinsch, E.; Albrecht, V. (2010): Entwicklung und Optimierung von Verfahren zur Elektrosortierung praxisrelevanter Kunststoffabfallgemische. AiF-Vorhaben-Nr. 14980 BR. Schlußbericht zum AiF-Projekt.
- Jakab et al. 2003 Jakab, E.; Uddin, Md.A; Bhaskar, T.; Sakata, Y. (2003): Thermal decomposition of flame-retarded high-impact polystyrene. In: Journal of Analytical and Applied Pyrolysis, 68 - 69, pp. 83 - 99.
- Jalalpoor et al. 2013 Jalalpoor, D.; Götze, R.; Rotter, V. S. (2013): Einsatz und Rückgewinnungspotential von Indium in LCD Geräten. In: Müll und Abfall, (6), pp. 312 - 319.
- Jofre, Morioka 2005 Jofre, S.; Morioka, T. (2005): Waste management of electric and electronic equipment. Comparative analysis of end-of-life strategies. In: Journal of Material Cycles and Waste Management, 7(1), pp. 24-32.
- Joung et al. 2006 Joung, H.-T.; Seo, Y.-C.; Kim, K.-H.; Seo, Y.-C. (2006): Effects of oxygen, catalyst and PVC on the formation of PCDDs, PCDFs and dioxin-like PCBs in pyrolysis products of automobile residues. In: Chemosphere, 65(9), pp. 1481 - 1489.

-
- Jung et al. 2012 Jung, S.-H.; Kim, S.-J.; Kim, J.-S. (2012): Fast pyrolysis of a waste fraction of high impact polystyrene (HIPS) containing brominated flame retardants in a fluidized bed reactor. The effects of various Ca-based additives (CaO, Ca(OH)₂ and oyster shells) on the removal of bromine. In: *Fuel*, 95, pp. 514 - 520.
- Kajiwara et al. 2008 Kajiwara, N.; Noma, Y.; Takigami, H. (2008): Photolysis Studies of Technical Decabromodiphenyl Ether (DecaBDE) and Ethane (DeBDethane) in Plastics under Natural Sunlight. In: *Environmental Science & Technology*, 42(12), pp. 4404 - 4409.
- Karama et al. 2013 Karama, J. P. B.; Béré, A.; Lemonon, J.; Daho, T.; Dissa, A.; Rogaume, Y.; Koulidiati, J. (2013): Modeling the emission of hydrogen chloride and free chlorine from the thermal treatment of polyvinyl chloride- (PVC-) based plastic materials. In: *Journal of Analytical and Applied Pyrolysis*, 101, pp. 209 - 214.
- Katano et al. 2014 Katano, S.; Wajima, T.; Nakagome, H. (2014): Recovery of Tantalum Sintered Compact from Used Tantalum Condenser Using Steam Gasification with Sodium Hydroxide. In: *APCBEE Procedia*, 10, pp. 182 - 186.
- Katz 2013 Katz, C. (2013): EUWID Recycling und Entsorgung. Umicore will 100 Mio € in Recycling-Standort Hoboken investieren. Last time checked: 2016, October 30. <http://www.euwid-recycling.de/news/wirtschaft/einzelansicht/Artikel/umicore-will-100-mio-EUR-in-recycling-standort-hoboken-investieren.html>.
- Katz 2016 Katz, C. (28.09.2016): Behandlungspreise für Siedlungsabfälle in MVA und MBA. Nov. 2015. Gernsbach.
- Kaune et al. 1999 Kaune, A.; Schramm, K.-W.; Lehnardt, R.; Kettrup, A.; Ollenschläger, I.; Rossel, H. (1999): Polychlorinated dibenzodioxins and dibenzofurans in the aluminium recycling process. In: *Journal of Analytical and Applied Pyrolysis*, 49(1 - 2), pp. 191 - 198.
- Kautz 2016 Kautz Vorrichtungsbau GmbH (2016): Stereoscopic picture of a pyrolysis pilot plant for 70 kg shredder residues per hour. Internal Data based on achievements of the BMBF-project "gagendta+". Willstätt-Legelshurst.

-
- Kawohl 2011 Kawohl, C. (11/02/2011): Multi-Metal Recycling bei der Aurubis AG. Berlin (Praxisdialog „Ressourcen- und materialeffiziente Produktgestaltung“).
- Kim et al. 2009 Kim, H.-J.; Kernbaum, S.; Seliger, G. (2009): Emulation-based control of a disassembly system for LCD monitors. In: The International Journal of Advanced Manufacturing Technology, 40(3-4), pp. 383 - 392.
- Kim et al. 2012 Kim, J.-Y.; Kim, T.-S.; Eom, I.-Y.; Kang, S. M.; Cho, T.-S.; Choi, I. G.; Choi, J. W. (2012): Characterization of pyrolytic products obtained from fast pyrolysis of chromated copper arsenate (CCA)- and alkaline copper quaternary compounds (ACQ)-treated wood biomasses. In: Journal of Hazardous Materials, 227-228, pp. 445 - 452.
- Knümann, Bockhorn 1994 Knümann, R.; Bockhorn, H. (1994): Investigation of the Kinetics of Pyrolysis of PVC by TG-MS-Analysis. In: Combustion Science and Technology, 101(1-6), pp. 285 - 299.
- Koch 2007 Koch, W. (Juli 2007): Entwicklung eines thermisch-chemischen Prozesses zur Verwertung von Abfällen aus Elektro- und Elektronikaltgeräten – die „Haloclean“-Pyrolyse. Dissertation. Stuttgart.
- Köhnlechner 2013 Köhnlechner, R. (2013): Sortenreine Separation schwarzer Kunststoff-Gemische. In: Thomé-Kozmiensky, Karl J.; Goldmann, Daniel (Eds.): Recycling und Rohstoffe. Neuruppin: TK, pp. 225 - 239.
- Köhnlechner 2014 Köhnlechner, R. (2014): Erzeugung sauberer PS- und ABS-Fraktionen. In: Thomé-Kozmiensky, Karl; Goldmann, Daniel (Eds.): Recycling und Rohstoffe. Neuruppin: TK, pp. 379 - 399.
- Kosuda et al. 2012 Kosuda, T.; Okada, T.; Nozaka, S.; Matsuzawa, Y.; Shimizu, T.; Hamanaka, S.; Mishima, S. (2012): Characteristics and mechanism of low temperature dehydrochlorination of poly(vinyl chloride) in the presence of zinc(II) oxide. In: Polymer Degradation and Stability, 97(4), pp. 584 - 591.
- Kramer 2013 Kramer, K. (18.06.2013): Mechanische Aufbereitung von Elektroaltgeräten. Dortmund (VDI-Wissensforum 2013 - Stoffliche und energetische Verwertung von Shredder-rückständen und Elektroschrott).

-
- Kuchta, Enzner Kuchta, K.; Enzner, V. (2015): Ressourceneffizienz der Metallrückgewinnung vor und nach der Verbrennung. In: Thomé-Kozmiensky, Karl J. (Ed.): Mineralische Nebenprodukte und Abfälle. Aschen, Schlacken, Stäube und Baurestmassen. Neuruppin: TK-Verl., pp. 107 - 116.
- Kumar et al. 2014 Kumar, M.; Lee, J.-C.; Kim, M.-S.; Jeong, J.; Yoo, K. (2014): Leaching of metals from waste printed circuit boards (WPCBs) using sulfuric and nitric acids. In: Environmental Engineering and Management Journal, 13(10), pp. 2601 - 2607.
- Kutz et al. 1990 Kutz, F. W.; Barnes, D. G.; Bottimore, D. P.; Greim, H.; Bretthauer, E. W. (1990): The international toxicity equivalency factor (I-TEF) method of risk assessment for complex mixtures of dioxins and related compounds. In: Chemosphere, 20(7-9), pp. 751–757.
- KWKG 2015 Gesetz für die Erhaltung, die Modernisierung und den Ausbau der Kraft-Wärme-Kopplung (Kraft-Wärme-Kopplungsgesetz - KWKG). KWKG (21.12.2015).
- Lai et al. 2007 Lai, Y.-C.; Lee, W.-J.; Li, H.-W.; Wang, L.-C.; Chang-Chien, G.-P. (2007): Inhibition of Polybrominated Dibenzo-*p*-dioxin and Dibenzofuran Formation from the Pyrolysis of Printed Circuit Boards. In: Environmental Science & Technology, 41(3), pp. 957 - 962.
- Lane et al. 2016 Lane, D. J.; Cook, N. J.; Grano, S. R.; Ehrig, K. (2016): Selective leaching of penalty elements from copper concentrates. A review. In: Minerals Engineering, 98, pp. 110 - 121.
- Lee et al. 2002 Lee, S.-Y.; Yoon, J.-H.; Kim, J.-R.; Park, D.-W. (2002): Degradation of polystyrene using clinoptilolite catalysts. In: Journal of Analytical and Applied Pyrolysis, 64(1), pp. 71 - 83.
- Lee et al. 2007 Lee, J.-C.; Song, H. T.; Yoo, J.-M. (2007): Present status of the recycling of waste electrical and electronic equipment in Korea. In: Resources, Conservation and Recycling, 50(4), pp. 380 - 397.
- Lewin 2001 Lewin, M. (2001): Synergism and catalysis in flame retardancy of polymers. In: Polymers for Advanced Technologies, 12(3-4), pp. 215 - 222.

-
- Linde 2016 Linde AG (2016): N₂, technical, 12x300 bar. München.
- Liu et al. 2013 Liu, W.-J.; Tian, K.; Jiang, H.; Zhang, X.-S.; Yang, G.-X. (2013): Preparation of liquid chemical feedstocks by co-pyrolysis of electronic waste and biomass without formation of polybrominated dibenzo-*p*-dioxins. In: Bioresource Technology, 128, pp. 1 - 7.
- López et al. 2011 López, A.; Marco, I. de; Caballero, B. M.; Laresgoiti, M. F.; Adrados, A.; Aranzabal, A. (2011): Catalytic pyrolysis of plastic wastes with two different types of catalysts. ZSM-5 zeolite and Red Mud. In: Applied Catalysis B: Environmental, 104(3-4), pp. 211 - 219.
- Lossin 2006 Lossin, A. (2006): Kupfer und Nickel. In: Winnacker, Karl; Küchler, Leopold (Eds.): Chemische Technik. Prozesse und Produkte. 5 edition. Weinheim: Wiley-VCH, pp. 609 - 668.
- Lu et al. 2012 Lu, R.; Ma, E.; Xu, Z. (2012): Application of pyrolysis process to remove and recover liquid crystal and films from waste liquid crystal display glass. In: Journal of Hazardous Materials, 243, pp. 311 - 318.
- Luda et al. 2002a Luda, M. P.; Balabanovich, A. I.; Camino, G. (2002): Thermal decomposition of fire retardant brominated epoxy resins. In: Journal of Analytical and Applied Pyrolysis, 65(1), pp. 25 - 40.
- Luda et al. 2002b Luda, M. P.; Camino, G.; Balabanovich, A. I.; Hornung, A. (2002): Scavenging of halogen in recycling of halogen-based polymer materials. In: Macromolecular Symposia, 180(1), pp. 141 - 152.
- Luda et al. 2005 Luda, M. P.; Euringer, N.; Moratti, U.; Zanetti, M. (2005): WEEE recycling: Pyrolysis of fire retardant model polymers. In: Waste Management, 25(2), pp. 203 - 208.
- Luda et al. 2010 Luda, M. P.; Balabanovich, A.I.; Zanetti, M. (2010): Pyrolysis of fire retardant anhydride-cured epoxy resins. In: Journal of Analytical and Applied Pyrolysis, 88(1), pp. 39 - 52.
- Luijk et al. 1991 Luijk, R.; Wever, H.; Olie, K.; Govers, H. A. J.; Boon, J. J. (1991): The influence of the polymer matrix on the formation of polybrominated dibenzo-*p*-dioxins (PBDDs) and polybrominated dibenzofurans (PBDFs). In: Chemosphere, 23(8-10), pp. 1173 - 1183.

-
- Luijk et al. 1992 Luijk, R.; Govers, H. A. J. (1992): The formation of poly-brominated dibenzo-*p*-dioxins (PBDDs) and dibenzofurans (PBDFs) during pyrolysis of polymer blends containing brominated flame retardants, 25(3), pp. 361 - 374.
- Lüngen et al. 2006 Lüngen, H. B.; Pluschkell, W.; Steffen, R.; Janke, D.; Volkova, O.; Senk, D.; Degner, M.; Lackinger, C.; Mauk, P.-J.; Ponge, D. (2006): Eisen und Stahl. In: Winnacker, Karl; Küchler, Leopold (Eds.): Chemische Technik. Prozesse und Produkte. 5th edition. Weinheim: Wiley-VCH, pp. 203 - 403.
- Luo et al. 2016 Luo, Y.; Hassan, E. B.; Guda, V.; Wijayapala, R.; Steele, P. H. (2016): Upgrading of syngas hydrotreated fractionated oxidized bio-oil to transportation grade hydrocarbons. In: Energy Conversion and Management, 115, pp. 159 - 166.
- LyondellBasell 2013 LyondellBasell Industries Holdings, B. V. (17.05.2013): Purell HP570U. Polypropylene, Homopolymer. Rotterdam. <https://www.lyondellbasell.com/en/polymers/p/Purell-HP570U/55cf143a-f735-484b-b14e-21b986854e36>.
- Ma et al. 2002 Ma, S.; Lu, J.; Gao, J. (2002): Study of the Low Temperature Pyrolysis of PVC. In: Energy & Fuels, 16(2), pp. 338 - 342.
- Ma, Xu 2013 Ma, E.; Xu, Z. (2013): Technological process and optimum design of organic materials vacuum pyrolysis and indium chlorinated separation from waste liquid crystal display panels. In: Journal of Hazardous Materials, 263 Pt 2, pp. 610 - 617.
- Ma et al. 2015 Ma, C.; Sun, L.; Jin, L.; Zhou, C.; Xiang, J.; Hu, S.; Su, S. (2015): Effect of polypropylene on the pyrolysis of flame retarded high impact polystyrene. In: Fuel Processing Technology, 135, pp. 150 - 156.
- Madorsky, Straus 1959 Madorsky, S. L.; Straus, S. (1959): Thermal Degradation of Polymers at High Temperatures. In: Journal of Research of the National Bureau of Standards - A. Physics and Chemistry, 63A(3), pp. 261 - 268.
- Magalini et al. 2012 Magalini, F.; Huisman, J.; Wang, F. (2012): Household WEEE generated in Italy. Analysis of Volumes & Consumer Disposal Behavior for Waste Electrical and Electronic Equipment.

-
- Mark et al. 2006 Mark, F. E.; Dresch, H.; Bergfeld, B.; Dima, B.; Fisher, M. M.; Grüttner, W.; Kleppmann, F.; Kramer, K.; Lehner, T.; Vehlouw, J. (August 2006): Large scale demonstration of the treatment of electrical and electronic shredder residue. by an co-incineraton in the Würzburg Municipal Solid Waste Incinerator. A Technical Report produced by: PlasticsEurope. Brussels.
- Marongio et al. 2003 Marongiu, A.; Faravelli, T.; Bozzano, G.; Dente, M.; Ranzi, E. (2003): Thermal degradation of poly(vinyl chloride). In: Journal of Analytical and Applied Pyrolysis, 70, pp. 519 - 553.
- Marongio et al. 2007 Marongiu, A.; Bozzano, G.; Dente, M.; Ranzi, E.; Faravelli, T. (2007): Detailed kinetic modeling of pyrolysis of tetrabromobisphenol A. In: Journal of Analytical and Applied Pyrolysis, 80(2), pp. 325 - 345.
- Masuda et al. 2006 Masuda, Y.; Uda, T.; Terakado, O.; Hirasawa, M. (2006): Pyrolysis study of poly(vinyl chloride)-metal oxide mixtures: Quantitative product analysis and the chlorine fixing ability of metal oxides. In: Journal of Analytical and Applied Pyrolysis, 77(2), pp. 159 - 168.
- Maurell-Lopez et al. 2012 Maurell-Lopez, S.; Ayhan, M.; Eschen, M.; Friedrich, B. (2012): Autotherme Metallrückgewinnung aus WEEE-Schrott. In: Thomé-Kozmiensky, Karl; Goldmann, Daniel (Eds.): Recycling und Rohstoffe. Neuruppin: TK Verlag Karl Thomé-Kozmiensky, pp. 413 - 427.
- MFA 2016 Mineral Fund Advisory (MFA) Pty. Ltd. (2016): MineralPrices.com. Last time checked: 30.09.2016 <http://mineralprices.com/>.
- Mineta, Okabe 2005 Mineta, K.; Okabe, T. H. (2005): Development of a recycling process for tantalum from capacitor scraps. In: Journal of Physics and Chemistry of Solids, 66(2-4), pp. 318 - 321.
- Miranda et al. 1999 Miranda, R.; Yang, J.; Roy, C.; Vasile C. (1999): Vacuum pyrolysis of PVC I. Kinetic study. In: Polymer Degradation and Stability, 64(1), pp. 127 - 144.
- Miskolczi et al. 2009 Miskolczi, N.; Bartha, L.; Angyal, A. (2009): Pyrolysis of Polyvinyl Chloride (PVC)-Containing Mixed Plastic Wastes for Recovery of Hydrocarbons. In: Energy & Fuels, 23(5), pp. 2743 - 2749.

-
- Miskolczi et al. 2008 Miskolczi, N.; Hall, W. J.; Angyal, A.; Bartha, L.; Williams, P. T. (2008): Production of oil with low organobromine content from the pyrolysis of flame retarded HIPS and ABS plastics. In: *Journal of Analytical and Applied Pyrolysis*, 83(1), pp. 115 - 123.
- Mitan et al. 2007 Mitan, N. M. M.; Brebu, M.; Bhaskar, T.; Muto, A.; Sakata, Y. (2007): Individual and simultaneous degradation of brominated high impact polystyrene and brominated acrylonitrile-butadiene-styrene and removal of heteroelements (Br, N, and O) from degradation oil by multiphase catalytic systems. In: *Journal of Material Cycles and Waste Management*, 9(1), pp. 56 - 61.
- Moltó et al. 2009 Moltó, J.; Font, R.; Gálvez, A.; Conesa, J.A. (2009): Pyrolysis and combustion of electronic wastes. In: *Journal of Analytical and Applied Pyrolysis*, 84(1), pp. 68 - 78.
- Morf, Taverna 2004 Morf, Leo S.; Taverna, Ruedi (2004): *Metallische und nichtmetallische Stoffe im Elektronikschrott. Stoffflussanalyse*. Bern (Schriftenreihe Umwelt, 374).
- Müller, Dongmann 1998 Müller, J.; Dongmann, G. (1998): Formation of aromatics during pyrolysis of PVC in the presence of metal chlorides. In: *Journal of Analytical and Applied Pyrolysis*, 45(1), pp. 59 - 74.
- Müller et al. 1997 Müller, J.; Dongmann, G.; Frischkorn, C. G. B. (1997): The effect of aluminium on the formation of PAH, Methyl-PAH and chlorinated aromatic compounds during thermal decomposition of PVC. In: *Journal of Analytical and Applied Pyrolysis*, 43(2), pp. 157 - 168.
- NEA 2016 National Electronics Alloys (NEA) (2016): 42alloy. Oakland, Santa Ana. Last time checked: 2016, October 30. http://www.nealloys.com/pdf/42_Alloy_Flyer.pdf.
- Nederkorn 2016 Nederkorn, H. (2016): *Sondermetallhandel Heinz Nederkorn*. www.metallankauf.org. Last time checked: 12.10.2016 <http://www.metallankauf.org/>.
- Neumann et al. 2016 Neumann, J.; Meyer, J.; Ouadi, M.; Apfelbacher, A.; Binder, S.; Hornung, A. (2016): The conversion of anaerobic digestion waste into biofuels via a novel Thermo-Catalytic Reforming process. In: *Waste management* (New York, N.Y.), 47(Pt A), pp. 141 - 148.

-
- Ni et al. 2012 Ni, M.; Xiao, H.; Chi, Y.; Yan, J.; Buekens, A.; Jin, Y.; Lu, S. (2012): Combustion and inorganic bromine emission of waste printed circuit boards in a high temperature furnace. In: Waste management (New York, N.Y.), 32(3), pp. 568 - 574.
- Nitschke-Kowsky et al. 2012 Nitschke-Kowsky, P.; Schenk, J.; Schley, P.; Altfeld, K. (2012): Gasbeschaffenheit in Deutschland. Gas quality in Germany. In: Gaswärme international, (6), pp. 55 - 60.
- Nuss, Eckelman 2014 Nuss, P.; Eckelman, M. J. (2014): Life cycle assessment of metals: a scientific synthesis. In: PloS one, 9(7), e101298.
- Oguchi et al. 2013 Oguchi, M.; Sakanakura, H.; Terazono, A. (2013): Toxic metals in WEEE: Characterization and substance flow analysis in waste treatment processes. In: Science of the Total Environment, 463-464, pp. 1124 - 1132.
- Oleszek et al. 2013a Oleszek, S.; Grabda, M.; Shibata, E.; Nakamura, T. (2013): Distribution of copper, silver and gold during thermal treatment with brominated flame retardants. In: Waste Management, 33(9), pp. 1835 - 1842.
- Oleszek et al. 2013b Oleszek, S.; Grabda, M.; Shibata, E.; Nakamura, T. (2013): Study of the reactions between tetrabromobisphenol A and PbO and Fe₂O₃ in inert and oxidizing atmospheres by various thermal methods. In: Thermochimica Acta, 566, pp. 218 - 225.
- Oleszek et al. 2013c Oleszek, S.; Grabda, M.; Shibata, E.; Nakamura, T. (2013): Fate of lead oxide during thermal treatment with tetrabromobisphenol A. In: Journal of Hazardous Materials, 261, pp. 163 - 171.
- Ortuño et al. 2014 Ortuño, N.; Conesa, J. A.; Moltó, J.; Font, R. (2014): Pollutant emissions during pyrolysis and combustion of waste printed circuit boards, before and after metal removal. In: Science of the Total Environment, 499, pp. 27 - 35.
- Ouchi, Honda 1959 Ouchi, K.; Honda, H. (1959): Pyrolysis of coal. 1. Thermal cracking of phenolformaldehyde resins taken as coal models. In: Fuel, 38(4), pp. 429 - 443.

-
- Pang, Gillham 1989 Pang, K. P.; Gillham, J. K. (1989): Anomalous behavior of cured epoxy resins. Density at room temperature versus time and temperature of cure. In: *Journal of Applied Polymer Science*, 37(7), pp. 1969 - 1991.
- Pape 2009 Pape, U. (2009): Grundlagen der Finanzierung und Investition. Mit Fallbeispielen und Übungen. München: Oldenbourg.
- Park et al. 2009 Park, K.-S.; Sato, W.; Grause, G.; Kameda, T.; Yoshioka, T. (2009): Recovery of indium from In_2O_3 and liquid crystal display powder via a chloride volatilization process using polyvinyl chloride. In: *Thermochimica Acta*, 493(1-2), pp. 105 - 108.
- Perry, Phillips 1995 Perry, D. L.; Phillips, S. L. (1995): Handbook of inorganic compounds. Boca Raton: CRC Press.
- Pomiro et al. 2015a Pomiro, F. J.; Fouga, G. G.; Gaviría, J. P.; Bohé, Ana E. (2015): Thermogravimetry study of Gd_2O_3 chlorination. In: *Journal of Thermal Analysis and Calorimetry*, 122(2), pp. 679 - 687.
- Pomiro et al. 2015b Pomiro, F. J.; Fouga, G. G.; Gaviría, J. P.; Bohé, Ana E. (2015): Study of the Reaction Stages and Kinetics of the Europium Oxide Carbochlorination. In: *Metallurgical and Materials Transactions B*, 46(1), pp. 304 - 315.
- Pretz, Meier-Kortwig 1998 Pretz, T.; Meier-Kortwig, J. (1998): Aufbereitung von Müllschlacken unter besonderer Berücksichtigung der Metallrückgewinnung. Aachen. Last time checked: 2013, June 20. http://www.iar.rwth-aachen.de/www/upload/Publikationen/download/bis1999/v06_sfb525.pdf.
- Quan et al. 2009 Quan, C.; Li, A.; Gao, N. (2009): Thermogravimetric analysis and kinetic study on large particles of printed circuit board wastes. In: *Waste Management*, 29(8), pp. 2353 - 2360.
- Quicker 2016 Quicker, P. (05/11/2016): Disintegration of metal-rich composite fractions from WEEE through pyrolysis. Nancy (International Conference in Analytical and Applied Pyrolysis Pyro2016).

-
- Quicker et al. 2014 Quicker, P.; Neuerburg, F.; Noël, Y.; Huras, A.; Eyssen, R. G.; Vehlow, J.; Thomé-Kozmiensky, Karl J. (1. August 2014): Sachstand zu den alternativen Verfahren für die thermische Entsorgung von Abfällen. Schlussbericht. Im Auftrag des Umweltbundesamts. Dessau-Roßlau.
- Reinhard, Richers 2004 Reinhard, T.; Richers, U. (2004): Entsorgung von Shredder-rückständen - ein aktueller Überblick (FZKA 6940).
- Ren et al. 2011 Ren, M.; Peng, P.; Cai, Y.; Chen, D.; Zhou, L.; Chen, P.; Hu, J. (2011): PBDD/F impurities in some commercial deca-BDE. In: Environmental pollution (Barking, Essex : 1987), 159(5), pp. 1375 - 1380.
- Reuter et al. 2013 Reuter, M.; Hudson, C.; van Schaik, A.; Heiskanen, K.; Meskers, C.; Hagelüken, C. (2013): Metal recycling. Opportunities, limits, infrastructure. A Report of the Working Group on the Global Metal Flows to the International Resource Panel. Nairobi (International resource panel, 2b).
- Rzyman et al. 2010 Rzyman, M.; Grabda, M.; Oleszek-Kudlak, S.; Shibata, E.; Nakamura, T. (2010): Studies on bromination and evaporation of antimony oxide during thermal treatment of tetrabromobisphenol A (TBBPA). In: Journal of Analytical and Applied Pyrolysis, 88(1), pp. 14 - 21.
- Sakai et al. 2001 Sakai, S.-I.; Watanabe, J.; Honda, Y.; Takatsuki, H.; Aoki, I.; Futamatsu, M.; Shiozaki, K. (2001): Combustion of brominated flame retardants and behavior of its byproducts. In: Chemosphere, 42(5-7), pp. 519 - 531.
- Sander et al. 2012 Sander, K.; Schilling, S.; Marscheider-Weidemann, F.; Wilts, H.; Gries, N. von; Hobohm, J. (August 2012): Abfall-wirtschaftliche Produktverantwortung unter Ressourcen-schutzaspekten. Ökopol GmbH, Fraunhofer ISI, TU Darmstadt und TU Hamburg-Harburg im Auftrag des Umweltbundesamtes. Meilensteinbericht August 2012. Dessau-Roßlau.
- Savilotidou et al. 2014 Savilotidou, V.; Hahladakis, J. N.; Gidaracos, E. (2014): Determination of toxic metals in discarded Liquid Crystal Displays (LCDs). In: Resources, Conservation and Recycling, 92, pp. 108 - 115.

-
- Schlummer et al. 2007 Schlummer, M.; Gruber, L.; Mäurer, A.; Wolz, G.; van Eldik, R. (2007): Characterisation of polymer fractions from waste electrical and electronic equipment (WEEE) and implications for waste management. In: *Chemosphere*, 67(9), pp. 1866–1876.
- Schneider et al. 2001 Schneider, L.; Berger, M.; Finkbeiner, M. (2011): The anthropogenic stock extended abiotic depletion potential (AADP) as a new parameterisation to model the depletion of abiotic resources. In: *The International Journal of Life Cycle Assessment*, 16(9), pp. 929 - 936.
- Scholz et al. 2001 Scholz, R.; Beckmann, M.; Schulenburg, F. (2001): Abfallbehandlung in thermischen Verfahren. Verbrennung, Vergasung, Pyrolyse, Verfahrens- und Anlagenkonzepte. Stuttgart: Teubner
- Scott et al. 1990 Scott, D. S.; Czernik, S. R.; Piskorz, J.; Radlein, D. S. A. G. (1990): Fast Pyrolysis of Plastic Wastes. In: *Energy & Fuels*, 4, pp. 407 - 411.
- Shi et al. 2013 Shi, Q.; Huang, Y.; Jing, C. (2013): Synthesis, characterization and application of lanthanum-impregnated activated alumina for F removal. In: *Journal of Materials Chemistry A*, 1(41), p. 12797 - 12803.
- Shi et al. 2015 Shi, Q.; Yan, L.; Chan, T.; Jing, C. (2015): Arsenic Adsorption on Lanthanum-Impregnated Activated Alumina: Spectroscopic and DFT Study. In: *ACS applied materials & interfaces*, 7(48), pp. 26735 - 26741.
- Shie et al. 2002 Shie, J.-L.; Chen, Y.-H.; Chang, C.-Y.; Lin, J.-P.; Lee, D.-J.; Wu, C.-H. (2002): Thermal Pyrolysis of Poly(vinyl alcohol) and Its Major Products. In: *Energy & Fuels*, 16(1), pp. 109 - 118.
- Sivalingam et al. 2003 Sivalingam, G.; Karthik, R.; Madras, G. (2003): Effect of Metal Oxides on Thermal Degradation of Poly(vinyl acetate) and Poly(vinyl chloride) and Their Blends. In: *Industrial & Engineering Chemistry Research*, 42(16), pp. 3647 - 3653.
- Statista 2016 Statista GmbH (2016): Inflationsrate in Deutschland von 1992 bis 2015. Veränderung des Verbraucherpreisindex gegenüber Vorjahr. Last time checked: 2016, October 30. <https://de.statista.com/statistik/daten/studie/1046/umfrage/inflationsrate-veraenderung-des-verbraucherpreisindex-zum-vorjahr/>.

-
- Staub et al. 2015 Staub & Co. Silbermann (2015): Angebot Aktivkohle. Last time checked: 2016, October 30. <http://www.staub-silbermann.de/>.
- Steinfeld et al. 2002 Steinfeldt, M.; Petschow, U.; Keil, M. (2002): Ökonomische Bewertung von Systemen zur Verwertung von biologisch-organischen Abfällen. Bericht des Instituts für ökologische Wirtschaftsforschung (IÖW) gGmbH im Rahmen des Gesamtprojektes "Untersuchungen zur Umweltverträglichkeit von Systemen zur Verwertung von biologisch-organischen Abfällen". Berlin: IÖW.
- Suzuki, Wilkie 1995 Suzuki, M.; Wilkie, C. A. (1995): The thermal degradation of acrylonitrile-butadiene-styrene terpolymer as studied by TGA/FTIR. In: *Polymer Degradation and Stability*, 47, pp. 217 - 221.
- Tanner 2011 Tanner, N. (2011): Energetische Optimierung von Abfallverbrennungsanlagen. – am Beispiel des MHKW Kassel –. In: Thomé-Kozmiensky, Karl; Beckmann, Michael (Eds.): *Energie aus Abfall: TK Verlag Karl Thomé-Kozmiensky*, pp. 31 - 68.
- Terakado, Hirasawa 2005 Terakado, O.; Hirasawa, M. (2005): Effect of metal oxides on the pyrolysis residues of poly(ethylene terephthalate). Formation of carbonaceous submicron, nano-scale filaments and mesoporous compounds. In: *Journal of Analytical and Applied Pyrolysis*, 73(2), pp. 248 - 256.
- Terakado et al. 2011 Terakado, O.; Ohhashi, R.; Hirasawa, M. (2011): Thermal degradation study of tetrabromobisphenol A under the presence metal oxide: Comparison of bromine fixation ability. In: *Journal of Analytical and Applied Pyrolysis*, 91(2), pp. 303 - 309.
- Terakado et al. 2013 Terakado, O.; Ohhashi, R.; Hirasawa, M. (2013): Bromine fixation by metal oxide in pyrolysis of printed circuit board containing brominated flame retardant. In: *Journal of Analytical and Applied Pyrolysis*, 103, pp. 216 - 221.
- Thoma et al. 1987 Thoma, H.; Hauschulz, G.; Knorr, E.; Hutzinger, O. (1987): Polybrominated dibenzofurans (PBDF) and dibenzodioxins (PBDD) from the pyrolysis of neat brominated diphenylethers, biphenyls and plastic mixtures of these compounds. In: *Chemosphere*, 16(1), pp. 277 - 285.

-
- Trick et al. 1995 Trick, Kimberly A.; Saliba, Tony E. (1995): Mechanisms of the pyrolysis of phenolic resin in a carbon/phenolic composite. In: Carbon, 33(11), pp. 1509 - 1515.
- USGS 2016 U.S. Department of the Interior; U.S. Geological Survey (USGS) (2016): Mineral Commodity Summaries 2016. Reston, Virginia. 9781411340114.
- Uddin et al. 2002 Uddin, M. A.; Bhaskar, T.; Kaneko, J.; Muto, A.; Sakata, Y.; Matsui, T. (2002): Dehydrohalogenation during pyrolysis of brominated flame retardant containing high impact polystyrene (HIPS-Br) mixed with polyvinylchloride (PVC). In: Fuel, 81, pp. 1819 - 1825.
- UBA 2007 Umweltbundesamt (UBA) (Februar 2007): Bromierte Flamm-schutzmittel in Elektro- und Elektronikgeräten: Das Flamm-schutzmittel Decabromdiphenylether (DecaBDE) ist durch umweltverträglichere Alternativen ersetzbar. Fachpapier Februar 2007. Dessau-Roßlau. Last time checked: 2016, October 11. <http://www.umweltbundesamt.de/sites/default/files/medien/419/dokumente/fachpapierdecabde.pdf>.
- UBA 2008 Umweltbundesamt (UBA) (Oktober 2008): Stellenwert der Abfallverbrennung in Deutschland. Dessau-Roßlau.
- UBA 2014 Umweltbundesamt (UBA) (2014): Dioxindatenbank des Bundes und der Länder. Toxizität und Bewertung (Berechnungsmodelle). Last time checked: 2016, November 28. http://www.dioxindb.de/f_stoffe_teqs2.html.
- van der Avert et al. 2004 van der Avert, P.; Podkolzin, S. G.; Manoilova, O.; de Winne, H.; Weckhuysen, B. M. (2004): Low-Temperature Destruction of Carbon Tetrachloride over Lanthanide Oxide-Based Catalysts: From Destructive Adsorption to a Catalytic Reaction Cycle. In: Chemistry - A European Journal, 10(7), pp. 1637 - 1646.
- van der Avert,
Weckhuysen 2004 van der Avert, Pieter; Weckhuysen, Bert M. (2004): Low-temperature catalytic destruction of CCl₄, CHCl₃ and CH₂Cl₂ over basic oxides. In: Physical Chemistry Chemical Physics, 6(22), p. 5256 - 5262.
- Vasile et al. 2008 Vasile, C.; Brebu, M. A.; Totolin, M.; Yanik, J.; Karayildirim, T.; Darie, H. (2008): Feedstock Recycling from the Printed Circuit Boards of Used Computers. In: Energy & Fuels, 22(3), pp. 1658 - 1665.

-
- VDI 2012 Verein Deutscher Ingenieure (VDI), VDI-Gesellschaft Energie und Umwelt (January 2012): Recycling elektrischer und elektronischer Geräte - Aufbereitung / Recycling of electrical and electronic equipment - Preparation techniques, 13.030.50 (VDI 2343 Part 4). Berlin: Beuth Verlag.
- VDI 2014 Verein Deutscher Ingenieure (VDI), VDI-Gesellschaft Energie und Umwelt (November 2014): Recycling elektrischer und elektronischer Geräte - Stoffliche und energetische Verwertung und Beseitigung / Recycling of electrical and electronic equipment - Material and thermal recycling and removal, 13.030.50 (VDI 2343 Part 5). Berlin: Beuth Verlag.
- Vishay 2015 Vishay (12/09/2015): Guide for Molded Tantalum Capacitors (Molded Guide, Vishay Sprague, 40074). Last time checked: 2016, October 30. www.vishay.com.
- VWR 2016 VWR International GmbH (2016): Natriumhydroxid TECHNICAL. 28240.460. Last time checked: 2016, October 30. www.vwr.com.
- Wang et al. 1992 Wang, C.-S.; Lin, Y.-S.; Fritz, D. B. (1992): m-Bromophenolic epoxy resins for electronic packaging. In: Angewandte Makromolekulare Chemie, 198(1), pp. 51 - 60.
- Wang et al. 2015a Wang, R.; Chen, Y.; Xu, Z. (2015a): Recycling acetic acid from polarizing film of waste liquid crystal display panels by sub/supercritical water treatments. In: Environmental science & technology, 49(10), pp. 5999 - 6008.
- Wang et al. 2015b Wang, Z.; Guo, H.; Shen, F.; Yang, G.; Zhang, Y.; Zeng, Y.; Wang, L.; Xiao, H.; Deng, S. (2015b): Biochar produced from oak sawdust by Lanthanum (La)-involved pyrolysis for adsorption of ammonium (NH_4^+), nitrate (NO_3^-), and phosphate (PO_4^{3-}). In: Chemosphere, 119, pp. 646 - 653.
- Wang, Xu 2014 Wang, R.; Xu, Z. (2014): Pyrolysis mechanism for recycle renewable resource from polarizing film of waste liquid crystal display panels. In: Journal of Hazardous Materials, 278, pp. 311 - 319.
- Wang, Xu 2016 Wang, R.; Xu, Z. (2016): Pyrolysis characteristics and pyrolysis products separation for recycling organic materials from waste liquid crystal display panels. In: Journal of Hazardous Materials, 302, pp. 45 - 56.

-
- Wang et al. 2016 Wang, Z.; Shen, D.; Shen, F.; Li, T. (2016): Phosphate adsorption on lanthanum loaded biochar. In: *Chemosphere*, 150, pp. 1 - 7.
- Weber, Kuch 2003 Weber, R.; Kuch, B. (2003): Relevance of BFRs and thermal conditions on the formation pathways of brominated and brominated-chlorinated dibenzodioxins and dibenzofurans. In: *Environment International*, 29(6), pp. 699 - 710.
- Widmer et al. 2015 Widmer, R.; Du, X.; Haag, O.; Restrepo, E.; Wäger, P. A. (2015): Scarce Metals in Conventional Passenger Vehicles and End-of-Life Vehicle Shredder Output. In: *Environmental Science & Technology*, 49(7), pp. 4591 - 4599.
- Williams 2010 Williams, P. T. (2010): Valorization of Printed Circuit Boards from Waste Electrical and Electronic Equipment by Pyrolysis. In: *Waste and Biomass Valorization*, 1(1), pp. 107 - 120.
- Wöhe et al. 2016 Wöhe, G.; Döring, U.; Brösel, G. (2016): Einführung in die allgemeine Betriebswirtschaftslehre, 26th edition. München, Verlag Franz Vahlen.
- Wong et al. 2015 Wong, H.-W.; Peck, J.; Bonomi, R. E.; Assif, J.; Panerai, F.; Reinisch, G.; Lachaud, J.; Mansour, N. N. (2015): Quantitative determination of species production from phenol-formaldehyde resin pyrolysis. In: *Polymer Degradation and Stability*, 112, pp. 122 - 131.
- Wood et al. 2013 Wood, S.; Fanning, M.; Venn, M.; Whiting, K. (January 2013): Review of state-of-the-art waste-to-energy technologies. Stage Two – Case Studies. Perth. Last time checked: 2016, October 30. http://www.wtert.com.br/home2010/arquivo/noticias_eventos/WSP%20Waste%20to%20Energy%20Technical%20Report%20Stage%20Two.pdf.
- Wu et al. 2014 Wu, H.; Shen, Y.; Harada, N.; An, Q.; Yoshikawa, K. (2014): Production of Pyrolysis Oil with Low Bromine and Antimony Contents from Plastic Material Containing Brominated Flame Retardants and Antimony Trioxide. In: *Energy and Environment Research*, 4(3), pp. 105 - 118.
- Yang et al. 2013a Yang, J.; Retegan, T.; Ekberg, C. (2013): Indium recovery from discarded LCD panel glass by solvent extraction. In: *Hydrometallurgy*, 137, pp. 68 - 77.

-
- Yang et al. 2013b Yang, X.; Sun, L.; Xiang, J.; Hu, S.; Su, S. (2013): Pyrolysis and dehalogenation of plastics from waste electrical and electronic equipment (WEEE): A review. In: *Waste Management*, 33(2), pp. 462 - 473.
- Yanik et al. 2001 Yanik, J.; Uddin, Md. A.; Ikeuchi, K.; Sakata, Y. (2001): The catalytic effect of Red Mud on the degradation of poly (vinyl chloride) containing polymer mixture into fuel oil. In: *Polymer Degradation and Stability*, 73(2), pp. 335 - 346.
- Yoshioka et al. 2005 Yoshioka, T.; Handa, T.; Grause, G.; Lei, Z.; Inomata, H.; Mizoguchi, T. (2005): Effects of metal oxides on the pyrolysis of poly(ethylene terephthalate). In: *Journal of Analytical and Applied Pyrolysis*, 73, pp. 139 - 144.
- Zhan et al. 2000 Zhang, B.; Yan, X.-Y.; Shibata, K.; Uda, T.; Tada, M.; Hirasawa, M. (2000): Thermogravimetric-Mass Spectrometric Analysis of the Reactions between Oxide (ZnO, Fe₂O₃ or ZnFe₂O₄) and Polyvinyl Chloride under Inert Atmosphere. In: *Materials Transactions, JIM*, 41(10), pp. 1342 - 1350.
- Zhang et al. 2015 Zhang, K.; Wu, Y.; Wang, W.; Li, B.; Zhang, Y.; Zuo, T. (2015): Recycling indium from waste LCDs. A review. In: *Resources, Conservation and Recycling*, 104, pp. 276 - 290.
- Zhu et al. 2008 Zhu, H. M.; Jiang, X. G.; Yan, J. H.; Chi, Y.; Cen, K. F. (2008): TG-FTIR analysis of PVC thermal degradation and HCl removal. In: *Journal of Analytical and Applied Pyrolysis*, 82(1), pp. 1 - 9.

Appendix

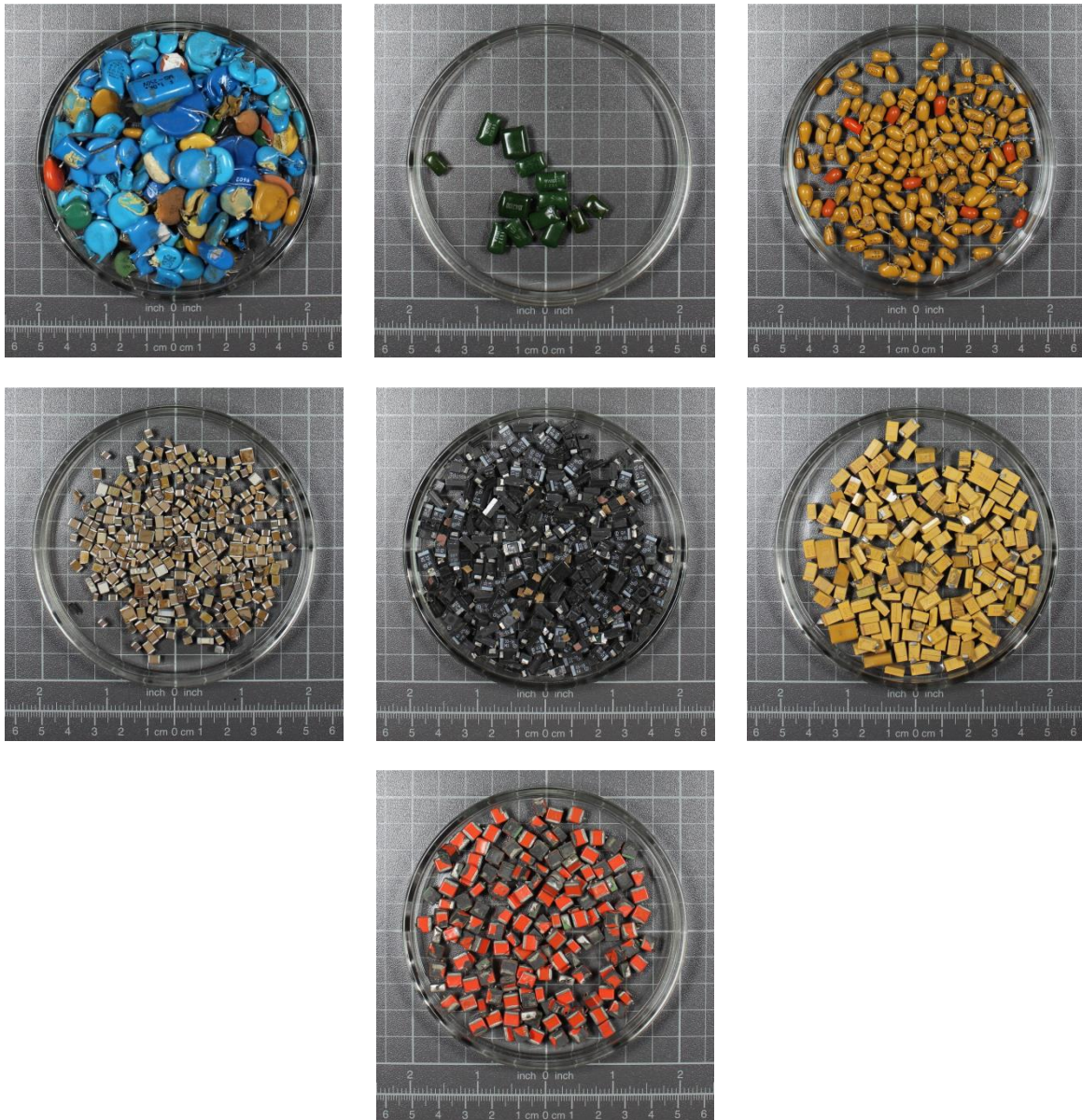
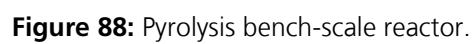


Figure 87: Different capacitor types: THT blue, yellow disks; THT green drops; THT orange, yellow drops; SMD brown; SMD black; SMD yellow; SMD orange.



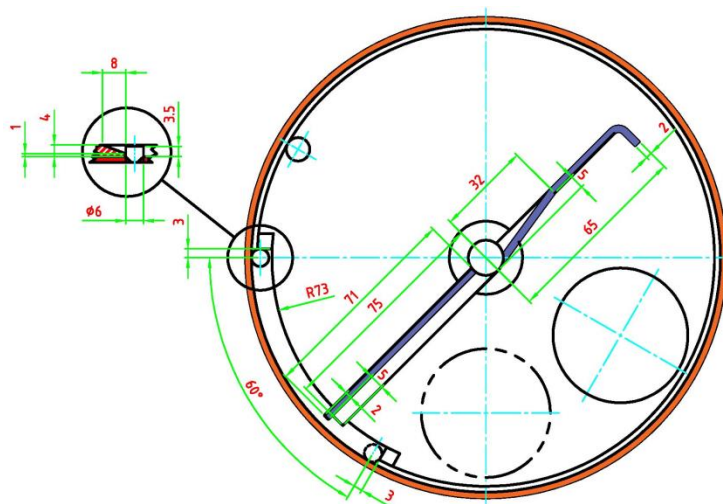


Figure 89: Bottom of pyrolysis bench-scale reactor.

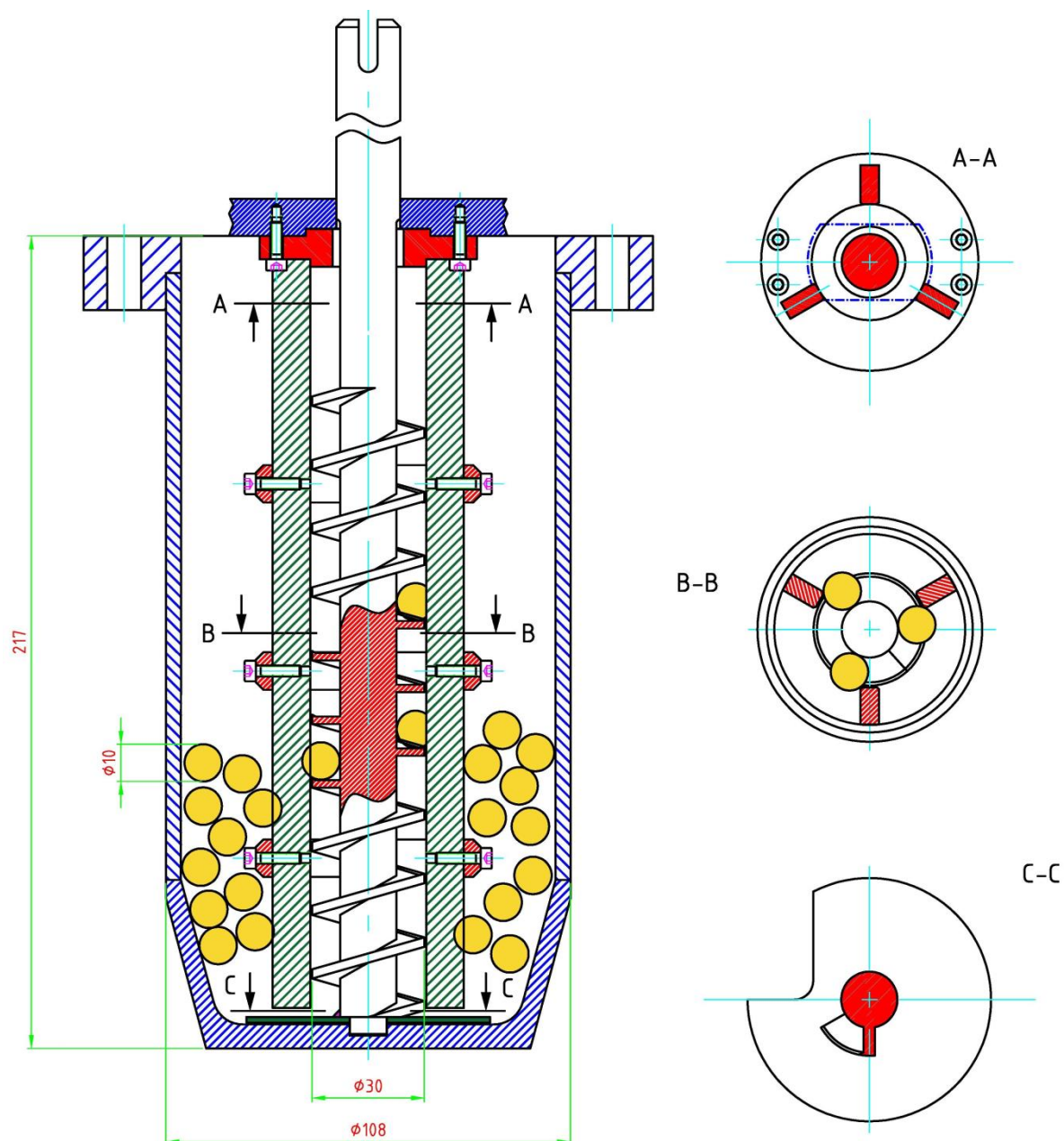


Figure 90: Polyolefin-reactor (based on [Hornung 1997]).

Table 48: List of all sums of PXDD/F and corresponding congeners according to the German act on restriction of chemicals (GGVSEB) and German chemicals prohibition ordinance (ChemVerbotsV).

Sum of PCDD/F	Congeners	Sum of PBDD/F	Congeners
4 PCDD/F	2,3,7,8-TetraCDD 1,2,3,7,8-PentaCDD 2,3,7,8-TetraCDF 2,3,4,7,8-PentaCDF	4 PBDD/F	2,3,7,8-TetraBDD 1,2,3,7,8-PentaBDD 2,3,7,8-TetraBDF 2,3,4,7,8-PentaBDF
12 PCDD/F	4 PCDD/F plus 1,2,3,4,7,8-HexaCDD 1,2,3,6,7,8-HexaCDD 1,2,3,7,8,9-HexaCDD 1,2,3,7,8-PentaCDF 1,2,3,4,7,8-HexaCDF 1,2,3,6,7,8-HexaCDF 1,2,3,7,8,9-HexaCDF 2,3,4,6,7,8-HexaCDF	8 PBDD/F	4 PBDD/F plus 1,2,3,4,7,8-/1,2,3,6,7,8-HexaBDD 1,2,3,7,8,9-HexaBDD 1,2,3,7,8-PentaBDF
17 PCDD/F	12 PCDD/F plus 1,2,3,4,6,7,8-HepaCDD 1,2,3,4,6,7,8,9-OctaCDD 1,2,3,4,6,7,8,9-HeptaCDF 1,2,3,4,7,8,9-HeptaCDF 1,2,3,4,6,7,8,9-OctaCDF		

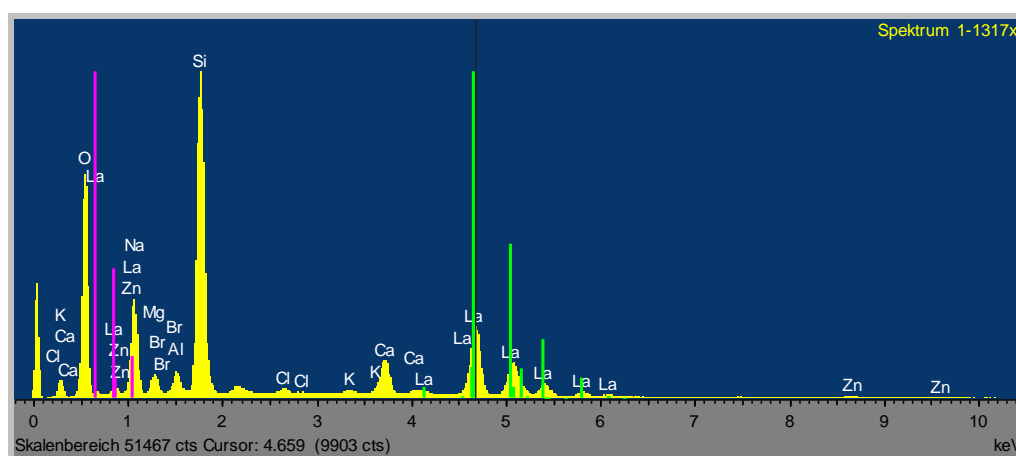


Figure 91: Spectra for EDXRF analysis from La coated glass spheres, spectrum from Figure 35a.

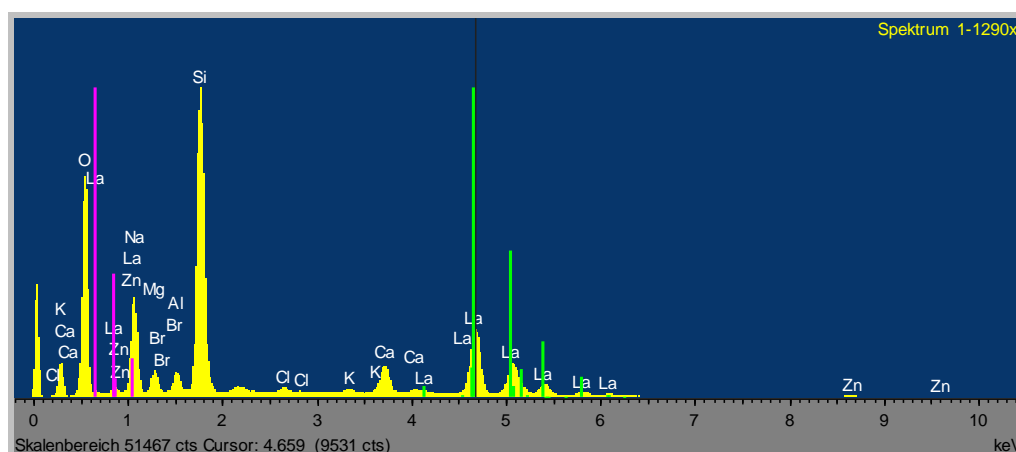


Figure 92: Spectra for EDXRF analysis from La coated glass spheres, spectrum from Figure 35b.

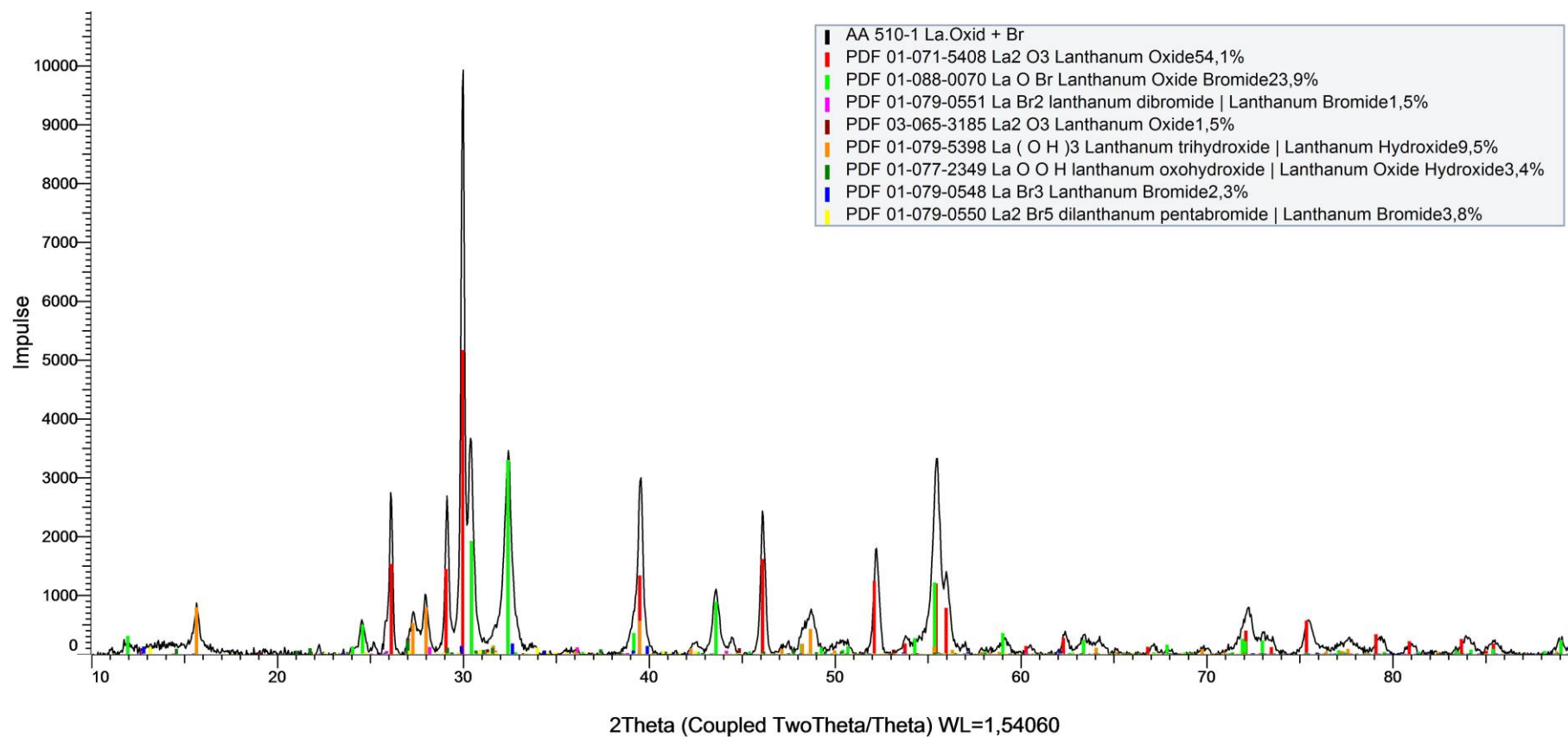


Figure 93: XRD pattern of spheres from absorption tests with Br₂ at 450 °C (%-values after normalization).

Table 49: Product allocation from tests with SR1 as feedstock.

Average Values ±Standard Deviation	Residence Time	Unit	450 °C	550 °C	650 °C
Yield Solids	30 min	wt.-%	58.64 ±0.79	53.54 ±3.10	55.35 ±1.23
	60 min		56.98 ±1.37	55.98 ±1.18	53.78 ±2.70
Yield Liquids, crude	30 min	wt.-%	20.25 ±2.54	22.70 ±0.76	19.91 ±0.88
	60 min		24.35 ±1.07	23.59 ±1.65	19.90 ±0.99
Yield Liquids, filtered	30 min	wt.-%	11.56 ±1.76	16.95 ±1.41	13.03 ±1.17
	60 min		14.54 ±2.23	17.22 ±4.05	13.16 ±1.06
Yield Waxes ³⁹	30 min	wt.-%	7.00 ±1.69	4.09 ±2.25	2.95 ±0.65
	60 min		6.54 ±0.55	3.49 ±0.45	2.74 ±0.46
Yield Tares ⁴⁰	30 min	wt.-%	0.80 ±0.39	0.40 ±0.14	0.47 ±0.13
	60 min		0.42 ±0.10	0.62 ±0.28	0.78 ±0.41
Yield Gases (by difference)	30 min	wt.-%	13.32	19.27	21.32
	60 min		11.72	16.32	22.80

³⁹ "Waxes" describe that amounts of residues, which were left in both cooling units.⁴⁰ "Tares" describe that amount of residue, which were left in the tar-cracking unit.

Table 50: Results of significance tests regarding product allocation with values <0.05.

Compared Pair of Values		450 – 550 (°C)			450 – 650 (°C)			550 – 650 (°C)			30 – 60 (min)		
		30 min	60 min	30 & 60 min	30 min	60 min	30 & 60 min	30 min	60 min	30 & 60 min	450 °C	550 °C	650 °C
Product Allocation	Yield Solid Products	-2.79E ⁻⁰²		-3.78E ⁻⁰³	-7.37E ⁻⁰⁵	-4.22E ⁻⁰²	-6.94E ⁻⁰⁵						
	Yield liquid Product (unfiltered)					-1.07E ⁻⁰²		-1.97E ⁻⁰³	-2.18E ⁰²	1.75E ⁻⁰⁴			
	Yield liquid Product (filtered)	6.68E ⁻⁰³		2.84E ⁻⁰²			2.55E ⁻⁰²						
	Yield Wax			-1.27E ⁻⁰³	-2.31E ⁻⁰²		-1.25E ⁻⁰³						
	Yield Tar												

Table 51: Results of significance tests regarding quality of solid products with values <0.05.

Compared Pair of Values		450 – 550 (°C)			450 – 650 (°C)			550 – 650 (°C)			30 – 60 (min)		
		30 min	60 min	30 & 60 min	30 min	60 min	30 & 60 min	30 min	60 min	30 & 60 min	450 °C	550 °C	650 °C
Solid Pyrolysis Products	HHV	-4.44E ⁻⁰⁴	-3.72E ⁰²	-1.60E ⁻⁰⁵	-2.34E ⁻⁰⁴	-6.60E ⁰³	-9.37E ⁻⁰⁶		7.98E ⁰³				-1.82E ⁻⁰³
	Ignition Loss												
	Content C				-2.88E ⁻⁰²		-2.59E ⁻⁰³						2.17E ⁰³
	Content H				-3.13E ⁻⁰²	-2.44E ⁰²	-1.49E ⁻⁰³			-6.57E ⁻⁰³			
	Content N				-3.17E ⁻⁰²	-1.59E ⁻⁰²	-9.91E ⁻⁰⁴						4.01E ⁻⁰²
	Content S												

Table 52: Results of significance tests regarding quality of liquid products with values <0.05.

Compared Pair of Values		450 – 550 (°C)			450 – 650 (°C)			550 – 650 (°C)			30 – 60 (min)		
		30 min	60 min	30 & 60 min	30 min	60 min	30 & 60 min	30 min	60 min	30 & 60 min	450 °C	550 °C	650 °C
Liquid Pyrolysis Products	HHV	-2.26E ⁻⁰²	-3.61E ⁻⁰²	2.84E ⁻⁰²	-1.70E ⁻⁰³	-1.03E ⁻⁰²	2.55E ⁻⁰²		-2.97E ⁻⁰²	-3.53E ⁻⁰³			
	TAN			-7.01E ⁻⁰⁴			-1.22E ⁻⁰⁵		-7.24E ⁻⁰³	-3.24E ⁻⁰²			
	H ₂ O						4.49E ⁻⁰²	-2.05E ⁻⁰²					
	Content C						-5.00E ⁻¹⁰	2.33E ⁻⁰³		4.43E ⁻⁰²			-6.54E ⁻⁰³
	Content H	-2.56E ⁻⁰³		-3.34E ⁻⁰⁶	-3.95E ⁻⁰⁴				-7.30E ⁻⁰³	-7.26E ⁻⁰⁴			
	Content N	1.10E ⁻⁰²		2.80E ⁻⁰³	4.25E ⁻⁰²	1.00E ⁻⁰³	1.63E ⁻⁰⁴		4.59E ⁻⁰²				5.75E ⁻⁰³
	Content S			1.73E ⁻⁰²									
	Ratio C/H	9.51E ⁻⁰³	3.70E ⁻⁰²	7.56E ⁻⁰⁴	1.09E ⁻⁰³	5.75E ⁻⁰⁴	2.40E ⁻⁰⁷	3.77E ⁻⁰²	1.21E ⁻⁰⁴	3.97E ⁻⁰⁵		-3.04E ⁻⁰²	

Table 53: Results of significance tests regarding quality of gaseous products with values <0.05.

Compared Pair of Values		450 – 550 (°C)			450 – 650 (°C)			550 – 650 (°C)			30 – 60 (min)		
		30 min	60 min	30 & 60 min	30 min	60 min	30 & 60 min	30 min	60 min	30 & 60 min	450 °C	550 °C	650 °C
Gaseous Pyrolysis Products	H ₂ , corr	3.94E ⁻⁰³	7.96E ⁻⁰⁸	1.10E ⁻¹⁰	2.48E ⁻⁰³	5.00E ⁻⁰⁹	1.85E ⁻¹¹	1.60E ⁻⁰³	9.24E ⁻⁰⁵	1.01E ⁻⁰⁶			
	CO	2.23E ⁻⁰⁴	6.73E ⁻⁰³	9.51E ⁻⁰⁸	1.82E ⁻⁰⁴	1.24E ⁻⁰⁶	1.28E ⁻¹⁴	1.47E ⁻⁰²	2.78E ⁻⁰²	1.75E ⁻⁰³			
	CO ₂		-6.47E ⁻⁰³			-1.27E ⁻⁰⁷	-5.22E ⁻⁰³		-6.80E ⁻⁰⁴	-5.77E ⁻⁰⁴			-4.76E ⁻⁰⁴
	HHV	1.73E ⁻⁰³		1.25E ⁻⁰³	1.21E ⁻⁰⁵	2.89E ⁻⁰³	8.59E ⁻⁰⁶	3.48E ⁻⁰²		6.79E ⁻⁰³			
	Density	1.19E ⁻⁰²	-3.89E ⁻⁰²	-1.85E ⁻⁰³	-1.91E ⁻⁰⁴	-1.37E ⁻⁰⁴	-7.25E ⁻⁰⁶		-2.90E ⁻⁰²	-1.84E ⁻⁰²			-1.88E ⁻⁰²
	Volume produced	8.90E ⁻⁰⁴			2.64E ⁻⁰⁶							1.52E ⁻⁰³	
	Duration												
	Gas Production	3.72E ⁻⁰⁴			1.65E ⁻⁰³	-8.09E ⁻⁰³			-2.38E ⁻⁰²		1.40E ⁻⁰⁴	1.82E ⁻⁰²	

Table 54: Results of chi-squared test *HHV* (in MJ·kg⁻¹) versus H₂corr (in vol.-%).

Measured Frequencies		HHV (MJ·kg ⁻¹)					SUM
		10.0 - 14.9	15.0 - 19.9	20.0 - 24.9	25.0 - 29.9	30.0 - 34.9	
H ₂ corr (vol.-%)	4.0 - 7.9	3	3	0	0	0	6
	8.0 - 11.9	1	1	0	1	0	3
	12.0 - 15.9	0	0	2	3	0	5
	16.0 - 19.9	0	0	2	1	7	10
SUM		4	4	4	5	7	24
Test statistic χ^2 : 32.72					Critical Value ($\alpha = 0.95$): 21.03		

Table 55: Results of chi-squared test *HHV* (in MJ·kg⁻¹) versus CO (in vol.-%).

Measured Frequencies		HHV (MJ·kg ⁻¹)					SUM
		10.0 - 14.9	15.0 - 19.9	20.0 - 24.9	25.0 - 29.9	30.0 - 34.9	
CO (vol.-%)	0.0 - 3.9	4	4	0	0	0	8
	4.0 - 7.9	0	0	0	3	0	3
	8.0 - 11.9	0	0	4	2	2	8
	12.0 - 15.9	0	0	2	0	6	8
SUM		4	4	6	5	8	27
Test statistic χ^2 : 45.94					Critical Value ($\alpha = 0.95$): 21.03		

Table 56: Results of chi-squared test *HHV* (in MJ·kg⁻¹) versus CO₂ (in vol.-%).

Measured Frequencies		HHV (MJ·kg ⁻¹)					SUM
		10.0 - 14.9	15.0 - 19.9	20.0 - 24.9	25.0 - 29.9	30.0 - 34.9	
CO ₂ (vol.-%)	10.0 - 24.9	0	0	0	0	3	3
	25.0 - 39.9	0	0	4	0	3	7
	40.0 - 64.9	1	1	2	3	9	7
	65.0 - 80.0	0	3	0	0	0	3
SUM		1	4	6	3	6	20
Test statistic χ^2 : 37.72					Critical Value ($\alpha = 0.95$): 21.03		

Table 57: Results of chi-squared test *HHV* (in MJ·kg⁻¹) versus C_xH_y (in vol.-%).

Measured Frequencies		HHV (MJ·kg ⁻¹)					SUM
		10.0 - 14.9	15.0 - 19.9	20.0 - 24.9	25.0 - 29.9	30.0 - 34.9	
C _x H _y (vol.-%)	0.00 - 2.49	3	0	0	0	0	3
	2.50 - 4.99	1	4	0	0	0	5
	5.00 - 7.49	0	0	0	0	1	1
	7.50 - 9.99	0	0	3	0	2	5
SUM		4	4	3	0	3	14
Test statistic χ^2 : 41.37					Critical Value ($\alpha = 0.95$): 21.03		

Table 58: Dataset about concentrations of PCDD/F in feedstock and pyrolysis solid products.

Sample	Feedstock	Pyrolysis solid products					
Pyrolysis conditions	---	"low heating rate"	450 °C 60 min	550 °C 60 min	550 °C 90 min	650 °C 30 min	650 °C 60 min
PCDD 2,3,7,8-Congeners							
2,3,7,8-TetraCDD	<0.001	<0.002	<0.002	<0.001	<0.001	<0.001	<0.001
1,2,3,7,8-PentaCDD	<0.002	<0.003	<0.003	<0.002	<0.002	<0.002	<0.002
1,2,3,4,7,8-HexaCDD	<0.003	<0.003	<0.003	<0.003	<0.003	<0.003	<0.003
1,2,3,6,7,8-HexaCDD	<0.003	<0.003	<0.003	<0.003	<0.003	<0.003	<0.003
1,2,3,7,8,9-HexaCDD	<0.003	<0.003	<0.003	<0.003	<0.003	<0.003	<0.003
1,2,3,4,6,7,8-HeptaCDD	0.038	<0.015	<0.015	<0.015	<0.015	<0.015	<0.015
1,2,3,4,6,7,8,9-OctaCDD	0.283	<0.045	<0.045	<0.045	<0.045	<0.045	<0.045
PCDF 2,3,7,8-Congeners							
2,3,7,8-TetraCDF	0.0164	1.580	0.934	0.680	0.00105	0.0298	0.403
1,2,3,7,8-PentaCDF	0.00461	2.120	1.120	0.789	<0.002	0.0347	0.391
2,3,4,7,8-PentaCDF	0.0126	1.912	0.851	0.590	<0.002	0.0337	0.470
1,2,3,4,7,8-HexaCDF	0.00703	0.737	0.376	0.267	<0.003	0.0156	0.180
1,2,3,6,7,8-HexaCDF	<0.003	0.945	0.511	0.358	<0.003	0.0191	0.236
1,2,3,7,8,9-HexaCDF	<0.003	0.518	0.207	0.119	<0.003	0.00546	0.0816
2,3,4,6,7,8-HexaCDF	<0.003	0.632	0.327	0.215	<0.003	0.0165	0.150
1,2,3,4,6,7,8-HeptaCDF	<0.015	0.4678	0.303	0.205	<0.015	<0.015	0.152
1,2,3,4,7,8,9-HeptaCDF	<0.015	0.279	0.112	0.659	<0.015	<0.015	0.0478
1,2,3,4,6,7,8,9-OctaCDF	<0.045	0.102	0.0529	<0.045	<0.045	<0.045	<0.045
TEQ-Values¹							
PCDD/F excl. DL ²	0.000953	1.510	0.722	0.501	0.000105	0.0327	0.367
PCDD/F incl. DL ²	0.0137	1.551	0.726	0.504	0.00584	0.0362	0.370

¹ TEQ: Toxic Equivalency Factors with 2,3,7,8-TetraCDD = 1.0 according to NATO/CCMS-Modell (1988)² DL: Detection Limit

Table 59: Dataset about concentrations of PBDD/F in feedstock and pyrolysis solid products.

Sample	Feedstock	Pyrolysis solid products					
Pyrolysis conditions	---	"low heating rate"	450 °C 60 min	550 °C 60 min	550 °C 90 min	650 °C 30 min	650 °C 60 min
PBDD 2,3,7,8-Congeners							
2,3,7,8-TetraBDD	<0.10	<0.10	<0.010	<0.010	<0.010	<0.010	<0.010
1,2,3,7,8-PentaBDD	<0.40	<0.40	<0.020	<0.020	<0.020	<0.020	<0.020
1,2,3,4,7,8-/1,2,3,6,7,8-HexaBDD	<0.40	<0.40	<0.040	<0.040	<0.040	<0.040	<0.040
1,2,3,7,8,9-HexaBDD	<0.80	<0.80	<0.040	<0.040	<0.040	<0.040	<0.040
1,2,3,4,6,7,8-HeptaBDD	2.45	<2.0	<0.100	<0.100	<0.100	<0.100	<0.100
1,2,3,4,6,7,8,9-OctaBDD	6.49	<5.0	<0.250	<0.250	<0.250	<0.250	<0.250
PBDF 2,3,7,8-Congeners							
2,3,7,8-TetraBDF	0.687	3.53	0.171	0.162	<0.0050	0.105	0.189
1,2,3,7,8-PentaBDF	0.584	1.3	0.171	0.0806	<0.020	0.0814	0.0919
2,3,4,7,8-PentaBDF	1.77	2.57	0.215	0.107	<0.020	0.1253	0.128
1,2,3,4,7,8-/1,2,3,6,7,8-HexaBDF	4.5	5.87	0.364	0.138	<0.040	0.283	0.215
1,2,3,7,8,9-HexaBDF	<0.80	<0.80	<0.040	<0.040	<0.040	<0.040	<0.040
2,3,4,6,7,8-HexaBDF	<6.0	<3.0	0.172	0.0697	<0.040	<0.040	0.1113
1,2,3,4,6,7,8-HeptaBDF	117	8.65	0.603	0.274	<0.100	0.431	0.498
1,2,3,4,7,8,9-HeptaBDF	<2.0	<2.0	<0.100	<0.100	<0.100	<0.100	<0.100
1,2,3,4,6,7,8,9-OctaBDF	328	<5.0	<0.250	<0.250	<0.250	<0.250	<0.250
TEQ-Values¹							
PBDD/F excl. DL ²	0.982	1.70	0.133	0.0736	n.c. ³	0.0772	0.0875
PBDD/F incl. DL ²	1.44	2.16	0.161	0.102	0.0345	0.1000	0.1155

¹ TEQ: Toxic Equivalency Factors with 2,3,7,8-TetraCDD = 1.0 according to [Kutz et al. 1990]² DL: Detection Limit³ n.c.: Value not calculated, because no congener was detected above detection limit.

Table 60: Dataset about concentrations of PXDD/F in feedstock and pyrolysis liquid products.

Pyrolysis	Pyrolysis liquid products				
Temperature [°C]	550 °C	650 °C	650 °C	650	650
Residence Time [min]	60 min	60 min	30 min	30	30
PO-Reactor			PP	PP+La-1.5¹	PP+La-4.5²
PCDD 2,3,7,8-Congeners					
2,3,7,8-TetraCDD	0.0722	0.0664	<0.06	<0.01	<0.02
1,2,3,7,8-PentaCDD	0.0714	0.16	<0.03	<0.02	<0.02
1,2,3,4,7,8-HexaCDD	<0.03	0.0571	<0.03	<0.03	<0.03
1,2,3,6,7,8-HexaCDD	0.0617	<0.03	<0.03	<0.03	<0.03
1,2,3,7,8,9-HexaCDD	0.0347	<0.03	<0.03	<0.03	<0.03
1,2,3,4,6,7,8-HeptaCDD	<0.15	<0.15	<0.15	<0.15	<0.15
1,2,3,4,6,7,8,9-OctaCDD	<0.45	<0.45	0.592	<0.45	<0.45
PCDF 2,3,7,8-Congeners					
2,3,7,8-TetraCDF	14.3	14.4	9.49	12.30	12.40
1,2,3,7,8-PentaCDF	33.6	15.8	3.84	6.46	6.07
2,3,4,7,8-PentaCDF	30.2	19.7	7.95	10.10	10.20
1,2,3,4,7,8-HexaCDF	11.2	4.28	1.09	1.91	1.58
1,2,3,6,7,8-HexaCDF	14.8	6.25	1.26	2.68	2.00
1,2,3,7,8,9-HexaCDF	4.93	1.07	0.34	0.62	1.22
2,3,4,6,7,8-HexaCDF	12.4	5.45	1.36	2.32	2.20
1,2,3,4,6,7,8-HeptaCDF	8.01	2.93	0.84	1.26	1.10
1,2,3,4,7,8,9-HeptaCDF	4.45	1.09	0.34	0.599	0.505
1,2,3,4,6,7,8,9-OctaCDF	1.53	0.487	0.88	<0.45	0.573
PBDD 2,3,7,8-Congeners					
2,3,7,8-TetraBDD	<0.30	<0.40	<0.15	<0.40	<0.03
1,2,3,7,8-PentaBDD	<1.0	<0.40	<0.10	<0.40	<0.10
1,2,3,4,7,8-/1,2,3,6,7,8-HexaBDD	<0.80	<0.80	<0.20	<0.80	<0.20
1,2,3,7,8,9-HexaBDD	<0.80	<0.80	<0.20	<0.80	<0.20
1,2,3,4,6,7,8-HeptaBDD	<2.0	<2.0	<0.50	<2.0	<0.50
1,2,3,4,6,7,8,9-OctaBDD	<5.0	<5.0	<1.25	<5.0	<1.25
PBDF 2,3,7,8-Congeners					
2,3,7,8-TetraBDF	25.1	4.57	2.05	5.37	1.27
1,2,3,7,8-PentaBDF	11.8	1.28	0.408	1.15	0.195
2,3,4,7,8-PentaBDF	21.3	2.07	0.676	2.16	0.288
1,2,3,4,7,8-/1,2,3,6,7,8-HexaBDF	22.5	1.36	0.374	1.23	0.202
1,2,3,7,8,9-HexaBDF	<0.80	<0.80	<0.20	<0.80	<0.20
2,3,4,6,7,8-HexaBDF	<12.0	<0.80	<0.20	<0.80	<0.20
1,2,3,4,6,7,8-HeptaBDF	24.1	<2.0	<0.5	<2.0	<0.5
1,2,3,4,7,8,9-HeptaBDF	<2.0	<2.0	<0.5	<2.0	<0.5
1,2,3,4,6,7,8,9-OctaBDF	<5.0	<5.0	<1.25	<5.0	<1.25
TEQ-Values¹					
PCDD/F excl. DL ²	22.8	14.0	5.54	7.48	7.33
PCDD/F incl. DL ²	22.8	14.0	5.62	7.48	7.38
PBDD/F excl. DL ²	13.8	1.55	0.563	1.68	0.281
PBDD/F incl. DL ²	14.7	2.31	0.803	2.14	0.396

¹ Blend of PP La(OH)₃/LaOOH (100:1.412 by weight).² Blend of PP La(OH)₃/LaOOH (100:0.468 by weight).³ TEQ: Toxic Equivalency Factors with 2,3,7,8-TetraCDD = 1.0 according to [Kutz et al. 1990]⁴ DL: Detection Limit

Table 61: Allocation of metals, halogens, and P from pyrolysis at 650 °C for 30 min with polyolefin-reactor (normalized, in wt.-%); analyses based on ICP-MS-/OES analyses.

Element	Allocation (normalized) [wt.-%]				Element	Allocation (normalized) [wt.-%]			
	Solid Product	PP-Residue	Filtration Residue	Filtered Liquids		Solid Product	PP-Residue	Filtration Residue	Filtered Liquids
Al	99.57	0.04	0.11	0.27	Mn	99.85	0.14	0.01	<0.01
As	96.44	1.27	---	2.29	Mo	12.13	86.21	---	1.66
Ba	100.00	---	---	---	Na	100.00	---	---	---
Br	91.76	1.03	2.79	4.41	Nb	100.00	---	---	---
Ca	99.85	0.04	0.08	0.08	Ni	98.97	0.99	0.02	0.01
Cd	---	2.14	15.51	82.35	Os	100.00	---	---	---
Ce	100.00	---	---	---	P	94.00	0.43	1.92	3.64
Cl	90.63	0.41	2.62	6.35	Pb	99.82	0.03	0.10	0.05
Cr	93.23	6.65	0.09	0.04	Sb	98.79	0.15	0.55	0.52
Cu	99.99	0.01	<0.01	<0.01	Si	99.56	0.03	0.14	0.27
Eu	100.00	---	---	---	Sn	99.56	---	0.17	0.26
Fe	99.55	0.40	0.03	0.02	Sr	100.00	---	---	<0.01
Ga	100.00	---	---	---	Te	100.00	---	---	---
In	---	---	---	100.00	Ti	99.99	---	---	0.01
Ir	100.00	---	---	---	Yb	98.70	---	1.30	---
K	99.97	0.02	0.01	---	Zn	99.33	0.09	0.34	0.24
La	---	100.00	---	---	Zr	99.98	---	---	0.02
Mg	99.60	---	0.10	0.30					

Table 62: Allocations of metals, Br, Cl, P, and S from pyrolysis solid product to sieve fractions (Pyrolysis at 650 °C for 30 min with polyolefin-reactor, normalized, in wt.-%); analyses based on EDXRF with C, H, N given and O as missing component.

Sieve Fraction [µm]	<63	63 - 125	125 - 250	250 - 500	500 - 1 000	1 000 - 2 000	>2 000
Element	Allocation (normalized) [wt.-%]						
Al	48.11	10.51	9.16	13.35	12.61	4.12	2.14
As	---	---	---	---	64.72	4.09	31.19
Ba	71.75	21.44	5.93	0.46	0.22	0.18	0.02
Br	87.41	7.35	1.26	0.94	1.8	0.90	0.34
Ca	77.29	11.56	3.87	2.04	3.12	1.36	0.76
Ce	8.28	71.47	9.87	---	---	---	10.39
Cl	76.23	8.60	2.60	2.84	5.98	2.11	1.64
Cr	39.47	---	1.91	9.12	1.14	7.74	40.63
Cu	8.88	1.92	2.48	18.93	49.92	6.58	11.78
Eu	82.08	11.26	3.04	1.51	1.16	0.95	0.43
Fe	79.64	10.72	2.43	1.76	2.37	1.61	1.47
Ga	100.00	---	---	---	---	---	---
Ir	55.26	14.16	6.00	23.43	---	1.15	---
K	66.08	20.40	8.02	1.77	2.28	1.07	0.38
Mg	68.86	11.27	4.72	4.01	6.64	2.16	2.53
Mn	82.82	8.83	2.03	1.57	1.89	0.98	0.88
Mo	---	---	---	---	---	23.68	76.32
Na	59.77	25.42	10.24	2.71	---	0.96	0.89
Nb	---	---	---	---	---	3.90	96.10
Ni	29.49	3.45	1.71	4.59	37.08	2.61	21.07
Os	25.88	41.00	33.12	---	---	---	---
P	66.25	14.18	5.01	3.91	6.38	1.96	2.32
Pb	56.63	14.20	5.69	8.77	12.80	1.46	0.44
S	91.83	1.86	---	---	3.84	1.14	0.33
Sb	87.73	8.25	1.85	0.66	1.17	0.25	0.09
Si	62.67	20.06	8.13	2.87	3.73	1.29	1.25
Sn	42.90	10.29	8.61	15.84	16.70	3.12	2.54
Sr	66.14	23.24	8.57	0.86	0.70	0.35	0.13
Te	75.22	18.70	6.08	---	---	---	---
Ti	77.26	11.57	3.02	2.04	3.53	1.59	0.98
Yb	---	---	---	51.54	...	11.61	36.85
Zn	68.13	7.16	2.41	3.69	4.04	2.76	11.81
Zr	67.02	23.27	8.43	0.99	---	0.29	---

Table 63: Retention times and absolute abundances of compounds in pyrolysis liquid products from different pyrolysis temperatures, detected by GC-MS.

Compound	450 °C 30 min		550 °C 30 min		650 °C 30 min	
	Ret. Time	Absolute Abund.	Ret. Time	Absolute Abund.	Ret. Time	Absolute Abund.
	min	%	min	%	min	%
Ethylbenzene	6.389	0.67	6.343	1.21	6.550 6.794	3.18
1,2-dimethylbenzene	6.903	1.45	6.832	1.72	6.909	0.41
Styrene	7.602	6.93	7.234 7.551	8.16	7.316 7.522	10.48
Trimethylbenzene	8.365	0.25	8.327	0.25	8.301	0.12
Phenol	9.547	0.97	9.571 ⁴	2.72 ⁴	9.544 ⁴	1.73 ⁴
Isopropenylbenzene	9.591	1.66	9.571 ⁴	2.72 ⁴	9.544 ⁴	1.73 ⁴
Benzonitrile	9.650	0.26	9.626	0.38	9.604	0.52
2-methylstyrene	10.482	0.12	10.455	0.14	10.440	0.12
4-ethyl-1,2-dimethoxybenzene	10.969	0.36	10.965	0.50	10.952	0.59
Alkene	11.421 14.998 15.240 18.740	1.34	11.420 14.967 15.212 18.750	0.68	11.494 14.950 15.200 18.299	1.23
2,4-dimethylphenol	11.922	0.20	11.921	0.25	11.910	0.19
Naphthalene	13.270	0.13	13.271	0.20	13.259	1.07
Isopropyl phenol	13.836	0.44	13.844	0.34	13.841	0.12
Benzenebutanenitrile	15.480	0.83	15.489	0.52	15.483	0.19
Biphenyl	16.128	0.11	16.135	0.16	16.122	0.36
1,3-diphenylpropane	19.505	1.16	19.517	0.42	19.435	0.55
1,1-diphenyl-2-methylpropene	19.802	0.13	19.812	0.05		
2,4-diphenyl-1-butene ²	20.274	0.29	20.285	0.07	20.213	0.28
Methylstilbene	20.415	0.32	20.430	0.15	20.448	0.07
1-phenyl-1,2,3,4-tetrahydronaphthalene	20.878	0.22	20.887	0.07	20.845	0.08
Dihydronaphthalene	21.142	0.33	21.154	0.09	21.149	0.05
1-phenylnaphthalene	21.808	0.17	21.824	0.12	21.814	0.14
2-phenylnaphthalene	22.983	0.27	22.982	0.19	22.970	0.32
2-benzyl naphthalene	24.202	0.18	24.215	0.08	24.249	0.22
1,4-diphenylbenzene	24.610	0.19	24.618	0.07	24.619	0.06
2,4,6-triphenyl-1-hexene ^{2,3}	27.130 27.997	0.36			27.275 27.867	0.119

¹ Styrene dimer² Styrene trimer³ Isomer⁴ Co-elution of phenol and isopropenylbenzene

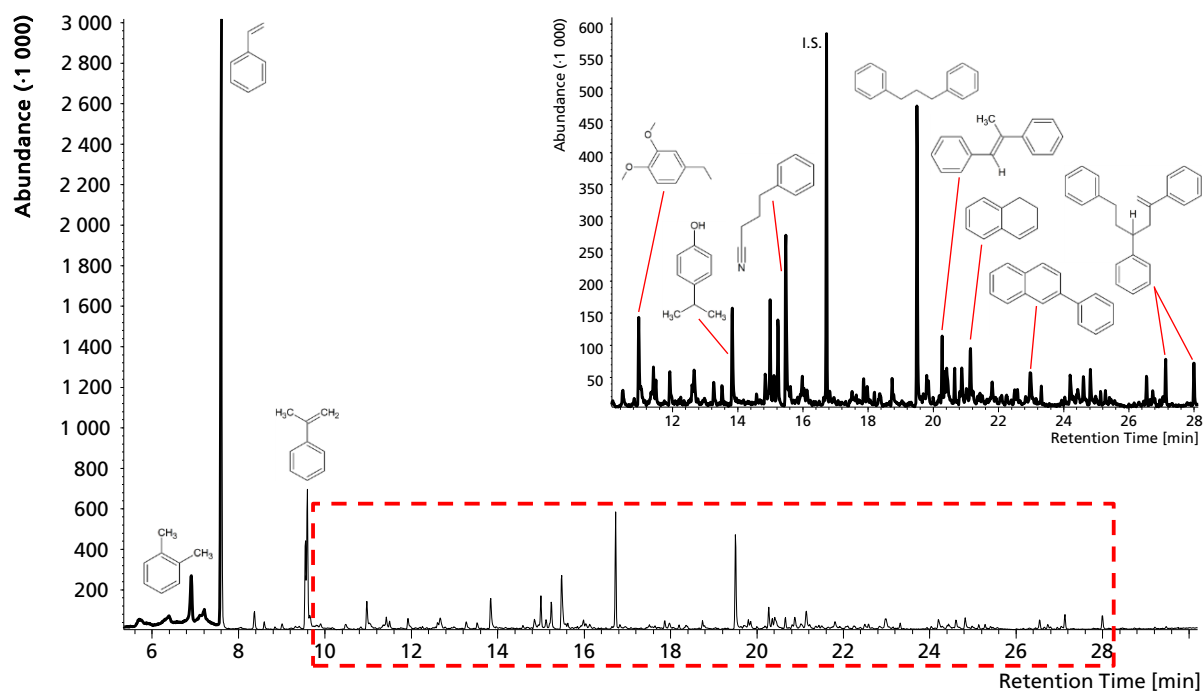


Figure 94: GC-MS Chromatogram of pyrolysis liquid product (450 °C, 30 min).

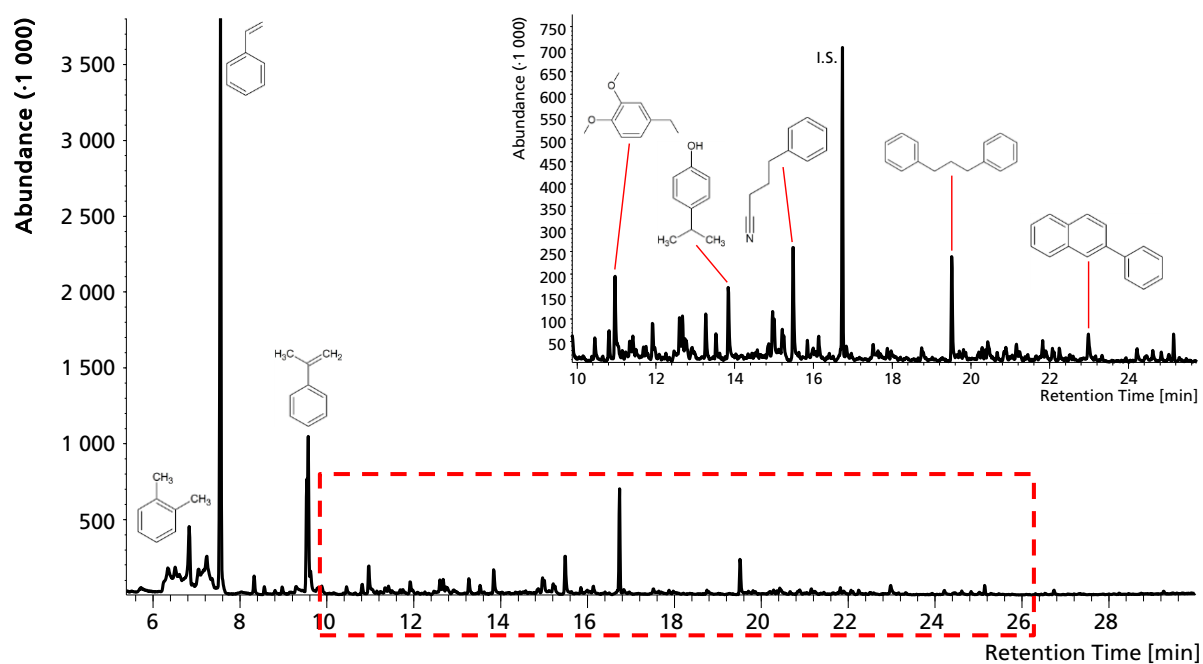


Figure 95: GC-MS Chromatogram of pyrolysis liquid product (550 °C, 30 min).

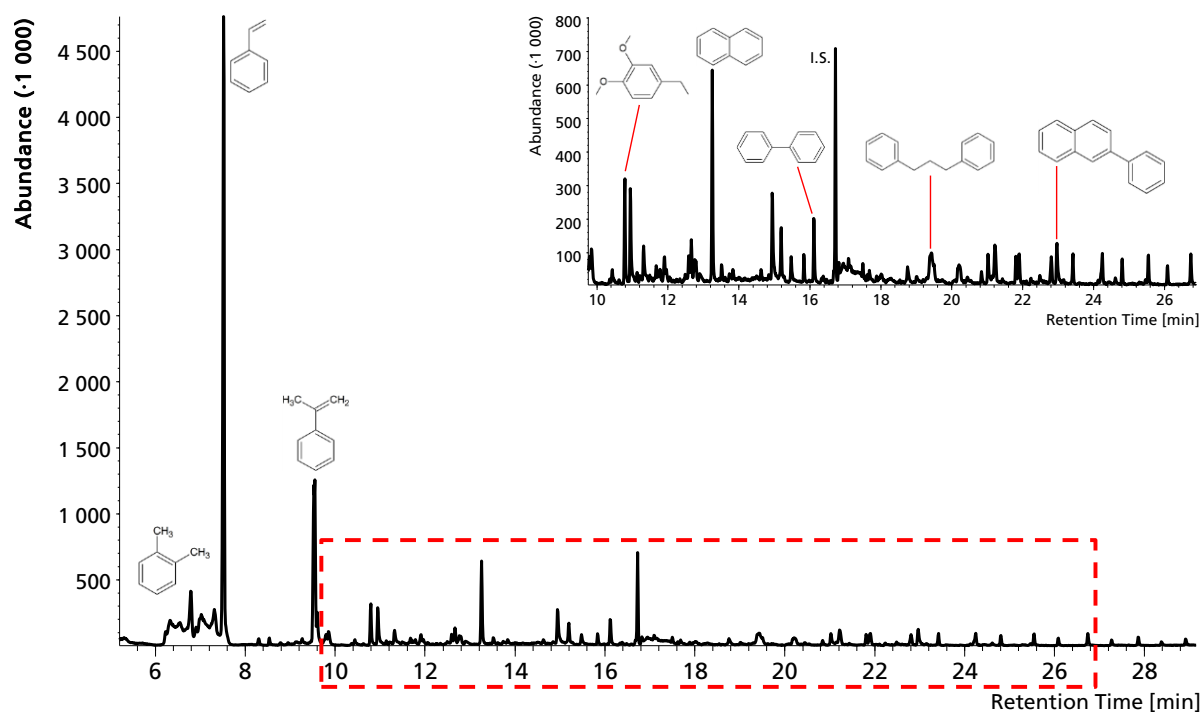


Figure 96: GC-MS Chromatogram of pyrolysis liquid product (650 °C, 30 min).

Table 64: Retention times and absolute abundances of compounds in pyrolysis liquid products from pyrolysis tests with polyolefin-reactor, detected by GC-MS.

Compound	650 °C + PP		650 °C + PP+La1.5		650 °C + PP+La4.5	
	Ret. Time	Absolute Abund.	Ret. Time	Absolute Abund.	Ret. Time	Absolute Abund.
	min	%	min	%	min	%
Ethylbenzene	6.403	0.99	6.418	1.04	6.404	1.10
1,2-dimethylbenzene	6.880	1.86	6.832	1.50	6.888	1.91
Styrene	7.591	10.37	7.218	9.08	7.592	7.15
			7.548			
Trimethylbenzene	8.352	0.11	8.321	0.11	8.356	0-11
Phenol	9.545	1.57	9.526	1.32	9.550 ⁴	3.33 ⁴
Isopropenylbenzene	9.579	1.65	9.560	1.41	9.550 ⁴	3.33 ⁴
Benzonitrile	9.639	0.41	9.615	0.42	9.642	0.44
2-methylstyrene	10.461	0.08	10.447	0.08	9.833	0.19
1-propynylbenzene			10.798	0.38		
4-ethyl-1,2-dimethoxybenzene	10.961	0.55	10.951	0.41	10.960	0.59
Alkene	11.416	0.93	11.405	1.68	11.414	1.48
	14.993		14.989		14.995	
	15.235		15.231		15.236	
	18.758		18.752		18.760	
	20.352					
	20.448					
2,4-dimethylphenol	11.915	0.12	11.908	0.11	11.914	0.16
Naphthalene	13.259	0.97	13.251	0.80	13.258	1.19
Isopropyl phenol	13.845	0.08	13.839	0.09	13.844	0.08
Benzenebutanenitrile	15.484	0.14	15.481	0.13	15.484	0.14
Biphenyl	16.117	0.33	16.114	0.29	16.118	0.38
1,3-diphenylpropane	19.516	0.06	19.516	0.07	19.517	0.07
Methylstilbene			20.443	0.10		
1-phenyl-1,2,3,4-tetrahydronaphthalene	20.841	0.08	20.882	0.05	20.840	0.12
Dihydronaphthalene			21.146	0.11	21.144	0.14
1-phenylnaphthalene	21.810	0.12	21.807	0.11	21.809	0.15
2-phenylnaphthalene	22.979	0.21	22.983	0.24	22.974	0.27
2-benzyl naphthalene					24.211	0.07
1,4-diphenylbenzene	24.600	0.05	24.601	0.05	24.610	0.02

¹ Styrene dimer² Styrene trimer³ Isomer⁴ Co-elution of phenol and isopropenylbenzene.

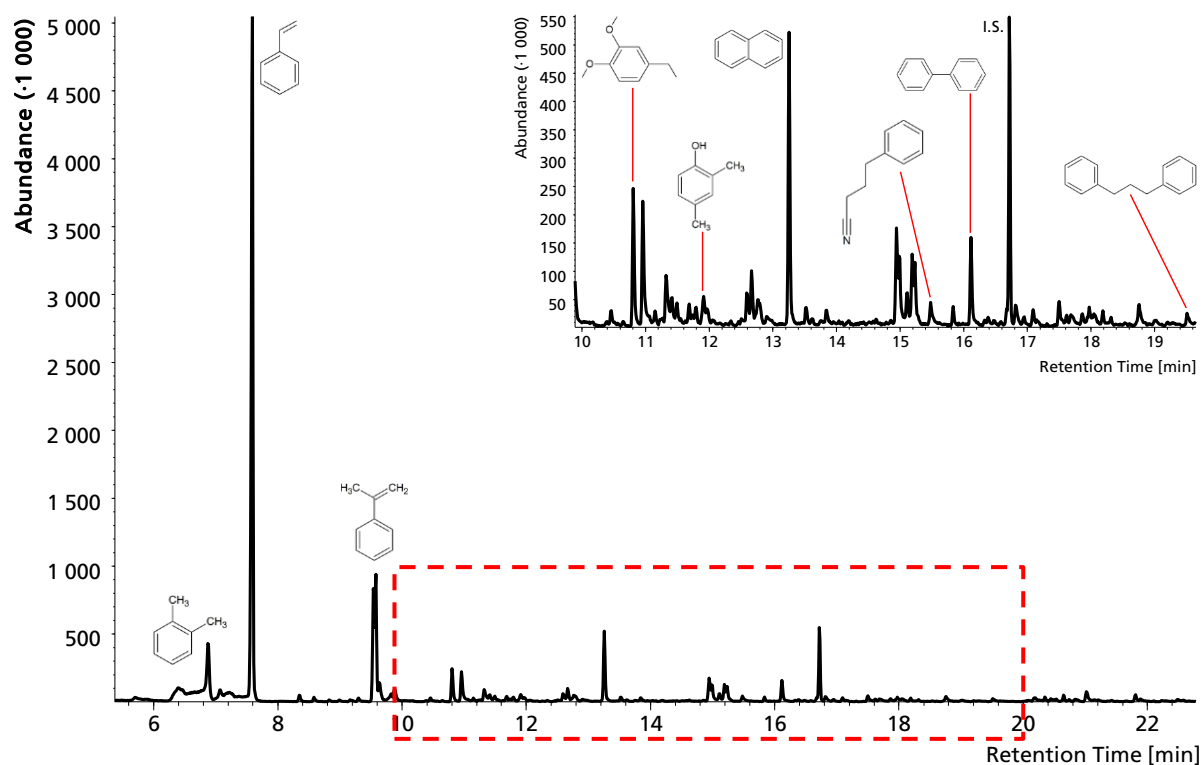


Figure 97: GC-MS Chromatogram of pyrolysis liquid product (650 °C, 30 min, PP, H.F.).

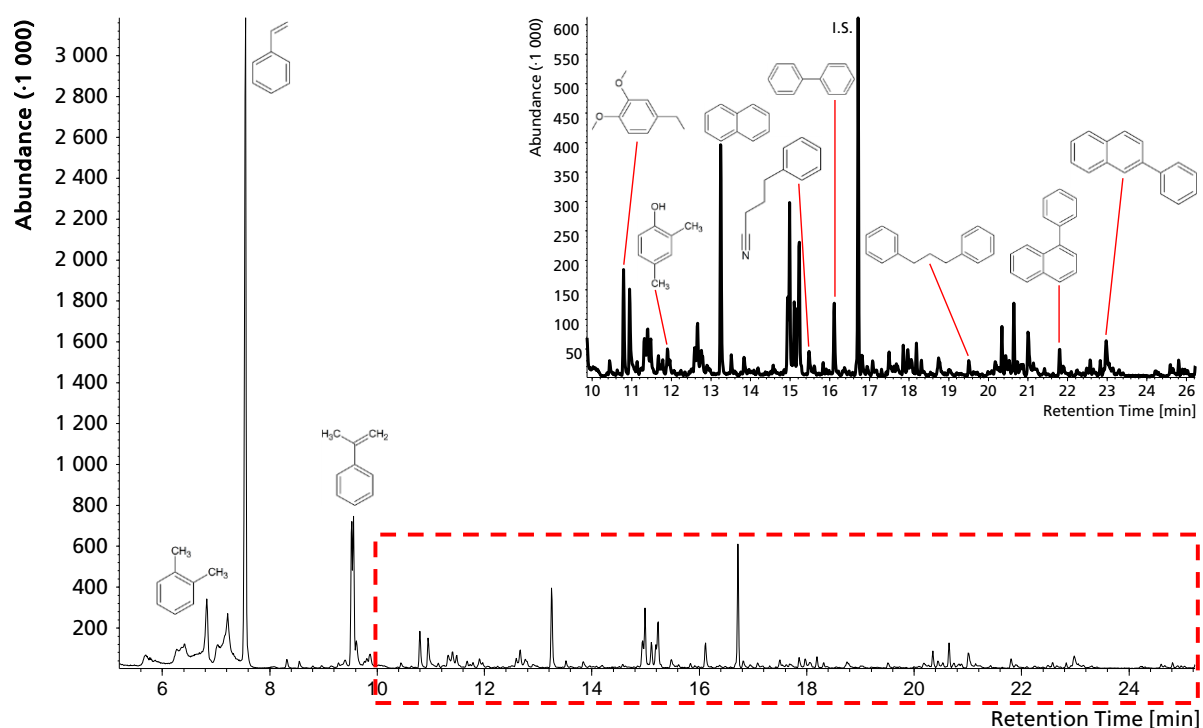


Figure 98: GC-MS Chromatogram of pyrolysis liquid product (650 °C, 30 min, PP+La1.5, H.F.).

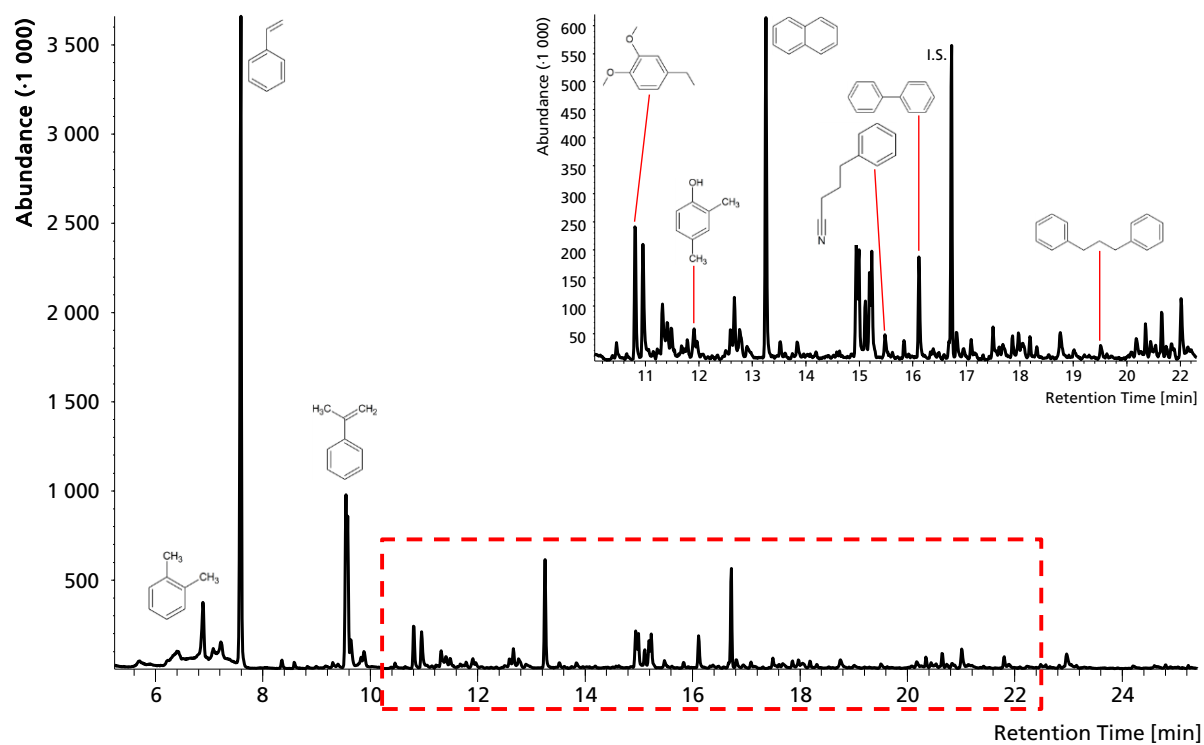


Figure 99: GC-MS Chromatogram of pyrolysis liquid product (650 °C, 30 min, PP+La4.5, H.F.).

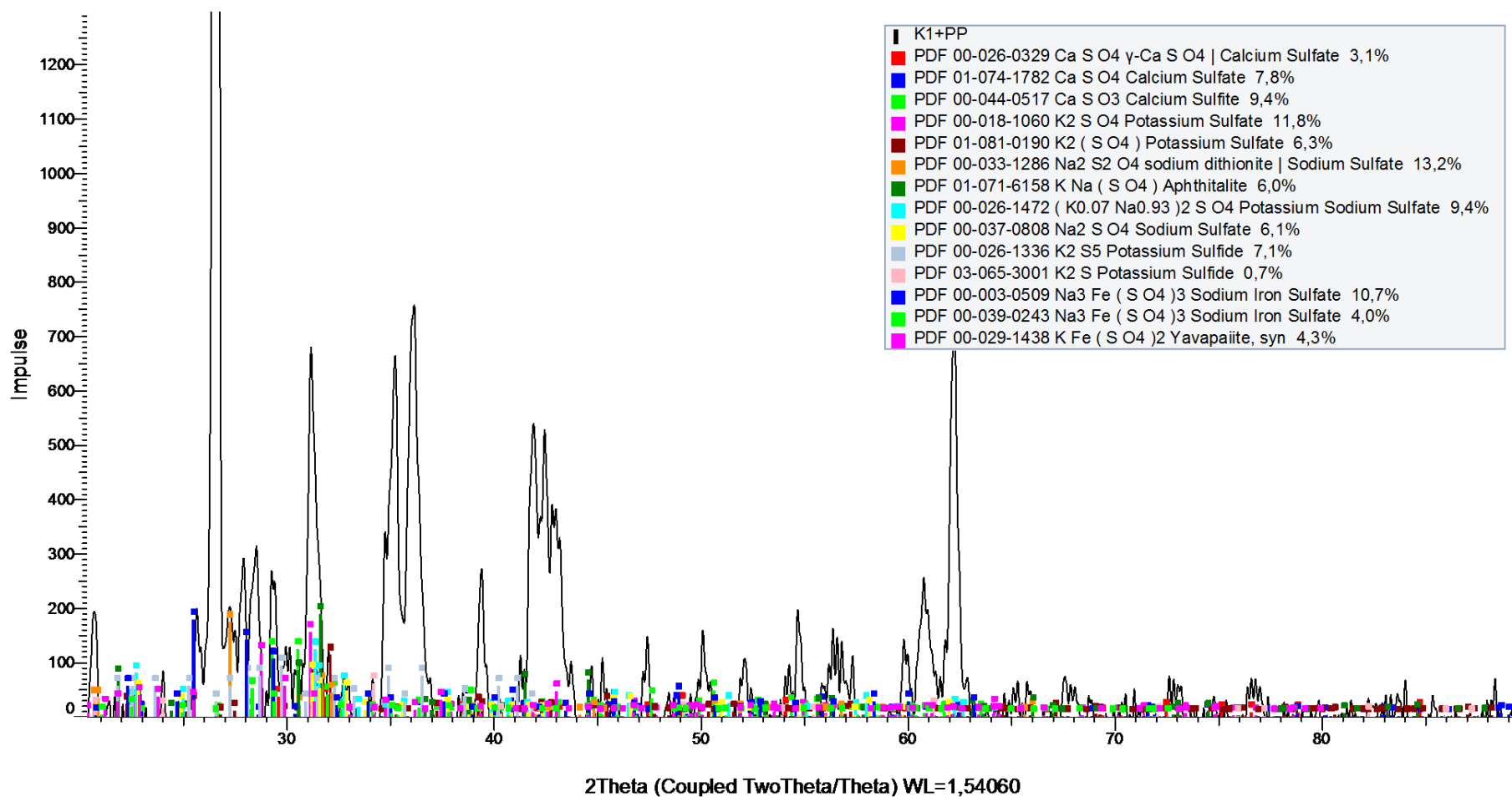


Figure 100: XRD pattern of pyrolysis sieve fraction <63 µm from pyrolysis tests with SR1 (650 °C, 30 min) regarding S compounds (%-values after normalization).

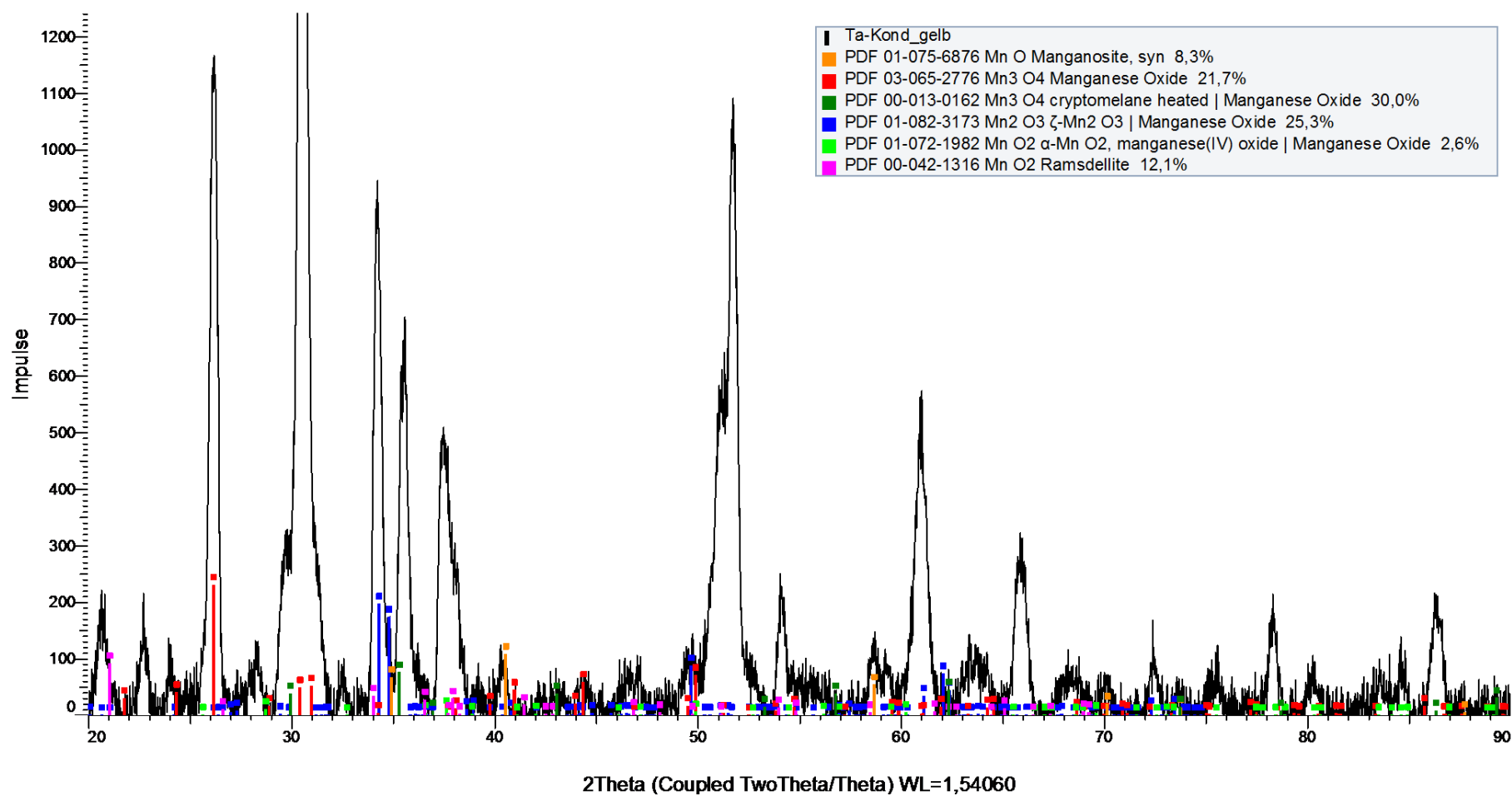


Figure 101: XRD pattern of fine fraction (<500 µm) from pyrolysis tests with Ta capacitors (550 °C, 30 min) regarding Mn oxides (%-values after normalization).

Table 65: Degree of enrichment of metals found in filtration residue and filtered liquids from pyrolysis tests (650 °C, 30 min, polyolefin-reactor with PP+La1.5) with corresponding melting and boiling points of metals, its oxides and halides (in °C) determined using ICP-MS/-OES [DGUV 2016; Holleman et al. 2007; Perry, Phillips 1995].

Metal	Degree of Enrichment		Metal		Me _x O _y			Me _x Cl _y			Me _x Br _y		
	Filtration Residue	Filtered Liquids	M _p (°C)	B _p (°C)	Form	M _p (°C)	B _p (°C)	Form	M _p (°C)	B _p (°C)	Form	M _p (°C)	B _p (°C)
As	0.24211	0.13684		616 ¹	As ₂ O ₃	313	460	AsCl ₃	-16	130.2	AsBr ₃	31	221
Cu	0.00027	---	1 083.4	2 595	CuO	1 326		CuCl	430	1490	CuBr ₂	498	900
Fe	0.00805	---	1 535	3 070	FeO	1 368		FeCl ₂	676	1 012	FeBr ₂	684	934
Ga	0.01827	---	29.78	2 403	Ga ₂ O ₃	1 725		GaCl ₃	77.9	201.3	GaBr ₃	122.5	279
In	0.07492	---	156.61	2 070	In ₂ O ₃			InCl ₃	586	600 ¹	InBr ₃	436	
Mg	0.00997	---	648.8	1 105	MgO	2 832	3 600	MgCl ₂	714	1 412	MgBr ₂	711	1 229.9
Mn	0.00703	---	1 244	2 030	Mn ₃ O ₄	1 705		MnCl ₂	652	1 230.9	MnBr ₂	695	1 027
Na	0.04435	---	97.82	881.3	Na ₂ O	1 132		NaCl	801	1 413	NaBr	747	1 390
Ni	0.00295	---	1 453	2 730	NiO	1 984		NiCl ₂	1 001	987	NiBr ₂	963	
Pb	0.03463	0.00056	327.43	1 751	PbO	897	1 470	PbCl ₂	498	954	PbBr ₂	373	916
Sb	0.69848	0.03167	630.7	1 635	Sb ₂ O ₃	655	1 425	SbCl ₃	73.4	223	SbBr ₃	96	288
Se	0.36667	---	220.5	684.8	SeO ₂	340	315 ¹	SeCl ₄	306	196	SeBr ₄	75	123
Sn	0.02256	0.00275	231.91	2 687	SnO ₂	1 630	1 800	SnCl ₂	247	623	SnBr ₂	216	619
Sr	0.00560	---	768	1 380	SrO	2 430	3 000	SrCl ₂	873	1 250	SrBr ₂	657	2 146
Ti	0.05231	---	1 667	3 285	TiO ₂	1 843	2 500 ²	TiCl ₄	-24.1	136.5	TiBr ₄	38.3	233.5
Zn	0.07721	0.00395	419.6	908.5	ZnO	1 975		ZnCl ₂	290	732	ZnBr ₂	394	650

¹ Sublimation

² 2 500 - 3 000 °C [Perry, Phillips 1995]